Coventry University

DOCTOR OF PHILOSOPHY

Development Of Novel Approaches For High Resolution Direction Of Arrival Estimation Techniques

Balasubramanian, Ramaswamy K.

Award date:
2016

Awarding institution:
Coventry University

Link to publication

General rights
Copyright and moral rights for the publications made accessible in the public portal are retained by the authors and/or other copyright owners and it is a condition of accessing publications that users recognise and abide by the legal requirements associated with these rights.

- Users may download and print one copy of this thesis for personal non-commercial research or study
- This thesis cannot be reproduced or quoted extensively from without first obtaining permission from the copyright holder(s)
- You may not further distribute the material or use it for any profit-making activity or commercial gain
- You may freely distribute the URL identifying the publication in the public portal

Take down policy
If you believe that this document breaches copyright please contact us providing details, and we will remove access to the work immediately and investigate your claim.

Download date: 04. Jul. 2025

DEVELOPMENT OF NOVEL APPROACHES FOR HIGH RESOLUTION DIRECTION OF ARRIVAL ESTIMATION TECHNIQUES

By

RAMASWAMY KARTHIKEYAN BALASUBRAMANIAN

September 2015

A thesis submitted in partial fulfilment of the University's requirements for the Degree of Doctor of Philosophy

CERTIFICATE

This is to certify that the Doctoral Dissertation titled "Development of Novel Approaches for Direction of Arrival Estimation Techniques" is a bonafide record of the work carried out by Mr. Ramaswamy Karthikeyan Balasubramanian in partial fulfilment of requirements for the award of Doctor of Philosophy Degree of Coventry University

September - 2015

Dr. Govind R. Kadambi
Diretor of Studies
M.S.Ramaiah School of Advanced Studies, Bangalore

Dr. Govind R. Kadambi
Supervisor
M.S.Ramaiah School of Advanced Studies, Bangalore

Dr. Yuri A. Vershinin
Supervisor
Coventry University, U.K.

ACKNOWLEDGEMENT

The successful completion of any task would be incomplete without complementing those who made it possible and whose guidance and encouragement ensured its success.

I thank my mother **Mrs. B. Thilakavathi** and my father **Mr. R. Balasubramanian** for their unconditional love and support. I am forever indebted to them and very sincerely acknowledge their forbearance during this period. Their support has steadfastly sustained my motivation to culminate all my doctoral research work into this thesis.

I am overwhelmed at this point of time to express my sincere and heartfelt gratitude to my supervisor **Professor Govind R. Kadambi**, Pro-Vice Chancellor, M S Ramaiah University of Applied Sciences, Bangalore. His guidance and sustained motivation are the backbone in the progress of this research. I profusely thank him for the same.

I am thankful to my supervisor **Dr. Yuri A. Vershinin**, Senior Lecturer, Coventry University, U.K. His guidance and monitoring of my research progress and thesis preparation helps me to reach this level.

With deep sense of gratitude and indebtedness, I acknowledge the support, guidance and encouragement rendered by, **Professor S.R. Shankapal**, Vice Chancellor, M S Ramaiah University of Applied Sciences. While his advice have been a source of inspiration, his suggestions and feedback proved to be valuable course correctors throughout the tenure of my research work at MSRSAS.

I thank **Professor M.D. Deshpande**, Head, Research Department, MSRSAS, for providing necessary resources, facilities and an excellent environment conducive to research work. His politeness and conduction of research reviews are worthy of emulation.

I take this opportunity to express my gratitude to **Professor Peter White**, Coventry University, U.K. for his thought provoking suggestions and also key inputs provided during the progress review meetings. His comments helped me a lot in understanding the purpose of research. I am ever grateful to him for his kindness and patient listening during review meetings.

I offer my most humble submission and thanks to **ALMIGHTY GOD** for his grace and immeasurable blessings.

ABSTRACT

This thesis presents the development of MUSIC algorithm based novel approaches for the estimation of Direction of Arrival (DOA) of electromagnetic sources. For the 2D-DOA estimation, this thesis proposes orthogonally polarized linear array configuration rather than the conventionally invoked two dimensional array. An elegant one dimensional search technique to compute 2D-DOA estimation for a single source scenario has been proposed. To facilitate one dimensional search for 2D-DOA estimation, a closed form relationship between the azimuth and elevation angles of the 2D-DOA is derived using the analytical expressions of radiation patterns of Rectangular Waveguide (RWG) and Circular Waveguide (CWG). The computation time for the proposed one dimensional search technique is reduced by a factor of 50 and 150 for 1° and 0.5° search interval respectively. To improve the accuracy and the resolution of 2D-DOA estimation in case of closely spaced sources, this thesis proposes novel array configurations such as orthogonally polarized planar array, orthogonally mounted linear array and orthogonally polarized linear array. Through numerous simulation studies, a relative performance comparison of 2D-DOA estimation realized through various proposed novel array configurations has been carried out to highlight the accuracy and resolution under wide range of SNR conditions. The thesis presents a discussion on the analysis of effect of spatial de correlation in lieu of the employed orthogonally polarized elements in the array configuration on the improved accuracy and resolution of the 2D-DOA estimation.

This thesis also deals with the utility of the proposed orthogonally polarized array configurations for tracking of 2D-DOA angles of non-stationary signal sources. The weighting factor and forgetting factor approaches for smoothing the time-varying covariance matrix of the non-stationary sources are studied. The simulation studies on 2D-DOA tracking by invoking proposed array configurations along with the proposed smoothing techniques prove that orthogonal polarized array configuration track the DOA source angle with minimum estimation errors. The thesis proposes the replacement of computationally intensive numerical schemes in Multiple Signal Classification (MUSIC) algorithm such as eigen decomposition and singular value decomposition with the subspace tracking techniques such as Bi-Iterative Singular Value Decomposition (Bi-SVD) algorithm. Invoking the concept of sub-band processing, the thesis addresses the validity of the extension of the presented 2D-DOA estimation analysis to wide band signal. A two subband filter approach is proposed for the estimation 2D-DOA of single and two wideband sources. The simulation study of the two subband filter approach along with the orthogonal polarized array configurations confirms the better estimation accuracy as well as the lesser computation time.

CONTENTS

LIST OF TABLES

LIST OF FIGURES

Nomenclature

a	-	Width of the RWG (mm) or (cm)
b	-	Height of the RWG (mm) or (cm)
c	-	Electromagnetic Velocity (m/s)
d	-	Inter-element spacing (mm) or (cm)
e^x	-	Exponential of x
f	-	Frequency (Hz) (MHz) (GHz)
j	-	Imaginary component of the complex term
k	-	Wave number
m	-	Index to denote m^{th} antenna of the array
n	-	Index to denote n^{th} sampling instant
p	-	Index to denote p^{th} source
q	-	Order of the Smoothing Filter
t	-	Index to denote t^{th} time instant
x	-	x coordinate
y	-	y coordinate
z	-	z coordinate
α	-	Weighting Factor
β	-	Forgetting Factor
β_{mn}	-	Propagation Constant of RWG Exited in mode mn
λ	-	Wavelength (mm) or (cm) or (m)
λ_i	-	i^{th} Eigenvalue
μ	-	Free Space Permeability
ε	-	Free Space Permittivity
ρ	-	Radius of CWG
θ	-	Elevation angle in Degrees
ϕ	-	Azimuth angle in Degrees
σ_i	-	i^{th} Singular Value
σ^2	-	Noise variance

ω	-	Angular Frequency
60°	-	Denoting 60 Degrees
E	-	E field of EM wave or E Plane
$E(.)$	-	Mathematical Expectation
H	-	H field of EM wave or H Plane
$(.)^H$	-	Hermitian Conjugate (Transpose) of a Matrix
$(.)^T$	-	Matrix Transpose
$J_1(.)$	-	First Order Bessel Function
$J_1^{'}(.)$	-	Derivative of the First Order Bessel Function
M	-	Number of Antenna Elements in Array
N	-	Number of Samples
P	-	Number of Sources
$E_\phi(\theta,\phi)$	-	Vertical Polarized Component of Radiation Pattern
$E_\theta(\theta,\phi)$	-	Horizontal Polarized Component of Radiation Pattern
$\mathbf{a}$	-	Array Steering Vector
$\mathbf{x}$	-	Array Observation Vector
$\mathbf{x}_h$	-	Data Observation Vector from Antenna elements along H plane
$\mathbf{x}_e$	-	Data Observation Vector from Antenna elements along E plane
$\mathbf{s}$	-	Signal Vector
$\mathbf{v}$	-	Eigenvector
$\mathbf{w}$	-	Additive White Gaussian Noise Vector
$\mathbf{A}$	-	Array Steering Matrix
$\mathbf{I}$	-	Identity Matrix
$\mathbf{R}$	-	Covariance Matrix
$\mathbf{S}$	-	Signal Data Matrix
$\mathbf{R_{xx}}$	-	Covariance Matrix
$\mathbf{R_s}$	-	Signal Covariance Matrix
$\mathbf{U}$	-	Matrix with the columns of Left Singular Vectors
$\mathbf{V}$	-	Matrix with the columns of Right Singular Vectors or Eigenvectors
$\mathbf{V}_n$	-	Noise Subspace Matrix
Λ	-	Diagonal Matrix with Eigenvalues on Diagonal
Σ	-	Diagonal Matrix with Singular values on Diagonal

List of Abbreviations

1D	-	One Dimension
2D	-	Two Dimension
3D	-	Three Dimension
dB	-	Decibel
mm	-	Millimetre
cm	-	Centimetre
AMI	-	Array Manifold Interpolation
AIC	-	Akaike Information Criterion
BER	-	Bit Error Rate
Bi-SVD	-	Bi Iteration Singular Value Decomposition
BWFN	-	Beamwidth Between First Null
CCM	-	Cross Covariance Matrix
CWG	-	Circular Waveguide
CSSM	-	Coherent Signal Subspace Method
DFS	-	Direction Finding System
DOA	-	Direction of Arrival
OPAST	-	Orthonormal Projection Approximation Subspace Tracking
EM	-	Electromagnetic
ESPRIT	-	Estimation of Signal Parameters via Rotational Invariance Technique
ETOPS	-	Extended Test of Orthogonality of Projected Subspaces
EVD	-	Eigen Value Decomposition
HPBW	-	Half Power Beamwidth
ICM	-	Incoherent Method
KFVM	-	Kalman Filter with a Variable Number of Measurements
MAC	-	Multiply Accumulate
MANET	-	Mobile Ad-Hoc Network
MDL	-	Minimum Description Length
ME	-	Maximum Entropy

ML	-	Maximum Likelihood
MPAST	-	Modified Projection Approximation Subspace Tracking
MSE	-	Mean Square Error
MUSIC	-	Multiple Signal Classification
MVDR	-	Minimum Variance Distortionless Response
NS	-	Noise Subspace
OMLA	-	Orthogonal Mounted Linear Array
OPLA	-	Orthogonal Polarized Linear Array
OPPA	-	Orthogonal Polarized Planar Array
PAST	-	Projection Approximation Subspace Tracking
PM	-	Propagator Method
RF	-	Radio Frequency
RFID	-	Radio Frequency Identification
RLS	-	Recursive Least Squares
RWG	-	Rectangular Waveguide
RMSE	-	Root Mean Square Error
R-CSM	-	Robust Coherent Signal Subspace Method
SLA	-	Sparse Linear Array
SVD	-	Singular Value Decomposition
SNR	-	Signal to Noise Ratio
SURE	-	Subspace Rotation Estimation
SS	-	Signal Subspace
SS-MUSIC	-	Spatial Smoothing MUSIC
SSS-MUSIC	-	Signal Subspace Scaled Multiple Signal Classification
TOPS	-	Test of Orthogonality of Projected Subspaces
ULA	-	Uniform Linear Array
UPA	-	Uniform Planar Array
UCA	-	Uniform Circular Array
WAVES	-	Weighted Average of Signal Subspaces
W-SpSF	-	Wideband Sparse Spectrum Fitting

Chapter 1

Introduction

1.1 Introduction to DOA Estimation

Antenna array processing has been in the forefront during the last several decades catering to the research progress of radar and wireless communication engineering. Estimation of signal parameters has been a topic of considerable research interest to various disciplines coming under the purview of communication systems designed to meet the system applications of radar and wireless technologies. The Direction of Arrival (DOA) is a technique for the estimation of angular direction of the signal sources impinging on the array of sensing elements by subjecting the received data samples to the array signal processing algorithms. The localization of the impinging source (signal) on the array of sensor elements is the theme of DOA estimation technique. The DOA estimation finds many applications in various disciplines of engineering. In radar and communication engineering, sensing elements are usually antennas which are part of the base station to identify the signals as well as interference. The system which performs the DOA estimation is also widely referred to as Direction Finding System (DFS).

Array signal processing is a broad field of research interest in advanced antenna systems. Development of algorithms in array signal processing for advanced antenna techniques, is of great relevance to wireless communication as well as radar engineering. The spatial samples of the signals emitted from various sources are received by the antenna elements of the array. The received data samples depend on the characteristics of the sources, the channels, the noise, and the measurement devices. Typically, the data are processed to estimate the parameters such as number of sources, location of sources, range or distance as well as velocity of the moving sources of signals. Estimation of these parameters opens up an avenue for a large number of studies involving different system models and signal processing objectives. Over the past decades, many researchers have been fascinated by the realisable novelties and niceties offered by the domain of estimation algorithm. The

demand for the performance enhancement of estimation algorithms has drawn attention and focus of applied mathematicians and signal processing researchers. Many researchers have attempted and contributed numerous techniques to this discipline. The source localization using smart antennas is one such problem which has evolved from the classical direction finding problem in radar signal processing. Through collection of received time samples and by processing of spatial signals, detection of multiple incoming sources and estimation of their DOAs can be realised (Krim & Viberg, 1996).

The spatial samples received through the elements of antenna array are processed to estimate the DOA. The algorithms of earlier DOA estimation techniques were either Fourier based or beamforming based. Later the arrival of subspace based approaches laid foundation for the development of algorithms for DOA estimation with higher resolution. The subspace algorithms are based on Eigen Value Decomposition (EVD) and Singular Value Decomposition (SVD) techniques (Golub & Van Loan, 2012). EVD plays a crucial role in signal processing, because it can split a mixture of complex signals into a set of desired and undesired subspace components. Thus, eigen based methods have been extensively researched in adaptive signal processing. These algorithms were initially developed to find the one dimensional DOA and later extended for two dimensional DOA estimation.

1.2 Applications of DOA Estimation

The DOA estimations find utility in diversified system applications and the following are a few examples, where DOA estimation schemes are employed (Van Trees, 2004) and (J. C. Chen, Yao, & Hudson, 2002); RADAR systems installed as phased array radar and air-traffic control radar; SONAR systems deploy DOA estimation schemes to estimate the far-field sources with localization and classification. In mobile communications, smart antennas with suitable adaptive signal processing sensor array are adopted. This technique will be able to locate mobile users with the use of DOA estimation techniques. In radio astronomy, the radio telescopes are used for the detection of radio waves from an astronomical object or celestial bodies. The accuracy and resolution of DOA estimation algorithms play a significant role. Seismology which deals with scientific study of earthquakes and the propagation of elastic waves through the earth finds the utility of DOA estimation algorithms to determine the origin of the seismic waves. In wireless communication, multipath channel characteristics of radio channel can be analysed using DOA estimation

algorithms. The angle of arrival statistics and time of arrival statistics are incorporated in channel models to characterise the multipath channels more accurately (Fuhl, Rossi, & Bonek, 1997; Rappaport, Reed, & Woerner, 1996). Recently, DFS has been identified for its potential in mobile communication systems for the characterisation of channel statistics in a multipath scenario. The DOA of interfering signal can also be estimated using DFS. The DOA estimation technique has paramount importance in tracking of signal sources in civilian and commercial applications. The DOA technique is a multi specialization entity embarking on the speciality domains of antenna engineering, algorithms of array signal processing and estimation techniques of communication engineering (Chryssomallis, 2000).

Recently, the potential of directional antennas and their significance for Mobile Ad-Hoc Networks (MANETs) have been steadily explored by researchers. Typically, the MANET nodes are employed with omni-directional antennas. The communication between sending and receiving nodes of MANET is through the packets routing, in which the route (path) is established through routing algorithms. These routing algorithms identify the nodes within the range of communication, and route the data packets from source node to destination node through multiple hops in the path established (Choudhury & Vaidya, 2003). In such a case, if the directional antennas are employed in place of omni-directional antennas, a directional antenna with its enhanced range of communication in lieu of higher gain would lead to minimization of the number of hops in routing of the packets. The scenario of transmitting data packets with omni-directional antenna and directional antenna for reduced hopping in the packet transmission are shown in Figures 1.1 and 1.2. From the Friis transmission formula (Kraus, 1992) and Shannon channel capacity theorem (S. Haykin, 2008), the higher gain of directional antenna will improve the channel characteristics as well as range of communication. This will be lead to realization of higher Signal to Noise Ratio (SNR) and reduced Bit Error Rate (BER). Since, the number of hops is reduced, it minimizes the packet transmission latency, saves transmission power and battery energy of the nodes in the network (Kolar, 2004).

The potential utility of directional antennas can be realized if only the task of placing the directional beam of the antenna towards the intended communication direction is achieved. Precise placement of directional beam of the antenna warrants the associated desirable accuracy and resolution of DOA estimation algorithm. Thus the algorithms

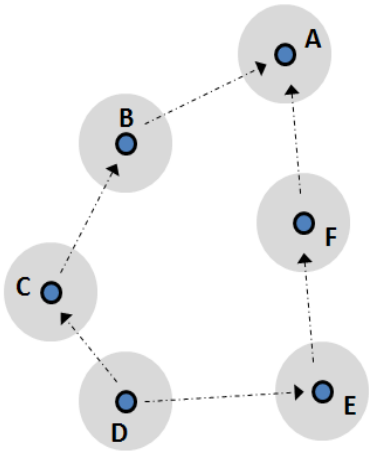

Figure 1.1: MANETs with Omni Directional Antennas

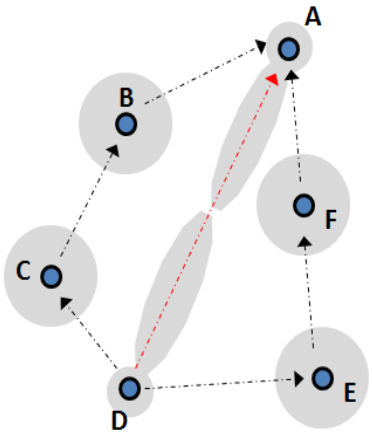

Figure 1.2: MANETs with Directional Antennas

of DOA estimation with higher accuracy and resolution have significant role to play in MANETs, satellite tracking and radar applications.

1.3 DOA Estimation Algorithms

Multiple Signal Classification (MUSIC) (Schmidt, 1986) and Estimation of Signal Parameters via Rotational Invariance (ESPRIT) (Roy & Kailath, 1989) are the classical high resolution Eigen-structure based algorithms for the estimation of DOA of the incoming sources. These algorithms are based on the assumption that the desired array signal response is orthogonal to the noise subspace. The orthogonality implies that the estimated covariance matrix is decomposed into the signal and noise subspaces (Eigenvectors) (Chandran, 2005).

The signal subspace based ESPRIT algorithm and noise subspace based MUSIC algorithm are the classical subspace based parameter estimation algorithms. In temporal signal processing, the estimation of frequency components from the mixture of complex sinusoids is carried with these algorithms. In array signal processing, these algorithms facilitate the estimation of azimuth and elevation angles of incoming signal sources through data processing of the spatial signal samples received by the antenna elements of the signal sensing array. The phase relationship between the array elements is utilized to construct an array steering vector which is a function of DOA angles. The ESPRIT algorithm has been limited only to uniform linear array configuration, since its computation is based on rotational invariance property of the subspace components. The estimation in ESPRIT algorithm, involves finding the roots of the polynomial and obtaining a least squares solution. The MUSIC algorithm can be invoked with an array of arbitrary geometric configuration and the estimation is based on the orthogonality of signal and noise subspaces. The DOA estimation is carried out through spectral peak search method. The construction of covariance matrix of the data for a fixed order, has significant role in these subspace based estimation algorithms. The covariance matrix should be decomposed to signal and noise subspaces. The computationally intensive EVD or SVD techniques are used in both of these algorithms for decomposition of signal and noise subspaces.

The ESPRIT algorithm is computationally efficient, since it does not involve a search approach, whereas the MUSIC technique is a computationally intensive approach. In case of one dimensional DOA, (say for only elevation angle θ), the search is along one dimension, and for two dimensional DOA (both the elevation angle θ and azimuth angle ϕ), two dimensional search is required. Hence the order of computation in search approach of MUSIC algorithm is increased from $O(n)$ to $O(n^2)$.
The statistical analysis of MUSIC and ESPRIT reveals that, in case of temporal signal processing for the estimation of frequency components from complex mixture of sinusoids, the ESPRIT algorithm is slightly more accurate than MUSIC algorithm. Whereas, in array signal processing, the MUSIC algorithm yields more accurate estimation than ESPRIT algorithm (Stoica & Söderström, 1991).

The MUSIC algorithm has the vast utility of being amenable to any arbitrary array configurations, despite its intensive computation. The need for reduction of computation

in the MUSIC algorithm for array signal processing based parameter (DOA) estimation problems is a single significant motivation factor to pursue research pertaining to estimation algorithms. The conventional DFS utilizes an antenna array, in which the elements are excited in single polarization. Typically, the performance of DOA estimation is studied with an assumption of isotropic radiating elements in the antenna array. In this, the gain of the antenna is assumed to be unity in all angles. The gain of the antenna element in the array is not considered in the DOA estimation, since it will be a scaling factor that is uniform across all the elements of the array. The assumption of unity gain of the antenna elements is valid in DOA estimation involving spatial signal samples obtained through single polarized antenna array with identical elements.

The scope of improving the estimation accuracy and resolution of MUSIC algorithm, is yet another direction of research which encourages to design diversely polarized antenna arrays. The antenna array with diversely polarized (vertical and horizontal polarization) antenna elements will not have uniform gain across the array and hence the unity gain assumption is not valid in such a case. Thus, the radiation pattern of individual antenna elements of the array must be considered along with their respective polarization for estimation of DOA angles of interest.
The difference in the gain of the vertical and horizontal polarized antenna elements present in the diversely polarized antenna array provides a difference in the covariance of the data received through the vertical and horizontal polarized array elements. The perfect orthogonality between the signal and noise subspaces is expected in the decomposition of the covariance matrix, which cannot occur in the practical scenario, because of the additive noise present in the signal reception. The difference in the covariance of the data through orthogonal polarized elements leads to the improved orthogonality between the signal and noise subspace components accomplished through EVD or SVD of the covariance matrix of the data samples. This improvement in the subspace decomposition directly reflects in the improved estimation accuracy and resolution of the DOA angles. The improved accuracy of DOA estimation from the diversely polarized array, warrants the analysis and design of novel array configurations named as orthogonal polarized array configurations, with its antenna elements having a combination of horizontal and vertical polarized elements in different geometric configurations. These orthogonal polarized array configurations must be evaluated for their performance in DOA estimation for wide range of SNR scenarios. The correlation property associated with the covariance matrix of the data samples obtained

through the antenna elements of the diversely (orthogonally) polarized array configurations is likely to not only improve the accuracy of the DOA estimation, but also the resolution to distinguish the closely spaced sources.
The DOA estimation by classical algorithms such as MUSIC and ESPRIT for stationary (fixed) sources is straight forward through the well established procedures. However the non-stationary sources (moving sources) pose challenges in DOA estimation. In simple terms, DOA tracking is nothing but estimation of DOA of non stationary sources and tracking the movements of the sources. The dynamic changes in the moving sources lead to fluctuations in the covariance of the data matrix as and when the (instantaneous) samples are received. Hence, the sample covariance matrix is not the correct choice for DOA estimation, whereas as a smoothing filter which does the weighted average of covariance information from the current and past samples tends to improve the accuracy of DOA estimation. The improved accuracy of 2D-DOA estimation with orthogonal polarized arrays, along with the improved covariance matrix using smoothing filter can offer a cumulative advantage in the tracking of 2D-DOA of non-stationary sources.

The term signal bandwidth is defined as the difference between the highest (significant) frequency and the lowest (significant) frequency in the signal spectrum (Lathi, 1998). In a wideband signal, the signal power spreads over wide range of frequencies. The spread of signal power in a narrow band signal is limited to a narrow range of frequencies (S. Haykin, 2008). However the term bandwidth is relative with respect to which part of the EM spectrum the signal is occupying.

Most signal sources used in wireless or mobile communication channels are not a narrow band signal. The information modulated by a carrier wave will always have a fixed bandwidth. Such signals with a defined bandwidth are termed as wideband signals. The terms wideband and broadband are sometimes interchangeably used in the broad domain of communication engineering. The scope of the study in DOA estimation can be extended to investigate the effect of orthogonal polarized array configurations for wideband source scenarios. The phase difference between the array elements for narrow band signals is fixed, whereas the corresponding phase difference of wideband signal gets cumulatively added for every discrete frequency component present in the signal.The cumulative phase along with the additive noise lead to increased complexity in the DOA estimation. Typically, wideband DOA estimation is performed by processing the discrete frequency components

of a wide band signal. For the estimation of DOA of incoming wideband sources, the classical techniques of incoherent and the coherent approaches are widely used. The incoherent approach averages the DOA estimation from the all the subspace components of the discrete frequencies. The coherent approach uses a transformation matrix to focus the signal subspace components of every discrete frequency to a desired frequency. Several methods of focussing the signal subspace components are proposed in the literature (Di Claudio & Parisi, 2001; Sellone, 2006). The potential utility of conventional subband filtering approach used in the multirate filters (Vaidyanathan, 1993) and image processing (Woods & O'Neil, 1986) can be utilised for DOA estimation of wideband sources. The improved DOA estimation using orthogonal polarized array configurations along with the subband approach can be exploited to process the wideband signal, to enhance its capability of 2D-DOA estimation. This simple subband approach does not involve any focusing of subspace and will estimate the 2D-DOA of wideband in a consistent manner. The subband filter approach is also preferred for its lower computational complexity when compared to the conventional incoherent and coherent approaches.

1.4 Motivation of the Research

DFS as a whole is a multi-disciplinary domain. The DFS involves the antenna array, Radio Frequency (RF) modules and digital signal processing modules to perform computation. In the past, significant research work has been carried in the development of DOA estimation algorithm, in an isolated way with a number of assumptions. Most of the research in DOA estimation is oriented towards the development or improvement over the existing algorithms with reduced emphasis on antenna configurations. The researchers have preferred to deal the problem in an isolated way by assuming the isotropic elemental radiation pattern, even though most commonly used elements of the antenna array are not omni antennas. The simulation of DOA estimation algorithms with actual radiation pattern of antenna element will be helpful to analyse its effects on the accuracy and resolution of DFS. The study of DOA estimation with the consideration of elemental radiation pattern in turn can affect the resolution of the estimation.

This thesis aims to focus its research on the DOA estimation emphasising techniques, algorithms and approaches to improve the performance characteristics (resolution, accuracy) of the DOA estimation. In the framework of DOA estimation, several characteristics

play vital role in the performance of DFS system. They are

- Configuration of array and its elements
- Characteristics of the received signal
- Estimation Algorithm

A need for novel approaches in the 2D-DOA estimation technique with improved estimation accuracy and resolution with lesser computational complexity is justifiable. The requirement for improved signal processing algorithm suitable to track the 2D-DOA of the non-stationary sources with least computation is also valid. A performance enhancement in the estimation of 2D-DOA for the case of wideband signal sources will also be beneficial from practical consideration. In this context, the following questions have been formed to formulate the intended research pursuance.

1. Can different configurations of orthogonally polarized array be designed for improved accuracy and resolution of 2D-DOA estimation algorithms?
2. Will the designed orthogonal polarized array configurations be able to resolve DOA of multiple sources, if their angular separation between them is smaller?
3. Can the designed orthogonally polarized array configurations be utilized for effective tracking of dynamic sources?
4. Will the proposed orthogonal polarized array configurations be effective to treat the 2D-DOA of single and multiple wideband sources
5. For the retention of orthogonally polarized elements for higher accuracy and resolution of 2D-DOA estimation, what modifications are needed at algorithmic perspectives to make them more amenable for DOA estimation?
6. Is there a feasibility to reduce the computational complexity of the MUSIC algorithm in 2D-DOA estimations?

1.5 Objectives of the Thesis

This thesis envisages to address the above listed research questions through the realization of the following formulated objectives.

1. To review the literature pertaining to the DOA estimation algorithms, approaches with respect to improve the resolution

2. To design, simulate and analyse the array of antenna elements with adjacent elements orthogonally polarized

3. To develop a DOA estimation scheme using orthogonally polarized adjacent elements

4. To enhance the performance of subspace based DOA estimation techniques using subspace tracking algorithms

5. To propose a novel approach for DOA estimation of wideband incoming signals

1.6 Organization of the Thesis

The subsequent chapters of this thesis are organized as follows.

- Chapter 2 is intended to facilitate a succinct and yet an effective review of background theory of antennas, antenna array and various DOA estimation algorithms

- Chapter 3 deals with the novel linear array configuration with its alternate elements orthogonally polarised and such an array is termed as Orthogonally Polarised Linear Array (OPLA). A closed form solution for MUSIC based 2D-DOA estimation of a single source is proposed which involves only 1D search instead of conventional 2D search. The computational advantage of the proposed 1D search scheme is substantiated through relevant case studies.

- Chapter 4 proposes novel orthogonally polarised antenna array configurations which enhance the accuracy and resolution of 2D-DOA of multiple sources compared with conventional single polarized uniform planar array. This chapter also discusses simulation results to substantiate the significant advantages of orthogonally polarised antenna array configurations to distinguish the multiple sources with relatively closer angular separation between them. This chapter also discusses a comparative RMSE performance analysis of 2D-DOA estimation realised through the proposed orthogonally polarised arrays and conventional single polarized planar array.

- Chapter 5 deals with the formulation and solution technique to analyse the tracking behaviour of 2D-DOA estimation of dynamic sources using the proposed novel

orthogonally polarised antenna array configurations. In particular, this chapter emphasises the importance of the techniques used for the formation of covariance matrix of the data samples and their influence on the accuracy of 2D-DOA estimation.

- Chapter 6 presents an analysis for 2D-DOA estimation of wideband sources based on an elegant subband filtering technique. The simulation studies presented in this chapter substantiate the consistent and steady performance of subband based 2D-DOA estimation of wideband sources at all SNR levels. This chapter also compares the accuracy and resolution of 2D-DOA estimation realized through subband approach with the conventional coherent and incoherent methods.

- Chapter 7 is aimed at the summary and significance of the analytical formulations along with the associated simulation results presented in this thesis. The suggestions for further research studies on the topics coming under the purview of this thesis are also incorporated in this chapter.

Chapter 2

Review of Antenna Arrays and DOA Estimation Algorithms

This chapter intends to review the concepts of antennas, antenna array theory and various antenna array configurations applicable for two dimensional DOA estimation. This chapter also details the fundamental concepts of array signal processing and provides a detailed review on classical algorithms for 2D-DOA estimation. The techniques and algorithms required to extend conventional DOA estimation to dynamic sources are also covered in this chapter. The analytical consideration and the algorithms in the 2D-DOA estimation to deal with wideband sources are also presented in this chapter.

2.1 Antennas

An antenna facilitates the propagation of electromagnetic waves in free space. It is an interface between free space EM waves propagation and a guided medium. An antenna plays a significant role in the performance of wireless communication systems. The antenna array has been a preferred solution for applications such as radar and communications. Rapid technological progress in wireless communication has provided an impetus for advancement of antenna engineering. The fundamental parameters and radiation behaviour of the radiating elements are significant to facilitate a better understanding of antenna arrays.

2.1.1 Radiation Pattern

The radiation pattern is a two or three-dimensional representation of radiation of an antenna. According to the IEEE ("IEEE Standard Definitions of Terms for Antennas", 1983) the radiation pattern is defined as, *A mathematical function or a graphical representation of the radiation properties of the antenna as a function of space coordinates*. This parameter highly depends upon the application of the antenna.

The radiation pattern of an antenna can be depicted or illustrated through a two dimensional representation or three dimensional representation for a given distance of

measurement. In a two dimensional representation, the illustration is restricted to a particular plane of a given three dimensional space. For example, In a Cartesian measurement system, the three dimensional representation corresponds to the three orthogonal axes x, y and z. The radiation patterns of an antenna in xz, yz and xy planes correspond to two dimensional representation. In a spherical polar coordinate system, the two dimensional radiation pattern may correspond to a plane of a fixed θ and varying ϕ or vice versa. A three dimensional radiation pattern of antenna in a spherical polar coordinate, corresponds to the radiation pattern measured / computed for θ varying from 0° to 180° and ϕ varying from 0° to 360°.

The antenna radiation is measured in terms of a parameter called gain (dB). The antenna gain is defined as, *The ratio of the intensity, in a given direction, to the radiation intensity that would be obtained if the power accepted by the antenna were radiated isotropically* ("IEEE Standard Definitions of Terms for Antennas", 1983; Balanis, 2012). A plot of radiation pattern of an antenna as a two dimensional graph is as shown in Figure 2.1. The main beam of an antenna refers to the region of strong radiation from the antenna. The maximum gain of the main lobe is termed as the peak gain of the antenna and side lobe level of antenna determines the radiation in other directions.

This item has been removed due to 3rd Party Copyright. The unabridged version of the thesis can be found in the Lancester Library, Coventry University.

Figure 2.1: Antenna Radiation Pattern (Balanis, 2012)

This item has been removed due to 3rd Party Copyright. The unabridged version of the thesis can be found in the Lancester Library, Coventry University.

Figure 2.2: Coordinate System for Antenna Analysis (Balanis, 2012)

The radiation at exactly 180° from main lobe is called as back lobe. The Half Power Beam Width (HPBW) is the width of main lobe between half power points. The Beam Width between the First Nulls (BWFN) is a parameter measured as width of the mainlobe between the first null of the left and right side of the mainlobe. The HPBW and BWFN are the performance parameters to characterize the shape of the radiation pattern of the antenna or antenna array (Balanis, 2012, 2011). A coordinate system for radiation pattern analysis of an antenna is shown in Figure 2.2.

2.1.2 Antenna Polarization

Polarization is an important radiation characteristic of the antenna. In a broad sense an antenna exhibits two polarizations typically called as vertical and horizontal polarization. The Figure 2.3 shows that, in the far-field distance from a dipole antenna, the E-field (E-wave or Electric field) oscillates. The H-field (H-wave or Magnetic field) also oscillates

perpendicular to the E-field plane. Both E and H fields oscillate together along the propagation axis. The direction of the electric field orientation of the antenna with respect to a reference plane (typically azimuth) is referred as polarization of the antenna. In Figure

This item has been removed due to 3rd Party Copyright. The unabridged version of the thesis can be found in the Lancester Library, Coventry University.

Figure 2.3: E and H Fields in Far-Field

This item has been removed due to 3rd Party Copyright. The unabridged version of the thesis can be found in the Lancester Library, Coventry University.

Figure 2.4: Veritical E-Fields Orientation of Rectangular Wave Guide - Vertical Polarization

2.4, the E-field orientation is vertical. Thus an antenna is termed as a vertically polarized antenna. If the orientation of the E-field of the antenna is horizontal as shown in Figure 2.5, then the polarization of the antenna is horizontal. The mounting position of the antenna also decides the polarization characteristics.

The radiation pattern of an antenna with linear polarization is discussed with respect to the principal plane of interest. Typically, the principal planes are E or H planes. The E-plane radiation pattern of the antenna corresponds to the radiation pattern in the plane containing the E-field of aperture distribution and the direction of the wave propagation (maximum radiation). Referring to Figure 2.4, the E-plane radiation pattern of the antenna is measured in xz plane. Likewise, the H-plane radiation pattern of the antenna corresponds

This item has been removed due to 3rd Party Copyright. The unabridged version of the thesis can be found in the Lancester Library, Coventry University.

Figure 2.5: Horizontal E-Fields Orientation of (RWG) - Horizontal Polarization

to the radiation pattern in the plane containing the H-field of aperture distribution and the direction of wave propagation (maximum radiation). Referring to Figure 2.4, the H-plane of the radiation pattern of the antenna is measured in yz plane. Mostly, antennas are oriented to one of the principal planes where the antenna maximum radiation is coincident with it (Balanis, 2012; Allen & Ghavami, 2006).

The concepts of the dual polarization characteristics and dual polarized antenna are often misunderstood and interchangeably used in practice. A single antenna radiator fed with a single feed, that exhibits both the horizontal and vertical polarized components of equal or comparable amplitude in a plane (either azimuth or elevation) is called a dual polarized antenna. Any conventional antenna radiating in single polarization (say vertical) can be physically rotated by 90° (about its propagation (z) axis) to receive the other orthogonal polarized (horizontal) component of the signal. In such a case, the antenna should not be called as dual polarized antenna.

2.1.3 Illumination of Sources

The impinging angles (θ, ϕ) of a source on the array of antenna elements are classified as broad side illumination and endfire illumination. In antenna elements such as waveguides the maximum radiation occurs along the propagation axis of the antenna elements or in a direction perpendicular to the radiating surface of the antenna.

This item has been removed due to 3rd Party Copyright. The unabridged version of the thesis can be found in the Lancester Library, Coventry University.

Figure 2.6: Broadside Illumination of Sources

This item has been removed due to 3rd Party Copyright. The unabridged version of the thesis can be found in the Lancester Library, Coventry University.

Figure 2.7: Endfire Illumination of Sources

Illumination, when the incidence is perpendicular to the antenna surface or aperture is called broadside illumination. Illumination when incidence is parallel or nearly parallel to the radiating surface or aperture of the antenna is called endfire illumination. Antenna elements whose direction of maximum radiation is along the broadside illumination angle are called broadside antenna. An analogous definition holds for endfire antenna. The illumination of a broad side source is illustrated in the Figure 2.6 and endfire sources is shown in Figure 2.7.

2.2 Antenna Arrays

Two or more antennas arranged in a geometric configuration (Topology) constitute an antenna array. The weighted sum of array antenna response gives the flexibility of electronic beam steering, combined sum and difference patterns, and formation of multiple beams. The position and the direction of the antenna elements in the array are critical in determining how the array receives a far-field signal from any angle. The spatially distributed antenna elements have one of their antenna element as reference element. The phase difference between the reference antenna element and the other antenna elements determines the response of the array antenna. Mostly, the antenna elements used in the array have identical radiation pattern. If non-identical elements are used in an array, then characterisation of an array will not be a straightforward task.

2.2.1 Array Factor

The performance or response of an antenna array, independent of its element behaviour is called as array factor. The array factor is computed as defined in Equation (2.1) (Balanis, 2012; Visser, 2006; Hansen, 2009). The Figure 2.8 denotes the parameters of array factor in a planar array.

This item has been removed due to 3rd Party Copyright.
The unabridged version of the thesis can be found in the
Lancester Library, Coventry University.

Figure 2.8: Array Factor Parameters on Planar Array(Balanis, 2012)

$$AF(\theta,\phi) = \sum_{m=1}^{M} w_m \, e^{jk(x_m \sin\theta\cos\phi + y_m \sin\theta\sin\phi + z_m\cos\theta)} \tag{2.1}$$

where M is the number of antenna elements;
x_m, y_m and z_m are the co-ordinates of the m^{th} antenna element;
$k = \frac{2\pi}{\lambda}$ is the wave number, λ being wavelength;
w_m is the complex weight denoting amplitude and phase of the m^{th} antenna element.
The phase term of the array factor is only with respect to its positional coordinate of antenna elements as well as elevation and azimuth angles (θ, ϕ).

2.2.2 Pattern Multiplication

The radiation pattern of the single (individual) radiator is called element factor. The array factor denotes the radiation pattern of the array of M isotropic radiators. The product of element factor of the array element and array factor of the array determines the radiation pattern of the array antenna. The above product is termed as the pattern multiplication of the array antenna.

$$\text{Array Radiation Pattern} = \text{Array Factor } AF(\theta, \phi) \times \text{Element Radiation Pattern } (\theta, \phi)$$

For the pattern multiplication to hold well, all antenna elements in an array have to be mounted identically to receive or transmit the same polarization. If any of the antenna elements are having different orientation, its polarization or propagation axis will change. The phase term of a particular element in the array factor at angles (θ, ϕ) has to match with the individual radiation pattern of the respective element at angles (θ, ϕ). Thus, factoring the element pattern out side the array factor is not possible for dissimilar orientation of elements. The radiation pattern of individual elements of the array has to individually multiplied inside the array factor equation.

2.2.3 Array Manifold

The vector $\mathbf{a}(\theta, \phi)$ which is a function of both the azimuth angle ϕ and elevation angle θ in an array of M antenna elements is called the array manifold vector or array steering vector for a corresponding direction of (θ, ϕ). The response of an array antenna to a signal with specified incidence angle, is determined by the array structure and characteristics of antenna. The set of these steering vectors for all possible angles of incidence is defined as antenna array manifold. The array manifold vector is measured or calculated for a specified incident angle (J.-T. Kim, Kim, & Lee, 2013). The array manifold transforms the change in angle of wave incidence into a change in measurement vector (Tuncer

& Friedlander, 2009). The change in measurement vector is correlated with (computed) phases at the antenna terminals to steer the antenna beam towards the desired beam pointing angle. The array manifold is two-dimensional information lying in an M-dimensional space. The information about the positional co-ordinates and directional characteristics of all the elements are required to calculate the array manifold. Apart from the complete characterisation of an array, the array manifold represents the real array in M-dimensional complex space as, (Chandran, 2005)

$$\mathbf{a}(\theta,\phi) = \left[e^{-jkd\beta_1(\theta,\phi)}, \quad e^{-jkd\beta_2(\theta,\phi)}, \quad \cdots, \quad e^{-jkd\beta_M(\theta,\phi)}\right]^T \tag{2.2}$$

where

$$\beta_m(\theta,\phi) = x_m \sin\theta\cos\phi + y_m \sin\theta\sin\phi + z_m\cos\theta \tag{2.3}$$

The parameter $\beta_m(\theta,\phi)$ is the phase computation with respect to the m^{th} antenna element in the array along with its position coordinates.

In the case of spatial filtering or beamforming applications, the weighted sum of amplitude and phase along with radiation pattern of the antenna element are utilized to realize the radiation pattern of the array. In source localization and DOA estimation applications, the data samples are collected from the antenna elements of an array and the array manifold vector or array steering vector is employed in the estimation schemes / algorithms.

2.2.4 Effect of Antenna Element Pattern

The antenna array form cited in the array signal processing literature (Krim & Viberg, 1996; Inoue, Mori, & Arai, 2002), generally ignores the actual radiation pattern of antenna elements. Typically, the array factor or array steering vector, in isolation of the radiation pattern is considered for array signal processing. The radiation pattern of the antenna element accounted through the pattern multiplication will not completely reveal the real scenario. The use of an isotropic radiation pattern with point source as shown in Figure 2.9 is convenient for signal processing engineers to develop pattern synthesis techniques and array signal processing algorithms. In practice, the physical dimension of the antenna is a constraint, while utilizing the modern array algorithm. In array antenna theory, the inter element spacing d is bounded within the limit as $\frac{\lambda}{4} \leq d \leq \frac{\lambda}{2}$, where λ is the wavelength (Balanis, 2012). Figure 2.10 shows a rectangular waveguide operating in the dominant TE_{10} mode with its width $a = 0.75\lambda$ and height $b = 0.33\lambda$. (Here TE_{10} refers to Transverse Electric wave with $m = 1$ and $n = 0$ mode (dominant mode) of the rectangular

This item has been removed due
to 3rd Party Copyright. The
unabridged version of the thesis
can be found in the Lancester
Library, Coventry University.

Figure 2.9: Point Source Spacing

This item has been removed due to 3rd Party Copyright.
The unabridged version of the thesis can be found in
the Lancester Library, Coventry University.

Figure 2.10: Rectangular Waveguide Element Spacing

waveguide). The minimum of inter-element spacing d shown on Figure 2.10 occurs when the two waveguides are positioned such that the side walls of them touch each other and the resulting d is 0.75λ which is higher than $\lambda/2$. Thus when the actual waveguide is considered instead of approximating it by a point source, there will be a violation of the conventional upper limit of inter-element spacing of $\lambda/2$.

2.3 Antenna Array Configurations

An antenna array is an orderly positional configuration of multiple antenna elements to obtain desired beam characteristics. The spatial arrangement of the multiple antenna elements and their combined radiation characteristics will lead to the narrow beam antenna. The beam widths (HPBW and BWFN) of the antenna array shall be controlled through the inter-element spacing, spatial arrangement and the radiation pattern of the elements.
In array signal processing, the geometric configuration of array antenna elements is very important. The modification of antenna element and array configuration can be used to improve angular resolution of the DOA estimation in both the azimuth and elevation angles. The simplest antenna array configuration Uniform Linear Array (ULA) is well studied and analysed. A ULA is capable of estimating one-dimensional (1D) DOA angle. For singly

polarized ULA configuration, the placement of array elements either along x-axis or y-axis determines the DOA angles either azimuth angle ϕ or elevation angle θ only. For example ULA with its elements oriented along x-axis will determine only the azimuth DOA angle ϕ, since the antenna elements show spatial phase variation along the x-axis only. Likewise, ULA with its elements oriented along y-axis will facilitate the estimation of elevation DOA angle θ, since the antenna elements experience spatial phase variation only along y-axis.

2.3.1 One-Dimensional Array

A configuration of antenna elements arranged along a straight line with equal spacing between the elements is called Uniform Linear Array (ULA). The simplest form of array to realize many of the array signal processing algorithms is the ULA configuration. In a ULA the antenna elements are geometrically arranged along only one axis (either x or y axis) and is also called linear arrangement (Krim & Viberg, 1996; Visser, 2006; Hansen, 2009).

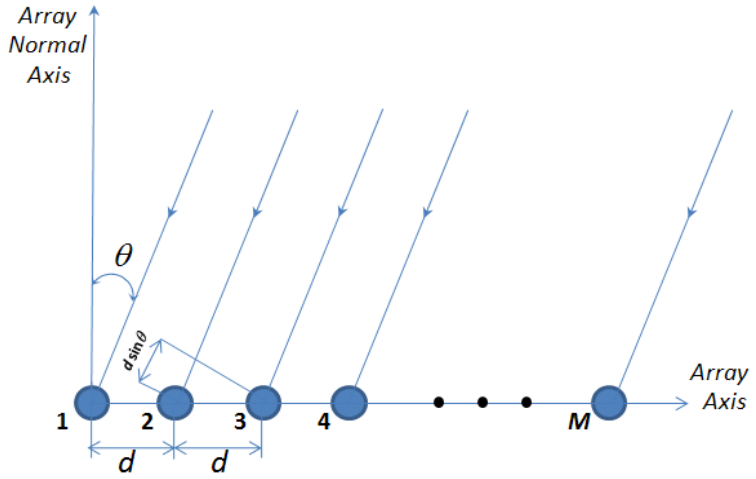

Figure 2.11: Uniform Linear Array

The Figure 2.11 shows the configuration of ULA. One of the antenna elements in the ULA is considered as a reference element. Usually it will be either the first element or the center element of the array. The signal impinging on the array will tend to have phase difference between two successive elements, due the linear arrangement and the reception of parallel wave fronts from far field. The received signal by the antenna elements will have integer multiples of phase difference.

2.3.2 Two-Dimensional Array

The two-dimensional(2D) array configuration is the primary requirement for the estimation of both the azimuth ϕ and elevation θ angles in DOA estimation. In 2D space, many array topologies are possible to configure the antenna elements. The commonly known two dimensional arrays are planar and circular arrangement of antenna elements. There are also several special two dimensional configurations such as orthogonal and L shaped configuration which are discussed in this section.

2.3.2.1 Uniform Planar Array

In the uniform planar array configuration, the antenna elements are arranged in a uniform planar grid, thereby resembling a matrix like arrangement. A typical Uniform Planar Array (UPA) is shown in Figure 2.12. In the UPA configuration, the antenna elements are

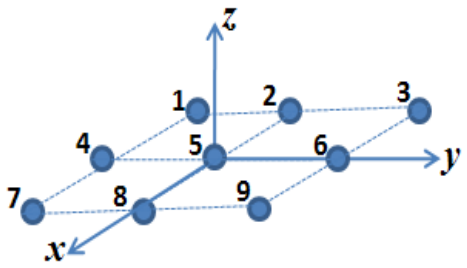

Figure 2.12: Uniform Planar Array Configuration

arranged over the planar grid formed over a plane and it is usually over the $x-y$ plane such that wave propagation direction is along the z axis only. Normally the center element of the grid topology is chosen as the reference element to compute the phase difference of the array elements. In Figure 2.12 the inter element spacing along the x axis and y axis is equal, and which in turn results in a square array. The UPA configuration can also be formed as a rectangular array with unequal number of elements oriented along the x and y axes with uniform or non uniform inter element spacing or equal number of elements with unequal inter element spacing.

2.3.2.2 Uniform Circular Array

In a 2D-array, the antenna elements can also be arranged in a circular fashion, such as along the circumference of the circle. The circular array is usually configured in the $x-y$

plane and the wave propagation will be along the z axis.

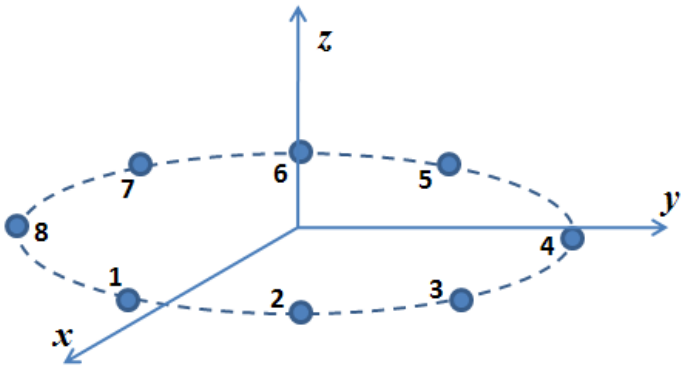

Figure 2.13: Uniform Circular Array Configuration

This array is also capable of estimating both the azimuth and elevation angles of DOA. A typical Uniform Circular Array (UCA) configuration is shown in Figure 2.13.

2.3.2.3 Cross Array

The cross array is a configuration, where the sensors or antenna elements are arranged on two linear axes orthogonal to each other as shown in Figure 2.14. In the cross array, the intersecting point of the orthogonally placed two linear axes may contain a common antenna element, which will be a reference element for the array processing (Hu et al., 2014).

This item has been removed due to 3rd Party Copyright. The unabridged version of the thesis can be found in the Lancester Library, Coventry University.

Figure 2.14: Cross Array Configuration (Hu et al., 2014)

2.3.2.4 Orthogonal Array

The cross array can be configured in an asymmetric form which is named as orthogonal array (N. A.-H. M. Tayem, 2005). The orthogonal array is shown in Figure 2.15.

This item has been removed due to 3rd Party Copyright. The unabridged version of the thesis can be found in the Lancester Library, Coventry University.

Figure 2.15: Orthogonal Array Configuration (N. A.-H. M. Tayem, 2005)

The intersection of x-axis and y-axis will be at the origin of the coordinate system, which can also be treated as a reference point. If an antenna is placed at the reference point, the data acquired from that antenna is used as reference.

2.3.3 Three Dimensional Array

The 2D array configuration can be extended to the third dimension (3D) which is the z-axis. The antenna elements are arranged in the three linear axes orthogonal to each other. This configuration is shown in the Figure 2.18. In 2D and 3D configurations, where the antenna elements are not only linearly spaced but also mutually orthogonally arranged. The array processing can be accomplished by segmenting the array into sub-arrays. Each sub-array is a linear array of antenna elements along its axis. The array steering vectors should be derived based on the geometric configuration of the antenna elements. The sub-array can be processed either independently or jointly and it depends on the algorithms used for DOA estimation.

2.3.3.1 L-Shaped Arrays

The antenna elements can be placed along x-axis, y-axis and z-axis as well as at the origin. Such an arrangement of antenna array has an L-shape structure. The L-Shape arrangement extended on the third dimension which is y-axis is as shown in the Figure 2.16.(N. A.-H. M. Tayem, 2005; Liang & Liu, 2011; Harabi, Changuel, & Gharsallah, 2007)

This item has been removed due to 3rd Party Copyright.
The unabridged version of the thesis can be found in the
Lancester Library, Coventry University.

Figure 2.16: L Shaped Array Configuration (N. A.-H. M. Tayem, 2005)

This item has been removed due to 3rd Party Copyright.
The unabridged version of the thesis can be found in the
Lancester Library, Coventry University.

Figure 2.17: One L Shaped Array Configuration (N. A.-H. M. Tayem, 2005)

Nizar Tayem (N. Tayem & Kwon, 2005) proposed a one L-shape array shown in Figure 2.17 as well as two L-shape arrays as shown in Figure 2.18 which is the array configurations

This item has been removed due to 3rd Party Copyright. The unabridged version of the thesis can be found in the Lancester Library, Coventry University.

Figure 2.18: Two L Shaped Array Configuration (N. A.-H. M. Tayem, 2005)

for two dimensional DOA estimation without any azimuth and elevation pair matching techniques. The authors claim that complete removal of the estimation pair matching between azimuth and elevation angles is possible with the proposed L-shape array and significant reduction in the RMSE of DOA estimation is also possible.

2.4 Review of DOA Estimation Algorithms

Antenna array signal processing has emerged under the broad engineering discipline of sensor array signal processing. This active area of research involves, processing of the data collected through antenna elements and fusing the data to perform the functions such as DOA estimation, digital beamforming and signal enhancement.

2.4.1 Antenna Array Signal Modelling

Array signal processing deals with the extraction of information from the simultaneous reception of data from the multiple elements of an antenna array. The estimation of parameters is carried out through fusion of temporal and spatial information obtained via

sampling of a signal. The information is obtained with appropriate positioning of antenna elements. A signal is generated or simulated through a finite number of transmitters. The simulated signal contains information to characterise parameters of the transmitters.
An array signal model is an absolute necessity for the success of any model based parameter estimation method. The signal modelling in the DOA estimation has the major dependence on the positions of antenna elements and the antenna array configuration. The common array configurations used are ULA, UPA and UCA. Usually identical antenna elements are used in the array. The non-identical elements can also be used, but the computation of the radiation pattern of an array will be cumbersome, and hence identical elements are always preferred.

2.4.2 Uniform Linear Array (ULA)

A ULA is composed of M antenna elements (sensors) placed in a straight line. The spacing between the adjacent elements is uniform. The antenna array receives P number of narrow band signals from different directions $\theta_1, \theta_2, \ldots, \theta_P$. The observed output from the array elements are the spatio-temporal samples at the time instant n, denoted as $\mathbf{x}(n)$, where $n = 1, 2, \ldots, N$; N is the total number of spatio-temporal samples or snapshots or period of observation. The observation output vector is modelled as an $M \times 1$ array (Krim & Viberg, 1996).

$$\mathbf{x} = \mathbf{A}\mathbf{s} + \mathbf{w} \tag{2.4}$$

where $\mathbf{A}$ is the array steering matrix; $\mathbf{s}$ is the signal vector and $\mathbf{w}$ is the spatially white Gaussian noise vector. The array steering matrix $\mathbf{A}$ spans the steering vector of each signal source through its column as

$$\mathbf{A} = \begin{bmatrix} \mathbf{a}(\theta_1) & \mathbf{a}(\theta_2) & \cdots & \mathbf{a}(\theta_P) \end{bmatrix} \tag{2.5}$$

The additive noise with the signal contents is assumed to have the property of ergodicity and is a spatial-temporal white stochastic process. The $\mathbf{a}(\theta)$ is the array steering vector which corresponds to the angle θ. This is also called as the array manifold vector and d is the inter element spacing chosen such that $\frac{\lambda}{4} \leq d \leq \frac{\lambda}{2}$.

$$\mathbf{a}(\theta) = \begin{bmatrix} 1, & e^{-jkd\cos\theta}, & \cdots, & e^{-jk(M-1)d\cos\theta} \end{bmatrix}^T \tag{2.6}$$

where $k = \frac{2\pi}{\lambda}$ is wave number. λ is the wavelength of the incoming signal. Keeping the first antenna as a reference element, the subsequent antenna elements in the array will

encounter an integer multiple of the phase differences with respect to the reference element. This will form a pattern called as Vandermonde structure as shown in Equation (2.6). The signal modelling of the observation output vector, received by the antenna array elements as a function of number of P incoming signals corresponding to P incoming angles is shown in Equation (2.7).

$$\begin{bmatrix} \\ \mathbf{x}(n) \\ \\ \end{bmatrix}_{M\times 1} = \begin{bmatrix} \\ \begin{bmatrix} \\ \mathbf{a}(\theta_1) \\ \\ \end{bmatrix} \begin{bmatrix} \\ \mathbf{a}(\theta_2) \\ \\ \end{bmatrix} \cdots \begin{bmatrix} \\ \mathbf{a}(\theta_P) \\ \\ \end{bmatrix} \\ \\ \end{bmatrix}_{M\times P} \times \begin{bmatrix} \\ \mathbf{s}(n) \\ \\ \end{bmatrix}_{P\times 1} + \begin{bmatrix} \\ \mathbf{w}(n) \\ \\ \end{bmatrix}_{M\times 1} \tag{2.7}$$

Equation (2.7) is written as

$$\mathbf{x}(n) = \mathbf{A}\mathbf{s}(n) + \mathbf{w}(n) \tag{2.8}$$

where $\mathbf{x}(n)$ is the observation vector at n^{th} instant;
$\mathbf{A}$ is the array response matrix with respect to the DOA of the incoming signals;
$\mathbf{s}(n)$ is the signal vector of size $P \times 1$;
$\mathbf{w}(n)$ is the zero mean white noise vector at the n^{th} instant, which is a vector of dimension $M \times 1$.
The signal received by the array is sampled at arbitrary time instants. The spatial covariance matrix has to be computed from the received spatio-temporal samples. The array covariance matrix can be written as

$$\mathbf{R} = E\left[\mathbf{x}\mathbf{x}^H\right] \tag{2.9}$$

Here, $E[\cdot]$ is the mathematical expectation operator and $(\cdot)^H$ is the hermitian conjugate. The covariance matrix $\mathbf{R}$ shall be decomposed in to signal and noise components (subspaces) as shown in Equation (2.10).

$$\mathbf{R} = \mathbf{A}\mathbf{R}_\mathbf{s}\mathbf{A}^H + \mathbf{Q} \tag{2.10}$$

The noise covariance $\mathbf{Q}$ is the diagonal matrix with σ^2 as variance. Hence the Equation (2.10) shall be written as

$$\mathbf{R} = \mathbf{A}\mathbf{R}_\mathbf{s}\mathbf{A}^H + \sigma^2\mathbf{I} \tag{2.11}$$

where $\mathbf{R}_\mathbf{s}$ is the signal covariance matrix of size $P \times P$;
$\mathbf{Q}$ is the noise covariance matrix of size $M \times M$;
$\mathbf{I}$ is the identity matrix of size $M \times M$.

The signal covariance $\mathbf{R_s}$ shall be equated to the average covariance of the signal vector as shown in Equation (2.12).

$$\mathbf{R_s} = E\left[\mathbf{s}(n)\mathbf{s}^H(n)\right] \tag{2.12}$$

The covariance matrix of the observed data samples is estimated as shown in Equation (2.13), where N is the number of data samples observed.

$$\hat{\mathbf{R}} = \frac{1}{N}\sum_{n=1}^{N}\mathbf{x}(n)\mathbf{x}^H(n) \tag{2.13}$$

2.4.3 Assumptions in the DOA Estimation Schemes

The process $\mathbf{x}(n)$ in Equation (2.13) is a multichannel random process. The first and second order statistics of signals and noise, characterise the above random process. An assumption of spatial decorrelation is associated with the impinging sources. The white noise added to the signal model is also uncorrelated with the signal sources. Coherent sources or highly correlated sources will lead to reduction in rank of the covariance matrix. Thus the source covariance matrix $\hat{\mathbf{R}}$ is often presumed to be non-singular or near-singular for highly correlated sources for the ease of computation.

In general, the distance of separation between the signal sources and antenna array is far greater than the array dimension. This facilitates to assume that parallel wave fronts are impinging on the array. The signals impinging on the antenna array are assumed to be originated from the far-field distance. Thus, the signal wave fronts arriving at the antenna array are parallel. The empirical formula for the far-field distance is $2D^2/\lambda$, where D is the maximum dimension of the antenna and λ is the wavelength.

If the received signal has spherical wave fronts, then the signal source is said to have originated from near-field region and the curvature of the wave front depends on the distance between the source and the antenna array. As the distance between the source and the antenna array becomes large, the antenna array receives the planar wave fronts (parallel rays). Hence the source is said to be in far field region with respect to the array.

For an impinging source located at a near-field of the sensing array, the localisation of the source is possible from the available information of relative time delays and the speed of propagation of source. The far-field sources which impinge on the array antennas have uniform time-delay as well as phase difference with respect to a reference antenna element. (Krim & Viberg, 1996; N. A.-H. M. Tayem, 2005). This thesis concentrates only on far-field source localization algorithms and approaches.

The multiple sources received by the antenna array are assumed to have a single carrier. Most of the algorithms cited in the literature (Krim & Viberg, 1996) deal with the signal model with narrow band signal sources.
The covariance matrix formed through the obtained data samples received by the antenna arrays elements, reflects the properties of the noise in the received signal by having common variance and de-correlation among all antennas. Such a noise is often termed as spatial white noise. For DOA estimation, the assumption of spatial white noise is common. On the contrary, other sources of man-made noise cannot be assumed to result in spatial white noise. In such a case pre-whitening of noise is a must, leading to assumption of complex white Gaussian process. The additive noise is derived from a zero mean, spatially uncorrelated random process, which is uncorrelated (independent) with the received signal sources. The noise has a common variance σ^2 at all the array elements and is uncorrelated among antenna elements. The analysis carried in this thesis neglects interference, atmospheric disturbances, static and other external noise sources.

2.5 Classification of DOA Estimation Algorithms

In general the DOA estimation algorithms can be broadly classified into two types

- Beamforming based estimation technique
- Subspace based estimation technique

2.5.1 Beamforming Based DOA Estimation Techniques

Beamforming is a technique which focuses Electromagnetic (EM) radiation in a particular direction. The antenna array essentially combines the effects of many antenna elements to form one or more beams. It is developed as a technique that could accurately direct or position a beam in free space. The formation of array and combinational effects permit the development of antennas of narrow beam-widths with high gain. The pointed or focussed beam will be used to scan the surrounding angular region. The weight and sum techniques are used to scan the angular region. In the process of scanning, the angle which maximizes the power of the received signal will be identified as the estimated DOA of the incoming signal. Bartlett's conventional beamforming or delay and sum beamformer (Bartlett, 1950) and Capon's minimum variance technique (Capon, 1969) are the classical beamforming techniques. The beamforming based techniques are formulated as spatial

filtering approaches to estimate the DOA. In these techniques, the main lobe of the antenna is used to scan the entire region of interest. The direction which maximizes the received signal power is determined as the DOA.

2.5.1.1 Bartlett's Conventional Beamformer

The conventional (Bartlett) beamformer (Bartlett, 1950) is a Fourier-based spectral analysis of spatio-temporal sampled data. This technique is also named as the delay and sum beamformer. As the name indicates *Delay and Sum*, complex weights will be applied to the received signal by the array elements and summed to obtain the output of the beamformer. The complex weights introduce the phase in the antenna elements which steers the pointing angle of antenna main lobe. This inturn suppresses the unwanted interference signal from other directions. The scan angle, which yields the maximum power of the received signal is determined as the DOA of the signal. This technique attempts to maximize the expected output power as stated in expression (2.14) by applying optimal weights to the signals received by the array elements, and thus improves the SNR of the signal (Van Veen & Buckley, 1988)

$$\max_{\mathbf{w}\, s.t\, \mathbf{w^H w}=1} E[\mathbf{w}^H \mathbf{x}(n)\mathbf{x}^H(n)\mathbf{w}]. \tag{2.14}$$

The optimal weight $\mathbf{w}_{opt}$ is computed such that, it is parallel to the $\mathbf{a}(\theta)$ as shown in Equation (2.15). Here $\mathbf{a}(\theta)$ is the steering vector for the DOA angle θ and $\mathbf{a}^H(\theta)$ is the Hermitian conjugate of the array steering vector.

$$\mathbf{w}_{opt} = \frac{\mathbf{a}(\theta)}{\sqrt{\mathbf{a}^H(\theta)\mathbf{a}(\theta)}} \tag{2.15}$$

The angular spectrum $P_B(\theta)$ for Bartlett's method is computed through the function given in Equation (2.16) for all the angles of θ (Krim & Viberg, 1996)

$$P_B(\theta) = \frac{\mathbf{a}^H(\theta)\mathbf{R}\mathbf{a}(\theta)}{\mathbf{a}^H(\theta)\mathbf{a}(\theta)} \tag{2.16}$$

The covariance matrix $\mathbf{R}$ is estimated from the samples received by the elements of antenna arrays. The DOA estimate is obtained by the highest peaks of the angular spectrum of the function of Equation (2.16). The beamformers developed invoking spatial-filtering were valid only for narrowband signals implying their characterisation only through a single frequency. This approach also suffers from fundamental limitation due to the beam width of the array elements. Its performance depends only on the physical size of the array (aperture). Further, the associated data collection time and Signal-to-Noise Ratio (SNR) have little significance (Bartlett, 1950; Coldrey & Viberg, 2006).

2.5.1.2 Capon's MVDR Algorithm

The limitation of the conventional beamformer is that, for the detection of multiple sources, the angular separation between the sources must be greater than the beamwidth of the array. This limitation is overcome by Capon's approach of Minimum Variance Distorsionless Response (MVDR). Bartlett's conventional beamformer uses every available degree of freedom to concentrate the received energy along one direction, namelythebearing angle of interest. This has been overcome by the minimization constraints of Capon's approach. Capons approach interprets minimization constraints as a sacrifice in the noise suppression capability to obtain more focused nulling in the directions other than the DOA sources present. Thus spectral leakage from closely spaced sources is reduced. The resolution capability of the Capon beamformer is dependent on the array aperture and the SNR (Krim & Viberg, 1996). The received samples have the mixed signal power of the desired DOA of the source as well as the undesired sources. This method attempts to minimize the signal of the undesired DOA sources, but keeping the gain of the desired sources fixed as a constraint. This constrained minimization results in a weight vector called as Minimum Variance Distortionless Response (MVDR). The weight vector $\mathbf{w}_c$ for the Capon's MVDR approach after the constrained optimization is given in Equation (2.17).

$$\mathbf{w}_c = \frac{\mathbf{R}\mathbf{a}(\theta)}{\mathbf{a}^H(\theta)\mathbf{R}\mathbf{a}(\theta)} \tag{2.17}$$

The angular spectrum $P_C(\theta)$ for computing DOA using Capon's method after applying the constraints is given by Equation (2.18)(Krim & Viberg, 1996).

$$P_C(\theta) = \frac{1}{\mathbf{a}^H(\theta)\mathbf{R}^{-1}\mathbf{a}(\theta)} \tag{2.18}$$

The Capon's method yields better response, compared to conventional beamformer in terms of sharpness of the peak estimation. It has higher complexity because it involves matrix inversion which is an intensive computation $O(N^3)$. It suffers when the correlated sources impinge on the array. The emergence of parameter estimation approach offers inspirations for the subsequent efforts in Maximum Entropy (ME) spectral estimation method and the initial applications of Maximum Likelihood (ML) principle (Hayes, 2009).

2.5.2 Subspace Based Estimation Techniques

The new age of high-resolution computations of DOA commenced with the subspace based estimation techniques. The class of algorithms known as subspace based techniques was

introduced in the mid 1970s and was a revolution in the field of high-end and computationally intensive estimation algorithms. The estimation is purely based on the underlying data model. This algorithm decomposes the vectors spanned by the correlation matrix into signal subspace and noise subspace. The significant aspect of these techniques is that the decomposed signal subspace and noise subspace vectors are orthogonal to each other. The orthogonality property is used for the search based estimation, polynomial rooting based estimation as well as least squares based estimation. The results of subspace based methods are much more promising in terms of accuracy and angular resolution of DOA when compared to other techniques such as Bartletts and Capon's method. The MUSIC and ESPRIT are the classical subspace based DOA estimation algorithms. The array aperture does not limit the resolution capability of subspace techniques.

The array covariance matrix $\mathbf{R}$ of the observed signal vector is given as

$$\mathbf{R} = E\left[\mathbf{x}\mathbf{x}^H\right] = \mathbf{A}\mathbf{R}_\mathbf{s}\mathbf{A}^H + \mathbf{Q} \tag{2.19}$$

where $\mathbf{x}$ is the observed signal vector from the antenna array;

$E(.)$ is the expectation operator to make sample covariance matrix as shown in Equation (2.13);

$(.)^H$ is the Hermitian transpose;

$\mathbf{A}$ is the array steering matrix as defined in Equation(2.5);

$\mathbf{R_s}$ is the signal covariance matrix;

$\mathbf{Q}$ is the noise covariance matrix. Assuming the number of sources P is known, the estimated source angles are calculated with respect to the reference element of the array as $\theta_1, \theta_2, \cdots, \theta_P$. The covariance matrix $\mathbf{R}$ is decomposed using eigen decomposition and shall be written using eigenvalues and eigenvectors as

$$\mathbf{R} = \sum_{i=1}^{M} \lambda_i \mathbf{v}_i \mathbf{v}_i^H = \mathbf{V}\Lambda\mathbf{V}^H \tag{2.20}$$

where, λ is the eigenvalue and $\mathbf{v}$ is the eigenvector. The eigenvalues are sorted in descending order such as $\lambda_1 \geq \lambda_2 \geq \cdots \geq \lambda_P$. The respective eigenvectors form the columns of the matrix $\mathbf{V}$ as shown in Equation (2.21).

$$\mathbf{V} = \begin{bmatrix} \mathbf{v}_1 & \mathbf{v}_2 & \cdots & \mathbf{v}_P & \mathbf{v}_{P+1} & \cdots & \mathbf{v}_M \end{bmatrix} \tag{2.21}$$

The eigenvalues will be arranged as diagonal elements of the matrix Λ as shown in Equation (2.22).

$$\Lambda = \begin{bmatrix} \lambda_1 & 0 & \cdots & & & \cdots & 0 \\ 0 & \lambda_2 & & & & & \vdots \\ \vdots & & \ddots & & & & \\ & & & \lambda_P & & & \\ & & & & \lambda_{P+1} & & \vdots \\ \vdots & & & & & \ddots & 0 \\ 0 & 0 & \cdots & & \cdots & 0 & \lambda_M \end{bmatrix} \tag{2.22}$$

The sum of eigenvalues λ_i, for $i > P$ is equal to the variance of the noise present in the data covariance matrix, stated in Equation (2.23).

$$\lambda_{P+1} + \lambda_{P+2} + \cdots + \lambda_M = \sigma^2 \tag{2.23}$$

The eigenvectors $\mathbf{v}_i$ for $i > P$ satisfy the condition as shown in Equation (2.24).

$$\mathbf{R}\mathbf{v}_i = \lambda_i \mathbf{v}_i = \sigma^2 \mathbf{v}_i \tag{2.24}$$

$$\mathbf{R}\mathbf{v}_i = \left(\mathbf{A}\mathbf{R}_\mathbf{s}\mathbf{A}^\mathbf{H} + \sigma^\mathbf{2}\mathbf{I}\right)\mathbf{v}_i \tag{2.25}$$

$$\left(\mathbf{A}\mathbf{R}_\mathbf{s}\mathbf{A}^\mathbf{H}\right)\mathbf{v}_i = 0 \tag{2.26}$$

By the full rank property, $\mathbf{A}$ and $\mathbf{R_s}$ in Equation (2.26) will be

$$\mathbf{v}_i^H \mathbf{A} = 0 \tag{2.27}$$

where $i > P$

$$\mathbf{G} = \mathbf{SS} + \mathbf{NS} \tag{2.28}$$

SS is the signal subspace and **NS** is the noise subspace which are described in Equations (2.29) and (2.30) and **G** is the sum of signal and noise subspace.

$$\mathbf{SS} = span\left[\mathbf{a}(\theta_1), \quad \mathbf{a}(\theta_2), \quad \cdots, \quad \mathbf{a}(\theta_P)\right] \tag{2.29}$$

$$\mathbf{NS} = span\left[\mathbf{v}_{P+1}, \quad \mathbf{v}_{P+2}, \quad \cdots, \quad \mathbf{v}_M\right]. \tag{2.30}$$

The mathematical steps or procedures describing in this section for the computation of covariance matrix and the decomposition of signal and noise subspace are applicable to both Pisarenko and MUSIC algorithms. Therefore the steps will not be repeated in the subsequent subsections.

2.5.2.1 Pisarenko Harmonic Decomposition

The Pisarenko method (Pisarenko, 1973) of parameter estimation was originally developed for the spectral estimation problems. This method acted as a base for the revolutionary emergence of the subspace based algorithms. This method assumes that a signal is composed of a finite number of complex exponentials in the presence of white noise. A priori knowledge of the number of complex exponential P present in the signal, is used to form the covariance matrix of size $(P+1)\times(P+1)$. The number of complex exponentials also refers to number of sources. The number of array elements M used in the case of Pisarenko method is one more than the number of sources, $M = P+1$. The covariance matrix of size $M \times M$ is decomposed into signal and noise subspace matrices. The signal subspace and the noise subspace are orthogonal to each other. The dimension of the noise subspace is always one and it is spanned by the eigenvectors corresponding to the least eigenvalue (Pisarenko, 1973; Hayes, 2009).

$$\widehat{P}_{PHD}(\theta) = \frac{1}{|\mathbf{v}_{min}^{H}\mathbf{a}(\theta)|^2} \tag{2.31}$$

The angular spectrum $\widehat{P}_{PHD}(\theta)$ estimation using Pisarenko harmonic decomposition is stated in Equation (2.31), in which $\mathbf{v}_{min}$ is the eigenvector corresponding to minimum eigenvalue, and $\mathbf{a}(\theta)$ is the array steering vector.

2.5.2.2 MUSIC Algorithm

The MUSIC Algorithm (Schmidt, 1986) is a classical high resolution subspace based algorithm to estimate the DOA of the signal sources. This algorithm is based on the property that the desired array signal response is orthogonal to the noise subspace. The orthogonality implies that the estimated autocorrelation matrix is decomposed (de-correlated) into the signal and noise subspaces (eigenvectors). The block diagram describing the computation flow of the MUSIC algorithm is shown in Figure 2.19. In a correlated environment some of the signal eigenvectors may diverge into noise eigenvectors, which in turn tends to degrade

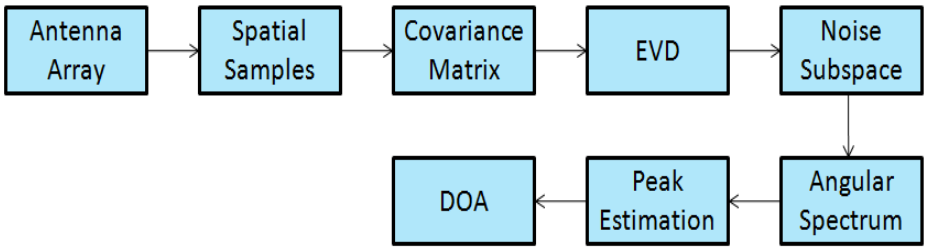

Figure 2.19: Block Diagram for DOA Using the MUSIC Algorithm

the performance of the algorithms severely.

$$P_{MUSIC}(\theta) = \frac{1}{\sum_{i=K+1}^{M} |\mathbf{v}_i^H \mathbf{a}(\theta)|^2} \tag{2.32}$$

The angular spectrum $P_{MUSIC}(\theta)$ of MUSIC algorithm can be estimated through Equation (2.32). In Equation (2.32), $\mathbf{v}_i$ is the i^{th} eigen vector after sorting in descending order and $\mathbf{a}(\theta)$ is the array steering vector.

2.5.2.3 Root MUSIC Algorithm

The root MUSIC is a polynomial rooting based technique is applicable for the linear array. In this approach, an M^{th} order polynomial is construct from the subspace components of the data. The roots of the constructed polynomial is obtained by the solving the polynomial. The obtained roots are plotted on a unit circle. The number of roots, that lie on the unit circle or very close to the unit circle denotes the signal components. The other roots lying inside and outside the unit circle represents noises.

2.5.2.4 ESPRIT Algorithm

The ESPRIT (Roy & Kailath, 1989) algorithm is a signal subspace based DOA estimation algorithm which reduces the computation and storage. In this algorithm, a set of uniform linear array elements is grouped to form a subarray such that many subarrays are formed and each subarray is called a doublet. The covariance matrix formed with the data received by the elements of the array is split accordingly with respect to the doublet and emphasizes the shift invariance in that, each doublet elements will have identical radiation (sensitivity) pattern. The translational separation of doublets is through a known constant displacement vector. The covariance matrix which corresponds to the doublets is related by a similarity transformation. The data sample received in the subarrays encounters only a linear translation of phase and hence the subarrays will have the same eigenvalues. The eigenvectors

which correspond to the covariance matrices of doublet are related by translation operator which can be solved in the least squares sense. Typically, two types of subarray namely non-overlapping and overlapping subarrays are used as shown in Figures 2.20 and 2.21.

Consider a ULA of M elements composed of two non-overlapping subarrays. The

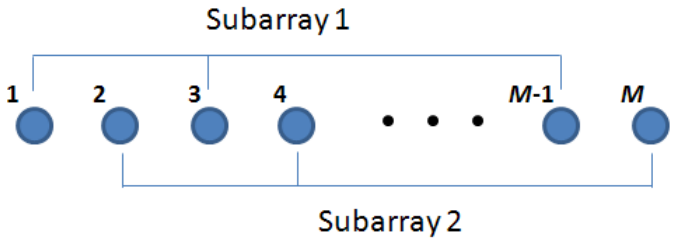

Figure 2.20: Non-Overlapping Subarrays

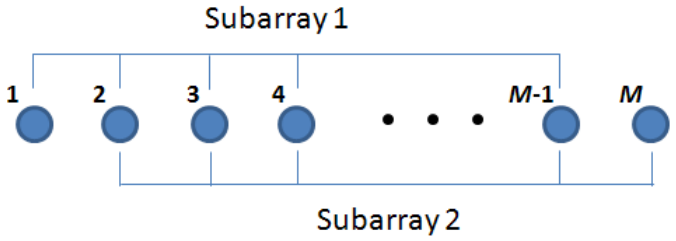

Figure 2.21: Overlapping Subarrays

samples received by the **y** and **z** subarrays of the i^{th} doublets group can be written as

$$\mathbf{y}_i(t) = \sum_{p=1}^{P} \mathbf{a}_i(\theta_p)\mathbf{s}_p(t) + \mathbf{n}_{\mathbf{y}i}(t) \tag{2.33}$$

$$\mathbf{z}_i(t) = \sum_{p=1}^{P} \mathbf{a}_i(\theta_p)e^{-j\frac{2\pi}{\lambda}d\cos\theta_p}\mathbf{s}_p(t) + \mathbf{n}_{\mathbf{z}i}(t) \tag{2.34}$$

where, $\mathbf{a}_i(\theta_p)$ is the array steering vector at angle θ_p for the i^{th} doublet;
$\mathbf{s}_p(t)$ is the p^{th} signal source; t is the time instant;
θ_p is the incoming angle of the p^{th} signal source;
d is the inter element spacing;
λ is the wavelength;
$\mathbf{n}_{\mathbf{y}i}(t)$ and $\mathbf{n}_{\mathbf{z}i}(t)$ are the additive white Gaussian noise vectors at the instant t for the

subarrays **y** and **z** respectively.
The matrix notation of Equations (2.33) and (2.34), can be represented as,

$$\mathbf{Y}(t) = \mathbf{A}(\theta)\mathbf{S}(t) + \mathbf{N_Y} \tag{2.35}$$

$$\mathbf{Z}(t) = \mathbf{A}(\theta)\Phi\mathbf{S}(t) + \mathbf{N_Z} \tag{2.36}$$

where $\mathbf{N_Y}$ and $\mathbf{N_Z}$ are the noise covariance matrices due to independent white noise vectors, whose components are zero mean and variance σ^2. The information required for DOA estimation of the impinging sources is contained in diagonal matrix Φ of dimension $P \times P$ as described in Equation (2.37).

$$\Phi = diag\left[e^{-j\frac{2\pi}{\lambda}d\cos\theta_1} \quad \ldots \quad e^{-j\frac{2\pi}{\lambda}d\cos\theta_P}\right] \tag{2.37}$$

Thus by computing the diagonal matrix Φ, the DOA can be estimated, and the procedure to estimate the matrix Φ is as follows. The sampled outputs of the subarrays $\mathbf{Y}$ and $\mathbf{Z}$ at the instant t are shown in the vector form in Equation (2.38).

$$\mathbf{R} = \begin{bmatrix}\mathbf{Y}(t)\\ \mathbf{Z}(t)\end{bmatrix} = \begin{bmatrix}\mathbf{A}\\ \mathbf{A}\Phi\end{bmatrix}\mathbf{S}(t) + \begin{bmatrix}N_y\\ N_z\end{bmatrix} \tag{2.38}$$

The covariance matrix $\mathbf{R_{YZ}}$ can be written as

$$\mathbf{R_{YZ}} = \mathbf{A}\mathbf{R_S}\mathbf{A}^H + \sigma^2\mathbf{I} \tag{2.39}$$

Using eigen decomposition the covariance matrix $\mathbf{R_{YZ}}$ is written as

$$\mathbf{R_{YZ}} = \mathbf{E}_s\Lambda_s\mathbf{E}_s^H + \mathbf{E}_n\Lambda_n\mathbf{E}_n^H \tag{2.40}$$

where Λ_s and $\mathbf{E}_s$ are the eigenvalues and eigenvectors corresponding to the signal subspace; Λ_n and $\mathbf{E}_n$ are the eigenvalues and eigenvectors of the noise subspace. The sources are uncorrelated, and hence the rank of the covariance matrix is P. The steering vector and eigen vector of the signal subspace can be written as

$$span\{\mathbf{A}\} = span\{\mathbf{E}_s\} \tag{2.41}$$

Since $span\{\mathbf{A}\} = span\{\mathbf{E}_s\}$, existence of a unique non-singular matrix $\mathbf{T}$ is realized, such that

$$\mathbf{E}_s = \mathbf{AT} \tag{2.42}$$

The signal subspace $\mathbf{E}_s$ shall be partitioned according to the samples of subarrays $\mathbf{Y}$ and $\mathbf{Z}$ formulated in the vector form shown in Equation (2.43).

$$\mathbf{E}_s = \begin{bmatrix} \mathbf{E_Y} \\ \mathbf{E_Z} \end{bmatrix} = \begin{bmatrix} \mathbf{AT} \\ \mathbf{A\Phi T} \end{bmatrix} \tag{2.43}$$

The signal subspaces $\mathbf{E_Y}$ and $\mathbf{E_Z}$ can also be stacked column wise as shown Equation (2.44).

$$\mathbf{E}_{s\mathbf{YZ}} = \begin{bmatrix} \mathbf{E_Y} & \mathbf{E_Z} \end{bmatrix} \tag{2.44}$$

Since the rank of $\mathbf{E}_{s\mathbf{YZ}}$ is also P, it implies the existence of matrix $\mathbf{F} \subset \mathbb{C}^{2P \times P}$ with rank P such that,

$$0 = \begin{bmatrix} \mathbf{E_Y} & \mathbf{E_Z} \end{bmatrix} \mathbf{F} = \mathbf{E_Y F_Y} + \mathbf{E_Z F_Z} \tag{2.45}$$

$$\mathbf{ATF_Y} + \mathbf{A\Phi TF_Z} = 0 \tag{2.46}$$

Here, $\mathbf{F}$ spans the null space of $\mathbf{E}_{s\mathbf{YZ}}$. A matrix Ψ of size $P \times P$ is defined as

$$\Psi = -\mathbf{F_Y F_Z^{-1}} \tag{2.47}$$

Equation (2.45) can be written as

$$\mathbf{AT\Psi T^{-1}} = \mathbf{A\Phi} \tag{2.48}$$

The implication of matrix $\mathbf{A}$ having full rank property, yields

$$\mathbf{T\Psi T^{-1}} = \Phi \tag{2.49}$$

Equation (2.49) can be rearranged to compute matrix Ψ as

$$\Psi = \mathbf{T^{-1}\Phi T} \tag{2.50}$$

The eigenvalues of Ψ are equal to the diagonal elements of Φ. The matrix $\mathbf{T}$ spans its column space with the eigenvectors of Ψ. This property leads to the development of ESPRIT algorithm.

The ESPRIT algorithm is also known as SUbspace Rotation Estimation (SURE). The accuracy of the MUSIC and ESPRIT techniques increases as M increases. In case of temporal data processing for frequency estimation, M refers to the temporal window size. In array signal processing, M denotes the number of sensors or antennas. However in

practical application, M cannot be very large. Both MUSIC and ESPRIT algorithms utilize eigen decomposition and the parameter M has the computational complexity of $O(M^3)$. M is fixed such that $M \ll N$. It is cited in (Stoica & Soderstrom, 1991), that the ESPRIT algorithm is preferred for its higher accuracy when compared to MUSIC algorithm for the case of temporal data processing. In case of the array signal processing, MUSIC algorithm is preferred over ESPRIT, due to processing of higher number samples. Generally, the ESPRIT algorithm is not required to search for all steering vectors as in the MUSIC algorithm. Hence its computational efficiency is more compared to the MUSIC algorithm. However, the ESPRIT algorithm is limited to operate with ULA geometries due to its rotational invariance property whereas, the MUSIC algorithm can be used with any arbitrary array configurations.

2.5.2.5 Other Methods

The de-correlation of the signal and noise eigenvectors has a critical role in the achievable resolution of the DOA estimators. Many attempts have been made in the past to improve the de-correlation between the signal and noise subspaces. Spatial Smoothing MUSIC (SS-MUSIC) and Signal Subspace-Scaled MUSIC (SSS-MUSIC) are some of the methods already available for improving the resolution. The above subspace based techniques are primarily signal processing based approach for improving the de-correlation (Shan, Wax, & Kailath, 1985; S.-W. Chen, Jen, & Chang, 2009).

The Matrix Pencil (MP) method utilizes the spatial samples received by the antenna array. In this method, individual snapshot (sample) based analysis is carried out to take care of non-stationary environments to facilitate ease of handling. The MP method does not require spatial smoothing for the DOA estimation in a multipath coherent environment. The reduction in computational complexity of covariance matrix is accomplished by the conversion of complex matrix to real matrix and its eigenvectors by a unitary transformation matrix. The transform matrix maps centro-Hermitian matrices to real matrices (Yilmazer, Koh, & Sarkar, 2006).

The subspace based Propagator Method (PM) is devoid of EVD or SVD of the Cross-Spectral Matrix (CSM) of the received signals. This method was perceived as a possible alternative to the MUSIC algorithm. The computational load is significantly smaller than the classical subspace based MUSIC and ESPRIT algorithms. The steering vectors of the array enable the extraction of the propagator (a linear operator) from the received data

(Marcos, Marsal, & Benidir, 1995).

2.6 Antenna Elements and Array Configuration for DOA Estimation

The several decades of research in array signal processing has been oriented towards the improvement of the estimation techniques and algorithms. However the emphasis of research towards the antenna array element and array configuration is rather limited. The geometry of the sensor array configuration has significant effects on the performance of DOA estimation algorithms. Research papers orient the estimation techniques with respect to the classical ULA, UCA and UPA configurations, because of their simplicity in implementation and straight forwardness. Some special configurations such cross array, L-type array have also been addressed for the two dimensional DOA estimation.

Most of the cited techniques and algorithms for DOA estimation (Krim & Viberg, 1996) assume the isotropic elements with omni-directional radiation pattern as element pattern for the antenna array element. Under the realistic scenario, this assumption is not valid. The antenna element designed for RF and Microwave frequencies are not omni-directional in practice. The assumption of identical antenna elemental characteristics is considered as fair one. The radiation pattern of the antenna elements of the array has significant impact on the DOA performance of estimation approaches.

The mutual coupling effect of the antenna elements in the array has interfering effects in the received signal, which may tend to degrade the performance of the estimation techniques. Formulation or analysis of approach to minimize the mutual coupling effect, which indirectly improves the DOA estimation has not been widely addressed in the literature. Initially, the large number of antenna elements in an array was used to produce the narrow pencil beam to detect and estimate the DOA of sources. The beamforming based methods are utilized in these approaches. After the arrival of subspace based techniques, lesser number of antenna elements are utilized to take advantage of the DOA estimation algorithm with higher resolution. Recently, research towards smaller antenna array to achieve high resolution DOA estimation has emerged.

The consequence of reduction in number of antenna elements will eventually will lead to lesser number of samples to be processed for DOA estimation. Therefore subspace based technique is getting prominence for high resolution DOA estimation.

It has been identified that, the polarization of the antenna is a factor to improve the DOA estimation schemes. In this regard, diversely polarized antenna elements have the potential

to improve the DOA estimation schemes. A mutually orthogonal arrangement of dipoles

This item has been removed due to 3rd Party Copyright. The unabridged version of the thesis can be found in the Lancester Library, Coventry University.

Figure 2.22: Mutually Orthogonal Arrangement of Dipoles (Chick et al., 2011)

and biconical antennas are proposed for DFS (Chick et al., 2011). In this paper, three biconical antennas with same angular cone are co-located. Thus the incident wave front rely only on the polarization of antenna. This mutually orthogonal arrangement cannot detect the phase delay between the antenna elements, since it is co-located. The mutually

This item has been removed due to 3rd Party Copyright. The unabridged version of the thesis can be found in the Lancester Library, Coventry University.

Figure 2.23: Mutually Orthogonal Arrangement of Antennas (Chick et al., 2011)

orthogonal arrangement of biconical antennas is shown in Figure 2.23. The computation of the vector which is perpendicular to the locus of the instantaneous electric field vector is utilized in this array configuration. The typical ML and MUSIC algorithms are used for DOA estimation.

A 3-axis orthogonal array antenna is proposed by Kim et al. (M. Kim et al., 2004) to determine the direction of the RFID tag. Three loop antennas of the same geometry and characteristics are arranged in 3-axis to form orthogonal array antenna as shown in Figure 2.24. The comparison of measured signal strength in each axis of the antenna yields the

direction information. Also the distance is estimated by phase shift obtained in each of the antenna.

This item has been removed due to 3rd Party Copyright. The unabridged version of the thesis can be found in the Lancester Library, Coventry University.

Figure 2.24: 3 Axis Orthogonal Antenna (M. Kim et al., 2004)

A patch antenna array with polarization discrimination is proposed by Yoshimura et al. in (Yoshimura et al., 2011). A 12 element antenna array with linear polarization discrimination circuit made up of diodes is proposed as shown in Figure 2.25.

This item has been removed due to 3rd Party Copyright. The unabridged version of the thesis can be found in the Lancester Library, Coventry University.

Figure 2.25: 12-Element Array Antenna for Orthogonal Polarization Discrimination (Yoshimura et al., 2011)

The received signals by the array 1 and array 2 are multiplied at the discriminating circuit and the multiplier output voltage corresponding to the polarization angle is obtained. Consequently, the received polarization angle is discriminated by the polarity of the output voltage of the multiplier. The direction of the fields is shown in Figure 2.26.

This item has been removed due to 3rd Party Copyright. The unabridged version of the thesis can be found in the Lancester Library, Coventry University.

Figure 2.26: Antenna Array Behaviour with Schematic Current Distributions (Yoshimura et al., 2011)

This antenna array can be utilized for dual linear polarization discrimination with very good cross polarization suppression. Simultaneous reception of both the horizontal and vertical polarized components cannot be achieved with this configuration. Wei and Guo (Wei & Guo, 2014) proposed a signal covariance technique with pair matching for 2D DOA estimation using the L-shaped array configuration of Figure 2.16. In this technique, two signal covariance matrices for each of the subarray are formed and a permutation matrix is formed for optimal matching of DOAs estimated through 1D subarrays. A technique for estimation of DOA using the Cross Covariance Matrix (CCM) realized through two arrays namely ULA and Sparse Linear Array (SLA) has been proposed by Gu et al. (Gu, Zhu, & Swamy, 2015).

2.7 DOA Tracking of Non Stationary Signal Sources

The classical high resolution DOA estimation techniques like MUSIC and ESPRIT addressed in (Schmidt, 1986; Roy & Kailath, 1989) are based on the eigen decomposition. These algorithms are associated with higher computational complexity because of the numerical techniques involved in the computation of eigenvectors for the sample covariance matrix. The major computation of algorithms is devoted to the decomposition of subspace itself. The subspace based robust DOA estimation algorithm without the direct

EVD computation is not adequately addressed in the published literature.
For the case of non-stationary sources, tracking DOA is essential for certain applications such as mobile communications. The computational complexity is increased by N folds, N refers to number of spatio temporal samples of the wave incident on the array. Due to time and space variation of the impinging signal characteristics, it is essential to estimate DOA for every sampling instant for higher accuracy. However, a single snapshot of the received sample, associated with noise cannot reveal the exact parameter of interest in the computation. It is preferred to utilize the past received samples of the impinging signal sources despite time and space variations present in it. The moving average and weighted average over the past received samples, tend to estimate the DOA more accurately when compared to the estimation through the instant samples alone. Processing of every new sample received along with the past sample increases computational complexity and time. As stated earlier, computing EVD or SVD alone occupies a significant computation load in the algorithm.

2.7.1 Singular Value Decomposition (SVD)

SVD decomposes the covariance matrix into left-hand and right-hand matrices. A descriptive diagonal matrix consisting of singular values, separates the two matrices. The SVD technique is utilized for the case of singular matrices or numerically very close to singular. Given a matrix $\mathbf{A}$ of order $M \times N$, where $M > N$, can be decomposed as shown in Equation (2.51).

$$\mathbf{A} = \mathbf{U}\Sigma\mathbf{V}^{\mathbf{T}} \tag{2.51}$$

$$\begin{bmatrix} \\ \mathbf{A} \\ \\ \end{bmatrix}_{M\times N} = \begin{bmatrix} \\ \mathbf{U} \\ \\ \end{bmatrix}_{M\times N} \begin{bmatrix} \sigma_1 & & \\ & \ddots & \\ & & \sigma_M \end{bmatrix}_{M\times N} \begin{bmatrix} \\ \mathbf{V} \\ \\ \end{bmatrix}^{T}_{M\times N} \tag{2.52}$$

The decomposition of matrix $\mathbf{A}$ is a product of $M \times N$ column orthogonal matrix $\mathbf{U}$, an $N \times N$ diagonal matrix Σ with positive or zero elements and the transpose of an $N \times N$ orthogonal matrix $\mathbf{V}$. The diagonal elements of matrix Σ are also called singular values. Also matrices $\mathbf{U}$ and $\mathbf{V}$ have their column span the left and right singular vectors of the matrix $\mathbf{A}$. The left and right singular vectors have similar properties of the eigen vectors. Mostly these singular vectors and eigenvectors are interchangeably used in the subspace algorithm. The computation of eigenvectors or singular vectors through the

classical approach like Jacobi or Power iteration methods involve higher computational complexities. The computation time is directly proportional to the order of the matrix under decomposition. The adaptive systems, uses this SVD technique for the reduction of computation resources (Vershinin, 2014).

2.7.2 Subspace Tracking Algorithms

The subspace tracking algorithms are more efficient than conventional SVD techniques to update the subspace components of the vector sequence. Initially, Karasalo proposed a method of signal subspace averaging in a least squares sense (Karasalo, 1986). Later the subspace tracking progressed from the exploitation of classical eigen structure techniques such as QR algorithm, Jacobi rotation, power iteration, and Lanczos method (Comon & Golub, 1990). The subspace tracking algorithms like BiSVD (Strobach, 1997), BiLS (Ouyang & Hua, 2005) are used for sequential updating of the subspace components.
The Projection Approximation Subspace Tracking (PAST) (B. Yang, 1995) attempts for solution to an exponentially weighted least square of the data matrix using unconstrained minimization. Based on well known Recursive Least Square (RLS) method, the signal subspace components are tracked efficiently. The obtained signal subspaces are not exactly orthonormal, which is a limitation of the PAST algorithm. Later the PAST algorithm is improved with orthonormal subspace components developed as Orthonormal PAST (OPAST) algorithm by (Abed-Meraim, Chkeif, & Hua, 2000). Estimation and tracking of DOA taking into account the mutual coupling between the elements of ULA has been proposed by Liao et al. (Liao, Zhang, & Chan, 2012). Liao et al. propose the joint estimation of DOAs and mutual coupling matrix by invoking the subspace tracking techniques such as Modified PAST (MPAST) and OPAST for slow varying subspace components. For the case of rapid changing subspace components, they propose Kalman Filter with variable number of measurements (KFVM). In the analysis of Liao et al., for higher number of samples, the term subspace leakage refers to the deviation of the sample covariance matrix from the true covariance matrix. The solution to the problem of subspace leakage has been addressed in (Shaghaghi & Vorobyov, 2015) through a root-swap method in the root MUSIC algorithm.

2.8 DOA Estimation of Wideband Signals

The signal with its energy spread over a broad range of frequencies is in general termed as wide-band or broad band signal. Initial attempts in the DOA estimation algorithms were directed only towards the narrowband signal sources, but many applications such as wireless communications warrant the localization of the wideband signal sources. The DOA estimation of wide-band signal sources has been attempted by many researchers in the past.

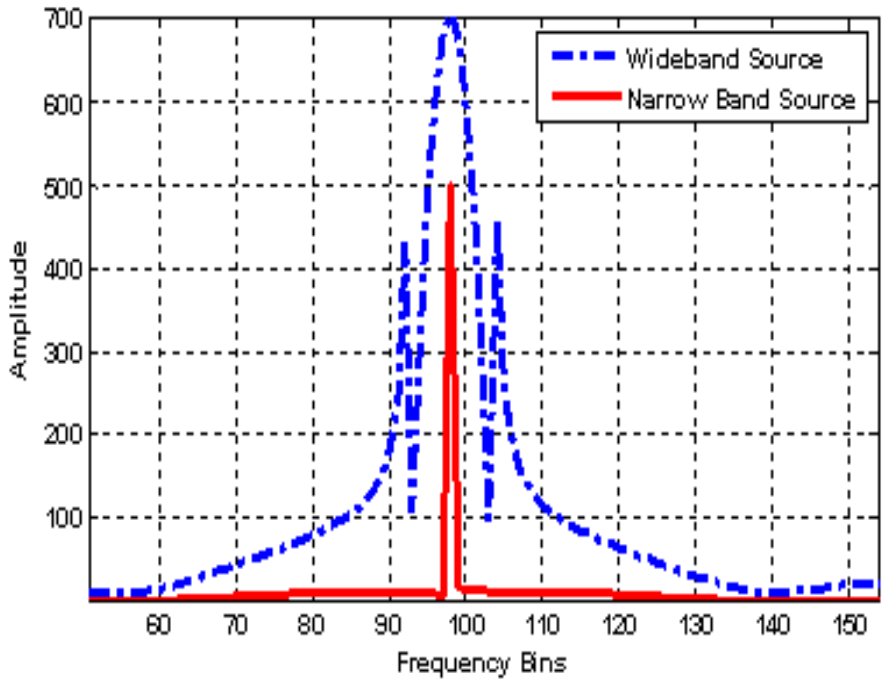

Figure 2.27: Narrowband and Wideband Signal Sources

Many concepts of DOA estimation in the narrow band case can be extended to the wideband situation. The design of a wideband beamformer involves a subband decomposition and subsequent design of beamformer for subband (narrow band) frequencies. This implies an application of spatio temporal filter to the samples received by the array. Hence such an array is often termed as filter and sum structure. Therefore the determination of the coefficients of the spatio-temporal filters constitutes the main task of the wideband beamformer. The narrow band and wideband sources are generated and its discrete frequency spectrum is shown the Figure 2.27. In a typical scenario, the narrow band signal appears as a spike at the corresponding frequency, where as the wideband signal spreads over the band

across the center frequency. The wideband source causes the spread of center frequency and adjacent frequency bins.

2.8.1 Approximation of Narrow Band Signal

A clear understanding of the approximations in the underlying concept of narrowband signal can provide an impetus for the development of wideband signal model. The complex representation of the p^{th} narrow band source signal over N observation time shall be represented by the Equation (2.53) (Stoica & Moses, 1997).

$$x(t) = w_p(t)\, e^{j\omega_o t} e^{jv_p(t)} \tag{2.53}$$

Here ω_o is the center frequency; and $p = 1,2,...,P$ where P denotes the number of sources and the sample index $t = 1,2,\ldots,N$. The amplitude and phase of the narrowband source are given by $w_p(t)$ and $v_p(t)$ respectively. The amplitude and phase of the narrowband signal are slowly varying function with respect to ω_o. The sequence $x(t)$ represents the p^{th} source signal waveform observed with respect to reference point in the array. The cumulative sum of all the P sources observed at time t is represented as

$$y_m(t) = \sum_{p=1}^{P} x_p(t - \Psi_{pm}) + u_m(t) \qquad \text{where} \quad t = 1,2,\ldots,N \quad \text{and} \quad m = 1,2,\ldots,M \tag{2.54}$$

where Ψ_{pm} is the propagation delay of the p^{th} source at the m^{th} antenna element from the reference antenna element of the array. In Equation (2.54), M denotes the number of antennas of the array and N is the number of samples.

$$\Psi_{pm} = (m-1)\pi \sin\theta_p \tag{2.55}$$

where θ_p is the direction of arrival of p^{th} signal source. The $u_m(t)$ is the additive white Gaussian noise at the m^{th} sensor. From the narrow band assumption, the variations of amplitude and phase are insignificant during the arrival time across the array. Now

$$x_p(t - \Psi_{pm}) = w_p(t - \Psi_{pm}) e^{j\omega_o(t-\Psi_{pm})} e^{jv_p\left(t-\Psi_{pm}\right)} \tag{2.56}$$

$$x_p(t - \Psi_{pm}) = w_p(t - \Psi_{pm}) e^{j\omega_o t} e^{-j\omega_o \Psi_{pm}} e^{jv_p\left(t-\Psi_{pm}\right)} \tag{2.57}$$

By narrowband approximation

$$w_p(t - \Psi_{pm}) \cong w_p(t) \tag{2.58}$$

and

$$v_p(t-\Psi_{pm}) \cong v_p(t) \tag{2.59}$$

$$x_p(t-\Psi_{pm}) \cong x_p(t)e^{j\omega_o\Psi_{pm}} \tag{2.60}$$

This implies that the time delay is transformed into only a phase delay. The center frequency, the inter element spacing and DOA determine this phase delay. However, it is independent of the time variable.

2.8.2 Wideband Signal Model for Linear Array

For the case where P number of far-field point sources are observed by M sensors arranged in a linear array geometry with additive white Gaussian noise, the spectral output of the array of the wideband sources for (narrowband) frequency f and time sample t is given by the Equations (2.61) and (2.62).

$$\mathbf{x}(f,t) = \mathbf{A}(f,\theta)\mathbf{s}(f,t) + \mathbf{n}(t) \tag{2.61}$$

$$= \sum_{p=1}^{P} \mathbf{a}(f,\theta_p)\mathbf{s}_p(f,t) + \mathbf{n}(f,t) \tag{2.62}$$

where the signal source is a vector $\mathbf{s}(f,t)$ represented as $\left[\mathbf{s}_1(f,t), \quad \mathbf{s}_2(f,t), \quad \ldots \quad ,\mathbf{s}_P(f,t)\right]^T$. The DOA (bearing) angle vector of the P sources is denoted as vector $\theta = \left[\theta_1, \quad \theta_2, \quad \ldots \quad ,\theta_P\right]$. The array manifold matrix of size $M \times P$ shall be defined as $\mathbf{A}(f,\theta) = \left[\mathbf{a}(f,\theta_1), \quad \mathbf{a}(f,\theta_2), \quad \ldots \quad ,\mathbf{a}(f,\theta_P)\right]$ with $\mathbf{a}(f,\theta_p)$ the array steering vector for the p^{th} source at frequency f and $\mathbf{n}(f,t)$ is the noise vector that is spectrally and spatially uncorrelated. The noise is also uncorrelated with the source signals.

The structure of the steering vector, $\mathbf{a}(f,\theta)$ changes significantly with the geometry of the array, since the steering vector establishes the relative phasing across the array to respond to source at a specific angle. For a ULA with M elements with spacing d between them, the steering vector takes the form

$$\mathbf{a}(f,\theta) = \begin{bmatrix} 1 \\ e^{j\frac{2\pi f}{c}d\sin\theta} \\ e^{j\frac{2\pi f}{c}2d\sin\theta} \\ \vdots \\ e^{j\frac{2\pi f}{c}(M-1)d\sin\theta} \end{bmatrix} \tag{2.63}$$

where c is the free space velocity of the EM wave. The first element in the ULA is the reference element with zero phase. The source impinging on the ULA at an angle θ from broadside causes a phase shifts between neighbouring antennas. The angle θ is a physical angle and the angle is a corresponding phase angle. The corresponding spatial spectral density matrix for the array output at frequency f is

$$\mathbf{P}_x(f) = \mathbf{A}(f,\theta)\mathbf{P}_s(f)\mathbf{A}^H(f,\theta) + \mathbf{P}_n(f) \tag{2.64}$$

where $\mathbf{P}_s(f) = E[\mathbf{s}(f,t)\mathbf{s}^H(f,t)]$ is the $P \times P$ Hermitian power spectral density matrix of the source vector, $\mathbf{s}(f)$, and it may include undesired signals such as interference and noises; $\mathbf{P}_n(f) = E[\mathbf{n}(f,t)\mathbf{n}^H(f,t)]$ is power spectral density matrix of the noise of size $M \times M$ at frequency f. The superscript $(\cdot)^H$ denotes the Hermitian transpose. It is assumed that $P < M$ and that the rank of $\mathbf{A}(f,\theta)$ is equal to P for all frequencies and angles.
The general phase-based DOA estimation methods such as MUSIC and ESPRIT rely on the correlation of the signal across the antenna elements. Therefore an approximation to the overall spectral density matrix is desired that yields the covariance matrix of array output over every frequency bin f_j, where $j = [1,J]$ and sample t as shown in Equation (2.65).

$$\mathbf{R}_{\mathbf{xx}}(f_j) = E[\mathbf{x}(f_j,t)\mathbf{x}^H(f_j,t)] \tag{2.65}$$

where $E[\cdot]$ is the expectation operator. The covariance matrix can be decomposed into signal component corresponding to the j^{th} frequency bin and noise component as shown in Equation (2.66)

$$\mathbf{R}_{\mathbf{xx}}(f_j) = \mathbf{A}(f_j,\theta)\mathbf{R}_s(f_j)\mathbf{A}^H(f_j,\theta) + \mathbf{R}_n(f) \tag{2.66}$$

In Equation (2.66), $\mathbf{R}_s(f_j)$ is the signal covariance matrix at j^{th} frequency bin and $\mathbf{R}_n(f)$ is the noise spatial covariance matrix. Typically, a limited number of samples are available for DOA estimation to obtain the spatial covariance matrix with sampling instants $\mathbf{x}(f_j,t)$ for $t = 1,...,N$.

$$\widehat{\mathbf{R}}_{\mathbf{xx}}(f_j) = \frac{1}{N}\sum_{t=1}^{N}\mathbf{x}(f_j,t)\mathbf{x}^H(f_j,t) \tag{2.67}$$

$$\widehat{\mathbf{R}}_{\mathbf{xx}}(f_j) = \mathbf{A}(f_j,t) \quad \frac{1}{N}\sum_{t=1}^{N}\mathbf{x}(f_j,t)\mathbf{x}^H(f_j,t)\Bigg)\Bigg(\mathbf{A}^H(f_j,t) + \frac{1}{N}\sum_{t=1}^{N}\mathbf{n}(f_j,t)\mathbf{n}^H(f_j,t) \tag{2.68}$$

$$\mathbf{x}(f_j) = \Big[x(f_j,1), \quad x(f_j,2), \quad \ldots \quad x(f_j,T)\Big]\Bigg(\tag{2.69}$$

Here t is the sample index and $\mathbf{x}(f_j)$ is the data matrix at frequency f_j. An adequate observation period, containing N number of samples must be chosen to facilitate the sample covariance matrices $\mathbf{P}_s = \frac{1}{N}\sum_{t=1}^{N}\mathbf{s}(f_j,t)\mathbf{s}^H(f_j,t)$ and $\mathbf{P}_n = \frac{1}{N}\sum_{t=1}^{N}\mathbf{n}(f_j,t)\mathbf{n}^H(f_j,t)$ to model signal $\mathbf{P}_s$ and noise $\mathbf{P}_n$ covariance matrices respectively.

2.8.3 DOA Estimation of Wideband Sources

The DOA estimation of wideband sources, based on each of the discrete frequency bins are classified as incoherent methods and coherent methods. The wideband DOA estimation by utilizing narrowband DOA estimation methods at each frequency bin and then combined to obtain the wide-band estimation is presented in this section. This approach is called incoherent approach. The subspace-based MUSIC algorithm decomposes the sample covariance matrix into subspace spanned by signal and noise components. A generic representation of the covariance matrix is of the form

$$\mathbf{R}_{\mathbf{xx}}(f_j) = \mathbf{A}(f_j,\theta)\mathbf{R}_s(f_j)\mathbf{A}^H(f_j,\theta) + \mathbf{R}_n(f) \tag{2.70}$$

The covariance matrix of Equation (2.70) can be decomposed using EVD as shown in Equation (2.71)

$$\mathbf{R}_{\mathbf{xx}}(f_j) = \begin{bmatrix}\mathbf{U}_s(f_j) & \mathbf{U}_n(f_j)\end{bmatrix}\begin{bmatrix}\sum_s(f_j) & 0\\ 0 & \sum_n(f_j)\end{bmatrix}\begin{bmatrix}\mathbf{U}_s^H(f_j)\\ \mathbf{U}_n^H(f_j)\end{bmatrix} \tag{2.71}$$

where the $\sum_s(f_j)$ and $\sum_n(f_j)$ are the eigen values of the covariance matrices corresponding the signal subspace and noise subspace respectively for the j^{th} frequency bin. These eigen values are sorted in the descending order of the diagonal matrix as shown in Equations (2.72 and 2.73). The matrices $\mathbf{U}_s(f_j)$ and $\mathbf{U}_n(f_j)$ in Equation (2.71) are signal and noise subspaces, respectively for the j^{th} frequency bin.

$$\sum_s(f_j) = diag\begin{bmatrix}\sigma_1(f_j) & \dots & \sigma_P(f_j)\end{bmatrix} \tag{2.72}$$

$$\sum_n(f_j) = diag\begin{bmatrix}\sigma_{P+1}(f_j) & \dots & \sigma_M(f_j)\end{bmatrix} \tag{2.73}$$

The P number of eigen values denoting $\sigma_1(f_j) > \sigma_2(f_j) > \cdots > \sigma_P(f_j)$ are principal components P signal sources and the remaining $\sigma_{P+1}(f_j) = \sigma_{P+2}(f_j) = \cdots = \sigma_M(f_j)$ correspond to the additive noise of the signal;

The standard assumptions of spatially uncorrelated and identically distributed noise ensure

that the noise covariance can be decomposed such that there is equal noise power in each of the array elements. Thus eigenvalues $\sigma_{P+1}(f_j) = \sigma_{P+2}(f_j) = \cdots = \sigma_M(f_j) = \sigma_n(f_j)$ where $\sigma_n(f_j)$ is the noise power such that the noise correlation can be written as

$$\mathbf{R}_n(f) \approx \sigma_n(f_j)\mathbf{U}_n(f_j)\mathbf{U}_n^H(f_j) \tag{2.74}$$

The $(M-P)$ eigenvalues associated with the noise have the same value $\sigma_n(f_j)$ which are used to estimate the size of the noise subspace. The matrix $\mathbf{U}_n(f_j)$ is a basis for the noise subspace, and its orthogonal complement $\mathbf{U}_s(f_j)$ is basis for the signal subspace. A method of estimating the signal direction vector can now be obtained by using the matrix $\mathbf{U}_n(f_j)$ whose size is $M \times (M-P)$ and whose columns are the $(M-P)$ noise eigenvectors. The square of the Euclidean distance between the vector $\mathbf{a}(f_j,\theta)$ (the steering vector) and the noise subspace can be represented as in Equation (2.75).

$$e^2(f_j,\theta) = \mathbf{a}^H(f_j,\theta)\mathbf{U}_n(f_j)\mathbf{U}_n^H(f_j)\mathbf{a}(f_j,\theta) \tag{2.75}$$

The minimum of this distance will be obtained when $\mathbf{a}(f_j,\phi)$ is in the same direction as the directional vectors of the signal, which are orthogonal to the noise subspace basis vectors. Inverting this distance, the MUSIC algorithm for the narrowband frequency bin, f_j, is obtained as given in Equation (2.76).

$$\mathbf{P}_{Music}(f_j,\theta) = \frac{1}{\mathbf{a}^H(f_j,\theta)\mathbf{U}_n(f_j)\mathbf{U}_n^H(f_j)\mathbf{a}(f_j,\theta)} \tag{2.76}$$

The In-Coherent Method (ICM) and Coherent Signal Subspace Methods (CSSM), which are the classical subspace based wideband DOA estimation algorithms were proposed by Wang and Kaveh (Wang & Kaveh, 1985).

2.8.4 Incoherent Method

The extension of the MUSIC algorithm to wideband sources consists of several MUSIC bearing responses that are determined from the signal subspace at each narrowband frequency and averaged together. Incoherent averaging was chosen to combine the MUSIC frequency spectra. The result from each narrowband MUSIC spectrum is averaged.

$$\mathbf{P}_{Music}(\theta) = \prod_{j=1}^{J} P_{Music}(f_j,\theta) = \prod_{j=1}^{J} \frac{1}{\mathbf{a}^H(f_j,\theta)\mathbf{U}_n(f_j)\mathbf{U}_n^H(f_j)\mathbf{a}(f_j,\theta)} \tag{2.77}$$

The Equation (2.77) denotes the incoherent method of averaging the spatial spectrum obtained for each of the narrow band frequency bin.

2.8.5 Coherent Signal Subspace Method

The Coherent Signal-Subspace Method (CSSM) is one of the widely adopted techniques and it is based on focusing matrices. Wang and Kaveh (Wang & Kaveh, 1985) proposed the CSSM approach in which a transformation matrix, transforms the covariance matrix and negates the influence of the frequencies other than the center frequency. After transformation, the covariance matrix represents a narrowband signal for center frequency.
The j^{th} frequency bin of the observed data sample $\mathbf{x}(f_j,t)$ and its covariance matrix shall be computed as shown in Equation (2.67). In CSSM method, data sample corresponding to j^{th} frequency bin is transformed to a center frequency f_0. This transformation is accomplished by focussing the signal subspace components of the data matrix to the center frequency (Doron & Weiss, 1992). The focussing of discrete frequencies is achieved by Equation (2.78).

$$\mathbf{y}(f_j,t) = \mathbf{T}(f_j)\,\mathbf{x}(f_j,t) \tag{2.78}$$

The focussing matrix $\mathbf{T}(f_j)$ defined in (Yoon, Kaplan, & McClellan, 2006) is represented in Equation (2.79).

$$\mathbf{T}(f_j) = \left[e^{i(k_j-k_0)\sin\theta}, \quad e^{i(k_j-k_0)d\sin\theta}, \quad \ldots \quad e^{i(k_j-k_0)(M-1)d\sin\theta}\right] \Bigg(\tag{2.79}$$

Here the k_j is the wave number corresponding to j^{th} frequency bin and k_0 is wave number corresponding to focussing frequency. Typically, the mid frequency of the wideband signal is chosen as the center frequency. The sample covariance matrix of j^{th} frequency bin after focussing is obtained by

$$\widehat{\mathbf{R}}_{\mathbf{yy}}(f_j) = E[\mathbf{y}(f_j,t)\mathbf{y}^H(f_j,t)] \tag{2.80}$$

The CSSM method of wideband DOA estimation using the classical MUSIC algorithm is computed through the Equation (2.81).

$$\mathbf{P}_{Music}(\theta) = \prod_{j=1}^{J} \frac{1}{\mathbf{a}^H(f_0,\theta)\mathbf{U}_n(f_j)\mathbf{U}_n^H(f_j)\mathbf{a}(f_0,\theta)} \tag{2.81}$$

In Equation (2.81), $\mathbf{U}_n(f_j)$ is the noise subspace corresponding to covariance matrix of j^{th} frequency bin $\widehat{\mathbf{R}}_{\mathbf{yy}}(f_j)$. The product of noise subspaces of all the frequency bins of the covariance matrix is computed. The array steering vector $\mathbf{a}(f_0,\theta)$ corresponding to the focussing frequency acts as actual signal subspace which is computed as defined in Equation (2.63).

Several researchers (Doran, Doron, Weiss, et al., 1993; Di Claudio & Parisi, 2001; Yoon et al., 2006; Zhang, Dai, & Ye, 2010; Yu, Liu, Huang, Zhou, & Xu, 2007; Sellone, 2006) have attempted to improve the focussing matrix by several techniques. Also the focusing matrix is parametrized to compute its focussing loss, and thus to relate the inaccuracies of the estimations is also addressed in the literature.

The CSSM attempts to focus (transform) its signal subspace components to a determined discrete frequency and averages to produce the search vector for the MUSIC like algorithm. A method named Array Manifold Interpolation (AMI) (Doran et al., 1993) attempts to linearly interpolate the array manifold vector for a desired frequency. These methods provide a array manifold interpolation matrix, which separates array manifold vector from the array geometry and direction θ. Further to CSSM, a Weighted Average of Signal Subspaces (WAVES) method (Di Claudio & Parisi, 2001) was developed by authors Di and Parisi. In WAVES, the signal subspace components subjected to weighed averaging to improve the focussing of the signal subspace. The Test of Orthogonality of Projected Subspaces (TOPS) proposed in (Yoon et al., 2006) for wideband DOA estimation accomplishes an intermediate performance between incoherent and coherent methods. Subsequently, an Extended TOPS (ETOPS) (Zhang et al., 2010) algorithm is based on incoherent method and TOPS algorithm further improved the focussing of signal subspaces at an reference frequency. The orthogonality between the signal and noise subspaces for each of the frequency components of the incoming sources is evaluated through TOFS method (Yu et al., 2007), to improve the focussing of signal subspaces over the CSSM method. The Robust Coherent Signal Subspace (R-CSM) (Sellone, 2006) proposed by Fabrizio Sellone shows a novel design of focussing matrices by minimizing the subspace focussing errors by optimising the Rotational Signal Subspace and Signal subspace transformation of focussing matrices. The Wideband-Sparse Spectrum Fitting (W-SpSF) estimation proposed by He et.al. in (He, Shi, Huang, & So, 2015) leverages the increased degrees of freedom of sparse spatial sampling available through co-array for under determined DOA.

2.9 Summary

This chapter aimed to present an overview of multi-disciplinary attributes of the broad domain of DOA estimation. It has provided a review of the basic concepts of antenna, antenna array and DOA estimation algorithms along with the associated mathematical techniques. After a brief discussion on important performance parameters of antenna, a

succinct review of various configurations such as 1D, 2D and 3D antenna arrays is presented in this chapter. The progression in the DOA estimation algorithms from Fourier based to subspace techniques has also been covered in this chapter with pertinent technical details. The assumptions associated with the determination of radiation pattern of antenna arrays used in DOA estimation algorithms have been briefly explained. The analytical details of classical subspace techniques like MUSIC and ESPRIT which are either extensively used or referred in this thesis have been dealt in detail. This chapter has presented a discussion on the existing techniques for the estimation of DOA of non-stationary sources. A review of available techniques for the estimation of DOA of wideband sources is also included in this chapter. The implicit/explicit constraints as well as the limitations of conventional antenna arrays and the existing DOA estimation algorithms are highlighted with a view to facilitate better appreciation of the novelties and the significance of the analysis/results to be presented in the subsequent chapters of this thesis.

Chapter 3

Formulation and Analysis of a Closed Form Solution for Two Dimensional DOA Estimation

3.1 Introduction

This chapter presents a formulation, for the minimization of computational complexity of two-dimensional DOA estimation algorithm for single incoming source scenario. Towards this end, a closed form expression for two-dimensional DOA estimation using the MUSIC algorithm is proposed which involves only one-dimensional search. This task has been accomplished by a novel one-dimensional antenna array configuration with its alternate array element's orthogonal orientation. These elements receive both the horizontal and vertical polarized field components simultaneously and these components are processed for 2D-DOA estimation. With prior knowledge of the analytical expressions for the radiation patterns of typical array elements, a closed form expression has been derived relating the azimuthal angle ϕ and elevation angle θ of DOA through the ratio of the amplitudes of horizontally and vertically polarized received fields. This concept is illustrated using the open ended Rectangular Wave Guide (RWG) and Circular Wave Guide (CWG) as an antenna element.

3.2 Review of 2D-DOA Estimation Techniques

A basic review on antenna array configuration and DOA estimation algorithms has already been presented in Chapter 2. In the discussion of antenna array for 2D-DOA estimation covered in Chapter 2, the emphasis was on antenna elements having identical (single) polarization only. In this section, the significance of diversely polarized antenna elements in DOA estimation is reviewed. Generally, two-dimensional array configurations such as planar, circular or three-dimensional array with linear subarrays along the three axes are used for the 2D-DOA estimation (N. Tayem & Kwon, 2005; Manikas, Alexiou, & Karimi, 1997). The general performance of a DOA estimation system is also directly influenced by

both the array geometry and the associated algorithm employed. Two-dimensional DOA estimation algorithms such as MUSIC (Schmidt, 1986) involves two-dimensional search and ESPIRIT (Roy & Kailath, 1989) uses polynomial rooting to determine the azimuth and elevation angles subtended by the distant source. This is true irrespective of number of sources.

In (Weiss & Friedlander, 1993), a diversely polarized array configuration along with array interpolation techniques are adopted for DOA estimation using a polynomial rooting method. In general, polynomial rooting methods are invoked for linear arrays, whereas in (Weiss & Friedlander, 1993) it is extended for arbitrary array configuration using diversely polarized array elements and interpolation techniques. In (Li, 1993), the polarization sensitive antenna elements such as crossed dipoles and loop antennas are used to exploit the invariance properties of the ESPRIT algorithm. The dipole and loops antennas are sensitive to the electric and magnetic fields of the incident waves. The invariance properties among the dipole and loop antennas are used to estimate the two-dimensional DOA and polarization of the incident waves. In (Wong, Li, & Zoltowski, 2004) antenna elements such as dipoles, loops and circularly polarized antennas oriented in L-shaped uniformly spaced grid array configuration are used for DOA estimation. In (Wong & Zoltowski, 1998) a closed form solution for DOA is presented with vector sensor array of irregular configuration. Each of the sensor consists of six co-located antennas to measure the three components of both E and H fields. The ESPRIT algorithm is applied multiple times to the distinct pairs of the six subarrays to extract the invariant factors to characterize the six EM field components of the impinging source. Both (Wong et al., 2004) and (Wong & Zoltowski, 1998), insist on the sensor array to capture the three cartesian components of E and H received fields. This chapter proposes a much simplified approach for 2D-DOA estimation utilizing only the two orthogonally polarized components of the received fields.

The focus of this chapter is to arrive at a formulation for the minimization of computational complexity of two-dimensional DOA estimation algorithm if the interest is of single source scenario. Towards this end, a closed form expression for two-dimensional DOA estimation using MUSIC algorithm is proposed which involves only a one-dimensional search. This task has been accomplished by a novel one-dimensional antenna array configuration with its alternate array element's orthogonal orientation. These elements receive both the horizontal and vertical polarized field components simultaneously and these components are processed for DOA estimation.

With prior knowledge of analytical expressions for the radiation patterns of array elements, a closed form expression shall be derived to relate the azimuthal angle ϕ and elevation angle θ of DOA through the ratio of the amplitudes of horizontally and vertically polarized fields. The analytical expressions for the radiation pattern of the open ended RWG and CWG are stated and validated in the literature (Silver, 1949). These analytical expressions are utilized to derive the closed form solution for 2D-DOA estimation with reduced computation complexity (Karthikeyan, Kadambi, & Vershinin, 2015).

3.3 Open Ended Waveguide as an Antenna Element

Open ended waveguides are classified under the category of aperture antennas in antenna engineering. The RWG and CWG are the fundamental canonical form of waveguides. These waveguides can serve as antenna as well as a transmission line to feed horn antennas. The aperture dimension of the waveguide is directly related to the operating frequency. The fundamental theory and different modes of operation of the RWG and CWG have been well addressed in the published literature (Silver, 1949; Kraus, 1992; Balanis, 2012). The cross sectional views of classical RWG and CWG are shown in Figures 3.1 and 3.2 respectively.

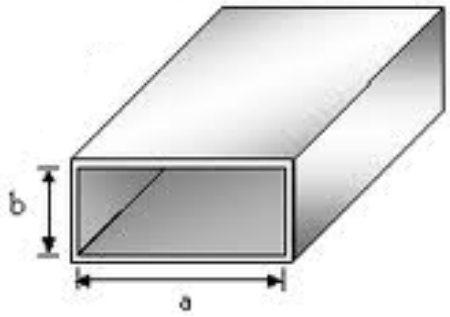

Figure 3.1: Rectangular Waveguide

It is well known through electromagnetic and antenna engineering that a wave guide exhibits its maximum potential when it is excited in its dominant mode. Closed form expressions to compute the azimuth and elevation plane radiation patterns of waveguides for a given mode of excitation and operating frequency are presented in (Silver, 1949). The normalized azimuth (H-Plane) and elevation (E-Plane) radiation patterns of an X-band RWG for a TE_{10} dominant mode, operated at 9.375 GHz are shown in Figure 3.3.

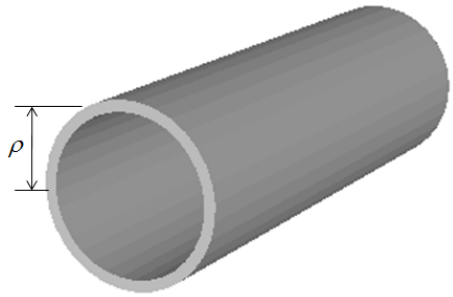

Figure 3.2: Circular Waveguide

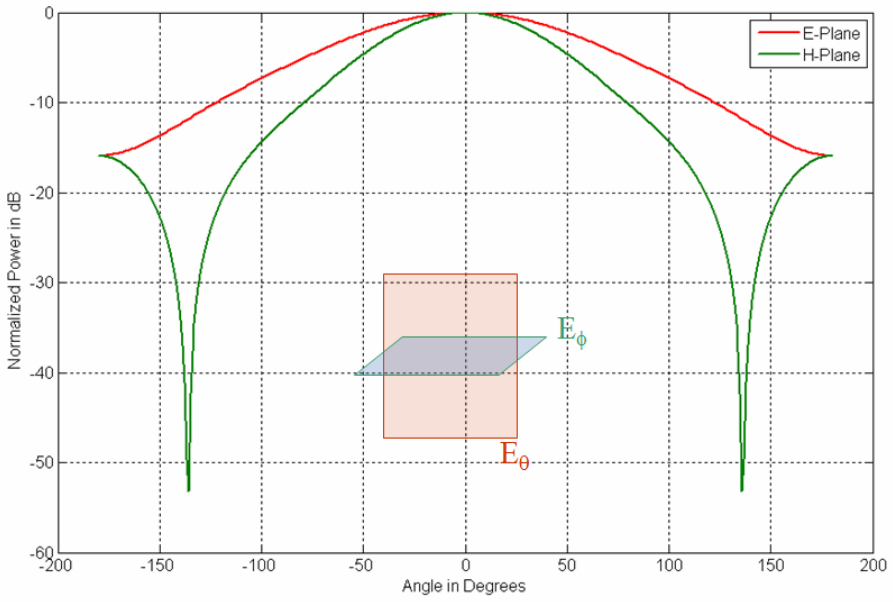

Figure 3.3: Normalized Radiation Pattern of a RWG

The Figure 3.4 indicate the copolar and cross polar components of the radiation of RWG. The significant difference between the copolar and cross polar justifies that, the cross polar component shall be ignored in the computations.

3.3.1 Proposed Orthogonally Polarized Linear Array Configuration

The RWG array is chosen for the proposed research based on the strong theoretical and practical considerations of RWG as an antenna element. The Orthogonally Polarized Linear Array (OPLA) configuration is proposed as shown in the Figure 3.5. In the proposed array configuration shown in Figure 3.6, the RWG elements are arranged in a straight line with the adjacent elements rotated by 90°. The adjacent elements of the array are orthogonally

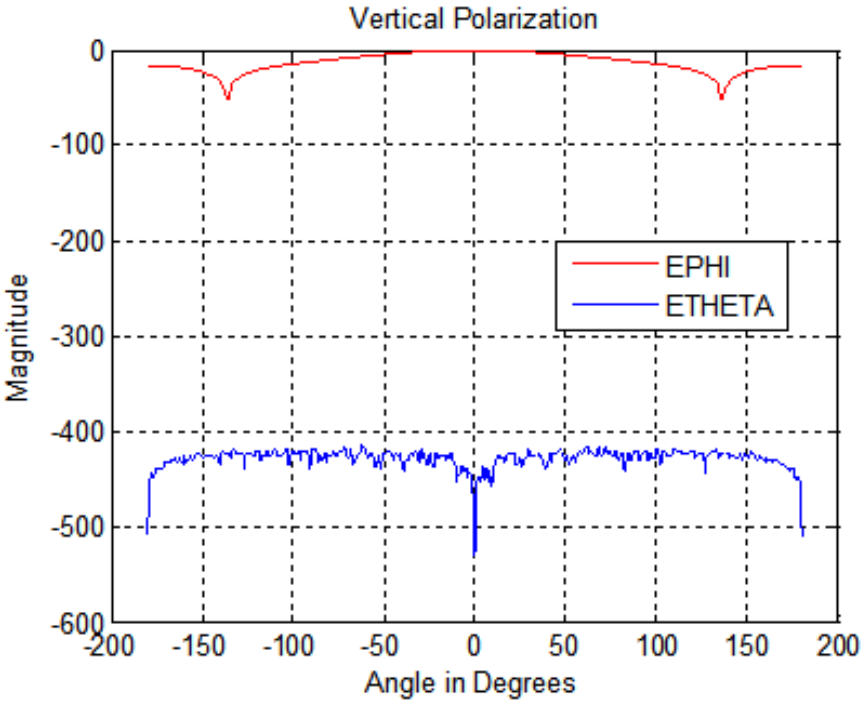

Figure 3.4: Co-polar and Cross Polar Radiation Pattern of a RWG

polarized with respect to each other. This configuration of dual polarized array will receive both the horizontal and vertically polarized components, which will be used to estimate the two dimensional DOA. For 2D-DOA estimation, a closed form expression to relate

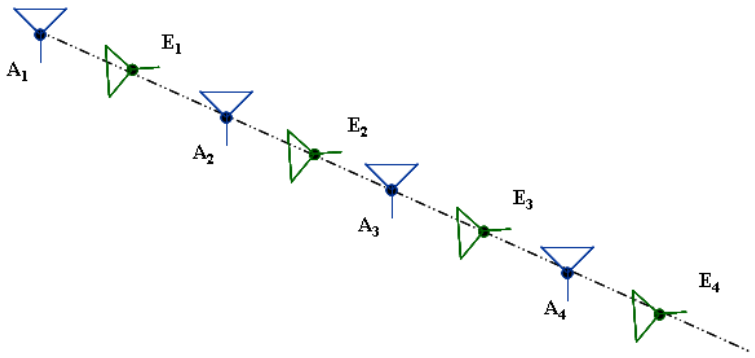

Figure 3.5: Proposed Orthogonally Polarized Linear Array

the azimuth angle ϕ and elevation angle θ is derived from the standard expressions of radiation patterns of RWG. The ratio between the horizontally polarized and vertically polarized received field, yields a unique value, which is used to estimate the DOA in the proposed algorithm. The sampled signal data received by the antennas are processed

using the standard MUSIC algorithm. As shown in the Figure 3.5, the alternate elements $A_1, A_2, \ldots, A_4$, receive the vertically polarized (azimuth) field components whereas, the $E_1, E_2, \ldots, E_4$ will receive the horizontally field polarized (elevation) components. The

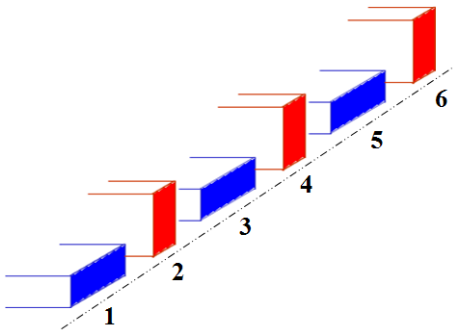

Figure 3.6: Orthogonally Polarized Linear Array Configuration using RWG Elements

RWG element in the proposed orthogonally polarized linear array configuration is shown in Figure 3.6. The elements are numbered with respect to its position Figure 3.6. The odd numbered elements correspond to the orientation to receive vertical polarization. Likewise, the even numbered elements correspond to horizontal polarization. The details of the polarization as an orientation of the electric field vectors are shown in the Figure 3.7.

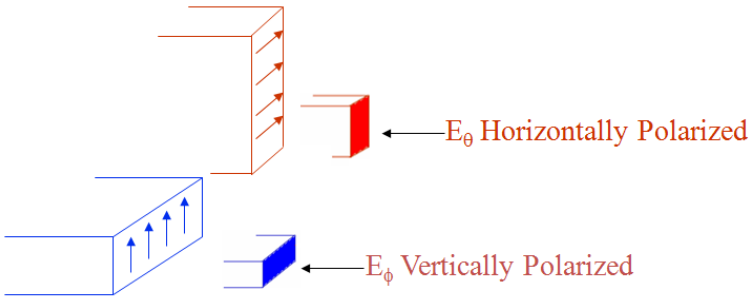

Figure 3.7: Polarization of RWG

3.4 Signal Modelling with RWG Array Elements

The RWG is considered as antenna elements for the array signal modelling. It is well known that for a waveguide mounted to radiate in one of its principal planes (E or H Plane), a physical rotation of 90° about its propagation axis (z axis) will result in change in polarization by 90° (Orthogonal Polarization). The signals received by antenna elements of the array are modelled in the matrix vector form as given in Equations (3.1) and (3.2).

$$\mathbf{x}_h = \mathbf{A}_h\mathbf{s} + \mathbf{n} \tag{3.1}$$

where $\mathbf{x}_h$ is the modelled signal vector received by the RWG elements oriented in H-Plane (Vertical Polarization) for the azimuth and elevation DOA angles (θ, ϕ). $\mathbf{A}_h$ is an array steering matrix for the Vertical Polarization; $\mathbf{s}$ and $\mathbf{n}$ are signal data and additive white Gaussian noise vector respectively.

$$\mathbf{x}_e = \mathbf{A}_e\mathbf{s} + \mathbf{n} \tag{3.2}$$

Similar description holds for $\mathbf{x}_e$ except that it refers to Horizontal Polarization or E-Plane. $\mathbf{A}_e$ is an array steering matrix for the Horizontal Polarization. The array steering matrix is a function of elevation angle θ, azimuth angle ϕ and the inter-element spacing d, which is defined as

$$\mathbf{a}_h(\theta,\phi) = E_\phi(\theta,\phi)\, e^{-jkdm_1 \sin\theta \cos\phi} \text{ where } m_1 = 1,2,\ldots,(M_h-1) \tag{3.3}$$

Similarly,

$$\mathbf{a}_e(\theta,\phi) = E_\theta(\theta,\phi)\, e^{-jkdm_2 \sin\theta \sin\phi} \text{ where } m_2 = 0.5,1.5,\ldots,(M_e-1)+0.5 \tag{3.4}$$

The columns of array steering matrices $\mathbf{A}_h$ and $\mathbf{A}_e$ are formed by the array steering vectors $\mathbf{a}_h$ and $\mathbf{a}_e$ respectively. Each column of the array steering matrix represents the steering

vector of the corresponding source angle (θ, ϕ). For the case of a single source, the array steering matrix has only one column, corresponding to the steering vector of the impinging source angle (θ, ϕ).

In Equations (3.3) and (3.4), M_h and M_e represent the number of antenna elements oriented in H-plane and E-plane respectively. k represents free space wave number. Typically, the inter-element spacing d is such that $\frac{\lambda}{4} \leq d \leq \frac{\lambda}{2}$, λ being the wavelength. The $E_\phi(\theta, \phi)$ and $E_\theta(\theta, \phi)$ are the amplitudes of vertically and horizontally polarized field components of the radiation pattern at (θ, ϕ).

The computation of the sample covariance matrix to invoke MUSIC algorithm (Schmidt, 1986) is carried out using Equation (3.5).

$$\mathbf{R_{xx}} = E\left[\mathbf{x}_e \mathbf{x}_e^H\right] \tag{3.5}$$

In Equation (3.5), $E[.]$ is the expectation operator and $(.)^H$ denotes the Hermitian conjugate. The covariance matrix $\mathbf{R_{xx}}$ can also be constructed using $\mathbf{x}_h$ data. The covariance matrix can be decomposed into signal and noise components through eigen decomposition shown in Equation (3.6).

$$\mathbf{R_{xx}} = \mathbf{ASA}^H + \sigma^2 \mathbf{I} \tag{3.6}$$

where $\mathbf{S} = E[ss^H]$ is the signal covariance matrix; $\mathbf{A}$ denotes the matrix representation of the array steering vector for the respective polarization as shown in Equations (3.3) and (3.4). σ^2 is the noise covariance, $\mathbf{I}$ is the identity matrix. The eigen vectors of the covariance matrix are decomposed into signal and noise subspace as stated in Equation (3.6) which are orthogonal to each other. The peak magnitude of MUSIC algorithm for the two-dimensional DOA estimation is given in Equation (3.7).

$$\arg\max_{(\theta,\phi)} P(\theta, \phi) = \frac{1}{\mathbf{a}(\theta, \phi)\, \mathbf{V}_n \mathbf{V}_n^H \mathbf{a}^H(\theta, \phi)} \tag{3.7}$$

where $\mathbf{a}(\theta, \phi)$ is a search vector. The matrix $\mathbf{V}_n$ spans the noise subspace vectors in its columns, which are the eigenvectors whose eigenvalues are equal to the σ^2.

3.5 2D-DOA Estimation Using Closed Form Solutions

For two-dimensional DOA estimation in the case of a single source, the two-dimensional search Equation (3.7) can be reduced to one-dimensional search which constitutes the

proposed research contribution of this chapter. The two-dimensional search vector $\mathbf{a}(\theta,\phi)$ is reduced to one-dimension by deriving compact expressions which relates the angle θ in terms of angle ϕ through the ratio of amplitudes of vertical polarized (E_ϕ) and horizontal polarized (E_θ) field components received by the RWG elements of the array.

3.5.1 Derivation to Relate Azimuth and Elevation DOA Angles with RWG

The analytical expressions of E_θ (Horizontal Polarization) and E_ϕ (Vertical Polarization) components of radiation patterns of the RWG with a dominant TE_{10} mode of propagation are given by Equations (3.8) and (3.9), respectively along with equation (3.10) (Silver, 1949). These closed form expressions are used to compute the E-Plane (horizontal) and H-Plane (vertical) polarized radiation pattern for a given operating frequency (9.375 GHz).

$$E_\theta(\theta,\phi) = -\left(\frac{\mu}{\varepsilon}\right)^{1/2} \frac{\pi a^2 b}{2\lambda^2 R}\cos\phi\left[\frac{\beta_{10}}{k}+\cos\theta\right]\Psi(\theta,\phi) \tag{3.8}$$

$$E_\phi(\theta,\phi) = -\left(\frac{\mu}{\varepsilon}\right)^{1/2} \frac{\pi a^2 b}{2\lambda^2 R}\sin\phi\left[1+\frac{\beta_{10}}{k}\cos\theta\right]\Psi(\theta,\phi) \tag{3.9}$$

where,

$$\Psi(\theta,\phi) = \left[\frac{\cos\left(\frac{\pi a}{\lambda}\sin\theta\cos\phi\right)}{\left(\frac{\pi a}{\lambda}\sin\theta\cos\phi\right)^2-\left(\frac{\pi}{a}\right)^2}\right]\left[\frac{\sin\left(\frac{\pi b}{\lambda}\sin\theta\sin\phi\right)}{\left(\frac{\pi b}{\lambda}\sin\theta\sin\phi\right)}\right] \tag{3.10}$$

For a rectangular waveguide, β_{10} is computed by

$$\beta_{mn} = \sqrt{k^2 - k_{mn}^2} \tag{3.11}$$

where

$$k_{mn} = \sqrt{\left(\frac{m\pi}{a}\right)^2+\left(\frac{n\pi}{b}\right)^2} \tag{3.12}$$

where θ is the elevation angle,

ϕ is the azimuth angle,

μ is the free space permeability,

ε is the free space permittivity

λ is the wavelength,

k is the wave number,

a is the width of the waveguide aperture,

b is the height of the waveguide aperture,

β_{10} is the propagation constant for the waveguide excited in dominant mode ($m=1, n=0$),

R is the distance between a reference point and a far-field distant point.

The ratio between the horizontal and vertical polarized field components of the received signal shall be derived as follows. Let

$$X = \frac{|E_\theta(\theta,\phi)|}{|E_\phi(\theta,\phi)|} \tag{3.13}$$

X denotes the ratio of amplitudes of horizontal and vertical polarized field components received by the RWG elements. With the substitution of Equations (3.8) and (3.9) in Equation (3.13).

$$X = \frac{\sin\phi\left[1+\frac{\beta_{10}}{k}\cos\theta\right]}{\cos\phi\left[\cos\theta+\frac{\beta_{10}}{k}\right]} \tag{3.14}$$

Further simplification of Equation (3.14) yields the separable closed form expressions relating the azimuth ϕ and elevation θ angles as shown in Equation (3.15) and (3.16).

$$\phi = \tan^{-1}\left(\frac{X\left(\cos\theta+\frac{\beta_{10}}{k}\right)}{\left(1+\frac{\beta_{10}}{k}\cos\theta\right.}\right) \tag{3.15}$$

$$\theta = \cos^{-1}\quad\frac{\tan\phi - X\frac{\beta_{10}}{k}}{X-\frac{\beta_{10}}{k}\tan\phi}\Bigg)\Bigg(\tag{3.16}$$

The exponential term of Equation (3.3) can be rewritten as shown in Equation (3.17) with the substitution of Equation (3.15).

$$e^{-j\frac{2\pi}{\lambda}d\sin\theta\cos\left(\tan^{-1}\left(\frac{X\left(\cos\theta+\frac{\beta_{10}}{k}\right)}{\left(1+\frac{\beta_{10}}{k}\cos\theta\right.}\right)\right)\Bigg(\Bigg(} \tag{3.17}$$

Thus, the exponential term of Equation(3.17) only involves the elevation angle θ. Similarly, the exponential term of Equation (3.3) shall also be rewritten after substituting Equation (3.16) in it. As a result, the exponential term of Equation (3.3) can be written to involve only the azimuth angle ϕ.

$$e^{-j\frac{2\pi}{\lambda}d\sin\quad\cos^{-1}\quad\frac{\tan\phi-X\frac{\beta_{10}}{k}}{X-\frac{\beta_{10}}{k}\tan\phi}\Bigg)\Bigg)\Bigg(\cos\phi} \tag{3.18}$$

The expressions (3.17) and (3.18) which relate the 2D-DOA (θ,ϕ) with only one angle say elevation θ (or azimuth ϕ) shall be utilized in the two-dimensional search vector $\mathbf{a}_h(\theta,\phi)$ in Equation (3.7) of the MUSIC algorithm.

3.5.2 Derivation to Relate Azimuth and Elevation DOA Angles with CWG

The derivation described for RWG has been extended to the case wherein the RWG is replaced by a CWG. Similar to the RWG, the analytical expressions of $E_\theta(\theta,\phi)$ and $E_\phi(\theta,\phi)$ components of radiation patterns of CWG with the TE_{11} dominant mode are given by Equations (3.19) and (3.20) (Silver, 1949).

$$E_\theta(\theta,\phi) = \frac{k\rho\omega\mu}{2R}\left[1+\frac{\beta_{11}}{k}\cos\theta\right]\left(J_1(k_{11}\rho)\frac{J_1(k\rho\sin\theta)}{k\rho\sin\theta}\sin\phi\right. \tag{3.19}$$

$$E_\phi(\theta,\phi) = \frac{k\rho\omega\mu}{2R}\left[\cos\theta+\frac{\beta_{11}}{k}\right]\left(J_1(k_{11}\rho)\frac{J_1'(k\rho\sin\theta)}{1-\left(\frac{k\rho\sin\theta}{k_{11}}\right)^2}\cos\phi\right. \tag{3.20}$$

For the dominant TE_{11} mode of a circular waveguide, β_{11} is computed as

$$\beta_{11} = \sqrt{k^2-\left(\frac{1.841}{\rho}\right)^2}$$

where ρ is the radius of the circular waveguide, k is the wave number, $J_1(.)$ is the first order Bessel function and $J_1'(.)$ is the derivative of the first order Bessel function. Similar to Equation (3.13), the ratio of amplitude of E_θ and E_ϕ field components received by the CWG elements of the array can be related through Equation (3.21).

$$X = \frac{|E_\theta(\theta,\phi)|}{|E_\phi(\theta,\phi)|} = \frac{1+\frac{\beta_{11}}{k}\cos\theta}{\cos\theta+\frac{\beta_{11}}{k}}\frac{\frac{J_1(k\rho\sin\theta)}{k\rho\sin\theta}}{\frac{J_1'(k\rho\sin\theta)}{1-\left(\frac{k\rho\sin\theta}{k_{11}}\right)^2}}\tan\phi \tag{3.21}$$

For the CWG, only the azimuth angle ϕ can be related in-terms of the elevation angle θ as shown in Equation (3.22).

$$\phi = \tan^{-1}\left(\frac{X\left(\cos\theta+\frac{\beta_{11}}{k}\right)}{1+\frac{\beta_{11}}{k}\cos\theta}\frac{J_m'(k\rho\sin\theta)}{1-\left(\frac{k\sin\theta}{k_{11}}\right)^2}\frac{k\rho\sin\theta}{J_1(k\rho\sin\theta)}\right)\left(\tag{3.22}$$

The exponential term of Equations (3.3) can be represented as shown in Equation (3.23) after the substitution of Equation (3.22).

$$e^{-jkd\sin\theta\cos\left(\left(\tan^{-1}\left(\frac{X\left(\cos\theta+\frac{\beta_{11}}{k}\right)}{1+\frac{\beta_{11}}{k}\cos\theta}\frac{J_m'(k\rho\sin\theta)}{1-\left(\frac{k\sin\theta}{k_{11}}\right)^2}\frac{k\rho\sin\theta}{J_1(k\rho\sin\theta)}\right)\right)\right)\left(\right.} \tag{3.23}$$

The derived Equation (3.22), relates the azimuth angle ϕ in-terms of only the elevation angle θ as shown in expression (3.23).

3.5.3 Reduction of Search Dimension of 2D DOA Estimation using Closed Form Solution

The expressions stated in Equations (3.17), (3.18) and (3.23) clearly indicate that, the exponential term is a function of only one angle. Hence the search dimension of steering vector $\mathbf{a}(\theta,\phi)$ in estimating $P(\theta,\phi)$ of Equation (3.7) is reduced to one-dimension. The conventional MUSIC algorithm as given in Equation (3.7) can be expressed in one-dimensional search form with the usage of the exponential term of Equation (3.17). The expression in Equation (3.24) shall be used for estimation of one of the angles of DOA say θ, which will estimate the angular peak of θ as shown in Figure. 3.8.

$$\arg\max_{\theta} P(\theta) = \frac{1}{\mathbf{a}(\theta,\phi)\mathbf{V}_n\mathbf{V}_n^H\mathbf{a}^H(\theta,\phi)} \tag{3.24}$$

The azimuth angle of two-dimensional DOA namely ϕ can be computed through the derived closed form Equation (3.15). Similarly, for the case of estimating azimuth angle

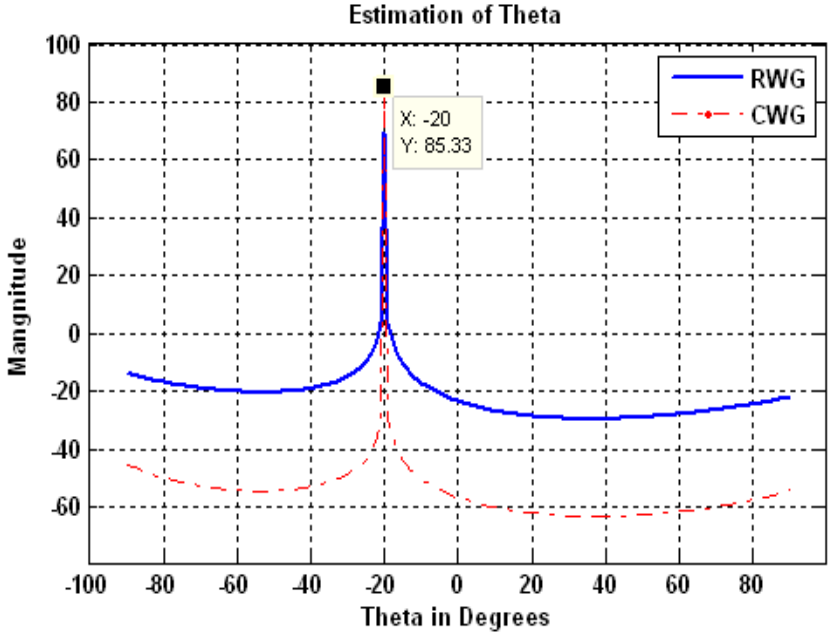

Figure 3.8: Estimation of Angle θ through the peak of One-Dimensional Search Technique for the DOA $(-20°, 25°)$

ϕ using the search vector of the MUSIC algorithm, the Equation (3.25) shall be used for estimation of angular peak of the ϕ angle.

$$\arg\max_{\phi} P(\phi) = \frac{1}{\mathbf{a}(\theta,\phi)\mathbf{V}_n\mathbf{V}_n^H\mathbf{a}^H(\theta,\phi)} \tag{3.25}$$

The elevation angle θ of the 2D-DOA, shall be computed through substituting the estimated peak angle ϕ in the derived closed form solution stated in Equation (3.16).
For the case of CWG as antenna elements, one dimensional search vector of the MUSIC algorithm given in Equation (3.24) should be used to estimate the angular peak of elevation angle θ, followed by substituting the angular peak θ in the derived closed form solution in Equation (3.22). Unlike the case of RWG, estimation of angular peak of azimuth angle ϕ using the one dimensional search vector and elevation angle θ using closed form is not possible with CWG antenna elements, in view of the radiation pattern functions of CWG. Table 3.1 summarizes the steps of one-dimensional search algorithm. The proposed array

Table 3.1: Summary of One Dimensional Search Algorithm

Steps of the Proposed Technique
1. Signal modeling as per equations (3.1) and (3.2) for a DOA (θ, ϕ)
2. Compute Ratio $X = \frac{\lvert E_\theta \rvert}{\lvert E_\phi \rvert}$ from a single sample of $\mathbf{x}_e$ and $\mathbf{x}_h$
3. Compute $\mathbf{R_{xx}}$ using $\mathbf{x}_e$ (or $\mathbf{x}_h$)
4. Compute noise subspace $\mathbf{V}_n$ through eigendecomposition of $\mathbf{R_{xx}}$
5. Compute $\mathbf{a}_e(\theta, \phi)$ substituting equation (3.17) in (3.4); (or $\mathbf{a}_h(\theta, \phi)$) (Here angle ϕ is equated through X and θ, similarly angle θ can also be equated using X and ϕ)
6. Find $\arg\max_\theta P(\theta)$ as in equation (3.24); $-90^\circ \leq \theta \leq 90^\circ$ (Here θ in the range can have a search interval of interest)
7. Compute ϕ using θ found as stated in equation (3.15)

configuration shown in Figure 3.5, detects the impinging sources at +/-90° in the E-plane and H-plane, which is not possible through the conventional singly polarized configuration. In the case of multiple sources, incoming wave received by the array will be the cumulative sum of the E-plane and H-plane field components of the multiple sources. Thus for the case of multiple sources, a unique combination of θ and ϕ cannot be determined to satisfy the resulting ratio X. Hence the proposed technique is limited to single source only. The array steering vectors for the proposed OPLA configuration is similar to the conventional linear array. The data received by both the horizontal and vertical polarized array elements are processed separately. The ratio of amplitudes of azimuth (vertical) polarized and elevation (horizontal) polarized received field components is calculated using a single snapshot received. A finite number of received samples is given as an input to classical

MUSIC algorithm. This is a typical one dimensional DOA estimation. The derived closed form expressions namely Equations (3.15) and (3.16) for RWG and Equation (3.22) for CWG are used to compute search in one dimension. With this procedure the azimuth DOA angle can be estimated using the Equation (3.15) for RWG or Equation (3.22) for CWG. The estimation of the elevation DOA can be substituted in the closed form expression to obtain azimuth DOA or vice versa. In this proposed method of 2D-DOA estimation, search computations are drastically reduced because of closed form relation of azimuth and elevation angles. In the proposed method, the searching dimension is now reduced to one dimensional (Equations (3.24) and (3.25)) instead of the two dimensional (Equation (3.7)) in typical 2D-DOA estimation algorithms.

3.5.4 Simulation Analysis of Proposed One Dimensional Search Technique for 2D-DOA

Conventionally for two-dimensional DOA estimation, a typical planar array configuration is used. A 2×2 planar array with RWG elements operating at 9.375 GHz was used to compute two-dimensional DOA. The signal was modeled for the incoming angles of actual DOA as stated in Table 3.2. In this analysis, a perfect mounting of the antenna elements in their principal (E and H) planes without mutual coupling between them is assumed. The spacing between the elements is $\lambda/4$.

The conventional two-dimensional search based MUSIC algorithm (Equation (3.7)) was used to estimate the ϕ and θ angles of DOA. Digital data modulated with a sinusoidal signal of frequency 9.375 GHz is modelled, which forms the spatio-temporal samples, as an input for the DOA analysis. The AWGN noise is considered with a SNR of 15 dB for the signal modelled for the array configuration. 100 number of spatio-temporal samples were considered for the simulation. The estimated DOA angles using the conventional two-dimensional search of MUSIC algorithm using Equation (3.7) are tabulated in Table 3.2. The signal was remodelled using Equations (3.1 and 3.2) for the proposed one-dimensional OPLA configuration for the same ϕ and θ angles of DOA as used for two-dimensional search technique of MUSIC. The steps for one-dimensional search algorithm for 2D-DOA estimation are provided in Table 3.1. The ratio between the horizontal and vertical polarized component of the impinging signal is computed form the signal model using the Equations (3.1 and 3.2).

Table 3.2: Comparison of Antenna Configurations for DOA and Timing Analysis

Configuration	**Actual DOA** $(\theta^\circ, \phi^\circ)$	**Estimated DOA at 1° Search Interval** $(\theta^\circ, \phi^\circ)$	**Computation Time with 1° Search Interval** (seconds)	**Estimated DOA at with 0.5° Search Interval** $(\theta^\circ, \phi^\circ)$	**Computation Time 0.5° Search Interval** (seconds)
2x2 Planar Array (Two-Dimensional DOA Search)	$(-20^\circ, 25^\circ)$	$(-20^\circ, 25^\circ)$	0.762	$(-20^\circ, 25^\circ)$	3.120
	$(50^\circ, -25^\circ)$	$(50^\circ, -25^\circ)$	0.761	$(50^\circ, -25^\circ)$	3.120
	$(-50^\circ, -25^\circ)$	$(-50^\circ, -25^\circ)$	0.764	$(-50^\circ, -25^\circ)$	3.120
	$(0^\circ, 0^\circ)$	$(0^\circ, 0^\circ)$	0.760	$(0^\circ, 0^\circ)$	3.120
1x4 Proposed Array (One-Dimensional DOA Search)	$(-20^\circ, 25^\circ)$	$(-20^\circ, 25^\circ)$	0.013	$(-20^\circ, 25^\circ)$	0.021
	$(50^\circ, -25^\circ)$	$(50^\circ, -25^\circ)$	0.013	$(50^\circ, -25^\circ)$	0.022
	$(-50^\circ, -25^\circ)$	$(-50^\circ, -25^\circ)$	0.013	$(-50^\circ, -25^\circ)$	0.025
	$(0^\circ, 0^\circ)$	$(0^\circ, 0^\circ)$	0.013	$(0^\circ, 0^\circ)$	0.021
	$(10^\circ, 90^\circ)$	$(10^\circ, 90^\circ)$	0.013	$(10^\circ, 90^\circ)$	0.021
	$(90^\circ, 10^\circ)$	$(90^\circ, 10^\circ)$	0.013	$(90^\circ, 10^\circ)$	0.021

The proposed one-dimensional search based MUSIC algorithm as stated in Equation (3.24) was used to estimate elevation angle θ first and then the azimuth angle ϕ was computed through the Equation (3.15). The results of the estimation of 2D-DOA (Table 3.2) through the conventional two-dimensional search approach and the proposed one-dimensional search technique are found to be exactly the same establishing the validity of the proposed technique.

The analysis of two-dimensional DOA computations was repeated with the CWG as array elements which also yielded the same DOA estimation as with RWG. The envelope of $P(\theta)$ of Equation (3.24) simulated with RWG and CWG for the desired elevation angle, θ = -20° is shown in Figure. 3.8. The tabulated computational time in Table 3.2 highlights the reduced computation of the proposed one dimensional search technique for the estimation of 2D-DOA. Simulations for both the one-dimensional search and two-dimensional search were performed on Intel core 2 Duo processor of 2.93 GHz clock speed platform. The computation time for the proposed one dimensional search technique of 2D-DOA estimation is reduced by a factor of 50 and 150 for 1° and 0.5° search intervals respectively, when compared with the conventional two-dimensional MUSIC search algorithm.

3.5.5 RMSE Analysis

The derived formulation of 2D-DOA estimation with 1D search approach is analysed for the range of SNR scenario 0 - 30 dB. The simulation for the wide range of SNR scenario is carried for signal model with DOA angles θ = -20°, ϕ = 25°. The RMSE of the estimation of elevation angle θ and azimuth angle ϕ is computed. The average estimation error from 200 simulation iteration for wide range of SNRs are computed and the results are shown in the Figure 3.9. The results reveal that estimation of θ angle has higher estimation error when compared to ϕ estimation error. The geometric configuration of the OPLA is linear. The spatial covariance of the received data samples is along only one direction, that is the array axis (x axis). Thus the θ estimation error is more than ϕ estimation error.

The results of the estimation of 2D-DOA OPLA configuration with one-dimensional search approach is compared with the conventional 2×2 uniform planar array configuration. The RMSE of 2D-DOA estimation for 2×2 UPA configuration is shown in Figure 3.10. The RMSE results shown in Figure 3.10 illustrate the importance of spatial phase variation with respect to geometric configuration of the array elements. The presence of spatial phase

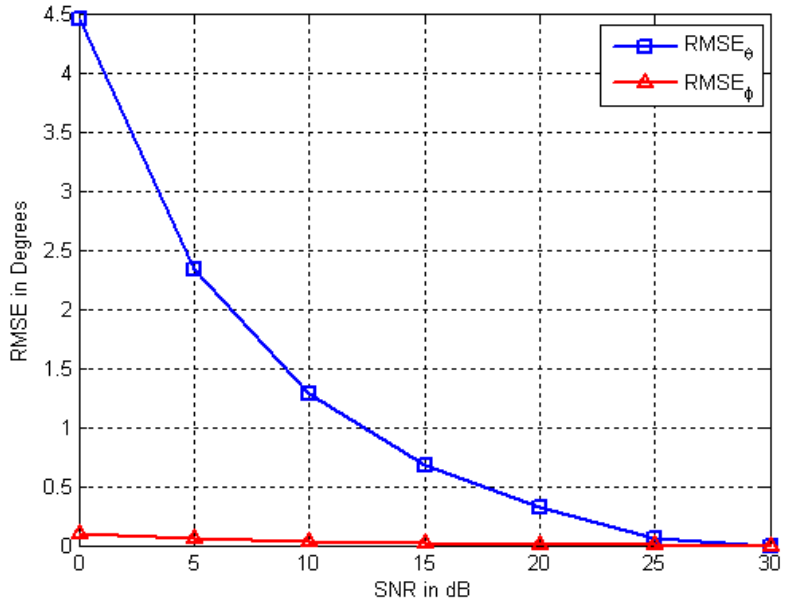

Figure 3.9: RMSE Plot for Estimation of θ and ϕ angle using One Dimensional Search Approach

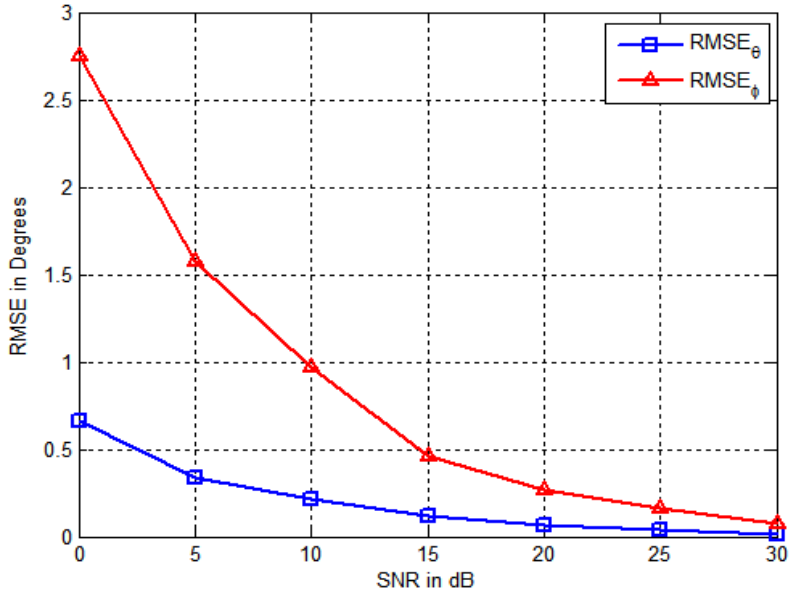

Figure 3.10: RMSE Plot for Estimation of θ and ϕ angle using 2x2 Planar Array with Conventioanl 2D-MUSIC

variation with both (x and y) axes influences, estimation accuracy and this can be seen through the reduction in $RMSE_\theta$ error when compared with the $RMSE_\theta$ results of OPLA configuration shown in Figure 3.9. Similarly, the linear phase variation with diversely

polarized array configuration of OPLA is advantageous with the estimation of $RMSE_\phi$ with least error, whereas poorer estimation accuracy in $RMSE_\phi$ is seen with the result of conventional UPA configuration due to its limited phase variation along x axis.

3.6 Summary

This chapter has presented an elegant one-dimensional search technique for two dimensional DOA estimation involving azimuth and elevation angles of distant sources. The proposed one-dimensional search is a consequence of utilizing the linear array configuration with alternate elements orthogonally polarized. The distinct feature of the proposed one-dimensional search technique leading to a significant reduction in the computation time for two-dimensional DOA estimation using MUSIC algorithm has been illustrated through the simulation studies. The proposed 2D-DOA estimation using one dimensional search is applicable only for a single source. Without loss of generality, the proposed formulation can be extended to any other antenna whose radiation pattern can be represented through an analytical expression involving separable form of elevation angle θ and azimuth angle ϕ.

The OPLA configuration can be used to estimate DOA with classical subspace based techniques. The derived closed form expression relation can be used along with the classical subspace based techniques to estimate 2D-DOA. The search dimensions are reduced to minimize the computation intensity in the proposed method. The proposed OPLA configuration minimizes the mutual EM coupling between the adjacent array elements. Reduced mutual coupling is obtained even when the antenna elements are very close to each other.

Chapter 4

Two Dimensional DOA Estimation using Dual Polarized Array for Single and Multiple Sources

4.1 Introduction

In this chapter, the diversely (dual) polarized array configurations are analysed for their performance in estimating 2D-DOA of the single and multiple sources. Discussion on various antenna array configurations for 2D-DOA estimation has been presented in Chapter 2. Subsequently, Chapter 3 covered the significance of antenna arrays with diversely polarized antenna elements. A novel OPLA configuration has been proposed for 2D-DOA estimation in Chapter 3. This chapter deals with other types of orthogonal polarized antenna arrays for 2D-DOA estimation. In this study, from antenna engineering perspective, dual polarization concept and different antenna array configurations are explored to improve the accuracy and resolution of DOA. Novel array configurations are proposed, where adjacent array elements have orthogonal polarization. The simulation studies confirm the proposed array geometries improve estimation accuracy of 2D-DOA estimations when compared with the single polarized array configuration.

4.1.1 Antenna Configurations for 2D-DOA Estimation

Typically, one dimensional array is used to estimate 1D-DOA (usually azimuth) and two or three dimensional array are used for 2D-DOA estimation. The conventional Uniform Planar Array (UPA) or Uniform Circular Array (UCA) (Balanis, 2012) configurations are used for the 2D-DOA estimation. Apart from this L-shaped array and 2L shaped array configurations addressed in (N. A.-H. M. Tayem, 2005; N. Tayem & Kwon, 2005) have been used for 2D-DOA estimation and involve pair matching computations.

4.2 Antenna Element Radiation Pattern in DOA

In the field of the array signal processing (especially in antenna arrays), generally researchers exclude the elemental radiation pattern (radiation pattern of element of the array), and utilize ideal steering matrix to validate the simulation model of the algorithms. However, in practice the elemental radiation characteristics, the mutual coupling and mounting inaccuracies of the array system distort measurements, which lead to less accurate DOA estimation. In this chapter, the actual antenna element pattern with its polarization are considered. The RWG as an antenna element is chosen to prove the proposed orthogonal array configuration. The mutual coupling and mounting inaccuracies are not considered in the 2D-DOA analysis.

4.3 Signal Model

The array configuration provides the spatial samples of the incoming signal waveform. The time domain discrete samples of the signal model at the n^{th} instant are represented by Equation (4.1).

$$\mathbf{x}(n) = \mathbf{A}\mathbf{s}(n) + \mathbf{n}(n) \tag{4.1}$$

where $\mathbf{x}(n)$ is the observed signal vector at the sensor of size $M \times 1$, $\mathbf{s}(n)$ is the signal vector at the instant n; $\mathbf{n}(n)$ is zero mean Gaussian distributed noise vector. $\mathbf{A}$ is the array steering matrix of order $M \times P$; P is the number of sources, where $M > P$ represented by

$$\mathbf{A} = \left[\mathbf{a}_1(\theta,\phi) \quad \mathbf{a}_2(\theta,\phi) \quad \cdots \quad \mathbf{a}_P(\theta,\phi)\right] \Bigg(\tag{4.2}$$

where

$$\mathbf{a}(\theta,\phi) = \left[e^{-jk\beta_1(\theta,\phi)}, \quad e^{-jk\beta_2(\theta,\phi)}, \quad \cdots, \quad e^{-jk\beta_M(\theta,\phi)}\right]^T \tag{4.3}$$

$$\beta_m(\theta,\phi) = x_m \sin\theta\cos\phi + y_m \sin\theta\sin\phi + z_m\cos\theta \tag{4.4}$$

x_m, y_m and z_m are co-ordinates of the m^{th} antenna element (sensors in general) positioned in the array; (θ,ϕ) denotes the elevation and azimuth angles of incoming source. In case of linear array sensor elements mounted along x-axis, its y and z co-ordinates of its elements will be zero. Similarly for a planar array mounted in $x-y$ plane, the z co-ordinate will be zero. For three dimensional array or conformal array, all the three axes take their co-ordinate values.

The matrix form of the signal model of the array for P number of signal sources is given as

$$\mathbf{X} = \mathbf{AS} + \mathbf{n} \tag{4.5}$$

where $\mathbf{X}$ is the observation samples constructed as a matrix of order $M \times N$; M is total number of antenna elements and N is the total number of samples. $\mathbf{A}$ is the array steering matrix consisting of the manifold vectors of each incoming source, whose size is $M \times P$; $\mathbf{S}$ is the data matrix of N discrete samples of the signal matrix of order $P \times N$, in which each row of the $\mathbf{S}$ matrix represents the data of a particular source.

4.4 Diversely (Dual) Polarized Antenna Array

The polarization of an antenna plays a key role in its receive mode performance. For typical communication purpose, an effective suppression of cross polarization is preferred in the antenna element design, where as in DOA estimation problem, the reception of orthogonally polarized components plays an important role in estimation algorithms.

In order to account for the antenna element characteristics in the array system, the elemental radiation pattern is multiplied with the array steering vector. According to the antenna array theory, the radiation pattern of the array is the product of the array factor (array steering vector) and element radiation pattern of the antenna.

$$\mathbf{a}_h(\theta,\phi) = \mathbf{a}(\theta,\phi) E_\phi(\theta,\phi) \tag{4.6}$$

$$\mathbf{a}_v(\theta,\phi) = \mathbf{a}(\theta,\phi) E_\theta(\theta,\phi) \tag{4.7}$$

In Equations (4.6) and (4.7), $\mathbf{a}(\theta,\phi)$ denotes the array factor; $E_\phi(\theta,\phi)$ and $E_\theta(\theta,\phi)$ vertical and horizontal polarized components of radiation pattern of the antenna elements in the array. Typically, identical elements are used in the array configurations, so that the element radiation pattern can be factored out and multiplied in final product. This is performed to simplify the multiplications. In a diversely polarized array configuration, element pattern of every element of the array should be accounted with due care for the polarization. The mounting position of the array element decides its electric field orientation.

If the array elements have dissimilar orientations, their polarization characteristics will not

be identical in the observation plane of interest. The respective polarization of the elements has major effects in the determination of the radiation pattern of the array. Under such a scenario it is not possible to factorize the element radiation pattern outside array steering vector. Rather it should be included within the steering vector. The array elements are denoted with numeric identity, which in-turn represents the co-ordinates of the position of the array element and thus there will a change in phase with respect to reference element. According to the array geometry of the design with respect to element orientation and its polarization characteristic, the corresponding elemental radiation pattern shall be multiplied with phase term of the array factor.

4.5 Antenna Array Configuration

For two dimensional DOA estimation, an antenna array of elements positioned at least in two axes is essential to estimate the azimuth ϕ and elevation θ angle of the DOA. In general, planar array configuration or L-shaped array are preferred for two dimensional DOA. In this thesis, the concept of diversely polarized array configurations are explored for two dimensional DOA estimation. The orthogonal polarized (vertical and horizontal polarized) RWG is used for the analysis in various array configurations. These orthogonally polarized array configurations are compared with the singly polarized conventional UPA configuration for the performance of two dimensional DOA through the simulation analysis.

To differentiate the influence of polarization in the antenna array configuration, different orthogonally polarized array configurations are proposed. The linear as well as planar array configurations with orthogonal polarization feature are proposed for determining 2D-DOA estimations. The proposed array configurations for the analysis are Orthogonally Polarized Planar Array (OPPA), Orthogonally Mounted Linear Array (OMLA) and Orthogonally Polarized Linear Array (OPLA). The 2D-DOA estimation of the proposed configurations are compared with the conventional singly polarized UPA configuration.

4.5.1 Uniform Planar Array (UPA)

A UPA chosen for analysis is a conventional 3×3 planar array configuration modelled as shown in Figure 4.1, where all the antenna elements are singly polarized (typically vertical). The planar arrangement of antenna spans square or rectangular grid in $x-y$ plane and antenna elements are indexed with spatial coordinates along x and y axes. In this

array configuration, the phase term in the array factor stated in Equation (4.4) reduces to Equation (4.8). Since there are no elements along the z- axis, the z coordinate of the phase term is ignored.

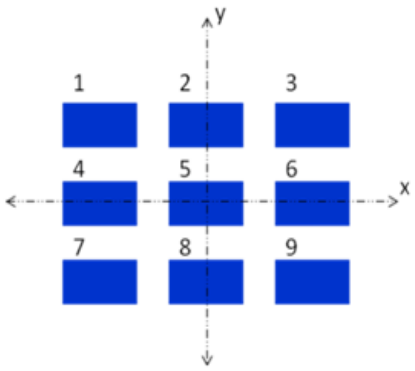

Figure 4.1: Conventional UPA

$$\beta_m(\theta,\phi) = x_m \sin\theta\cos\phi + y_m \sin\theta\sin\phi \tag{4.8}$$

4.5.2 Orthogonally Polarized Planar Array (OPPA)

A typical 3×3 planar array with adjacent elements rotated by 90°, which changes its polarization orthogonally with respect its adjacent elements is shown in Figure 4.2. In this array configuration, indices of the element are same as in the conventional planar array. The planar orthogonal array geometry is shown in Figure 4.2. The phase term in the array factor shall be accounted as expressed in Equation (4.8).

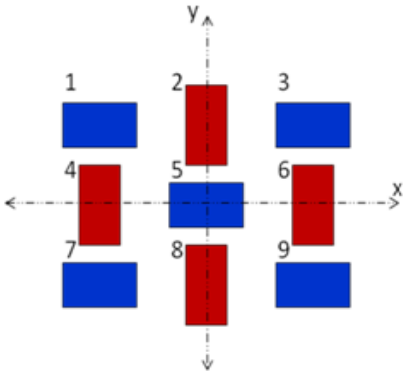

Figure 4.2: Orthogonal Polarized Planar Array

4.5.3 Orthogonally Mounted Linear Array (OMLA)

The OMLA configuration also involves both vertical and horizontal polarized elements. As shown in Figure 4.3, OMLA looks like a planar array. In the configuration of OMLA shown in Figure 4.3, the horizontally polarized antenna element '2' is placed on the vertically polarized antenna element '1' with no spacing between the edges of the mounted elements. However, these two orthogonally polarized elements exhibit a spacing of $(a+b)/2$ (center to center) along the y axis. There is a spacing along the x axis between successive like polarized elements. In view of the presence of the spatial variations of the elements along both x and y axes, the OMLA appears like a planar array. Since the size of array configuration shown in Figure 4.3 can be increased with the additional elements along the x axis only, this configuration tantamount to 'linear array'.

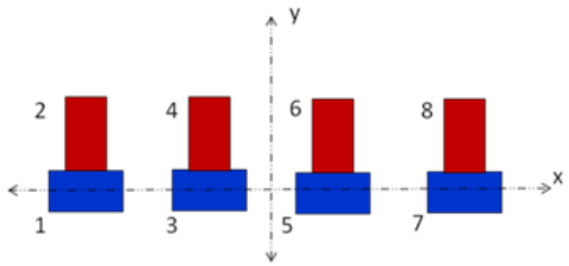

Figure 4.3: Orthogonal Mounted Linear Array

4.5.4 Orthogonally Polarized Linear Array (OPLA)

The classical linear array is modified to satisfy that adjacent elements are orthogonal to each other. In this array configuration, the antenna elements are mounted along only one axis (say x-axis). There is a the phase variation along the x-axis only. Thus the phase term mentioned in Equation (4.4) reduces to Equation (4.9).

$$\beta_m(\theta,\phi) = x_m \sin\theta\cos\phi \tag{4.9}$$

The OPLA is shown in Figure 4.4. Unlike typical linear array geometries, this OPLA configuration is capable of determining two dimensional DOA (both azimuth and elevation angles).

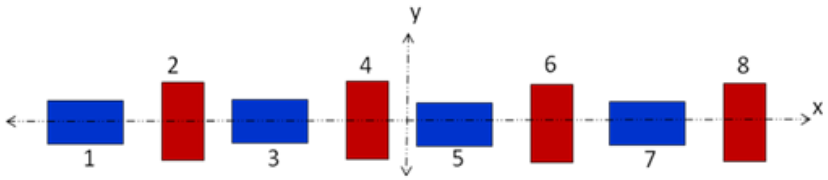

Figure 4.4: Orthogonally Polarized Linear Array

4.6 Simulation Environment

The simulation environment is configured through the signal modelling of the conventional uniform planar and proposed diversely polarized array configurations. As stated earlier X-band rectangular waveguide is chosen as an antenna for the analysis. The standard dimension of the X-band waveguide of width $a = 2.32cm$ and height $b = 1cm$ is considered. The RWG is operated at its TE_{10} dominant mode. The frequency and wavelength of the simulation setup are 9.375 GHz and 3.2cm respectively. The standard spectral MUSIC algorithm described in subsection 2.8.2.2 (Equations(2.32 and 3.7)) is used for the computation of the 2D-DOA estimation for the conventional and proposed orthogonal array configurations.

The elements of the array are oriented such that the array receives both the vertical and horizontal polarized components independently at their respective elements. The signals of opposite (orthogonal) polarization do not combine in space. However the samples received from the vertical and horizontal polarized antenna elements are combined to produce the spatial covariance matrix. The covariance between the vertical and horizontal polarized signal components are utilized to improve the accuracy and angular resolution of the DOA, when compared to the single polarized spatial covariance matrix of UPA.

4.7 Analysis of Accuracy of Estimation of 2D-DOA

The following simulation results illustrate the estimation accuracy of the proposed dual polarized array configurations and its results are compared with the singly polarized UPA configurations. The 2D-DOA estimation is analysed through the RMSE of the estimation for the SNR range of 0 - 30 dB and averaged over 200 Monte-Carlo iterations. In the comparison of estimation accuracy of 2D-DOA estimation, different array configurations namely UPA, OPPA, OMLA and OPLA are used.

4.7.1 Broadside Illumination

For the estimation accuracy of the 2D-DOA of single source of broadside illumination, a signal was modelled at azimuth angle $\phi = 35^\circ$ and elevation angle $\theta = 25^\circ$. The Figures 4.5, 4.6 and 4.7, 4.8 depict the accuracy through the RMSE of estimate of angles θ and ϕ respectively as the SNR is varied from 0 to 30 dB.

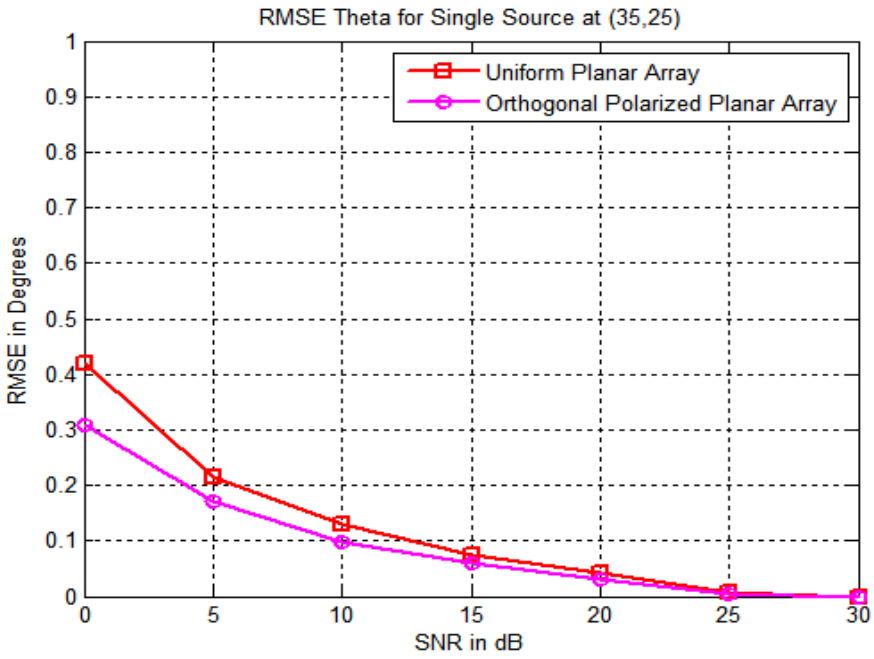

Figure 4.5: RMSE of Elevation Angle Estimation for Broadside Illumination at $(35^\circ, 25^\circ)$ for UPA and OPPA Configurations

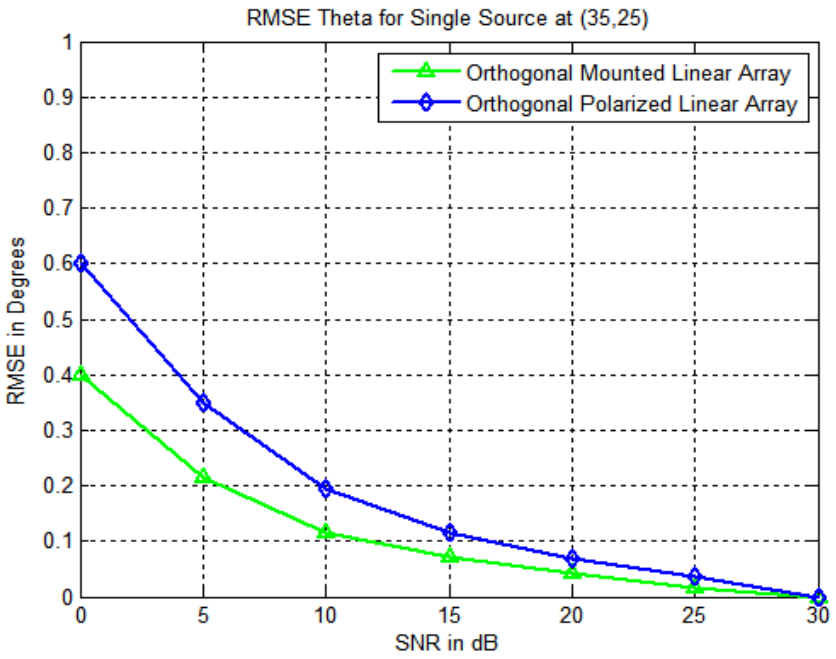

Figure 4.6: RMSE of Elevation Angle Estimation for Broadside Illumination at $(35°, 25°)$ for OMLA and OPLA Configurations

The results of RMSE of elevation angle θ of DOA estimation are shown in Figure 4.5 for UPA and OPPA as well as in Figure 4.6 for OMLA and OPLA. The results of Figures 4.5 and 4.6 illustrate that OPPA configuration exhibits least RMSE when compared to the UPA, OMLA and OPLA configurations. At low SNR scenario ($<$10 dB) a relative difference in RMSE is found to be (0.3°- 0.4°). At higher SNR, the relative difference in RMSE is still smaller. The ability of OPPA to estimate the elevation angle θ of DOA with least error is attributed to its elements which exhibit the spatial phase variation along x and y axes. The elements of OMLA configuration experience the spatial phase variation predominantly along x axis when compared to y axis and hence a small difference in RMSE with respect to that of OPPA is present. The complete absence of spatial phase variation along y axis leading to relatively higher increased RMSE can be seen in OPLA configuration. In UPA configurations, the antenna elements experience spatial phase variation along x and y axes. However, UPA configuration suffers from the absence of orthogonal polarized antenna elements leading to a slightly more RMSE compared to OPPA configuration. By comparing the planar array configurations for DOA estimation, UPA and OPPA show a relative reduction of RMSE at lower SNRs .

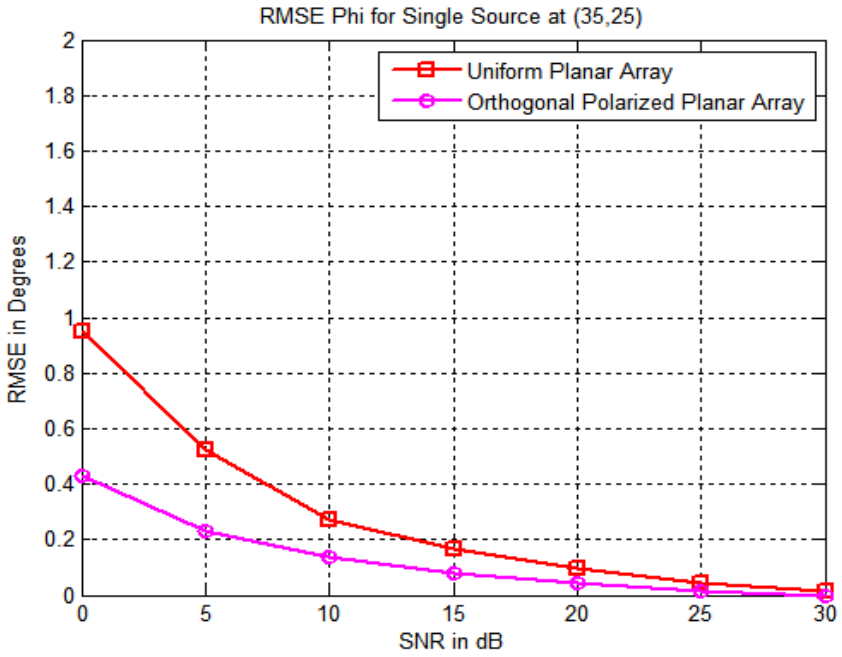

Figure 4.7: RMSE of Azimuth Angle Estimation for Broadside Illumination at $(35°, 25°)$ for UPA and OPPA Configurations

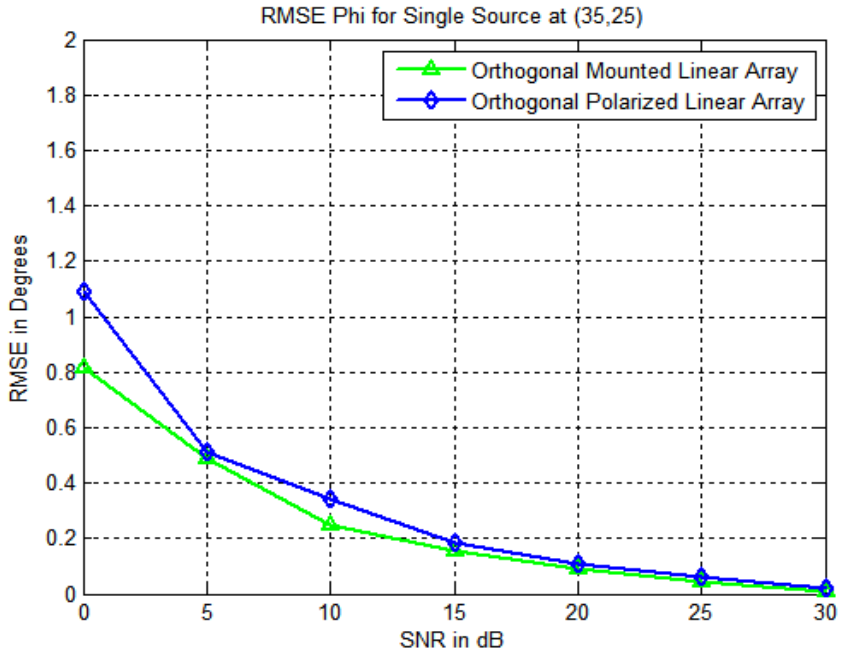

Figure 4.8: RMSE of Azimuth Angle Estimation for Broadside Illumination at $(35°, 25°)$ for OMLA and OPLA Configurations

Similarly, the results of RMSE of azimuth angle ϕ of DOA estimation are shown in Figure 4.7 for UPA and OPPA as well as Figure 4.8 for OMLA and OPLA. The results of Figure 4.7 and 4.8 reveal that the OPPA configuration exhibits the lowest RMSE compared to UPA, OMLA and OPLA configurations. The relative comparison of RMSE among the four different array configurations shows the same trend with respect to the azimuth and elevation angle estimations, which can be seen from the Figures 4.5, 4.6, 4.7 and 4.8. The RMSE of azimuth angle of DOA estimation is more (from Figure 4.7 and 4.8) when compared to the RMSE of elevation angle estimation (from Figure 4.5 and 4.6) since the incidence angle is modelled for broadside illumination. It is well known in array theory, that conventionally the linear and planar array configurations are more effectively utilized in broadside region rather endfire region.
The OPLA is featured with an inaccuracy to 0.6° at 0 dB SNR. The performance of singly polarized UPA and OMLA is not good with respect to other configurations. In case of the azimuth angle, the OPLA exhibits array inaccuracy up to 1.2° at 0 dB SNR. However in both the azimuth and elevation angular estimation, the OPPA is superior among all other array configurations.

4.7.2 End-fire Illumination

Similar to broad side illumination, accuracy of the 2D-DOA estimation of single source closer to End-fire illumination with azimuth angle $\phi = 60^{\circ}$ and elevation angle $\theta = 60^{\circ}$ is analysed. Figures 4.9, 4.10, 4.11 and 4.12 reveal the accuracy through the RMSE of the estimation of elevation angle θ and azimuth angle ϕ respectively.

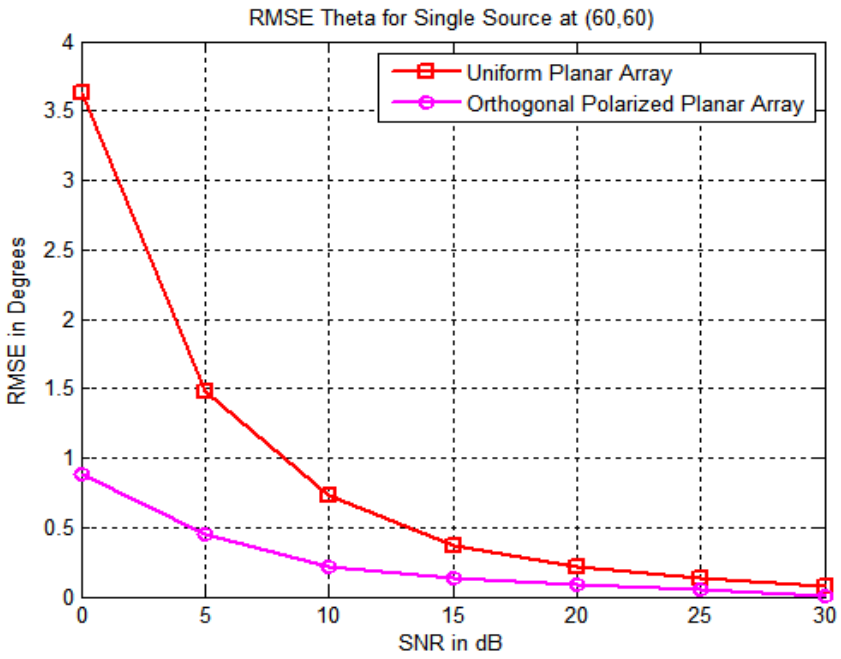

Figure 4.9: RMSE of Elevation Angle Estimation for End-fire Illumination at $(60°, 60°)$ for UPA and OPPA Configurations

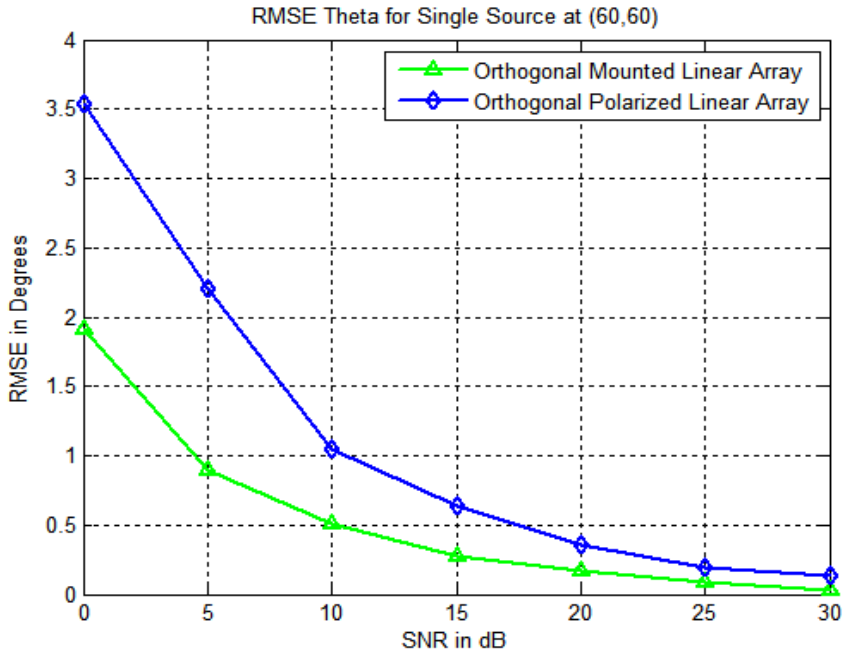

Figure 4.10: RMSE of Elevation Angle Estimation for End-fire Illumination at $(60°, 60°)$ for OMLA and OPLA Configurations

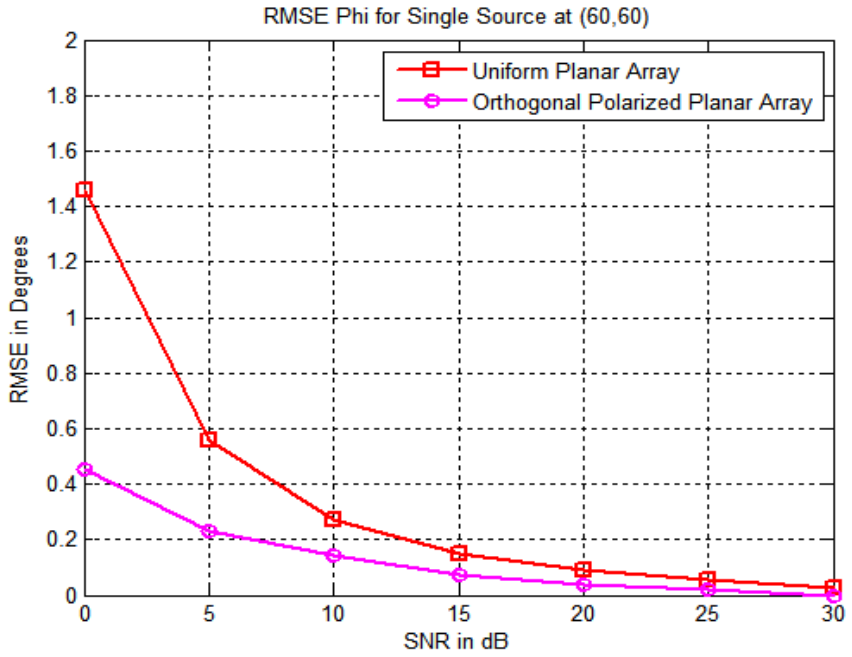

Figure 4.11: RMSE of Azimuth Angle Estimation for End-fire Illumination at $(60°, 60°)$ for UPA and OPPA Configurations

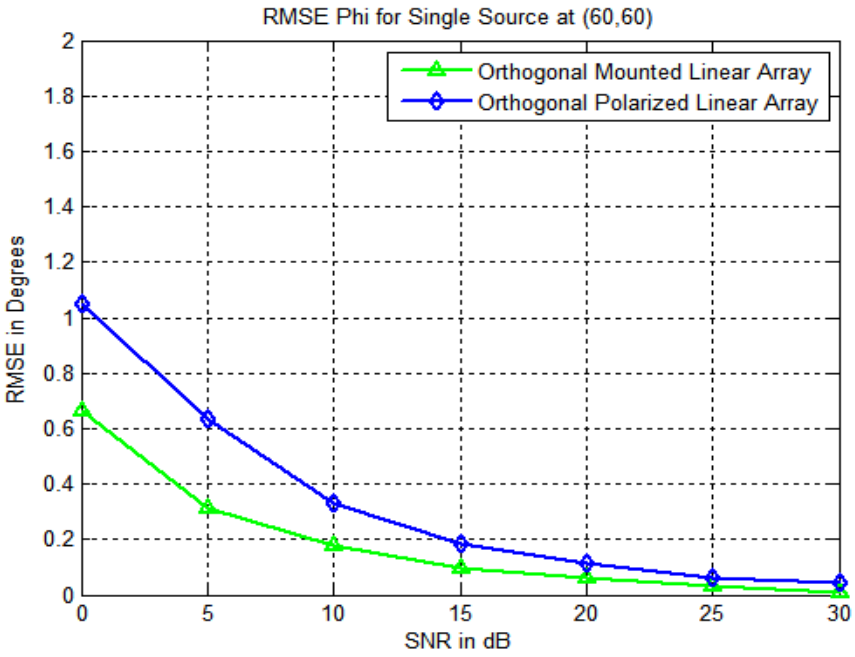

Figure 4.12: RMSE of Azimuth Angle Estimation for End-fire Illumination at $(60°, 60°)$ for OMLA and OPLA Configurations

The results of Figure 4.9 illustrate that a maximum error of 3.5° at SNR of 0 dB for both UPA configuration and OPLA configuration. The OPPA achieves a minimum RMSE of 0.8° at 0 dB. The OMLA exhibits a relatively poorer performance amongst the array configurations. The RMSE of the azimuth angle ranges between 0.5° to 1.5° for the different array configurations. The conventional UPA exhibits error of 1.5° at SNR of 0 dB and continues to perform similar to the OPLA configuration. The OMLA configuration continues to exhibit average performance and the OPPA shows superior performance among all other array configurations.

4.8 Discussion of Results on 2D-DOA of Single Source

The 2D-DOA estimations obtained through OPPA exhibit relatively better performance over singly polarized UPA and also with OPLA, implying that, diversely polarized planar array configuration is better than UPA configuration. From the simulation analysis it is also evident that in 2D-DOA estimation, the angle of illumination of sources is also a factor in the estimation accuracy provided the antenna element patterns are considered in the analysis. From the analysis of broadside and end-fire illumination of signal sources, it is shown that estimation accuracy depends on the region of illumination with respect to the antenna geometry and antenna radiation pattern. In general, the broadside illumination has lesser estimation error when compared to the end-fire illumination. When the azimuth and elevation angles of DOA broadly fall into broadside illumination, the estimation accuracy of elevation angle θ is greater than the source illuminated in end-fire region. This is due to higher gain of the radiation pattern in the broadside region and progressively reduced gain in the end-fire region. The accuracy of azimuth angle ϕ estimation is almost the same irrespective region of illumination. However minor changes are seen in the accuracy due to the spatial phase variations in the configuration. The RMSE of DOA estimation with OPLA is more compared to the conventional singly polarized array due to the linear arrangement of element of elements. The spatial phase variation only along the x axis is present in OPLA configuration, where as spatial phase variations in the both x and y axes are seen in the other array configuration. However it is evidently clear from the simulation analysis that, the OPLA although a geometrically linear configuration is a potential candidate to estimate 2D-DOA estimation. A conventional singly polarized linear array geometry is not adequate for 2D-DOA estimation.

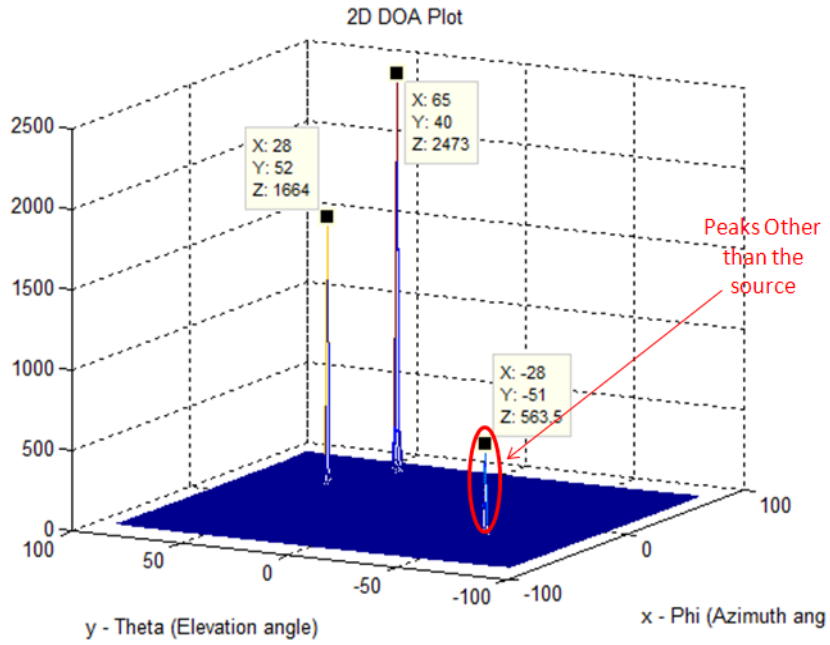

Figure 4.13: Two Dimensional DOA Estimation of Two Sources using UPA for 20 dB SNR

4.9 Analysis of 2D-DOA Estimation for Two Sources

After having established the validity of proposed array configurations for the 2D-DOA estimation with a single source, simulation studies have been performed to substantiate the performance of 2D-DOA estimation for two sources. The conventional UPA, OPPA, OMLA and OPLA as indicated in the Figures 4.1, 4.2, 4.3 and 4.4 respectively are considered for the analysis. The 2D-MUSIC algorithm is modelled for the various array configurations for the 2D-DOA estimation. Modelling of the two sources with arriving angles of $(\theta_1 = 52^\circ, \phi_1 = 28^\circ)$ and $(\theta_2 = 40^\circ, \phi_2 = 65^\circ)$ has been carried for the varying SNR values of 20 dB, 10 dB and 0 dB. This analysis is carried out to compare the distinguishing features of the estimation of DOA angles obtained with the various array configurations.

4.9.1 Results of 2D-DOA of Two Sources at 20 dB SNR

In this subsection, a detailed analysis of the simulation results of 2D-DOA estimation with two sources derived with various array configurations is presented. For the purpose of simulation studies, signal modelling has been performed with 2D-DOA azimuthal and elevation angles of two sources as $(\theta_1 = 52^\circ, \phi_1 = 28^\circ)$ and $(\theta_2 = 40^\circ, \phi_2 = 65^\circ)$.

Figure 4.13 illustrates the results of estimating 2D-DOA angles of two sources derived with conventional UPA. There is a perfect match between the 2D-DOA angles assumed in the signal modelling and the estimated angles derived through the MUSIC based DOA estimation algorithm. The noticeable observation in the results of Figure 4.13 is the presence of an additional peak whose magnitude is significantly lesser than the other two peaks. Based on this inference, one can ignore it as a fictitious one.

The appearance of additional peak in the UPA configuration is due to larger inter-element spacing between the array elements because of which there is an inadequacy of spatial samples during one wavelength of the signal. This in turn leads to spatial aliasing resulting in additional peak or peaks. The minimum inter-element spacing along the x axis for UPA configuration itself is greater than the half of the wavelength (considering the dimensions of X-band RWG as (2.32cmx1cm) at λ of 3.2cm corresponding to 9.375 GHz). Assuming negligibly small wall thickness of the waveguide, the minimum inter-element spacing along the x-axis is equal to 2.32cm, which is 0.725λ and along the y-axis it is 0.31λ. In the case of OPPA, the minimum spacing between the successive elements along both x and y axes is equal to 1.16 + 0.5 = 1.66 cm, which is equivalent to 0.518λ The inter-element spacing much greater than $\lambda/2$ in the case of UPA is due to the physical aperture and the geometrical arrangement of its elements. The orthogonal array configurations such as

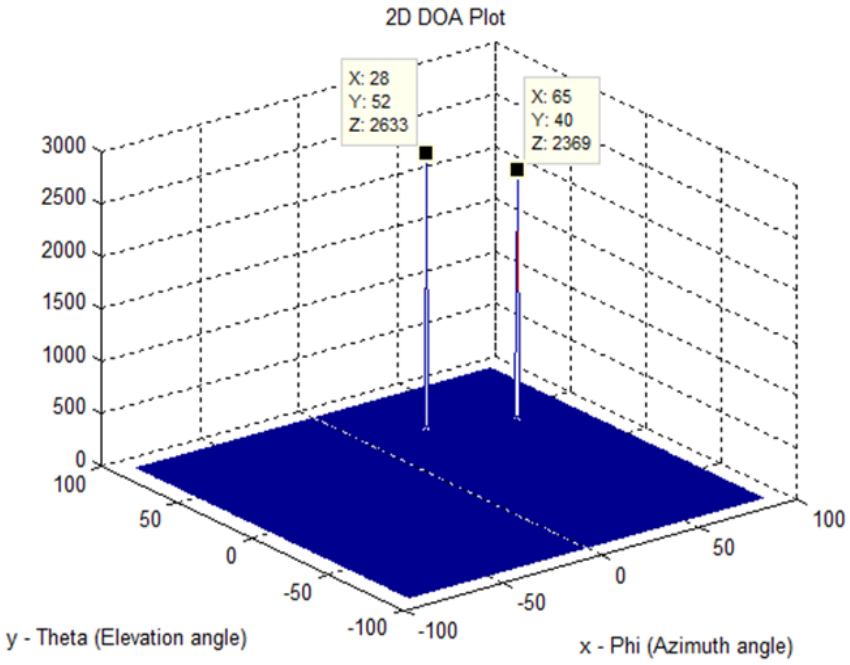

Figure 4.14: Two Dimensional DOA Estimation of Two Sources using OPPA for 20 dB SNR

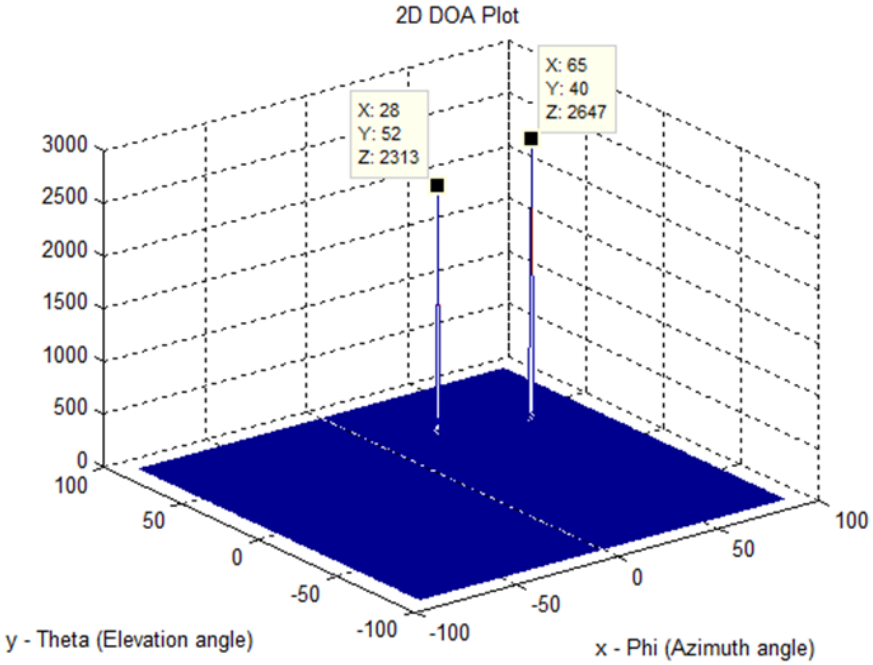

Figure 4.15: Two Dimensional DOA Estimation of Two Sources using OMLA for 20 dB SNR

OPPA, OMLA and OPLA have sufficient spatial samples due to their smaller inter-element spacing and hence the additional fictitious peaks do not occur.

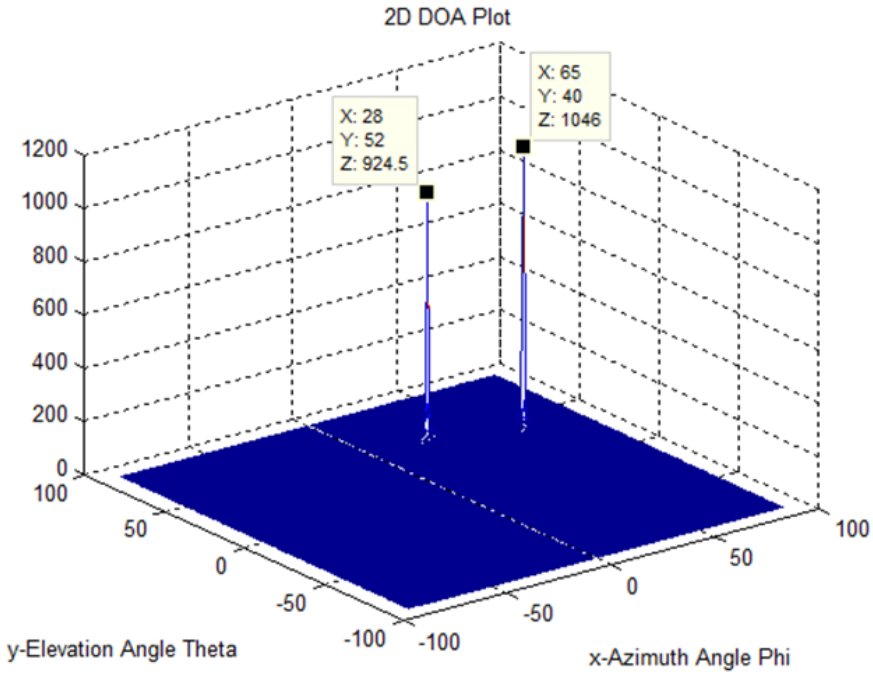

Figure 4.16: Two Dimensional DOA Estimation of Two Sources using OPLA for 20 dB SNR

The corresponding simulation results obtained with OPPA are shown in Figure 4.14. The results of 2D-DOA estimation shown in Figure 4.14 match exactly with the azimuth and elevation angle used in signal modelling. Unlike with UPA, 2D-DOA estimation with OPPA is not associated with any additional peaks.

The simulation results of 2D-DOA estimation with two sources derived through OMLA are shown in Figure 4.15. Similar to the case of OPPA, the simulation results of 2D-DOA with OMLA also produce only two peaks corresponding to the azimuth and elevation angle of two sources assumed in the signal modelling. Also, there are no additional or fictitious peaks. The analogous simulation results of 2D-DOA estimation with OPLA are shown in Figure 4.16. The estimation results of 2D-DOA azimuth and elevation angles of two sources derived through OPLA match with the azimuth and elevation angles of sources assumed in the signal modelling. The results of Figure 4.16 also do not show any additional peaks.

4.9.2 Results of 2D-DOA of Two Sources at 10 dB SNR

In this subsection, the influence of SNR assumed in the signal modelling on the reliability and accuracy of the 2D-DOA estimation derived through various antenna array configurations is analysed. In this subsection, the simulation studies assume an SNR of 10 dB. The simulation results of the 2D-DOA estimation with two sources derived through conventional UPA are shown in Figure 4.17. As in the case of SNR of 20 dB shown in Figure 4.13, even with SNR 10 dB, there is an additional peak predicted and the magnitude of the additional peak is relatively higher than the corresponding result with SNR of 20 dB. Figure 4.18 illustrates the 2D-DOA estimation with two sources for 10 dB SNR scenario derived with OPPA. The results with the configuration of OPPA also do not predict any additional peak thereby avoiding the ambiguity. The estimation of 2D-DOA angles of two sources exactly match with the azimuth and elevation angles of sources assumed in the signal modelling.

The simulation results of 2D-DOA with two sources derived with OMLA are depicted in Figure 4.19. The 2D-DOA estimation obtained with OMLA configuration of array also does not predict any additional peaks. The analogous results of 2D-DOA with two sources for 10 dB SNR derived with OPLA are shown in Figure 4.20. As with other OPPA, the

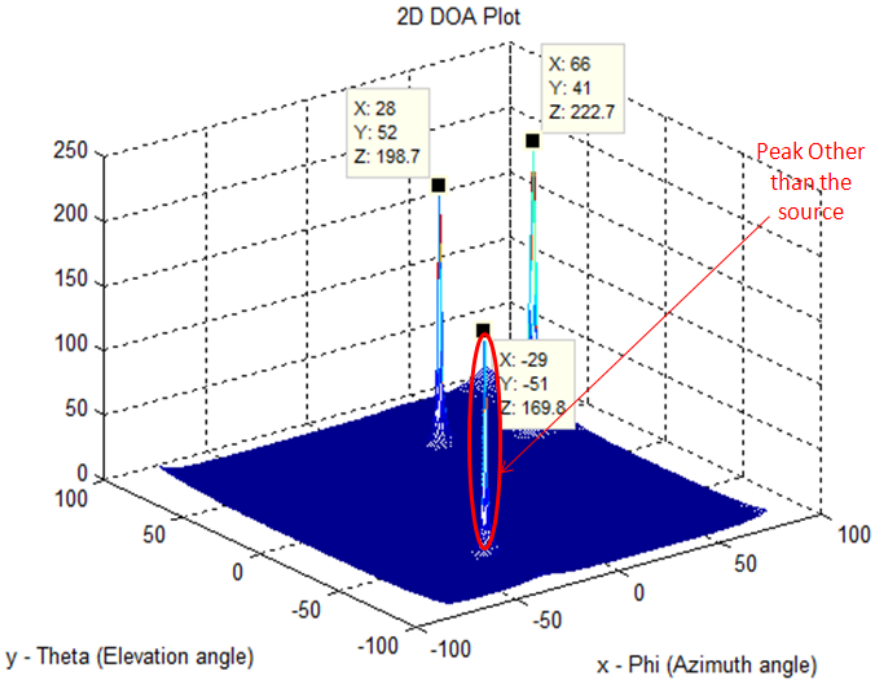

Figure 4.17: Two Dimensional DOA Estimation of Two Sources using UPA for 10 dB SNR

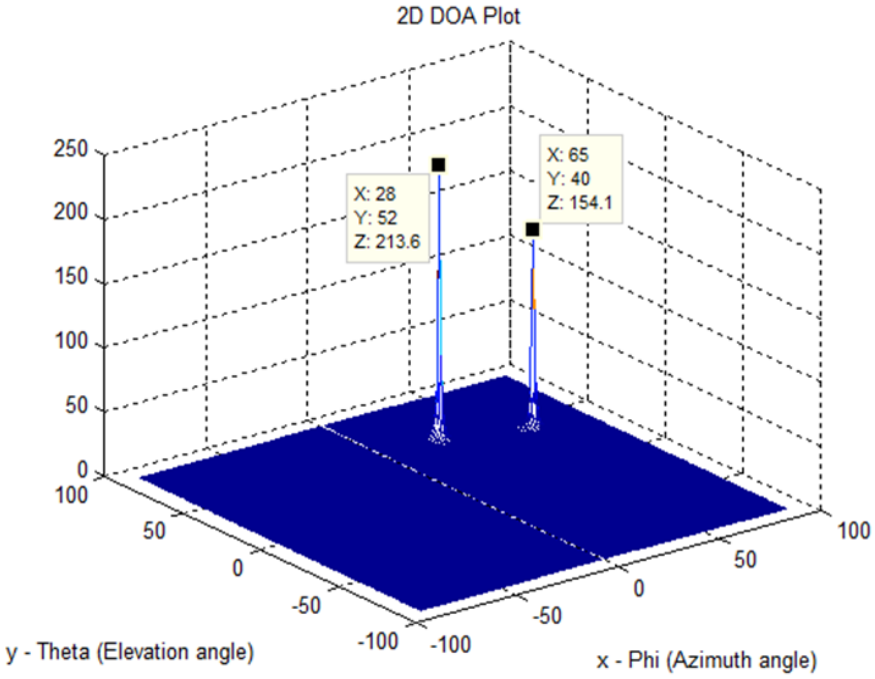

Figure 4.18: Two Dimensional DOA Estimation of Two Sources using OPPA for 10 dB SNR

simulation results of 2D-DOA estimation with OPLA do not predict any additional peak.

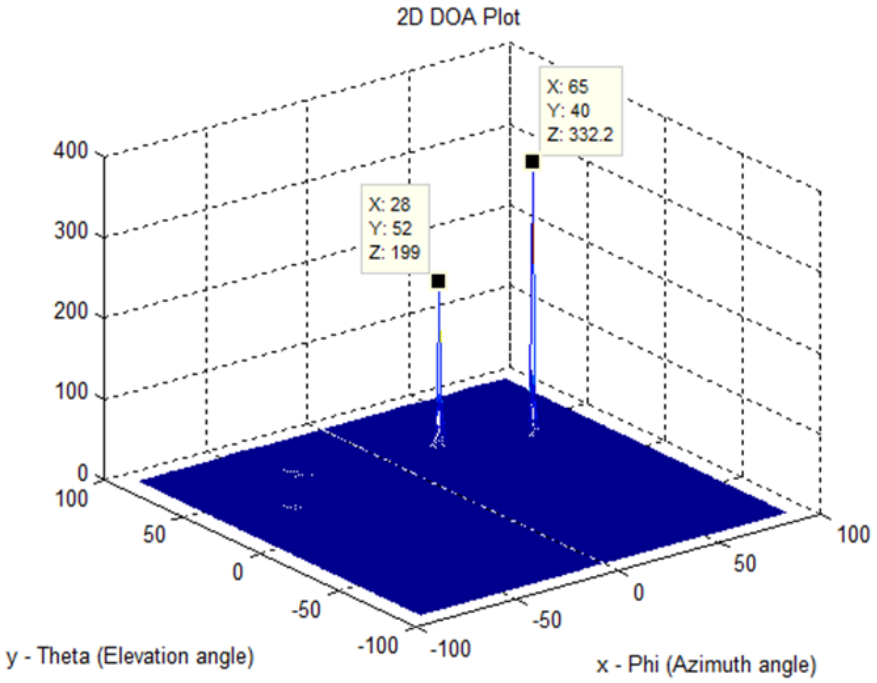

Figure 4.19: Two Dimensional DOA Estimation of Two Sources using OMLA for 10 dB SNR

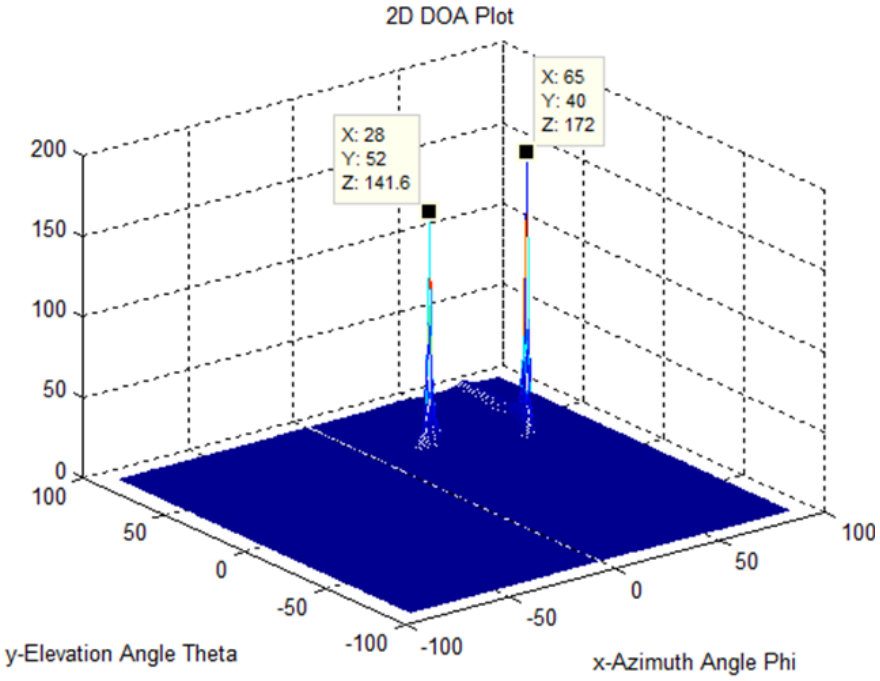

Figure 4.20: Two Dimensional DOA Estimation of Two Sources using OPLA for 10 dB SNR

4.9.3 Results of 2D-DOA of Two Sources at 0 dB SNR

In this subsection, the simulation studies emphasise the influence of 0 dB SNR on the accuracy of 2D-DOA estimation with two sources. A scenario of 0 dB SNR implies that

the signal power and noise power are equal.

The results of simulation studies on 2D-DOA obtained through conventional singly polarized UPA are shown in Figure 4.21. The results of Figure 4.21 indicate the presence of multiple additional peaks whose amplitudes are comparable or higher that those peaks which coincide with the true arrival angles of the two sources. From the simulation studies carried out with singly polarized UPA with SNR values varying from 0 to 20 dB, it is clearly evident that this UPA configuration results in additional fictitious peak leading to an ambiguity of estimating the true values of 2D-DOA angles of multiple sources. The

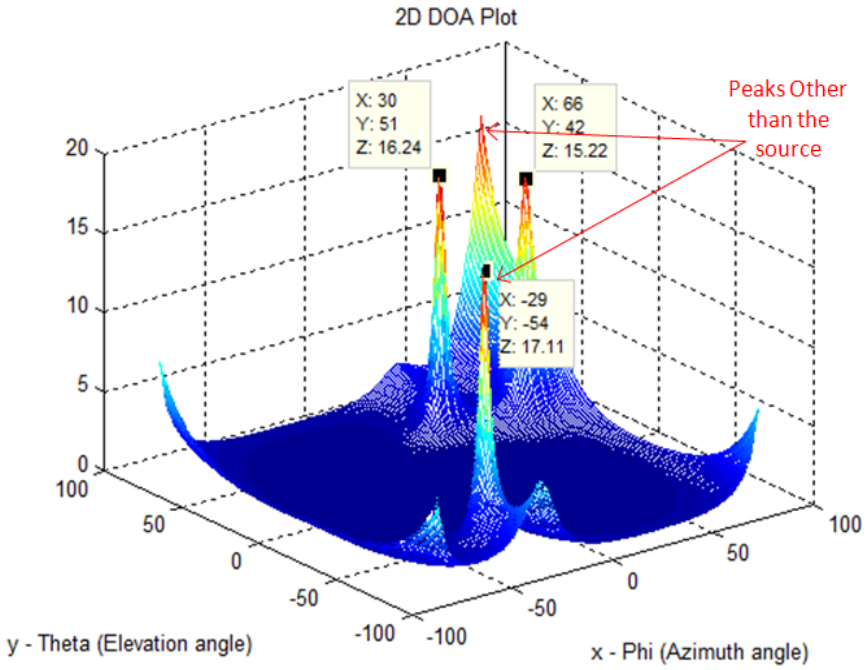

Figure 4.21: Two Dimensional DOA Estimation of Two Sources using UPA for 0 dB SNR

corresponding simulation results obtained through OPPA are shown in Figure 4.22. Like in cases of SNR of 20 dB and 10 dB, even in case of 0 dB SNR, the estimation of 2D-DOA angles with OPPA does not produce any additional peak. Figures 4.23 and 4.24 depict the analogous results on estimation of 2D-DOA angles with two sources obtained through OMLA and OPLA respectively. Apart from the accuracy of the estimated azimuth and elevation angles of the two sources, the noteworthy observation is the absence of additional peak and thus avoiding the ambiguity in ascertaining the true angles of arrival of distant sources.

From the simulation studies presented in this subsection, it is easy to infer that for the 2D-DOA estimation with the presence of two sources, the array configurations proposed in

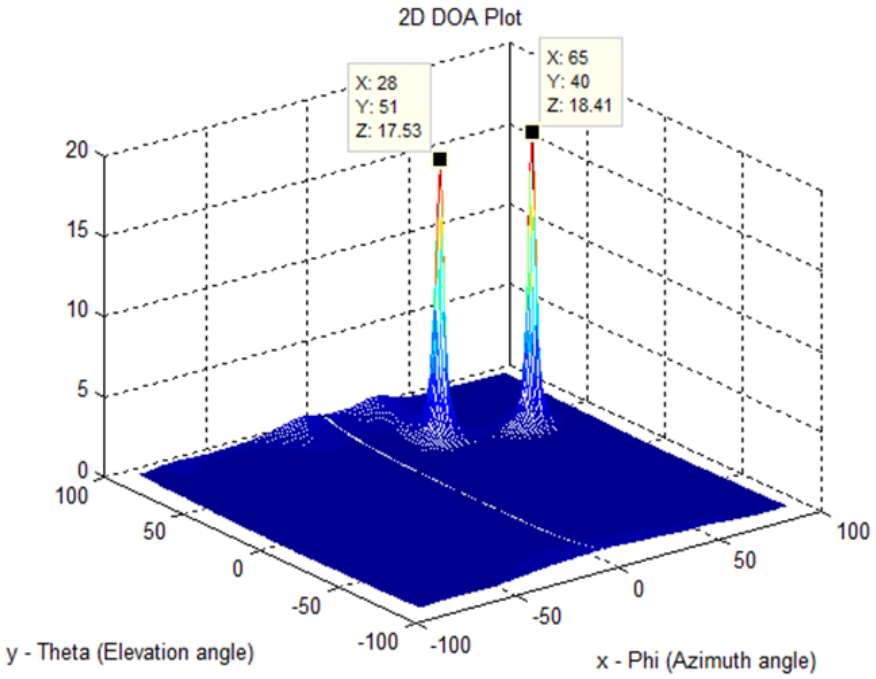

Figure 4.22: Two Dimensional DOA Estimation of Two Sources using OPPA for 0 dB SNR

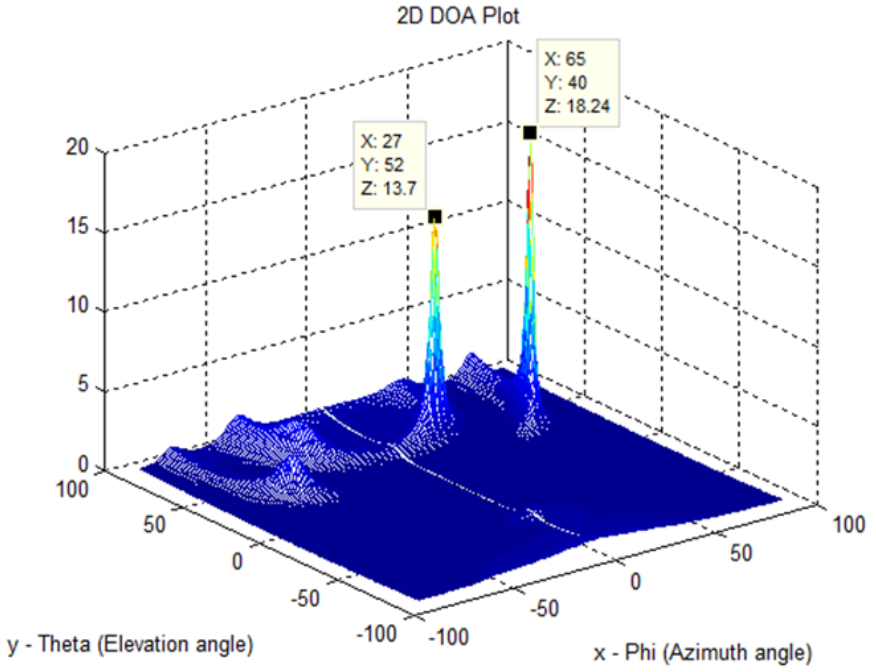

Figure 4.23: Two Dimensional DOA Estimation of Two Sources using OMLA for 0 dB SNR

the thesis that are featured with orthogonal polarization ensure relatively more accurate results and they are also associated with the distinct feature of absence of fictitious peaks.

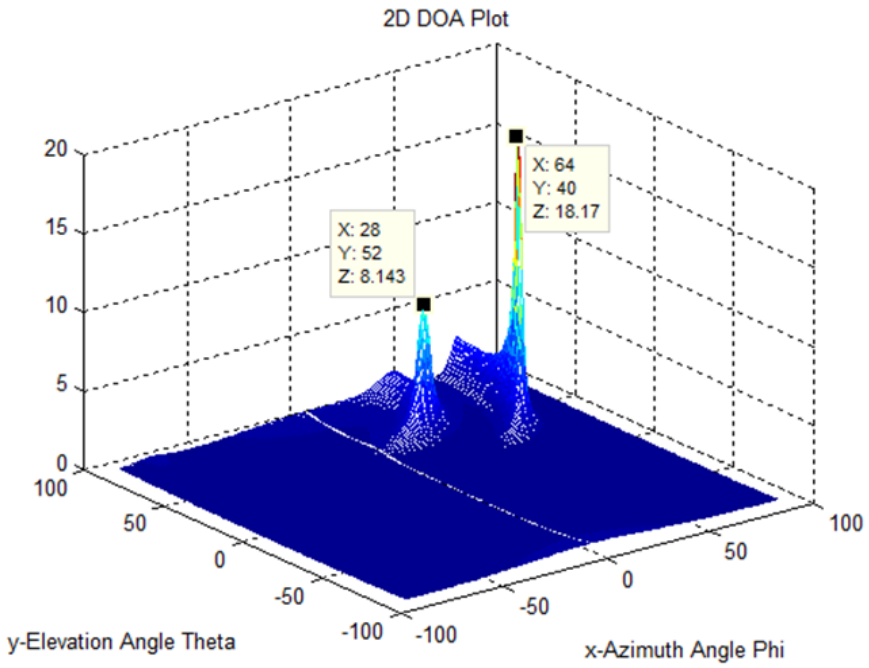

Figure 4.24: Two Dimensional DOA Estimation of Two Sources using OPLA for 0 dB SNR

The same observation cannot be extended to the case of array configuration featured with single polarization. This inference is valid for all the three cases of SNR values (20 dB, 10 dB and 0 dB) considered in the simulation studies.

4.9.4 Inference from the Results of 2D-DOA of Two Sources

From the results shown in Figures 4.13-4.24, it is evident that the proposed diversely (dual) polarized array configurations estimate the 2D-DOA of two sources accurately and detected peaks are clearly distinguishable. The single polarized conventional UPA configuration suffers in distinguishing the sources. This UPA exhibits extra peaks due to the non availability of spatial phase decorrelation of the polarized components. The results of UPA continues to produce extra peaks for all values of SNR ranging from 0 to 20 dB. The magnitude of the fictitious peak detected shows an increasing trend when the SNR decreases and may mislead to treating it as an actual DOA of sources in the lower SNRs scenarios.

In MUSIC algorithm, the distance between the signal subspace and the noise subspace components is computed. Since the signal subspace and noise subspace are orthogonal to each other, the distance should be ideally zero and its inverse leading to infinity. For

the case of lower SNR, the higher variance of noise overlaid on the signal disturbs the orthogonality between signal and noise subspace vectors. The magnitude of the DOA estimation peak is inversely proportional to orthogonality between the signal and noise subspace vectors. In higher SNR scenario, lesser variance of noise leads to improved orthogonality and therefore higher magnitude of estimation peaks. Hence SNR determines the magnitude of true DOA peak as well as the fictitious peaks.

The proposed diversely (orthogonally) polarized array configurations are able to distinguish multiple sources for all ranges of SNR values. However in the proposed diversely polarized configurations, the extra peaks are of diminished magnitude and are clearly distinguishable from the true peaks corresponding to the DOA of actual sources. A generic observation which holds uniformly to all the array configurations is that, the magnitude of detected peaks increases with increased value of SNR assumed in signal modelling.

4.9.5 Eigenvalues based Scheme for Distinguishing Sources

In the previous section, analysis of 2D-DOA estimation to distinguish the sources was on the basis of detectable peaks. In this section, the utility of eigenvalue to distinguish the number of sources is presented. The eigenvalue spread of the correlation matrix in any subspace based estimation technique is a significant parameter.

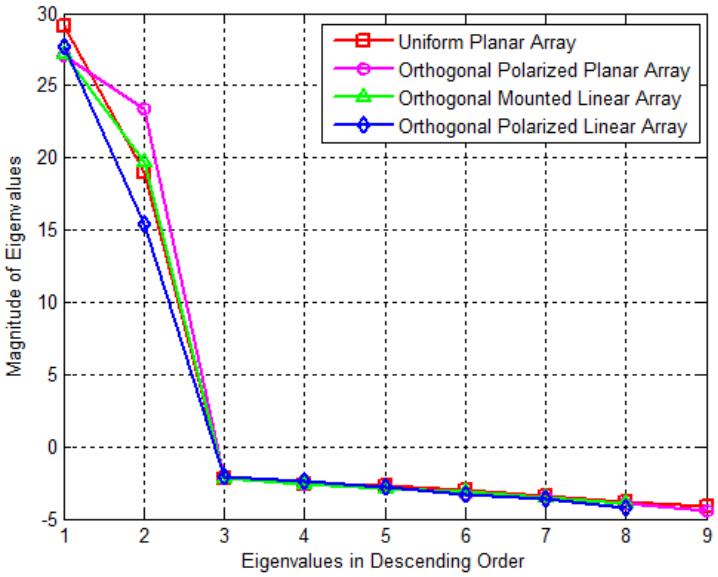

Figure 4.25: Eigenvalue Spread for Two Sources SNR = 20 dB

The spread of the eigenvalues are analysed in 2D-DOA for the two sources at $(\theta_1 = 52^\circ, \phi_1 = 28^\circ)$ and $(\theta_2 = 40^\circ, \phi_2 = 65^\circ)$. The analysis is carried for the range of SNR values like 20 dB, 10 dB, 5 dB and 0 dB. The eigenvalues are sorted in a descending order and have been compared for the different array configurations.

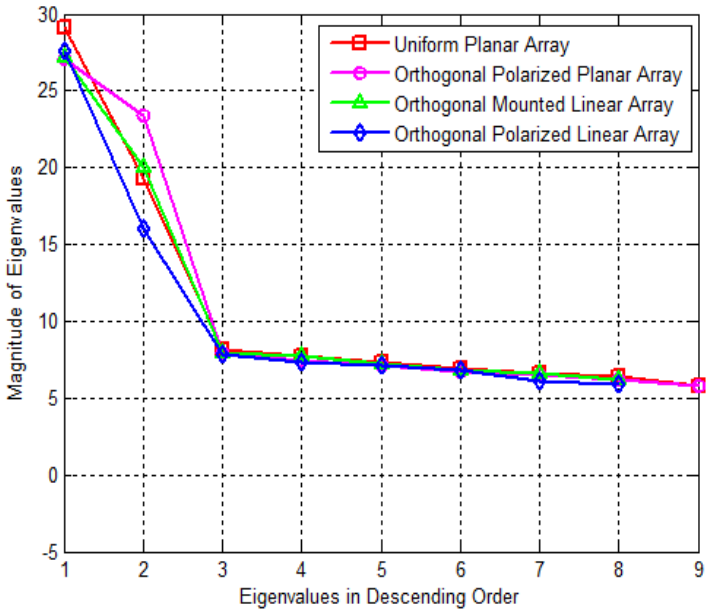

Figure 4.26: Eigenvalue Spread for Two Sources SNR = 10 dB

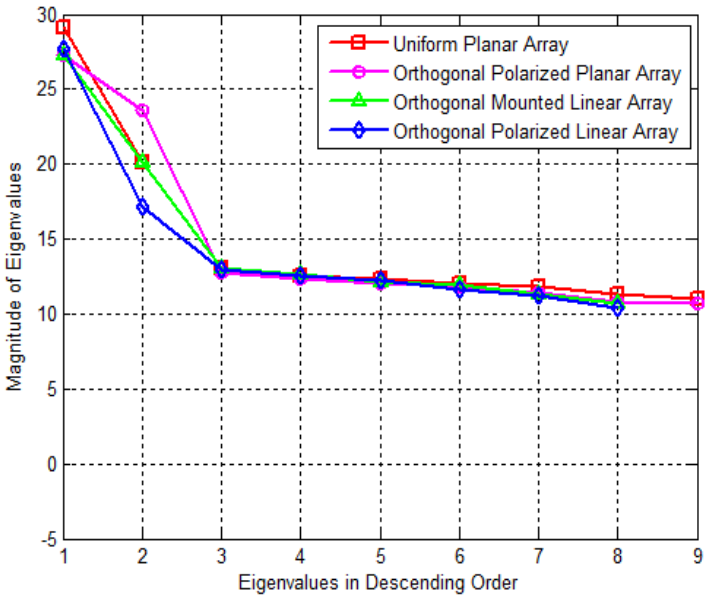

Figure 4.27: Eigenvalue Spread for Two Sources SNR = 5 dB

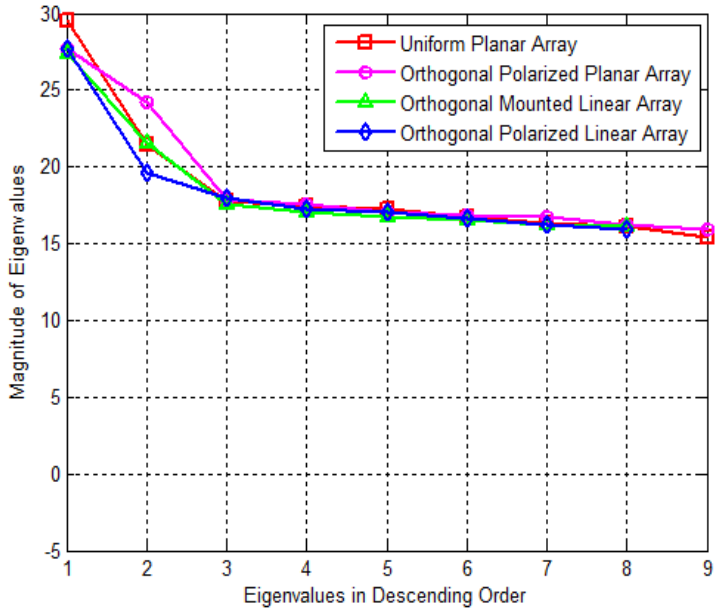

Figure 4.28: Eigenvalue Spread for Two Sources SNR = 0 dB

The sorted eigenvalues have highest magnitude corresponding to the actual DOA of sources (signals) initially. The magnitude of eigen values corresponding to noise power will be negligibly small and tends to zero. This can be distinguished as, the first P number

of eigenvalues correspond to the signal subspace and the remaining $P+1$ to M correspond the noise subspace eigenvectors, where P is number of incoming sources. Distinguishing the eigenvalues of signal subspace and eigenvalues of noise subspace can be achieved by the Minimum Discrimination Length (MDL) techniques and Akaike Information Criteria (AIC) algorithm (Wax, 1989; Wax & Kailath, 1985; Nadler, 2010). In this thesis, the simulation analysis assumes the total number of sources impinging on the array are aprior known and therefore performing MDL and AIC is beyond the scope of analysis. In this thesis, such an assumption is not only possible but is also not appropriate. Therefore the separation of eigenvalues belonging to signal subspace and noise subspace is beyond the scope of the work.

4.9.6 Inference of Eigenvalues under various SNRs

It is observed from the analysis, that eigenvalues corresponding to the noise subspace tends to be more towards zero as the SNR increases. This is true with the results obtained with all the array configurations. For two sources, the first two eigenvalues are corresponding to the signal subspace and the remaining eigen values correspond to the noise subspace.

The computed eigenvalues of the covariance matrix used for the estimation of 2D-DOA angles of two sources with SNR 20 dB are shown in Figure 4.25. From the results of Figure 4.25, it is seen that the first two eigenvalues which correspond to the two actual sources have significant amplitude. The magnitudes of other eigenvalues are considerably smaller nearing zero. Such an observation is valid for all the four array configurations considered in this thesis. As the SNR value is decreased to 10 dB, the magnitude of 3^{rd} to 9^{th} eigenvalues (belonging to noise subspace) increases as can be seen from the results of Figure 4.26. But the magnitude of the first two eigenvalues which belong to the signal subspace are much higher.

The significant magnitude of the first and second eigenvalue which are said to be primary eigenvalues (also called as principal components) indicate the clear distinguishing feature of the estimated DOA of two sources from the noise. The eigenvalues having least magnitudes and whose values significantly differ from the primary eigenvalues are also known as secondary eigenvalues. The sum of magnitudes of the secondary eigenvalues denote the amount of noise power present in the signal. The noise is measured as variance denoted by σ^2. Figures 4.27 and 4.28 depict the variation of amplitude of eigenvalues of

the covariance matrix for SNR of 5 dB and 0 dB respectively. With further decrease in SNR, the magnitude of eigenvalues from 3^{rd} to 9^{th} are relatively higher. But the magnitudes of 1^{st} and 2^{nd} eigenvalues are more prominent.

The divergence of signal component to the noise component is evident in the lower SNR scenario of 0 dB and 5 dB. The OPPA configuration shows better distinguishing capability even under lower SNR scenario, which is evident from the higher magnitudes of the primary eigenvalues (1^{st} and 2^{nd}) as can be observed from Figures 4.27 and 4.28. The raise of noise eigenvalues is obvious in the lower SNR case due to the increase in noise power. The other array configurations such as OMLA and UPA also exhibit similar performance. The OPLA shows better magnitude in the estimation of number of sources as seen from the results of Figures 4.27 and 4.28.

4.10 2D-DOA for Three Sources at SNR of 0 dB

Without incorporating any changes to array configurations, simulation studies have been carried out for 2D-DOA estimation with 3 sources. The simulation results of the

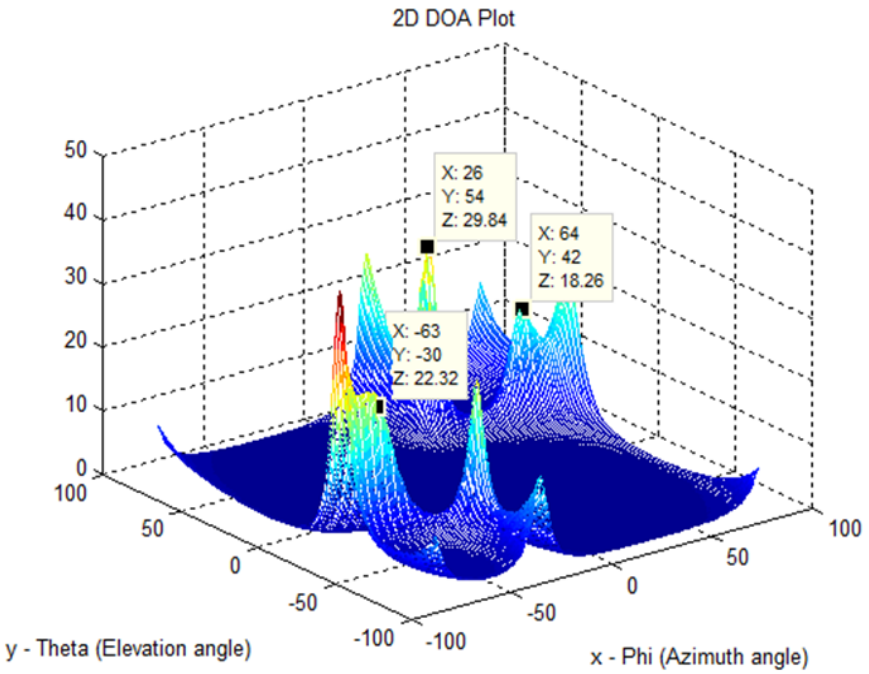

Figure 4.29: Two Dimensional DOA Estimation of Three Sources using UPA for 0 dB SNR

estimation of 2D-DOA angles with 3 sources under SNR scenario of 0 dB obtained with

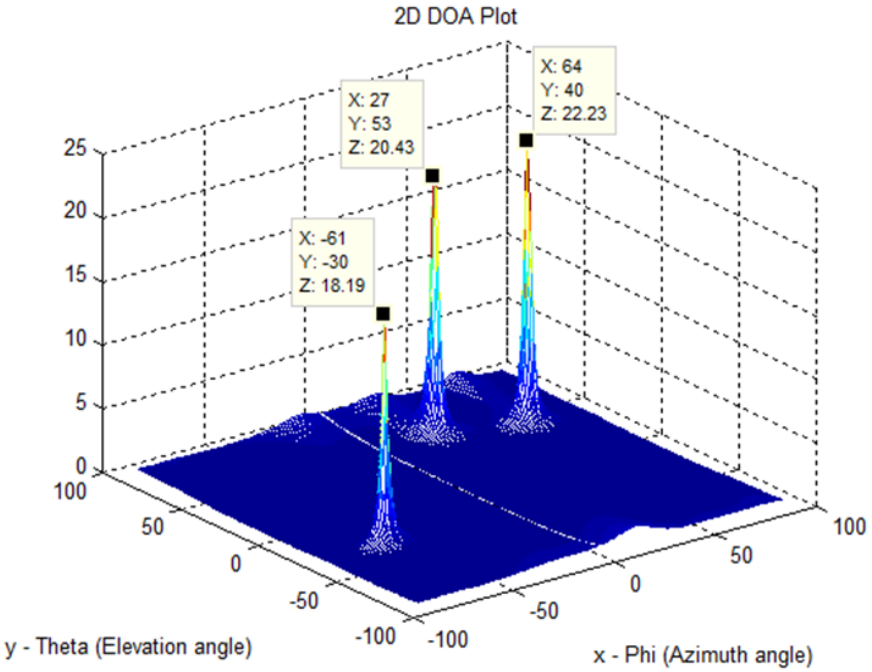

Figure 4.30: Two Dimensional DOA Estimation of Three Sources using OPPA for 0 dB SNR

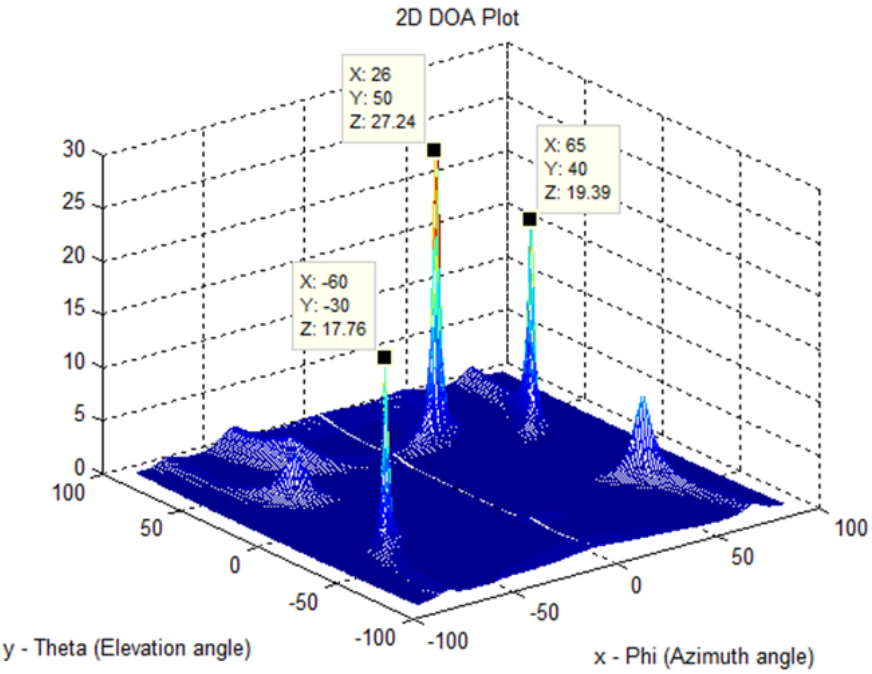

Figure 4.31: Two Dimensional DOA Estimation of Three Sources using OMLA configuration for 0 dB SNR

the conventional single polarized UPA are depicted in Figure 4.29. In the simulation studies with three sources, the azimuth and elevation angles used in the modelling of signal

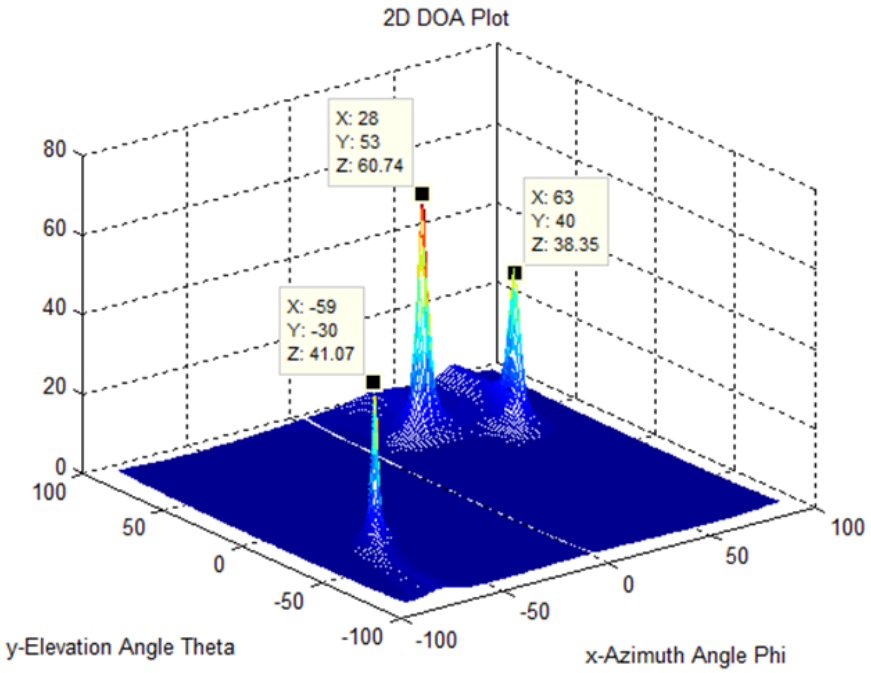

Figure 4.32: Two Dimensional DOA Estimation of Three Sources using OPLA for 0 dB SNR

impinging on the array configuration of DOA estimation system are $(\theta_1 = 52^\circ, \phi_1 = 28^\circ)$, $(\theta_2 = 40^\circ, \phi_2 = 65^\circ)$ and $(\theta_3 = -30^\circ, \phi_3 = -60^\circ)$.

As revealed by the results of Figure 4.29, the estimation of 2D-DOA with conventional UPA is associated with numerous additional peaks which are fictitious. In addition, the additional peaks which are supposed to have information on the DOA angles of true sources have angular coordinates which are different from the ones used to simulate the impinging signal.

The corresponding results derived through the OPPA are shown in Figure 4.30. As far the cases with single and two sources, the estimation of 2D-DOA angles with three sources using OPPA does not show any additional peaks thus avoiding the ambiguity. The estimated 2D-DOA angles of all the 3 sources are close to the ones assumed while modelling the signal impinging on the OPPA.

The analogous results of 2D-DOA estimation with 3 sources under 0 dB SNR scenario obtained with OMLA and OPLA are shown in Figures 4.31 and 4.32 respectively. The results shown in Figure 4.31 and 4.32 are also not associated with additional peaks. The estimated 2D-DOA angles of the three sources match closely with those assumed while modelling the 3 sources.

4.10.1 Inference from the Results of 2D-DOA on Estimation of Three Sources

The results of the Figures 4.29, 4.30, 4.31 and 4.32 show the performance of the 2D-DOA estimation of three sources using the four array configurations. The results illustrate that the proposed orthogonally polarized array configurations have satisfactory performance in distinguishing the sources. Whereas the conventional singly polarized 3×3 UPA fails to differentiate the actual DOA of sources and extra peaks. From the results of the Figures 4.29-4.32, it is inferred that, the OPLA and OPPA yield better performance and exhibit clear distinction of the DOA of sources. The orthogonally mounted linear array configuration has a minor fictitious extra peak appearance, but with its lower magnitude. Hence the fictitious peak can be distinguished from the peaks corresponding to the actual DOA of sources.

4.11 Analysis of Sharpness of Peak in 2D-DOA Estimation

In the previous section, a detailed discussion on the analysis of two dimensional DOA Estimation for the sources $(\theta_1 = 25^\circ, \phi_1 = 25^\circ)$ and $(\theta_2 = 45^\circ, \phi_2 = 45^\circ)$ was presented for 10 dB SNR. This section presents a relative comparison of sharpness profile of the curve that will facilitate the accurate prediction of the DOA angle of the impinging sources on the array. Figure 4.33 illustrates the sharpness of the profile of the curve to detect the two peaks which confirms the presence of two sources obtained from the estimation of 2D-DOA angles through conventional single polarized UPA. In the results of Figure 4.33, the true arrival angles of the two sources are $(25^\circ, 25^\circ)$ and $(45^\circ, 45^\circ)$. The corresponding results obtained through the estimation of 2D-DOA angles using OPPA are $(25^\circ, 25^\circ)$ and $(45^\circ, 45^\circ)$. A relative comparison of the results of Figures 4.33 and 4.34 reveal that the OPPA is associated with a sharper peak as well as larger amplitude of peak.

From the results shown in Figure 4.35 and 4.36, it is easy to infer that the OMLA also shows relatively sharper profile of the peak when compared to the OPLA. From the results of Figures 4.33 - 4.36, it is also evident that OPLA exhibits maximum amplitude of the two peaks.

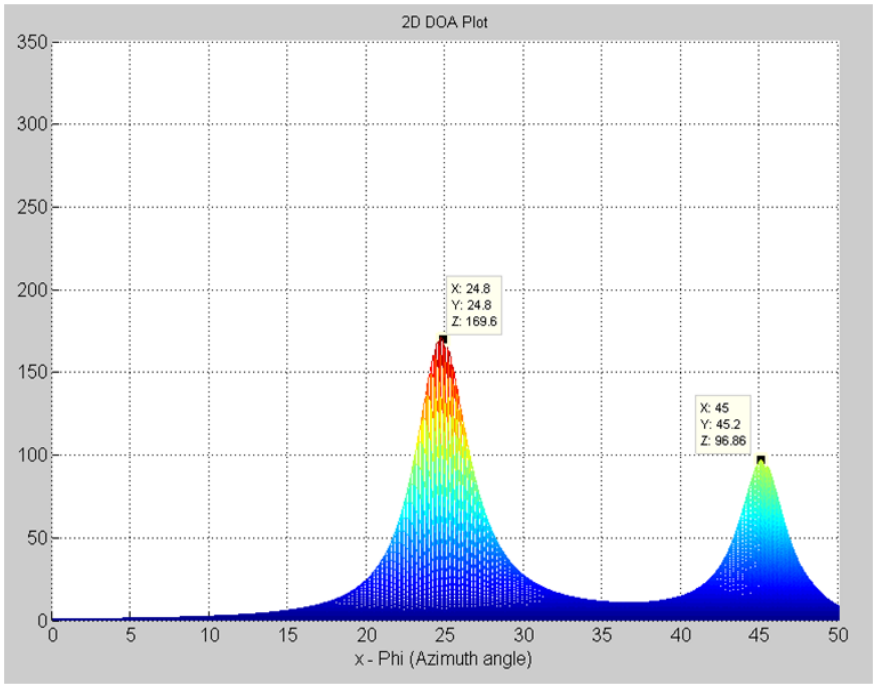

Figure 4.33: 2D-DOA Estimation using UPA Configuration for Two Sources at $(25°, 25°)$ and $(45°, 45°)$ for SNR of 10dB

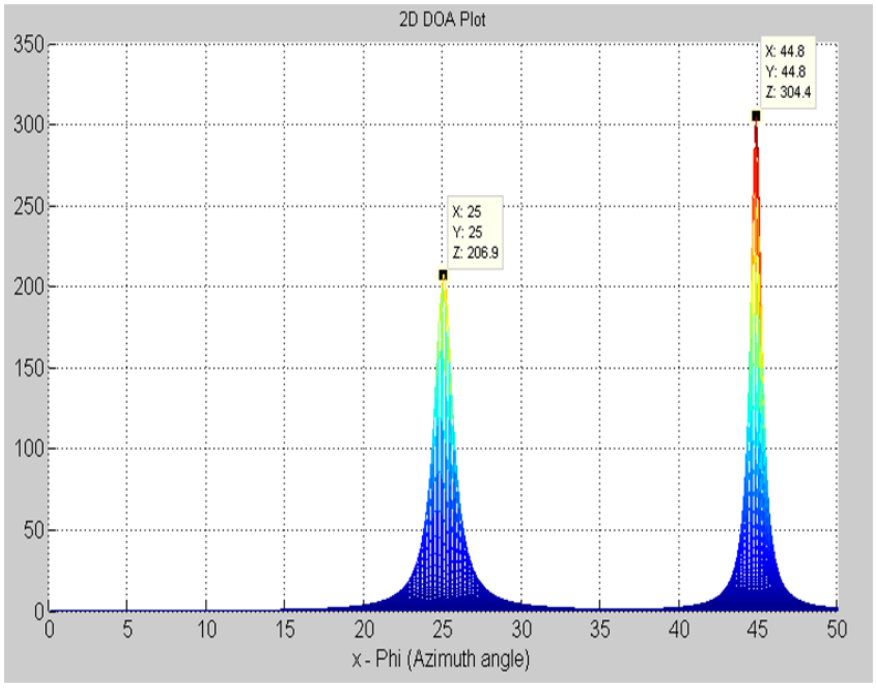

Figure 4.34: 2D-DOA Estimation using OPPA Configuration for Two Sources at $(25°, 25°)$ and $(45°, 45°)$ for SNR of 10dB

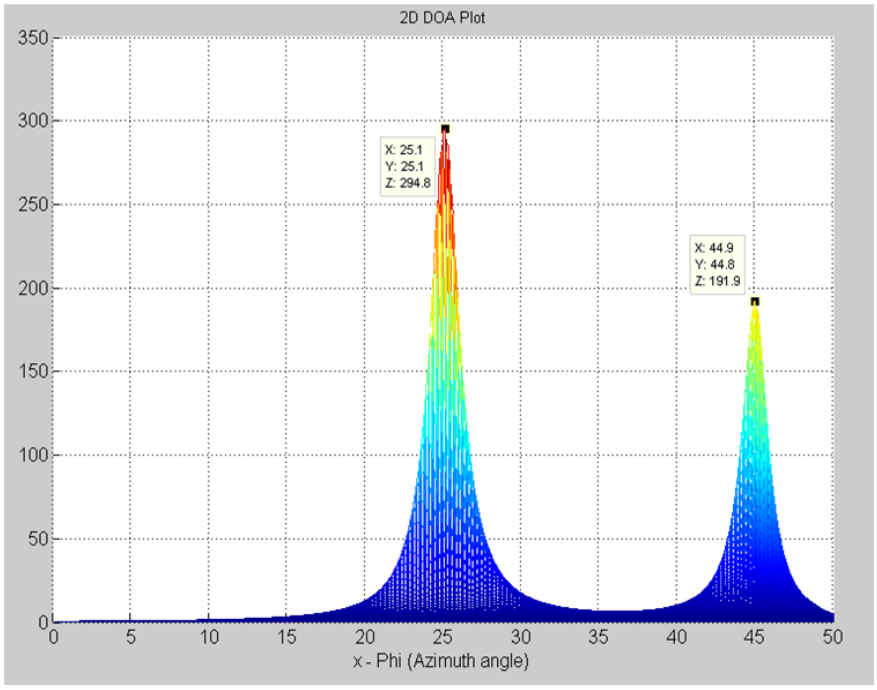

Figure 4.35: 2D-DOA Estimation using OMLA Configuration for Two Sources at $(25°, 25°)$) and $(45°, 45°)$ for SNR of 10dB

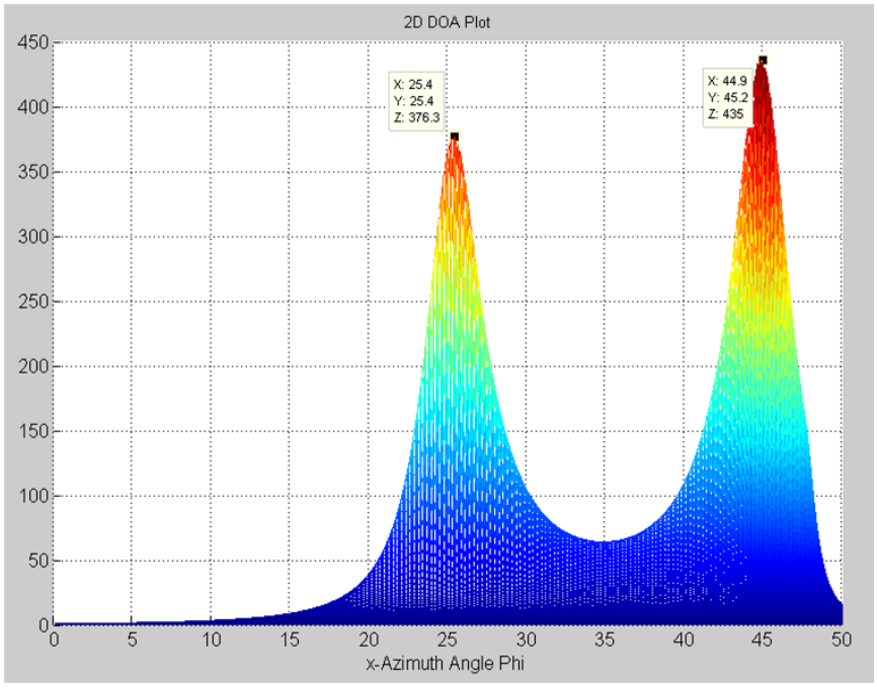

Figure 4.36: 2D-DOA Estimation using OPLA Configuration for Two Sources at $(25°, 25°)$ and $(45°, 45°)$ for SNR of 10dB

4.12 Resolution Analysis of 2D-DOA Estimation with Closely Spaced Two Sources

A principal focus of this thesis is to formulate and analyse the schemes for improved resolution and accuracy of estimation of 2D-DOA. A measure of resolvability of 2D-DOA estimation algorithm is the ability of the algorithm to distinguish the peaks even when the angular separation between the sources impinging on the array configuration is small. This section presents the simulation results pertaining to the resolvability of the MUSIC based 2D-DOA estimation using various array configurations described earlier in this chapter. The detection of the peaks resulting from the MUSIC algorithms based 2D-DOA estimation techniques usually involves a visualization of 3D graph. To illustrate the ability of MUSIC algorithm based 2D-DOA estimation technique to resolve closely spaced sources, a 2D representation is preferred, in which 3D graph is viewed in 2D perspectives.

4.12.1 Analysis of 2D-DOA Estimation of Closely Spaced Two Sources using UPA

The results of the 2D-DOA estimation using UPA configuration are shown in Figures 4.37, 4.38 and 4.39. For the simulations, the two sources are modelled with the arrival angles of $(\theta_1 = 25^\circ, \phi_1 = 25^\circ)$ and $(\theta_2 = 25^\circ, \phi_2 = 35^\circ)$.

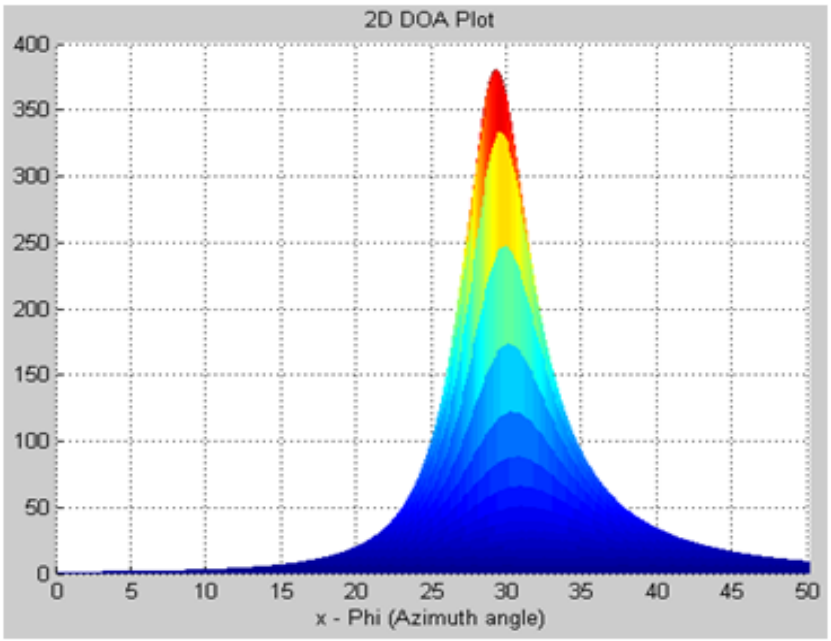

Figure 4.37: 2D-DOA Estimation of Closely Spaced Sources Estimation using UPA for Two Sources at $(25^\circ, 25^\circ)$ and $(25^\circ, 35^\circ)$

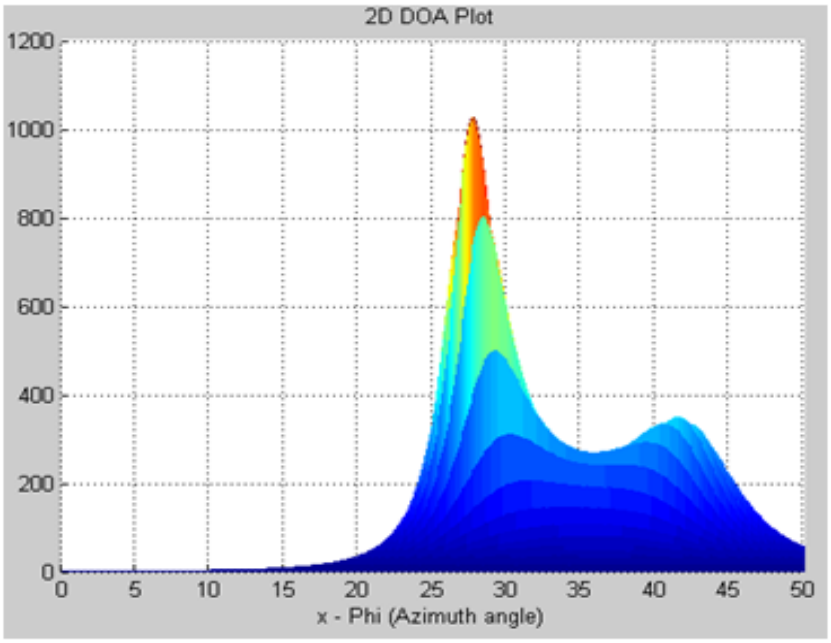

Figure 4.38: 2D-DOA Estimation of Closely Spaced Sources Estimation using UPA for Two Sources at $(25°, 25°)$ and $(25°, 40°)$

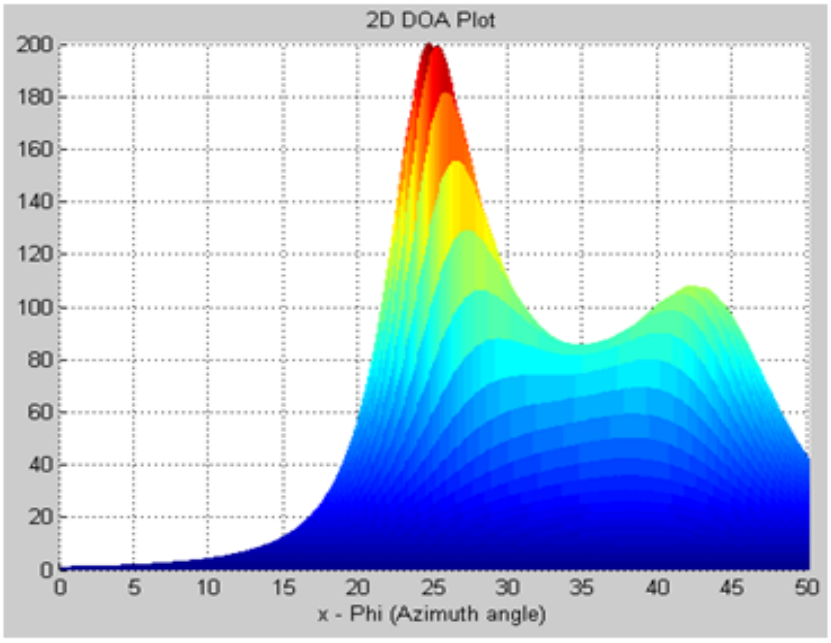

Figure 4.39: 2D-DOA Estimation of Closely Spaced Sources Estimation using UPA for Two Sources at $(25°, 25°)$ and $(25°, 43°)$

The simulation results of 2D-DOA estimation using single polarized UPA are shown in

Figure 4.37. The simulation results shown in Figure 4.37 confirm that the single polarized UPA fails to distinguish the two sources when their angular separation is less than 10°. When the azimuth angle of the second source was increased from 35° to 40°, the simulation results on 2D-DOA of Figure 4.38 reveal some improving trend of distinguishing the two closely spaced sources. When the azimuth angle of the second source is increased to 43°, the results of Figure 4.39 reveal further signs of conventional UPA being able to distinguish the two closely spaced sources with improved resolution.

4.12.2 Analysis of 2D-DOA of Closely Spaced Two Sources using OPPA

The results of the 2D-DOA with OPPA when the elevation and azimuth angles of the two sources are $(\theta_1 = 25°, \phi_1 = 25°)$ and $(\theta_2 = 25°, \phi_2 = 33°)$ are shown in Figure 4.40.

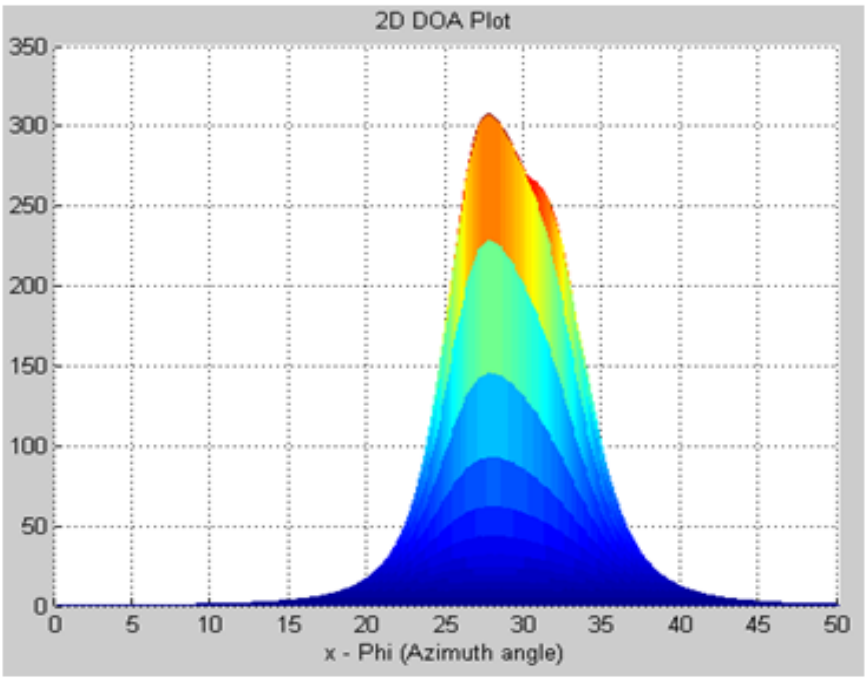

Figure 4.40: 2D-DOA Estimation of Closely Spaced Sources Estimation using OPPA for Two Sources at $(25°, 25°)$ and $(25°, 33°)$

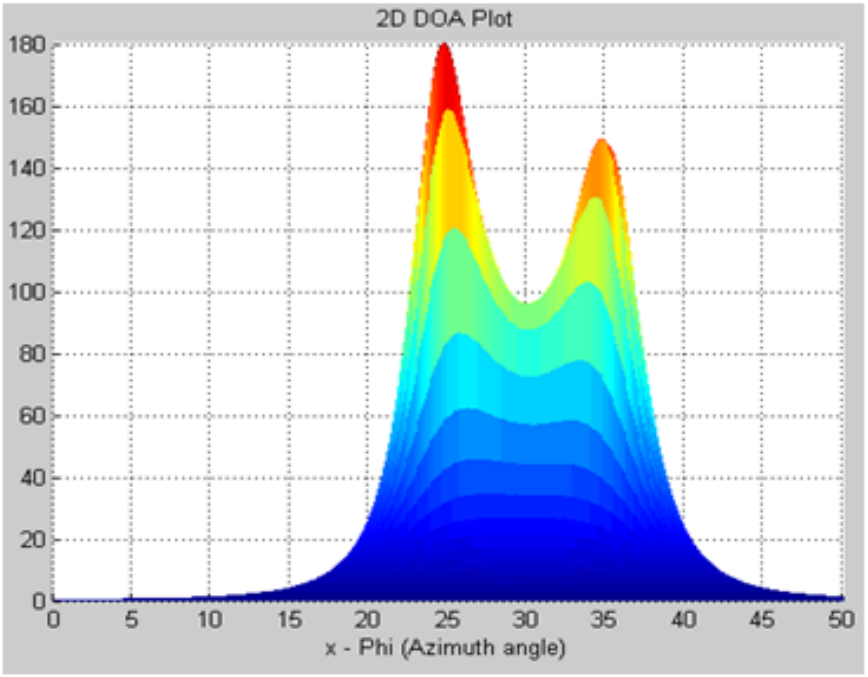

Figure 4.41: 2D-DOA Estimation of Closely Spaced Sources Estimation using OPPA for Two Sources at $(25^\circ, 25^\circ)$ and $(25^\circ, 35^\circ)$

As far the case of single polarized UPA configuration, the OPPA is not able to distinguish the two sources when the azimuth angles of the two sources differ by less than 10°. However, when the azimuth angle ϕ_2 of the second source is changed to 35°, the OPPA is able to distinguish the two sources distinctly as can be inferred from the results of Figure 4.41. This is contrary to case the of conventional single polarized UPA.

4.12.3 Analysis of 2D-DOA Estimation of Closely Spaced Two Sources using OMLA

The results of Figure 4.42 reveal that the OMLA is not able to distinguish the two sources whose elevation and azimuth angles of the two sources are $(\theta_1 = 25^\circ, \phi_1 = 25^\circ)$ and $(\theta_2 = 25^\circ, \phi_2 = 33^\circ)$. When the azimuth angle ϕ_2 of the second source is increased to 34° also, the OMLA is not able to distinguish the two sources as revealed by the results of Figure 4.43. However, when the angle ϕ_2 is changed to 35°, the OMLA shows its ability to infer the presence of two sources even though not with a distinctly visible second peak.

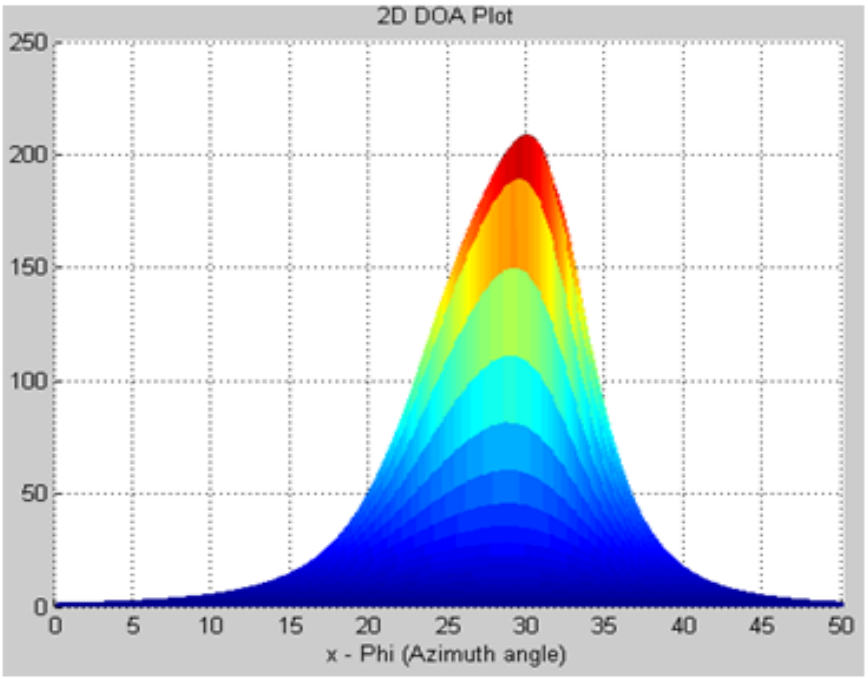

Figure 4.42: 2D-DOA Estimation of Closely Spaced Sources Estimation using OMLA for Two Sources at $(25°, 25°)$ and $(25°, 33°)$

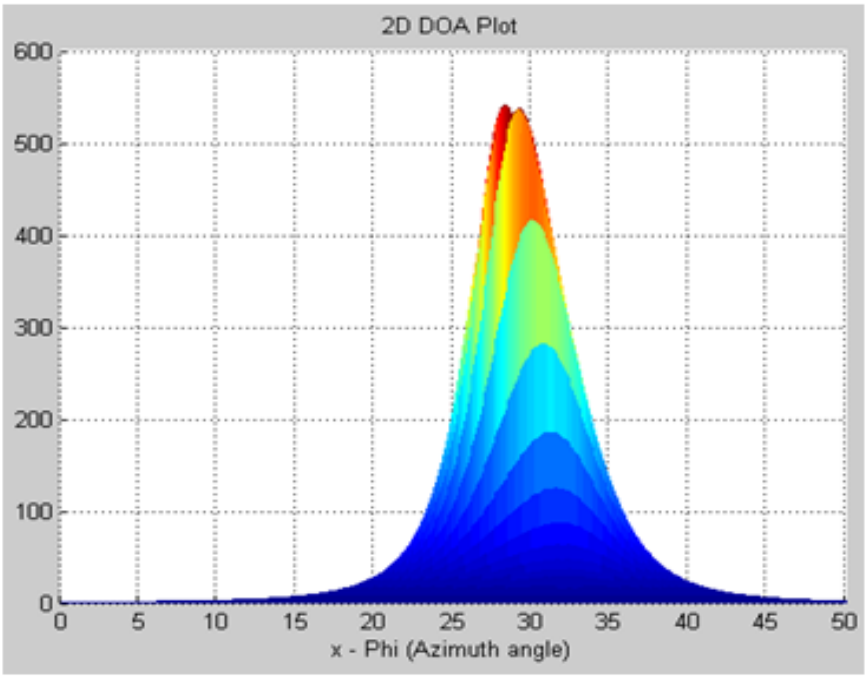

Figure 4.43: 2D-DOA Estimation of Closely Spaced Sources Estimation using OMLA for Two Sources at $(25°, 25°)$ and $(25°, 34°)$

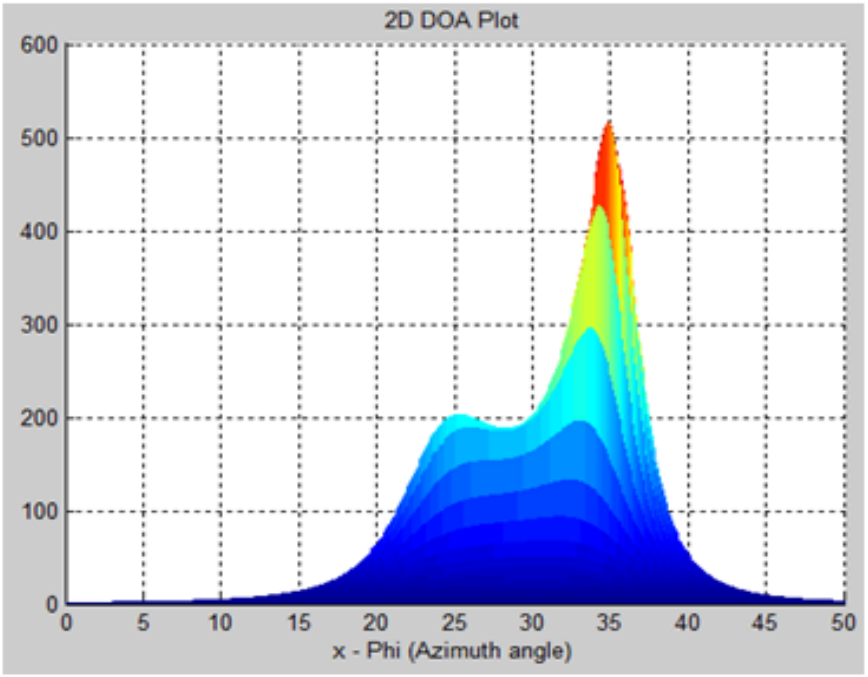

Figure 4.44: 2D-DOA Estimation of Closely Spaced Sources Estimation using OMLA for Two Sources at $(25°, 25°)$ and $(25°, 35°)$

4.12.4 Analysis of 2D-DOA Estimation of Closely Spaced Two Sources using OPLA

The OPLA is subjected to the analysis of 2D-DOA with closely spaced sources. This configuration is slightly inferior in distinguishing the closely spaced sources. The performance of the OPLA is analysed iteratively and identified that minimum angular separation of 25° is required for the clear distinguishing of the two closely spaced sources.

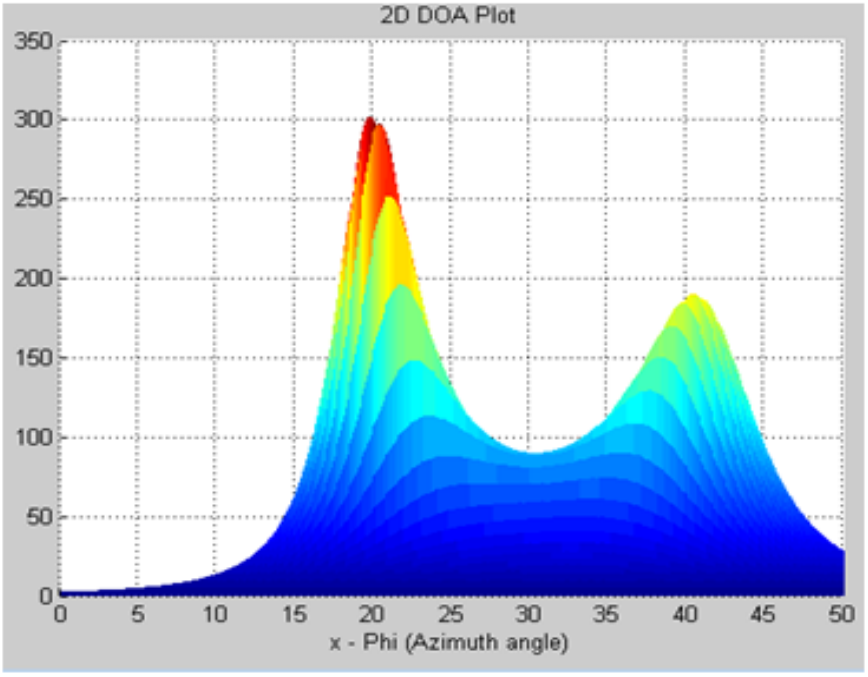

Figure 4.45: 2D-DOA Estimation of Closely Spaced Sources Estimation using OPLA for Two Sources at $(25°, 15°)$ and $(25°, 40°)$

The inferior performance of the OPLA configuration is due to the lack of variation of spatial component along the y axis. The results of the OPLA is shown in Figures 4.45, 4.46, 4.47 and 4.48.

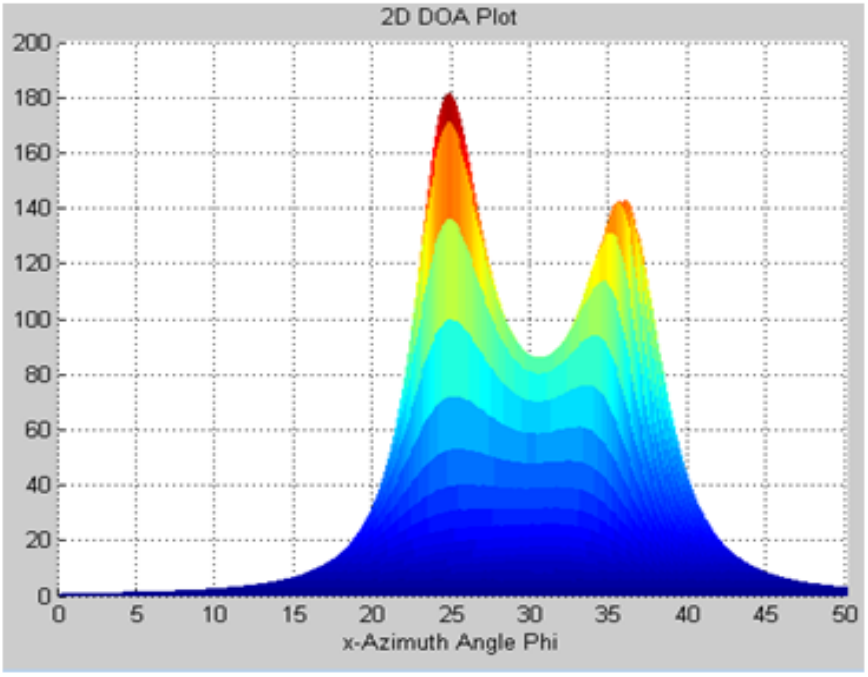

Figure 4.46: 2D-DOA Estimation of Closely Spaced Sources Estimation using OPLA for Two Sources at $(25°, 20°)$ and $(25°, 40°)$

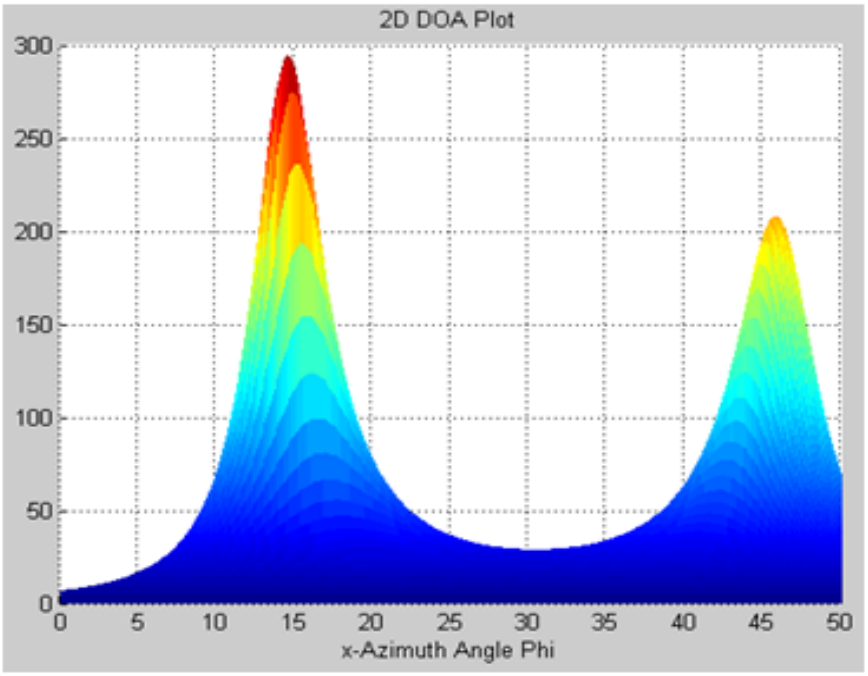

Figure 4.47: 2D-DOA Estimation of Closely Spaced Sources Estimation using OPLA for Two Sources at $(25°, 25°)$ and $(15°, 45°)$

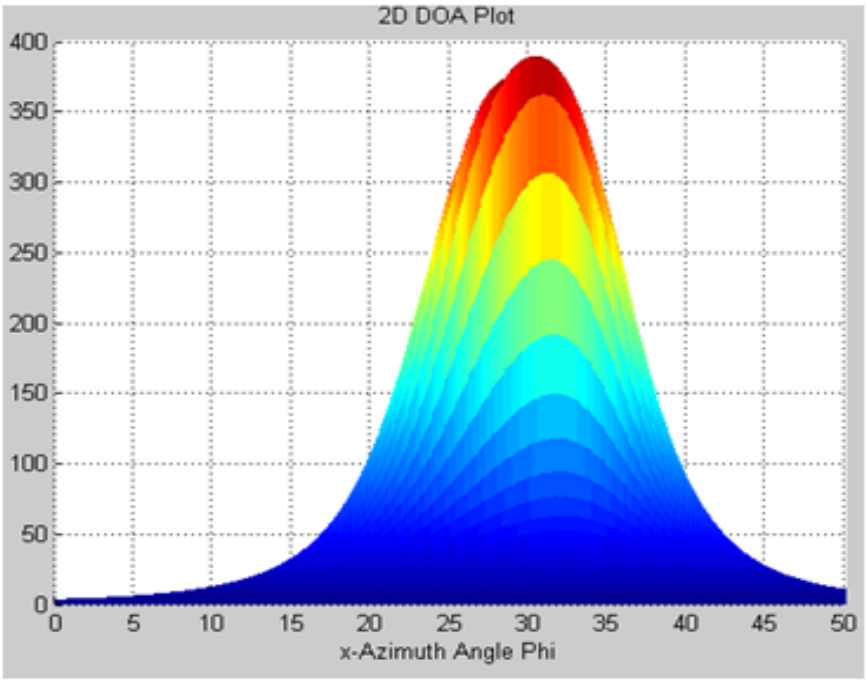

Figure 4.48: Closely Spaced Sources Estimation using OPLA for Two Sources at $(25^\circ, 25^\circ)$ and $(25^\circ, 40^\circ)$

4.13 Analysis of Effect of Inter Element Spacing on the 2D-DOA Estimation Performance

In this section, the influence of the inter element spacing of OPLA on the accuracy and performance of 2D-DOA estimation algorithm is presented. Among the orthogonally polarized array configurations, it is evident that the resolution and accuracy of 2D-DOA estimation realized with OPLA has been relatively poor. In an attempt to analyse the scheme for the performance enhancement of 2D-DOA estimation using OPLA, studies have been carried out to analyse the effect of change in the inter element spacing on the derived 2D-DOA estimation. As was stated in the section, in all the simulation studies presented so far in this chapter, the inter element spacing is $\lambda/4$ at the operating frequency of 9.375 GHz. The OPLA geometry was modified by doubling the inter element spacing implying that the earlier value of 5.56 cm has been changed to 11.2 cm. With the specific change, the simulation has been repeated for the estimation of 2D-DOA of the two sources whose angular coordinates of impinging on the array elements of OPLA are $(\theta_1 = 25^\circ, \phi_1 = 25^\circ)$ and $(\theta_2 = 25^\circ, \phi_2 = 35^\circ)$. Typically the inter element spacing is optimized to achieve the better performance of DOA estimators where antenna elements

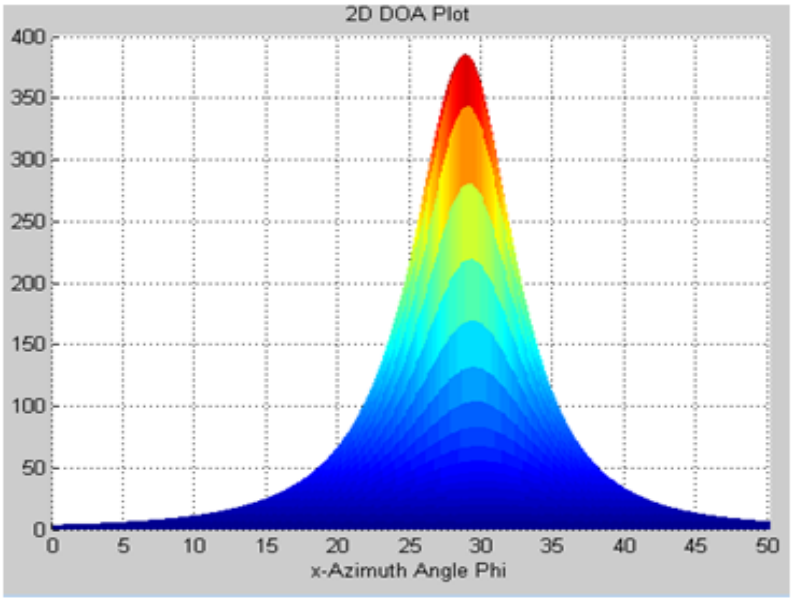

Figure 4.49: Estimation of DOA using OPLA for Two Sources at $(25°, 25°)$ and $(25°, 35°)$ with $d = 5.56cm$

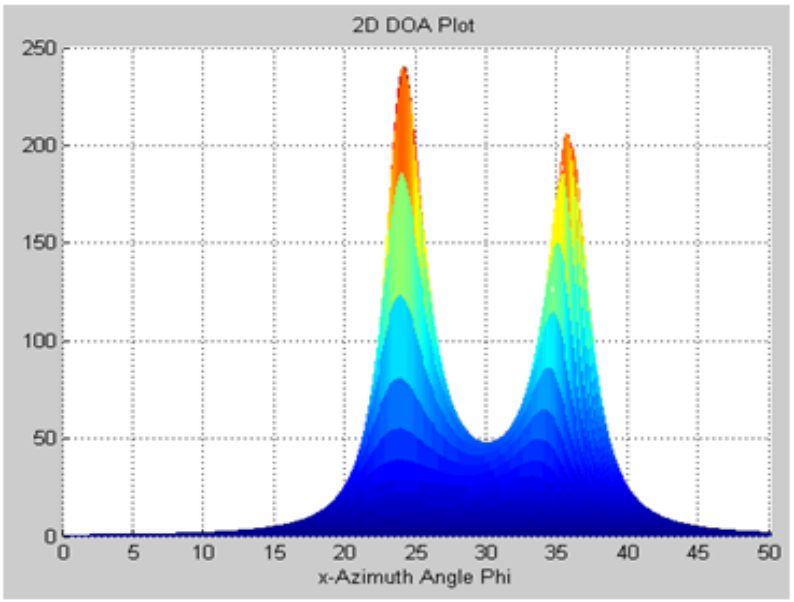

Figure 4.50: Estimation of DOA using OPLA for Two Sources at $(25°, 25°)$ and $(25°, 35°)$ with $d = 11.2cm$

are approximated as isotropic point sources. Consideration of actual radiation pattern of the antenna elements and their polarization, induces change in the amplitude of the signal reception with diversely polarized antenna elements. The change in amplitudes of the signal received by diversely polarized array elements is proportional to the magnitude

of radiation at that particular angle of incidence (DOA). Increased inter-element spacing approximating to half the wavelength leads to improved covariance of the received samples. This improvement in the covariance improves the DOA estimation.

The simulation results of 2D-DOA with increased inter elemental spacing using OPLA are shown in Figure 4.50. A comparison of results of Figure 4.50 with the results of Figure 4.49 clearly demonstrates that the larger inter elemental spacing has significantly improved the resolution of 2D-DOA results. The simulation results on estimation of 2D-DOA with the angular coordinate of the two sources being $(\theta_1 = 25^\circ, \phi_1 = 25^\circ)$ and $(\theta_2 = 25^\circ, \phi_2 = 35^\circ)$ derived through OPLA with d = 11.2 cm are shown in Figure 4.50. A comparison of results of Figure 4.49 with Figure 4.50 confirms that the sharpness of the peaks of 2D-DOA estimation improves with increased inter element spacing.

4.14 Summary

The simulations and analysis presented in this chapter confirm that the orthogonally polarized components of antenna array have significant influence in the accuracy and resolution of the 2D-DOA estimations. The proposed OPLA can be treated as an linear array. Thus a linear array configuration and its ability to estimate 2D-DOA is the novel part of the proposed OPLA. Among the proposed array configurations, OPPA has improved estimation accuracy and the OMLA configuration estimates the two sources with higher magnitude. The improved distinguishing capability of the OPPA for closely spaced sources is also realized through the simulations. The OPPA and the OMLA configuration clearly distinguish the sources with minimum angular separation of 10° with accurate estimation. The conventional single polarized UPA configuration resolves the 18° angular separation of sources which is inferior when compared with the proposed OPPA and OMLA configurations. The OPLA can resolve 10° angularly separated sources at the expense of increased inter-element spacing. The improved estimation accuracy and resolution of the proposed orthogonally polarized array configurations than the conventional single polarized UPA are realized for 2D-DOA for two sources and three sources under high and low SNR (weak coverage) conditions.

Chapter 5

Two Dimensional DOA Tracking of Non-Stationary Sources using Subspace Tracking Algorithms

5.1 Introduction

High resolution subspace based parameter estimation algorithms are widely applied in both temporal and spatial domain spectral analysis. Typical subspace based parameter estimation algorithms highly rely on the statistical stationary characteristics of the sampled received signal. Hence, the sample covariance data matrix obtained from the data samples observed over a period is adequate for the parameter estimation. In case of a dynamic scenario, where the moving signal sources have non-stationary signal characteristics, direct application of the subspace estimation algorithm warrants repeated eigen decompositions of the continuously updating data covariance matrix. In time varying systems, there will be a more frequent change in vector sequence with time. Also there may be significant overlap between new and old vector sequences. This warrants an analysis for the development of adaptive eigen decomposition and subspace tracking algorithms discussed in Chapter 2. This chapter intends to provide the simulation study on the analysis of tracking of 2D-DOA of non-stationary signal sources. The simulation study includes novel method of smoothing the covariance matrix of time varying non-stationary signal sources. The performance analysis of tracking of 2D-DOA estimation is evaluated for the single polarized UPA and the proposed orthogonal polarized array configurations for the range of SNR scenarios.

5.1.1 Adaptive Eigen Decomposition Algorithms

The adaptive eigen decomposition algorithm emerged in late 1970s, to avoid the repeated computation of intensive eigen decomposition of the covariance matrix. Many research contributions are reported in the literature for efficient updating and tracking of the subspace components of the covariance matrix. For every new sample, these algorithms attempt to recursively update the subspaces of eigen decomposition to avoid recomputing. A

significant reduction of computation complexity has been achieved through this approach. Initially, computation of signal subspace is developed through constrained optimization techniques. Subsequently, it is solved using stochastic gradient search approaches. These algorithms engage a Gram-Schmidt orthogonalization for every iteration (Owsley, 1978; J.-F. Yang & Kaveh, 1988).

Consequently, the concept of rank one updating of symmetric covariance matrix has evolved which was proposed by Golub (Golub, 1973). This concept was further improved by Bunch et al. (Bunch, Nielsen, & Sorensen, 1978). Several versions of rank one updating technique emerged from its variations and extension (Schreiber, 1986). The rank one updating algorithm exploits the low rank property of the covariance matrix of the new samples. It invokes an efficient eigen decomposition of updating covariance matrix than direct computation. The first order perturbation analysis of the covariance matrix due to the newer samples along with forgetting factor and exponential widowing is exploited in (Champagne, 1994).

5.1.2 Eigen Based DOA Tracking Algorithms

Eigen based methods were originally discussed in a block processing context. In sequential signal processing, the subspace components are updated by performing SVD of a data matrix recursively, on the arrival of new data snapshots. For example, it can be of great interest to compute, at each time step, some dominant singular values and the associated singular vectors of a data matrix.

Classical EVD and SVD are used in the context of block processing to estimate the subspace components. The signal and noise subspace based algorithms are widely adopted in adaptive signal processing and wireless communication control systems. For the scenario where the dynamic update of the signal subspace or the noise-subspace is required, it is sufficient to track the subspace components rather than compute the complete EVD or SVD. Subspace Tracking algorithms are used for sequential processing of data and recursively update the subspaces upon the arrival of new data. Bi-Iterative Singular Value Decomposition (Bi-SVD) is computationally efficient when compared to classical SVD algorithms. The computationally intensive SVD algorithm can be circumvented with QR decomposition algorithm in the bi-iteration manner. Bi-Iterative QR decomposition (Bi-SVD) is computationally efficient than classical SVD algorithms. The computationally intensive SVD algorithm can be computed with QR decomposition algorithm in the bi-

iteration manner. The subspace tracking algorithm Bi-SVD is detailed below. Many variations of the Bi-SVD algorithm cited in the [Strobach 1997] literature with different MACs of slow, fast and ultra fast.

5.1.3 Bi-SVD Algorithm

The Bi-SVD algorithm involves Bi-iteration of *QR* decomposition of the covariance matrix. This bi-iteration simplifies the computation of the left and right singular vectors of the classical SVD techniques. The steps to execute Bi-SVD algorithm are detailed in the following pseudo code to decompose the covariance matrix Φ with r principal components.

Pseudo code of Bi-SVD

i. Initialize $\mathbf{Q}_A = \begin{bmatrix} \mathbf{I}_r \\ \mathbf{0} \end{bmatrix}$; where $\mathbf{I}_r$ is the identity matrix of size $r \times r$ and r is the number of signal sources.

ii. $for\ i = 1, ..., until\ convergence$

$$\mathbf{B}_i = \Phi_i \mathbf{Q}_{A(i-1)}$$

$$\mathbf{Q}_{Bi}\mathbf{R}_{Bi} = QR(\mathbf{B}_i)$$

$$\mathbf{A}_i = \Phi_i^H \mathbf{Q}_{Bi}$$

$$\mathbf{Q}_{Ai}\mathbf{R}_{Ai} = QR(\mathbf{A}_i)$$

end

Here $QR(.)$ denotes the QR Decomposition of the matrix and $(.)^H$ refers to hermitian conjugate.

The step (ii.) is iterated until convergence, and after convergence the left and right singular vectors are settled in the **B** and **A** matrices respectively.

while the matrix $\mathbf{B}_i$ Settles for left dominant singular vectors, the matrix $\mathbf{A}_i$ Settles for right dominant singular vectors

In mathematical sense, the r dominant singular vectors are equivalent to r signal subspace vectors of eigen decomposition. Also the matrices $\mathbf{B}_i$ and $\mathbf{A}_i$ have the non-dominant singular vectors, which are equivalent of noise subspace of the eigen decomposition. The signal subspace based estimation algorithm requires to compute the dominant singular vectors. Where as the noise subspace based algorithm warrants the non-dominant singular vectors. Typically the signal subspace is associated with the principal components of the

covariance matrix, and noise subspace is associated with the non-principal components of the covariance matrix. The Bi-SVD algorithm converges for the dominant singular vectors first and later for the non-dominant vectors. The computationally intensive SVD algorithm can be circumvented with QR decomposition algorithm in the bi-iteration manner such as Bi-SVD and its variants.

5.2 Modelling of Signal Sources for Tracking of 2D-DOA

In DOA estimation, the data matrix or covariance matrix is processed for parameter estimation using either MUSIC or ESPRIT based algorithms, in which computationally intensive EVD or SVD technique are a routine must.

5.2.1 Modelling of Stationary Source

In case of the stationary sources, the array steering vector is fixed for all the samples and is independent of the time index n as shown in Equation (5.1). In other words, the azimuth (ϕ) and elevation (θ) angles are fixed for all the received samples of the array. The noise added to the signal model is white Gaussian noise of fixed variance for all the time samples.

$$\mathbf{a}(\theta,\phi) = \left[e^{-jk\beta_1(\theta,\phi)}, \quad e^{-jk\beta_2(\theta,\phi)}, \quad \cdots, \quad e^{-jk\beta_M(\theta,\phi)}\right]^T \tag{5.1}$$

where,

$$\beta_m(\theta,\phi) = x_m \sin\theta\cos\phi + y_m \sin\theta\sin\phi + z_m\cos\theta \tag{5.2}$$

The standard array signal model for stationary sources are shown in Equation (5.3).

$$\mathbf{x}(n) = \mathbf{a}(\theta,\phi)\,\mathbf{s}(n) + \mathbf{w}(n) \tag{5.3}$$

where, $\mathbf{x}(n)$ is the received sample at time instant n. $\mathbf{s}(n)$ signal sample at instant n. $\mathbf{w}(n)$ is the white Gaussian noise vector at instant n. The sample covariance matrix, $\mathbf{R_{xx}}$ is a simple computation as shown in Equation (5.4).

$$\mathbf{R_{xx}} = E\left[\mathbf{x}\mathbf{x}^H\right] \tag{5.4}$$

where $(.)^H$ refers to Hermitian conjugate.

5.2.2 Modelling of Non-stationary Source

In the case of non-stationary sources, the array steering vector is a function of time index n. The azimuth and elevation angles of the incoming signal sources change over time samples. The change in azimuth and elevation angles lead to change in phase of the received samples in the observation interval. Thus, it is essential to compute the covariance matrix independently for all the spatio-temporal samples. The time-varying source or non-stationary source or dynamic source model is shown in Equation (5.5).

$$\mathbf{x}(n) = \mathbf{a}(\theta, \phi, n)\mathbf{s}(n) + \mathbf{w}(n) \tag{5.5}$$

The covariance matrix is computed independently for all values of the time sample indices n.

$$\mathbf{R_{xx}}(n) = \mathbf{x}(n)\mathbf{x}^H(n) \tag{5.6}$$

The covariance matrices of instantaneous samples are computed in which the variance of the spatial samples is not retained over the successive received samples, due to the dynamic behaviour of the incoming sources. Retaining the second order statistical properties of the received signal over the observation interval is essential for the better estimation of the DOA. Various methods for the construction of covariance matrix are discussed in the following subsections.

5.2.3 Covariance Matrix by Weighting Factor α

The concept of weighting factor based covariance computation widely used in adaptive signal processing algorithms is utilized to retain the statistical properties of the incoming sources. The weighting factor approach is formulated based on the typical moving average filter (Hayes, 2009) and weighted average covariance matrix used in (Strobach, 1997). In the weighting factor approach, the current sample along with the immediate past sample are weighted, such that more weightage is for the current sample and less weightage for the previous sample. In this method, covariance matrix for n^{th} instant is computed by

$$\mathbf{RW_{xx}}(n) = (1-\alpha)\mathbf{R_{xx}}(n-1) + \alpha\mathbf{R_{xx}}(n) \tag{5.7}$$

where α is chosen such that $\frac{1}{2} \leq \alpha \leq 1$.

The weighted averaged covariance matrix used for DOA estimation carries the statistical properties of the signal from the beginning till the end. This in turn improves the DOA estimation of the non-stationary sources. The weighting factor based covariance matrix is shown in Equation (5.7)

5.2.4 Forgetting Factor β Method for Covariance Matrix

Similar to the weighting factor approach, concept of forgetting factor is introduced for the dynamic source models. The forgetting factor technique is widely adopted in RLS type of adaptive algorithms (S. S. Haykin, 2008). The concept of forgetting factor is to forget the older samples in the memory. The size of the memory is fixed, keeping in view the ease of the computation. It also depends on the dynamic behaviour of the source. In essence, it can be said as the weighted sum of moving average filter. The covariance method $\mathbf{Rff_{xx}}(n)$ through the forgetting factor method is represented through the Equation (5.8).

$$\mathbf{Rff_{xx}}(n) = \sum_{i=0}^{q} \beta^i \mathbf{R_{xx}}(n-i) \tag{5.8}$$

where β is chosen such that $0 \leq \beta \leq 1$.
The β and q are respectively the forgetting factor and the order of the filter. This approach carries the statistical property of the signal from the beginning more precisely than the weighting factor approach. The forgetting factor based covariance matrix is shown in Equation (5.8).

5.3 Simulation Analysis of DOA of Non-Stationary Sources

The simulation and performance analysis of DOA estimation are carried for the non-stationary moving sources utilizing the instantaneous samples, weighting factor and forgetting factor approaches on the covariance matrix computations.

5.3.1 Tracking of DOA with MUSIC Algorithm

For the tracking of non-stationary sources, the standard MUSIC algorithm is incorporated to estimate the DOA. The Root MUSIC algorithm can also be incorporated, which is variation of the standard spectral MUSIC algorithm, in which polynomial rooting approach is incorporated. The polynomial roots determined from the subspace components are utilized to estimate the DOA. However, the Root MUSIC algorithm has the limitation of array geometric configuration restricted to linear. The dynamic tracking of the moving sources involves, the decomposition of signal and noise subspace components. The classical EVD or SVD approaches intensify the computation over the observation interval. It is sufficient to track the subspace components of the moving sources. The methods incorporated involving weighting factor approach and forgetting factor approach carry the second order

information of the covariance of the moving sources.

Figures 5.1, 5.2 and 5.3 depict the tracking behaviour of 2D-DOA estimation for the non-stationary source model θ moving from source angle -25° to destination angle $+45^{\circ}$ using the instantaneous sample approach, Weighting factor approach and the forgetting factor approach respectively. The linear trajectory between the source angle and destination angle is assumed. 100 spatio-temporal samples for the linear trajectory between the source and destination angle are considered for the simulation. A scenario of 0 dB SNR with AWGN is chosen, where the signal power and noise power are equal for the simulation. The variations in DOA estimation can be clearly seen due to the noise influence of the techniques. The 0 dB SNR scenario addresses the estimation behaviour under the heavy influence of noise added to signal. At higher SNR the estimation algorithm should tend to behave distinctly better than 0 dB behaviour, since the noise influence is lesser at higher SNRs.

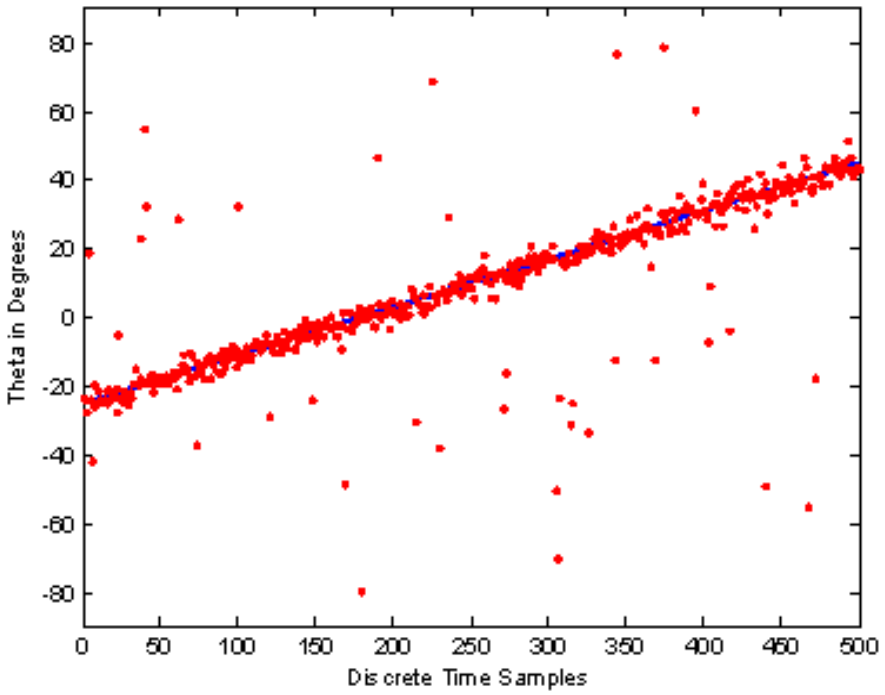

Figure 5.1: DOA Tracking by Instantaneous Samples Processed for SNR = 0 dB

The results of the tracking behaviour of DOA estimation of the three different approaches in computing the covariance matrix can be clearly seen from the above depicted Figures 5.1 to 5.3. As can be seen from the results of Figure 5.1, the estimation and tracking behaviour of DOA estimation using instantaneous samples approach is poor for

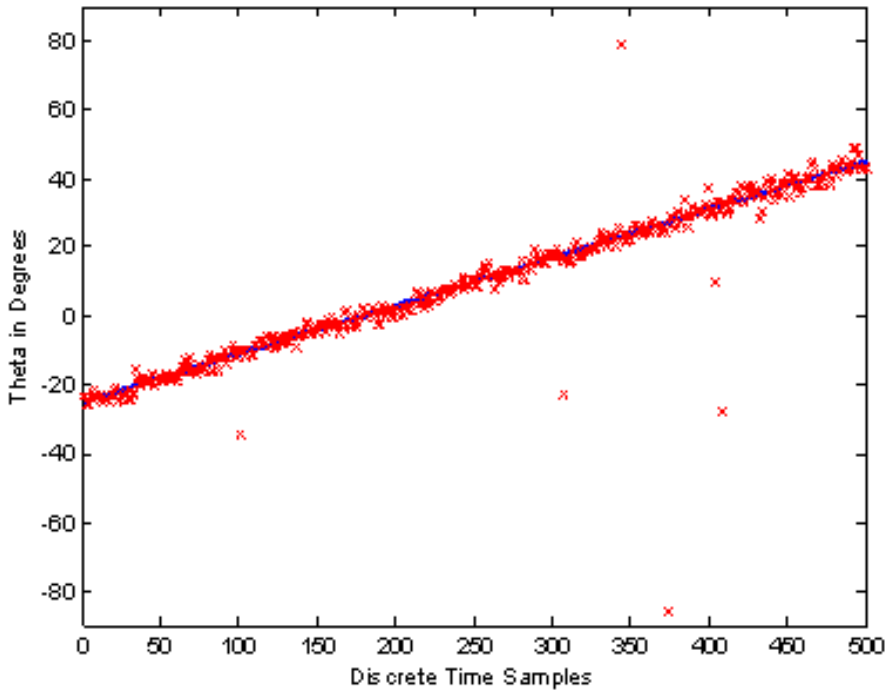

Figure 5.2: DOA Tracking by Weighting Factor Method $\alpha = 0.6$ for SNR = 0 dB

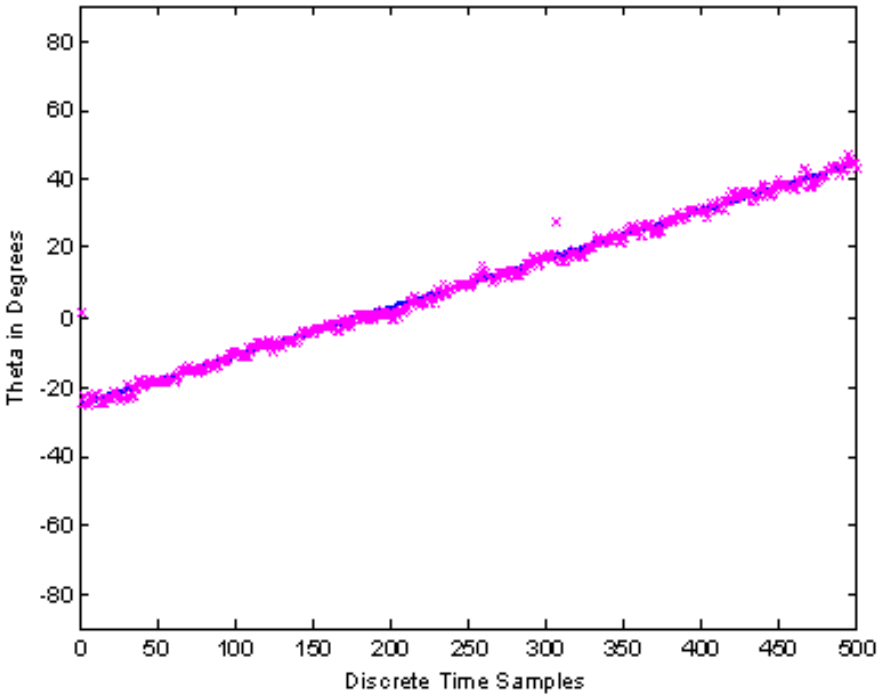

Figure 5.3: DOA Tracking by Forgetting Factor Method $\beta = 0.95$ $q = 5$ for SNR = 0 dB

the dynamic signal sources.
Further, the estimation and tracking characteristics of DOA derived through the weighted factor approach show marked improvement as is evident in Figure 5.2. On an average, the weighted factor approach for DOA estimation and tracking seems to be better than the instantaneous samples approach for dynamic sources.
The results depicted in Figure 5.3, clearly reveal that the forgetting factor based DOA estimation and tracking out performs the approaches based on instantaneous samples and weighted average. Since this method carries the second order statistics of the signal from the beginning of duration of sample collection, lesser variations in the covariance are realized when compared with the weighting factor approach.

5.4 Analysis of Weighting and Forgetting Factor in 2D-DOA Estimation and Tracking

In section 5.3, the focus was on estimation and tracking of 1D-DOA. In this section, the analysis of the previous section is extended to 2D-DOA. The covariance of the received data samples from the antenna array configuration has the major influence in the estimation accuracy of DOA. The second order statistics of the data covariance matrix need to be uniform for all the data samples received for the DOA tracking from the source angle to the destination angle. The instantaneous samples of the antenna array do not maintain the uniformity of second order statistics. Thus to maintain the uniformity of the statistics, it is essential to consider the past data samples also in to consideration, in the DOA estimation. The weighting factor approach and forgetting factor approach are proposed to construct the data covariance matrix with weighted average of the past data samples. These two approaches are analysed for the optimized choice of parameters for the tracking of DOA with low Mean Square Error (MSE) in the estimations. The signal for tracking of 2D-DOA using the OPLA configuration with source angle $(\theta = 25^\circ, \phi = 15^\circ)$ and destination angle $(\theta = 45^\circ, \phi = 50^\circ)$ is modelled for the analysis.

5.4.1 Weighting Factor Analysis for Tracking of Estimation of 2D-DOA

The weighted average approach is used in the signal model for the construction of data covariance matrix utilizing the Equation provided in (5.7). The use of immediate past data samples received from the antenna arrays, in the formation of data covariance matrix and its behaviour with various weights for the current and past data samples are analysed. The

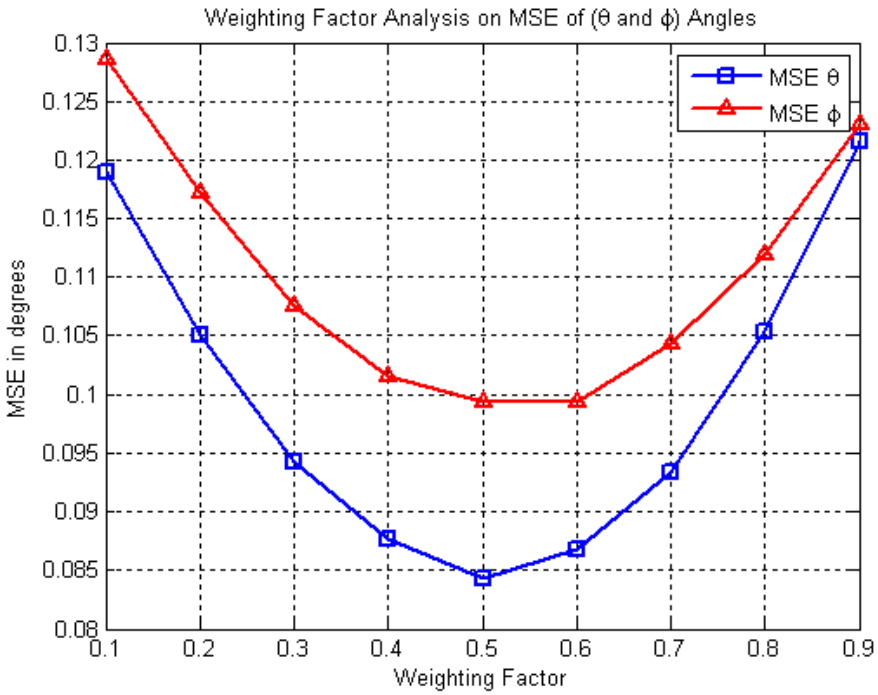

Figure 5.4: Analysis of Weighting Factor in 2D-DOA Tracking

weighting factor α in Equation (5.7) is varied in the range $0.1 \leq \alpha \leq 0.9$. The tracking behaviour of 2D-DOA estimation between the source and destination DOA angles are performed using the MUSIC algorithm. The MSE between the actual DOA trajectory and estimation angles for every data sample with weighted average is calculated. The Figure 5.4 illustrates the MSE of θ and ϕ angles of the tracking behaviour of 2D-DOA with each of the weighting factor in the range considered for the data covariance matrix. This analysis reveals that the weighting factor $\alpha = 0.5$ in the construction of covariance matrix yields the lowest MSE in tracking the estimation of 2D-DOA between the source and destination angles. This implies that equal weightage of the current and past samples will tend to track the estimation of θ and ϕ angles with lower MSE.

5.4.2 Forgetting Factor Analysis for Tracking of Estimation of 2D-DOA

Similar to the weighting factor approach, the forgetting factor approach is also subjected for the analysis of tracking behaviour of 2D-DOA estimation. Unlike the weighting factor approach, the forgetting factor approach includes several past samples, in the formation of the covariance matrix. The weighted average of the past several samples improves the smoothness in the tracking behaviour of estimation of 2D-DOA. The number of past

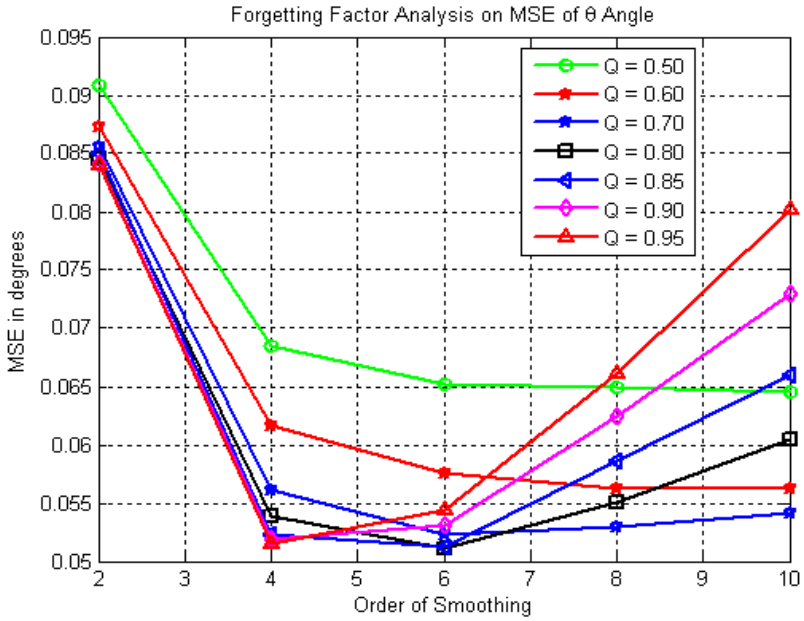

Figure 5.5: Analysis of Forgetting Factor in θ Estimation of 2D-DOA Tracking with Orthogonal Polarized Linear Array

samples q is said to be the order of smoothing filter and β is the forgetting factor. The parameters q and β of the Equation (5.8) are analysed using the signal model for tracking

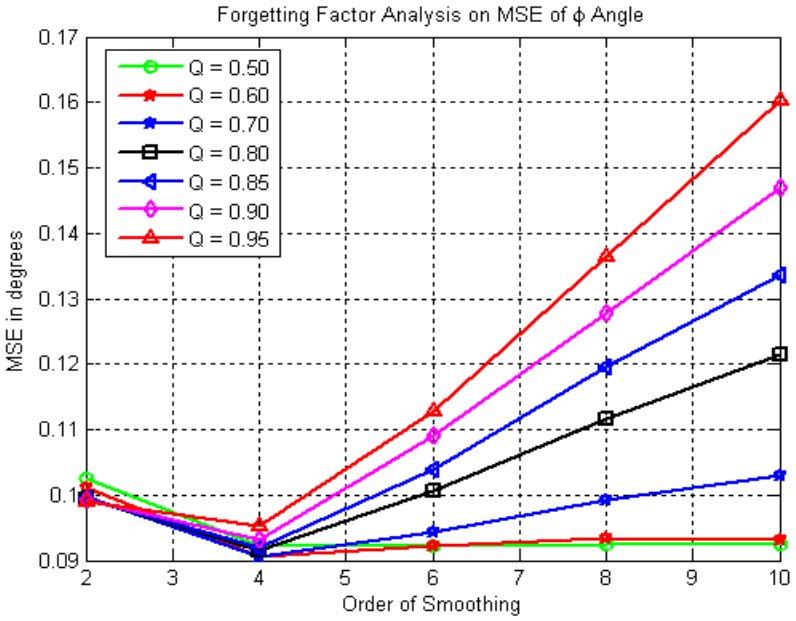

Figure 5.6: Analysis of Forgetting Factor in ϕ Estimation of 2D-DOA Tracking with Orthogonal Polarized Linear Array

behaviour of estimation of 2D-DOA for choosing the optimum choice of the filter order and forgetting factor.

The order of the smoothing filter q is subjected for the analysis in the range $2 \leq q \leq 10$ in steps of 2. The forgetting factor β in the range $0.5 \leq \beta \leq 0.95$ with order of the filter is analysed for the tracking behaviour of estimation of 2D-DOA. The results of the Figures 5.5 and 5.6 depict the MSE of θ and ϕ estimation respectively in 2D-DOA tracking behaviour between the source and destination DOA angles. The results of the Figures 5.5 and 5.6 reveal that, in both θ and ϕ estimation error is very less at smoothing filter order of q = 4. This in turn conveys that only the immediate past 4 samples should be utilized for the better estimation accuracy rather than considering the more number of past samples. The combined analysis of the θ and ϕ estimation error, the forgetting factor $\beta = 0.95$ is more suitable to be utilized for the lowest MSE with the filter order of q = 4, when compared with the other forgetting factors in the range.

5.5 Analysis of 2D-DOA Tracking Behaviour of Single and Orthogonal Polarized Arrays

The two-dimensional DOA tracking behaviour is analysed for the conventional single polarized and proposed orthogonal polarized array configurations. The following analyses illustrate 2D-DOA tracking behaviour for the single and orthogonal polarized using the instantaneous samples, weighting factor and forgetting factor approaches. The signal model for the 2D-DOA tracking with source angle $(\theta = 25^{\circ}, \phi = 15^{\circ})$ and destination angle $(\theta = 45^{\circ}, \phi = 50^{\circ})$ is modelled for the analysis with SNR of 20 dB. Between the source and destination angles, 100 data samples are modelled for the trajectory. The 2D MUSIC algorithm is used for the 2D tracking behaviour of the array configuration and average error of the 2D-DOA estimation per data sample is computed through the MSE performance analysis.

5.5.1 Tracking Behaviour of 2D-DOA Estimation with Single Polarized UPA

The conventional single polarized UPA configuration with rectangular waveguide shown in Figure 4.1, is analysed for its performance in the 2D-DOA tracking behaviour for the above mentioned signal model.

5.5.1.1 Tracking of 2D-DOA Estimation with UPA using Instantaneous Samples

The instantaneous data samples received in the conventional single polarized UPA configuration is used to construct the data covariance matrix, This data covariance matrix is used to estimate the 2D-DOA using 2D MUSIC algorithm. Thus every instant of the data samples and the respective data covariance will tend to estimate the 2D-DOA and track the trajectory of signal model.

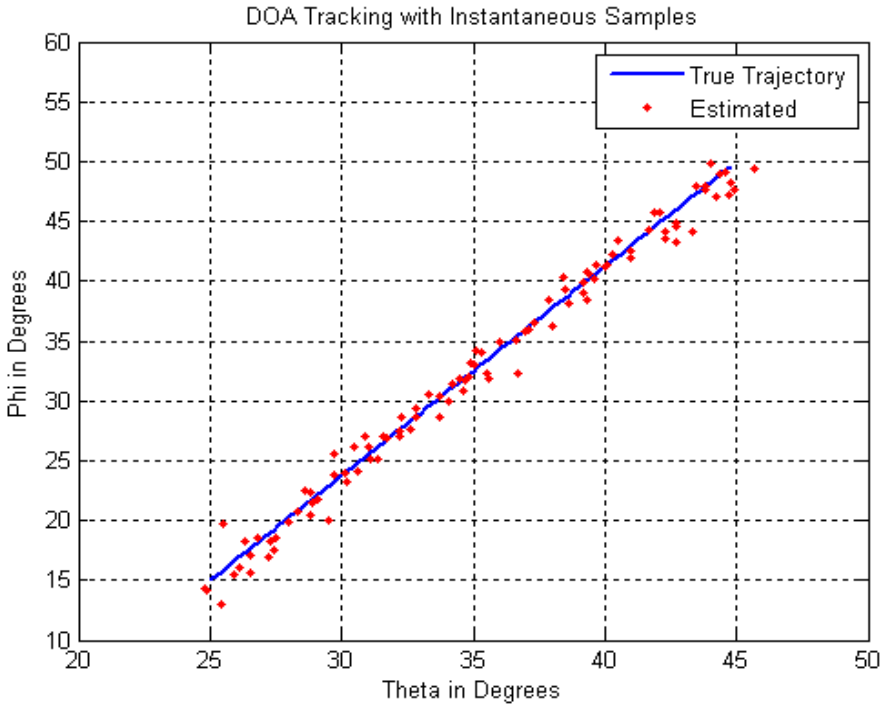

Figure 5.7: 2D-DOA Tracking with Uniform Planar Array with Instantaneous Samples with SNR 20 dB, $\theta_{mse} = 0.0826$ and $\phi_{mse} = 0.1304$

Figure 5.7 depicts the tracking behaviour using the instantaneous samples method. The estimated trajectory is compared with true trajectory of the signal model. The MSE between the true and estimated trajectories is calculated as $\theta_{mse} = 0.0826$ and $\phi_{mse} = 0.1304$.

5.5.1.2 Tracking of 2D-DOA Estimation with UPA using Weighting Factor

The conventional single polarized UPA is analysed for the 2D-DOA tracking behaviour with weighting factor based construction of data covariance matrix. The data samples of the signal model between the source and destination angles are utilized to form the

covariance matrix using the weighting factor approach. The weighting factor $\alpha = 0.5$ is chosen, and 2D-DOA tracking behaviour is analysed.

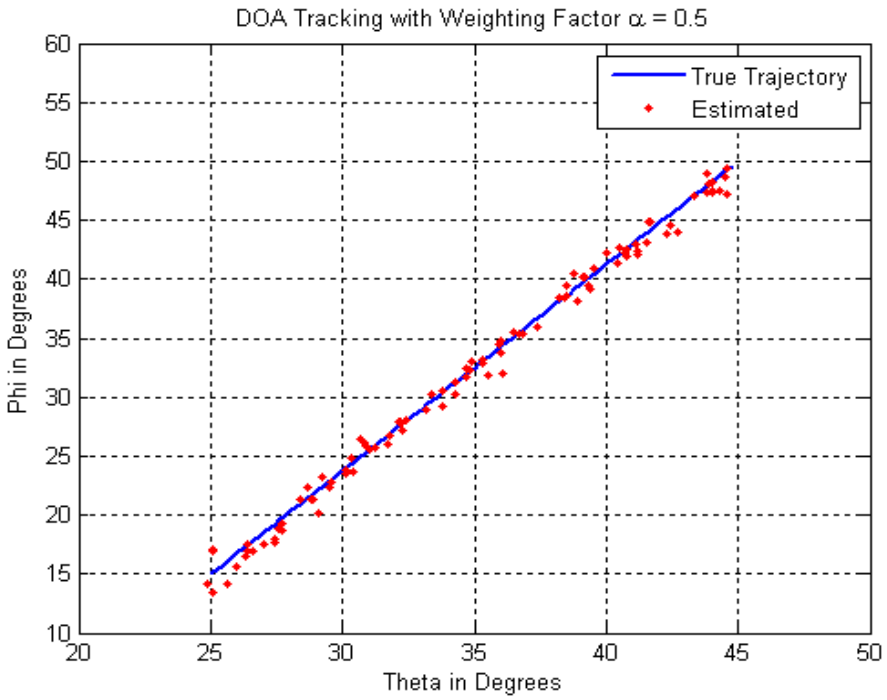

Figure 5.8: 2D-DOA Tracking with Uniform Planar Array with Weighting Factor with SNR 20 dB, $\theta_{mse} = 0.0559$ and $\phi_{mse} = 0.0939$

The performance of the tracking behaviour is analysed through computing the MSE of the θ and ϕ estimation of the tracking trajectory. The Figure 5.8 shows the tracking behaviour of the UPA utilizing weighting factor based data covariance matrix construction. The MSE of the tracking performance of DOA estimation is computed as $\theta_{mse} = 0.0559$ and $\phi_{mse} = 0.0939$. The weighting factor based tracking of 2D-DOA has lower error in both θ and ϕ estimations, when compared with the instantaneous samples based tracking behaviour.

5.5.1.3 Tracking of 2D-DOA Estimation with UPA using Forgetting Factor

The analysis of 2D-DOA estimation and tracking of dynamic sources has also been carried out with forgetting factor based construction of data covariance matrix. The parameters forgetting factor $\beta = 0.95$ and the order of smoothing filter $q = 4$ are fixed based on

performance analysis of the approach. The estimation error in θ and ϕ is computed through the MSE analysis.

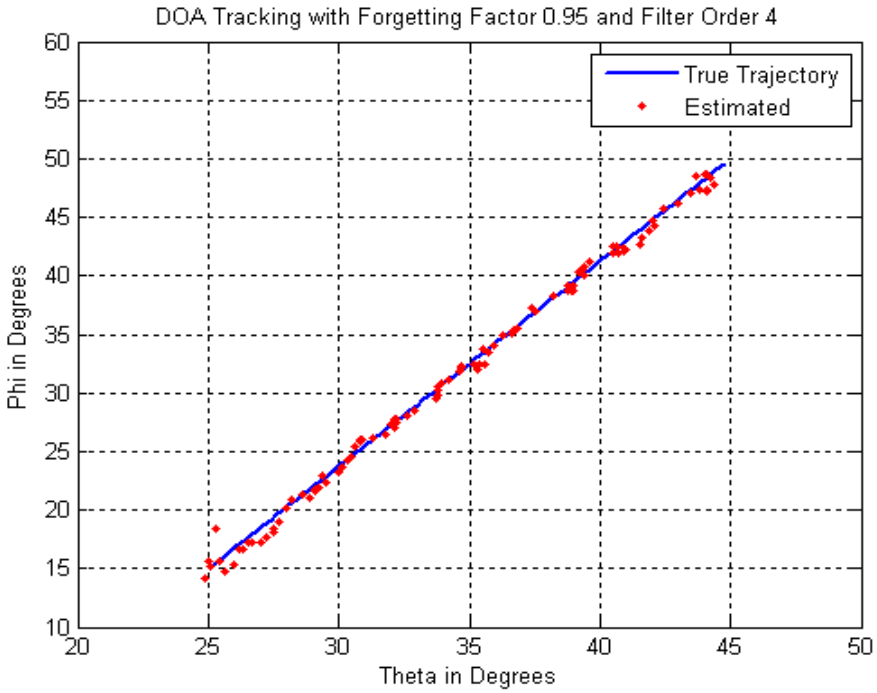

Figure 5.9: 2D-DOA Tracking with Uniform Planar Array with Forgetting Factor with SNR 20 dB, $\theta_{mse} = 0.0426$ and $\phi_{mse} = 0.0919$

Figure 5.9 depicts the tracking behaviour of the trajectory of the signal model. The MSE between the true trajectory and the estimated trajectory is computed as $\theta_{mse} = 0.0426$ and $\phi_{mse} = 0.0919$. Lowest MSE of the tracking behaviour of 2D-DOA estimation algorithm is realized with the forgetting factor approach. Due to presence of the forgetting factor as well as smoothing filter along with second order statistics of past data samples, improved tracking behaviour is realized using the forgetting factor based approach. The estimation and tracking performance of 2D-DOA estimation algorithm with forgetting factor approach tracking is better compared to instantaneous samples approach and weighting factor approach.

5.5.2 Tracking Behaviour of 2D-DOA Estimation with OPPA

The two dimensional DOA tracking behaviour analysis is performed for the proposed OPPA configuration. The OPPA configuration is as shown in Figure 4.2. The 2D-DOA

tracking is performed by tracking trajectory between with source angle $(\theta = 25^\circ, \phi = 15^\circ)$ and destination angle $(\theta = 45^\circ, \phi = 50^\circ)$ with 100 number of data samples between them. The signal model is used for the OPPA configuration, utilizing both horizontal and vertical polarized components of the RWG as per the geometric configuration shown in Figure 4.2. The tracking trajectory utilized for the analysis is maintained the same as with the case of conventional single polarized UPA configuration. Hence the comparison will reveal the influence of orthogonal polarized waveguide elements in the tracking behviour of the 2D-DOA estimation algorithm.

5.5.2.1 Tracking of 2D-DOA Estimation with OPPA using Instantaneous Samples

The OPPA configuration is subjected to estimate 2D-DOA, with the construction of data covariance matrix at every instant. This instantaneous sample based covariance matrix is utilized in 2D MUSIC algorithm for estimating both θ and ϕ angles of 2D-DOA for every data sample modelled in the trajectory.

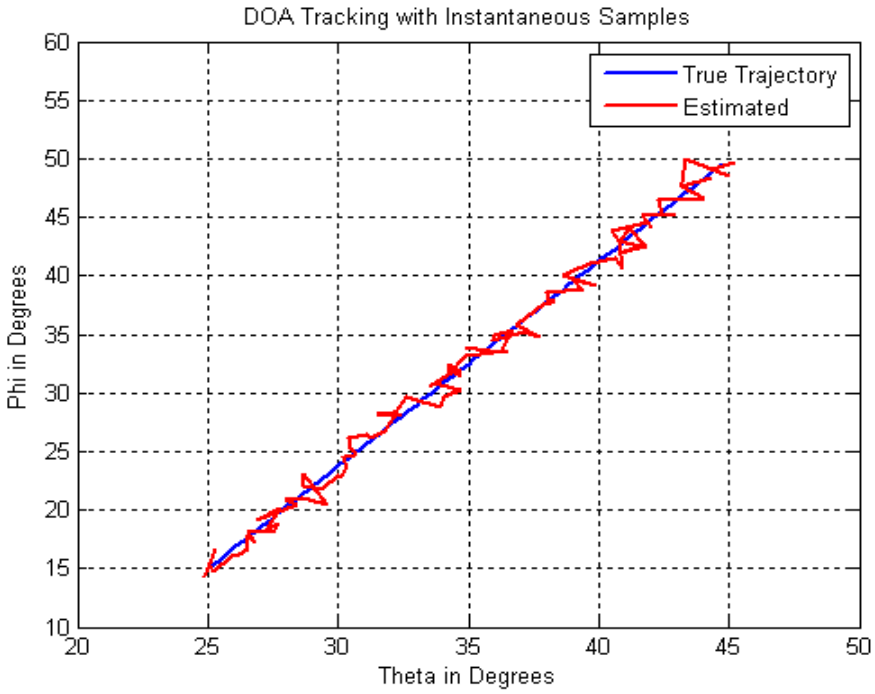

Figure 5.10: 2D-DOA Tracking with Orthogonal Polarized Planar Array with Instantaneous Samples with 20 dB SNR, $\theta_{mse} = 0.0499$ and $\phi_{mse} = 0.0559$

The tracking behaviour of estimation of 2D-DOA with the OPPA configuration is

shown in Figure 5.10. The comparison between the true trajectory and estimated trajectory reveals close agreement between them. The difference between the true trajectory of the signal model and the estimated trajectory through the DOA tracking algorithm is measured through the MSE between them. The computed average error per estimation for scenario of 20 dB SNR are $\theta_{mse} = 0.0499$ and $\phi_{mse} = 0.0559$. Comparatively the θ_{mse} and ϕ_{mse} are less, when compared with the single polarized UPA configuration. Hence, it can be concluded that, orthogonal polarized elements of the array configuration improve the estimation accuracy in tracking of 2D-DOA estimation.

5.5.2.2 Tracking of 2D-DOA Estimation with OPPA using Weighting Factor

The OPPA configuration is evaluated for its performance in 2D-DOA tracking behaviour by utilizing weighting factor based data covariance matrix construction. Keeping the signal model and tracking trajectory identical to the one used with instantaneous samples method, the weighting factor based data covariance method has been adopted in the estimation algorithm.

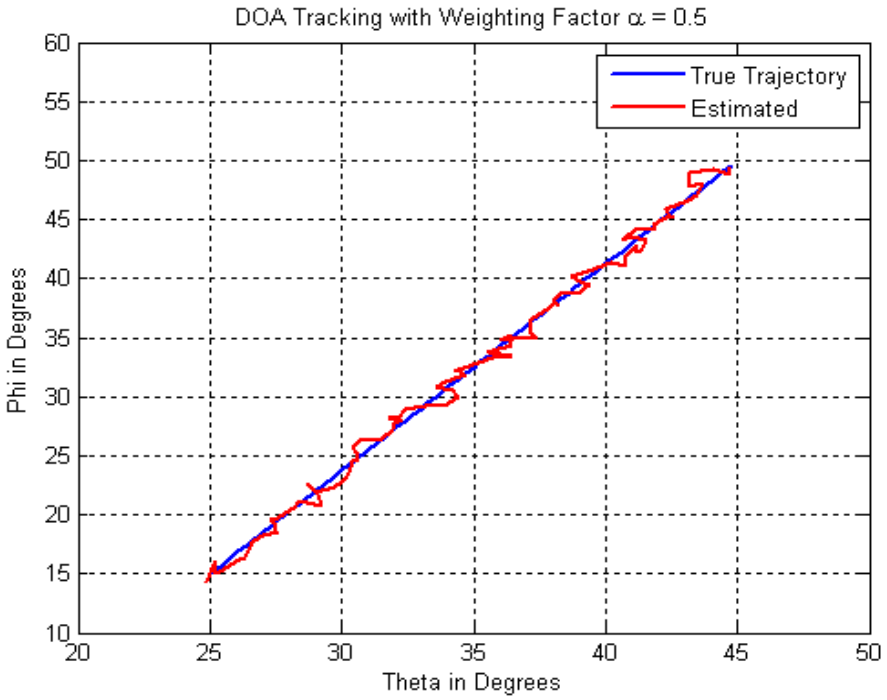

Figure 5.11: 2D-DOA Tracking with Orthogonal Polarized Planar Array with Weighting Factor 20 dB SNR, $\theta_{mse} = 0.0389$ and $\phi_{mse} = 0.0450$

The weighting factor α is fixed as 0.5, as per the analysis carried for this technique. This approach averages the current data sample received by the antenna array and immediate past sample with equal weights. The results of the tracking behaviour of 2D-DOA estimation with weighting factor approach are shown in Figure 5.11. The tracking behaviour shown in Figure 5.11 clearly depicts the close DOA tracking of the true trajectory. The computed MSE between true and estimated trajectories are $\theta_{mse} = 0.0389$ and $\phi_{mse} = 0.0450$. The MSE value indicates that, weighting factor approach improves estimation and tracking behaviour when compared to instantaneous sample approach. Also the influence of the orthogonal polarized elements in the array configuration is evident in realizing lesser MSE in the tracking, when compared with MSE of the single polarized UPA configuration.

5.5.2.3 Tracking of 2D-DOA Estimation with OPPA using Forgetting Factor

The tracking behaviour of the OPPA is also evaluated with forgetting factor approach.

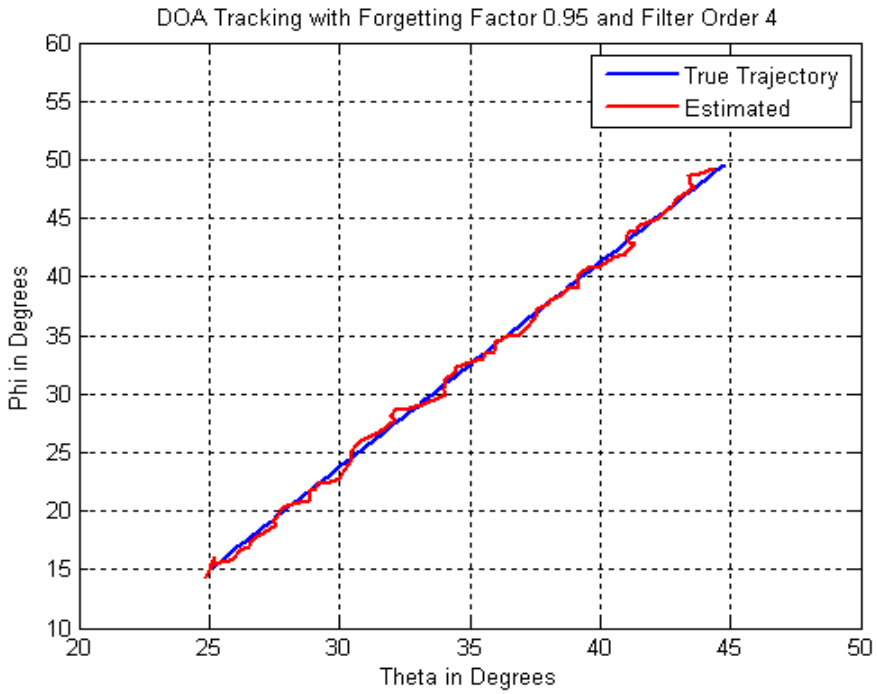

Figure 5.12: 2D-DOA Tracking with Orthogonal Polarized Planar Array with Forgetting Factor 20 dB SNR, $\theta_{mse} = 0.0380$ and $\phi_{mse} = 0.0622$

The analysis is carried by keeping the same signal model and trajectory model. The influence of orthogonal polarized wave guide elements present in the array configuration,

along with the forgetting factor based approach for the construction of covariance matrix in improving the estimation accuracy is analysed. The parameters, forgetting factor and order smoothing filter are fixed as $\beta = 0.95$ and $q = 4$ based on the detailed analysis carried for this approach. The improved tracking behaviour of OPPA is depicted in the Figure 5.12. It is seen from the results of the Figure 5.12, that there is a close agreement of estimated trajectory of DOA with true trajectory and the same is evident through the computation of MSE between them. The computed MSE between the estimated trajectory and true trajectory are $\theta_{mse} = 0.0380$ and $\phi_{mse} = 0.0622$. The MSE value depicts the lesser estimation error both in the θ and ϕ DOA angles, which has resulted in improved tracking behaviour. The combination of forgetting factor approach and the orthogonal polarized array elements is an effective combination in improving the estimation accuracy and the tracking behaviour of 2D-DOA estimation algorithm.

5.5.3 Tracking Behaviour of 2D-DOA Estimation with OMLA

The simulation analysis of the tracking behaviour of 2D-DOA estimation is extended for the OMLA configuration. In the OMLA, both the horizontal and vertical polarized waveguide elements are combined together to form the orthogonal mounting. This orthogonal mounting arrangement along the array axis as shown in Figure 4.3 is examined for its performance in tracking of a 2D-DOA trajectory between the source and destination angles. The signal model for the analysis is carried as per the geometric configuration of the array elements and the trajectory modelled between the source angle $(\theta = 25^\circ, \phi = 15^\circ)$ and destination angle $(\theta = 45^\circ, \phi = 50^\circ)$ with 100 number of data samples between them. The OMLA configuration also has the orthogonal polarized (both horizontal and vertical) elements. It is anticipated that, the estimation and tracking performance of 2D-DOA estimation will be similar to that with the OPPA configuration.

5.5.3.1 Tracking of 2D-DOA Estimation with OMLA using Instantaneous Samples

The signal model and trajectory model for the OMLA are evaluated for 2D-DOA tracking with the instantaneous sample method for the construction of data covariance matrix. The data covariance matrix is subjected to 2D-DOA estimation algorithm and the MSE performance of the 2D-DOA tracking is evaluated.

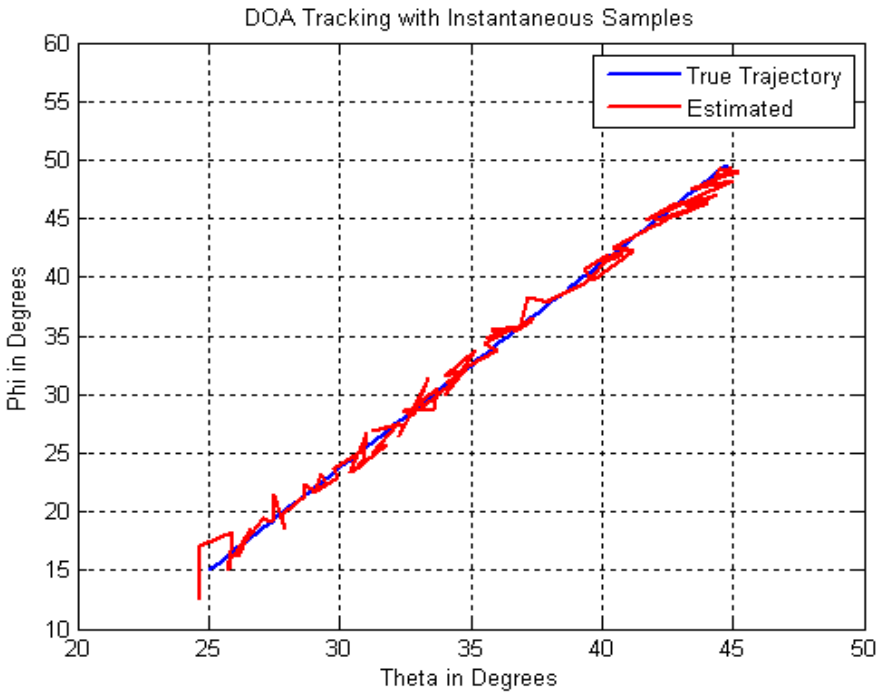

Figure 5.13: 2D-DOA Tracking with Orthogonal Mounted Linear Array with Instantaneous Samples with 20 dB SNR, $\theta_{mse} = 0.0499$ and $\phi_{mse} = 0.0559$

The results of the 2D tracking behaviour of OMLA configuration are shown in Figure 5.13. The simulation results of Figure 5.13 show relatively poor performance in the 2D-DOA estimation and tracking behaviour. The comparison of true and estimated trajectory is analysed through computing MSE of the θ and ϕ of data samples. The computed MSE of $\theta_{mse} = 0.0499$ and $\phi_{mse} = 0.0559$ in the tracking behaviour for the OMLA configuration is realized.

5.5.3.2 Tracking of 2D-DOA Estimation with OMLA using Weighting Factor

The simulation analysis of 2D-DOA tracking for the OMLA configuration is extended by utilizing the weighting factor based construction of data covariance matrix. The weighting factor $\alpha = 0.5$ reveals that it provides the data covariance matrix with the equal weighted average of the current and past data samples.

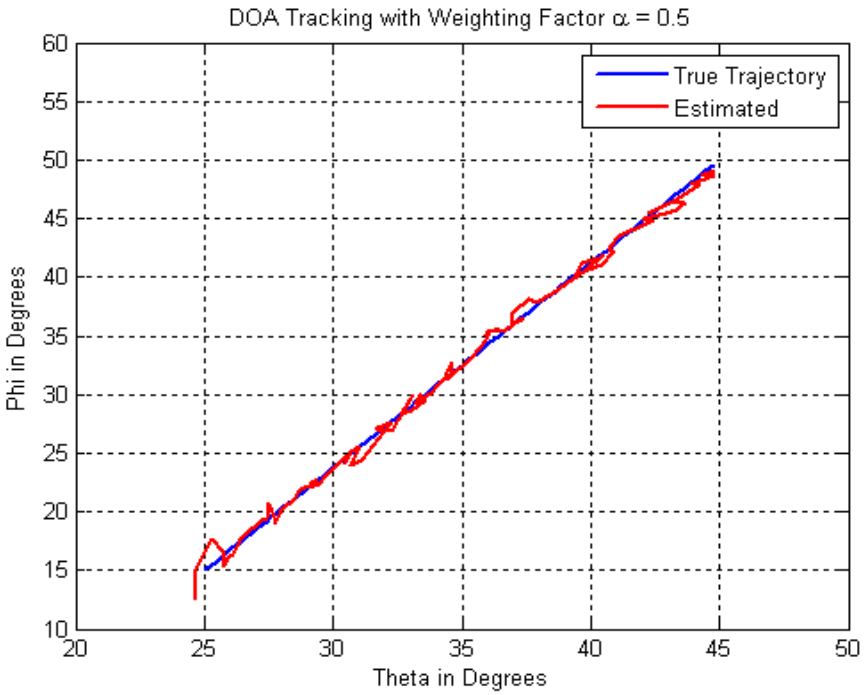

Figure 5.14: 2D-DOA Tracking with Orthogonal Mounted Linear Array with Weighting Factor 20 dB SNR, $\theta_{mse} = 0.0389$ and $\phi_{mse} = 0.0450$

The tracking of 2D-DOA estimation with OMLA is illustrated through the Figure 5.14. The results illustrated in Figure 5.14 depict that weighting factor approach improves the accuracy in the tracking behaviour of 2D-DOA when compared to instantaneous sample approach. The improved accuracy in the tracking behaviour is evident by comparing the difference between the true and estimation trajectories by computing MSE. The computed MSE $\theta_{mse} = 0.0389$ and $\phi_{mse} = 0.0450$ indicates the lesser MSE values when compared with the instantaneous sample approach. This signifies the benefit of weighting factor in the formation of the data covariance matrix of the 2D-DOA estimation algorithm.

5.5.3.3 Tracking of 2D-DOA Estimation with OMLA using Forgetting Factor

The OMLA configuration is analysed for its performance in tracking of 2D-DOA estimation by utilizing the forgetting factor based approach in the construction of data covariance matrix. The orthogonal polarized elements in the array configuration along with the forgetting factor techniques are anticipated to improve the tracking behaviour of 2D-DOA estimations. The forgetting factor $\beta = 0.95$ and order of the smoothing filter of $q = 4$ are fixed as per the earlier detailed study of this approach.

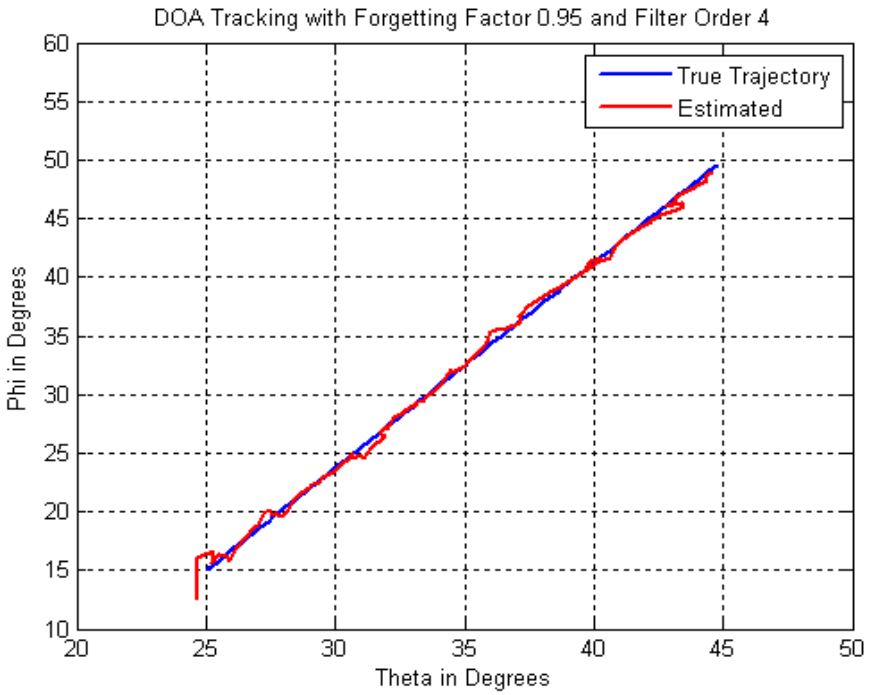

Figure 5.15: 2D-DOA Tracking with Orthogonal Mounted Linear Array with Forgetting Factor 20 dB SNR, $\theta_{mse} = 0.0380$ and $\phi_{mse} = 0.0622$

The tracking behaviour of 2D-DOA estimation using the OMLA is depicted in the Figure 5.15. The combination of the orthogonal polarized elements in the array and forgetting factor approach improves the 2D estimation and tracking behaviour. The improved tracking behaviour of 2D-DOA estimation is evident through the lesser MSE $\theta_{mse} = 0.0380$ and $\phi_{mse} = 0.0622$. The results of Figure 5.15 confirm the significance of utilizing the past data samples and the orthogonal polarized components of the received data.

5.5.4 Tracking Behaviour of 2D-DOA Estimation with OPLA

The simulation analysis for the tracking of 2D-DOA estimation is further extended to analyse the performance of the OPLA configuration. The OPLA configuration shown in Figure 4.4 has the linear arrangement of the RWG elements on the x axis with adjacent elements in orthogonal configuration. The signal model for the linear orthogonal array configuration is carried as per its geometric configuration shown in Figure 4.4. Without incorporating any changes in the trajectory model between the source angle $(\theta = 25^\circ, \phi = 15^\circ)$ and destination angle $(\theta = 45^\circ, \phi = 50^\circ)$ with 100 number of data samples, the tracking performance of 2D-DOA estimation is analysed. The performance of OPLA configuration performance

in tracking of 2D-DOA estimation is evaluated through computing the MSE between the true and estimated trajectories.

5.5.4.1 Tracking of 2D-DOA Estimation with OPLA using Instantaneous Samples

The signal model and the trajectory model are subjected to the tracking analysis of 2D-DOA estimation by utilizing the instantaneous samples of the model, for the formation of data covariance matrix. This data covariance matrix is incorporated into the 2D MUSIC algorithm, through which 2D-DOA estimation is performed.

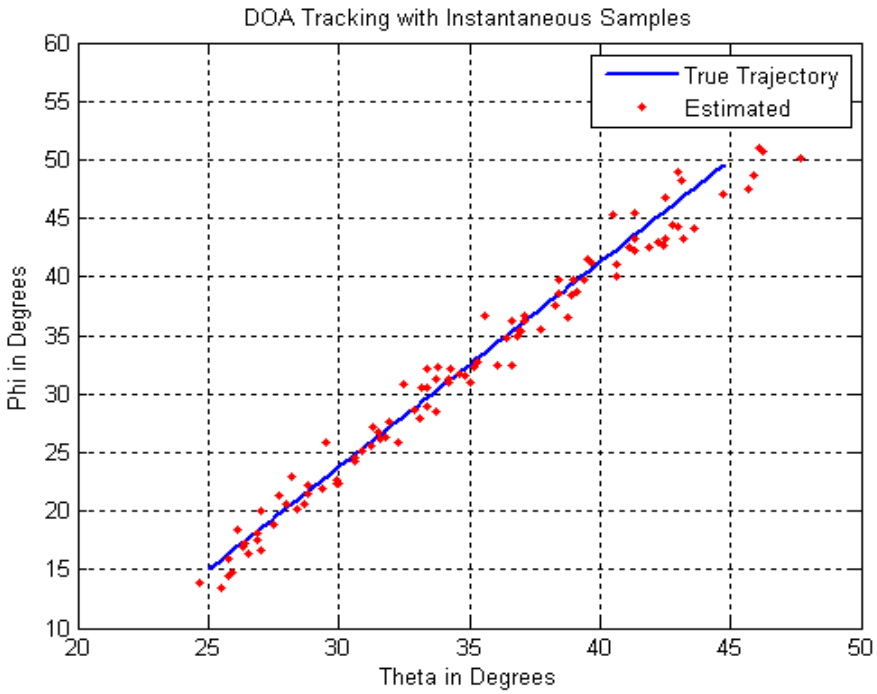

Figure 5.16: 2D-DOA Tracking with Orthogonal Polarized Linear Array with Instantaneous Samples with 20 dB SNR, $\theta_{mse} = 0.1386$ and $\phi_{mse} = 0.1351$

The OPLA exhibits its tracking behaviour of 2D-DOA estimation as shown in Figure 5.16. The comparison between the true trajectory and the estimated trajectory is computed is analysed through MSE between them, and the computed MSE is $\theta_{mse} = 0.1386$ and $\phi_{mse} = 0.1351$. The MSE of the 2D-DOA tracking with OPLA is slightly higher, when compared with the other array configurations presented earlier. Slightly higher MSE is attributed to the only linear arrangement of the array elements despite the presence of orthogonal elements.

5.5.4.2 Tracking of 2D-DOA Estimation with OPLA using Weighting Factor

The evaluation of OPLA is carried further by utilizing weighting factor, without incorporating any changes in the signal model and the trajectory model presented earlier in this section. The weighting factor based approach for the data covariance matrix in the 2D MUSIC algorithm is simulated and performance analysis of the OPLA is examined by comparing the true trajectory and the estimated trajectory.

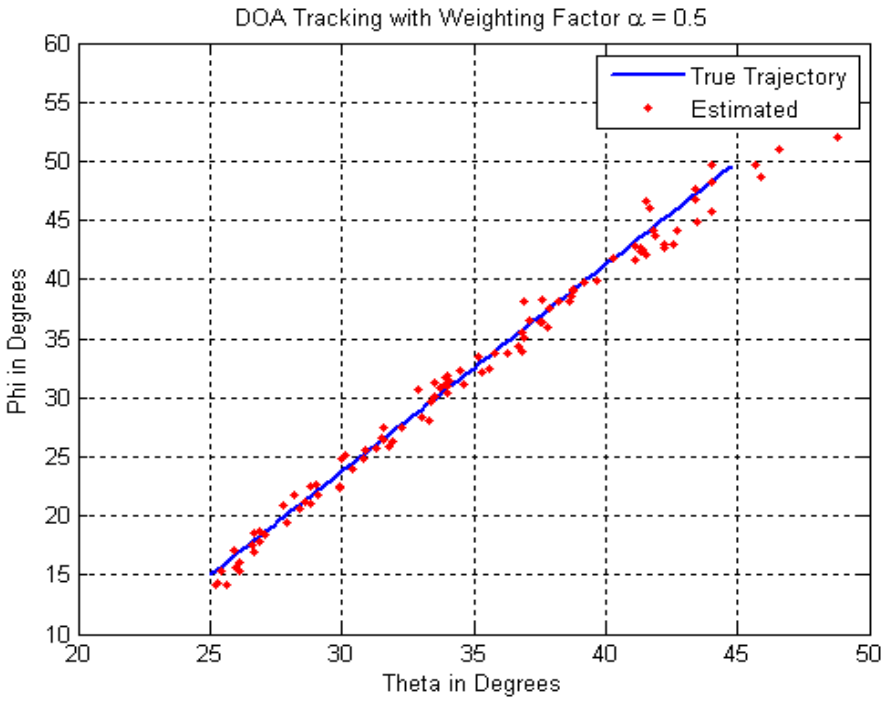

Figure 5.17: 2D-DOA Tracking with Orthogonal Polarized Linear Array with Weighting Factor 20 dB SNR, $\theta_{mse} = 0.0843$ and $\phi_{mse} = 0.0994$

The Figure 5.17 depicts the tracking behaviour of 2D-DOA estimation with OPLA. The tracking behaviour illustrates the improvement in trajectory tracking when compared to the instantaneous samples approach. However, due the linear arrangement of the array configuration, the MSE between the true and estimated trajectory is $\theta_{mse} = 0.0843$ and $\phi_{mse} = 0.0994$. This is higher when compared with single polarized UPA configuration.

5.5.4.3 Tracking of 2D-DOA Estimation with OPLA using Forgetting Factor

The OPLA configuration is studied for its performance in tracking behaviour of 2D-DOA estimation by incorporating forgetting factor approach in the 2D-DOA estimation. With

no modifications in the signal and trajectory model, simulation of OPLA with forgetting factor approach of covariance data matrix is performed and the performance is analysed through the MSE between the true and estimated trajectories.

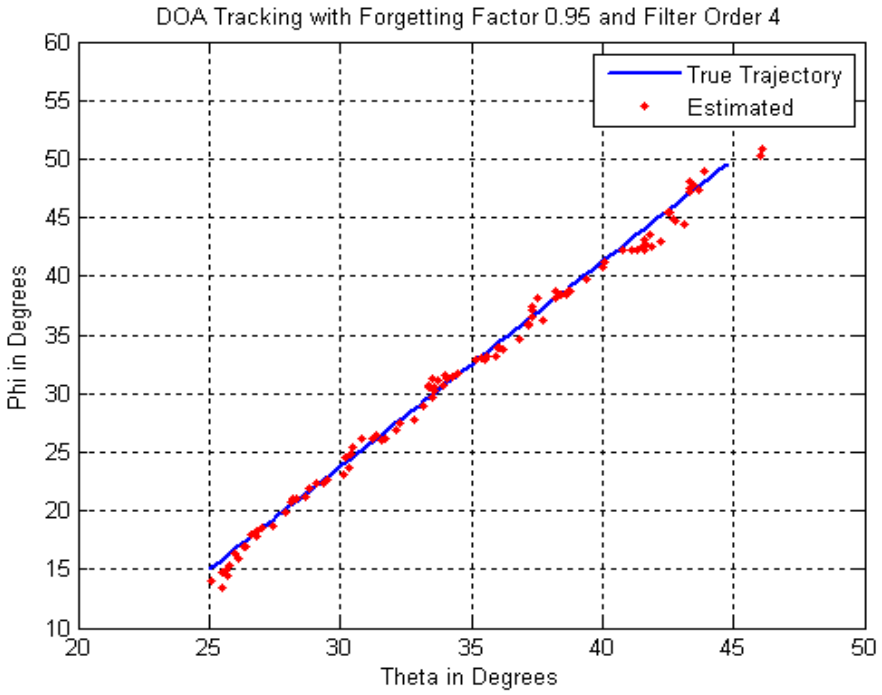

Figure 5.18: 2D-DOA Tracking with Orthogonal Polarized Linear Array with Forgetting Factor 20 dB SNR, $\theta_{mse} = 0.0515$ and $\phi_{mse} = 0.0952$

The results of the tracking of 2D-DOA estimation with OPLA are shown in Figure 5.18. The results of Figure 5.18 illustrate close agreement in tracking behaviour, by estimating the 2D-DOA to be very close to the actual DOAs. The improvement in the tracking behaviour of 2D-DOA estimation using forgetting factor approach is evident through lesser MSE between the estimation and true trajectories, which is computed as $\theta_{mse} = 0.0515$ and $\phi_{mse} = 0.0952$.

5.6 Computation Analysis of MSE versus SNR in Tracking Behaviour of 2D-DOA Estimation with Single Polarized and Orthogonal Polarized Arrays

In the previous section, the analysis of the tracking behaviour of 2D-DOA estimation is evaluated for single and orthogonal polarized array configurations with 20 dB SNR. The simulation analysis is extended further to analyse the tracking behaviour of 2D-DOA

estimation with lower and higher SNR values. The tracking behaviour of 2D-DOA estimation of the single polarized conventional UPA configuration and the proposed orthogonal polarized array configurations is examined by utilizing three different approaches for the construction of covariance matrix namely, instantaneous samples, weighting factor and forgetting factor approaches. The comparison of MSE of θ and ϕ angles for each of the approaches with both the conventional single polarized and orthogonal polarized array configuration is carried with respect to the SNR values of 10, 20 and 30 dB.

5.6.1 MSE Performance Analysis of Tracking Behaviour of 2D-DOA Estimation with Instantaneous Samples

The MSE between the true and estimated trajectories of the conventional single and orthogonal polarized array configurations is analysed by utilizing the instantaneous sample approach. Both the θ and ϕ angles of 2D-DOA estimation are analysed through its MSE performance. The results comparing the MSE θ_{mse} and ϕ_{mse} versus the low, medium and high SNR values, for the conventional single polarized UPA, and the proposed OPPA, OMLA and OPLA are illustrated in Figures 5.19 and 5.20.

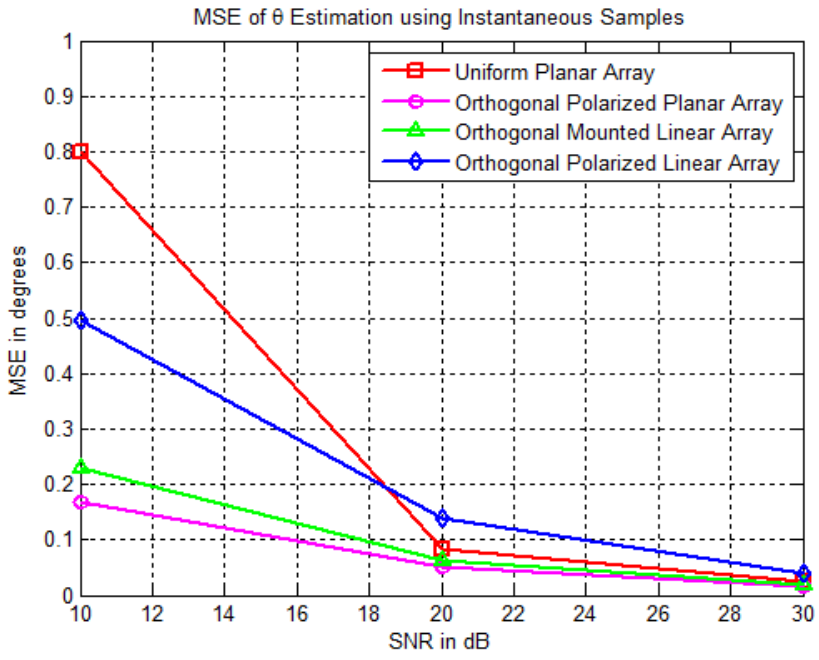

Figure 5.19: Comparison of MSE of θ Estimation using Instantaneous Samples

The results of the Figures 5.19 and 5.20 indicate that, for this trajectory model, θ_{mse}

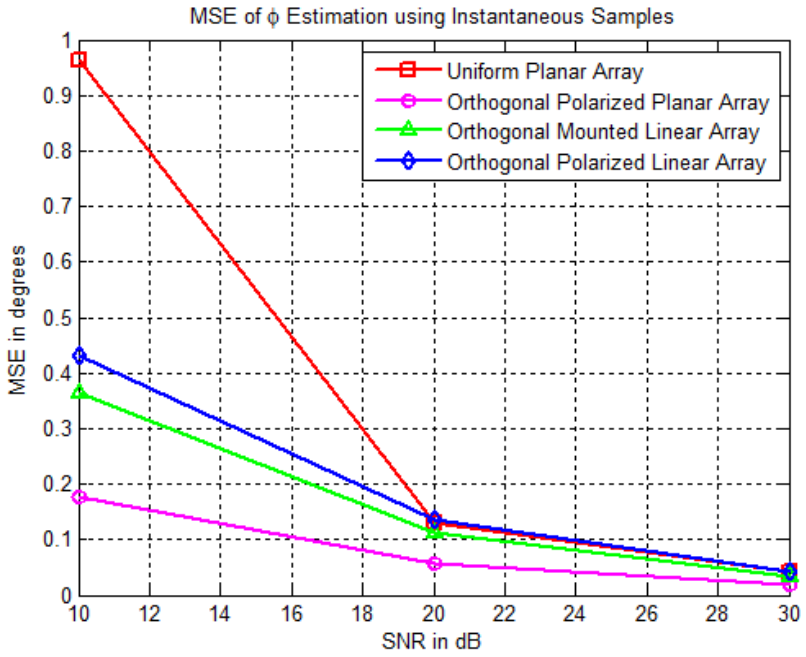

Figure 5.20: Comparison of MSE of ϕ Estimation using Instantaneous Samples

is very less when compared to ϕ_{mse} estimations. As expected, at low SNR, the MSE is more. At higher SNR, MSE is very low with (less than 0.1°), due to lesser noise. The MSE of the conventional signal polarized UPA exhibits higher estimation error in both θ and ϕ estimation angles. On the contrary, all the proposed orthogonal polarized array configurations show less MSE in the tracking behaviour. In both, the θ and ϕ estimation, the OPPA configuration exhibits superior performance in the tracking of 2D-DOA estimation among all other configurations. Also, the OMLA also performs better compared to OPLA and single polarized UPA configuration.

5.6.2 MSE Performance Analysis of Tracking Behaviour of 2D-DOA Estimation with Weighting Factor

The conventional single polarized UPA configuration and the proposed orthogonal configurations such as OPPA, OPMA and OPLA are invoked for the analysis of tracking behaviour of 2D-DOA estimation with low, medium and high SNR scenarios.

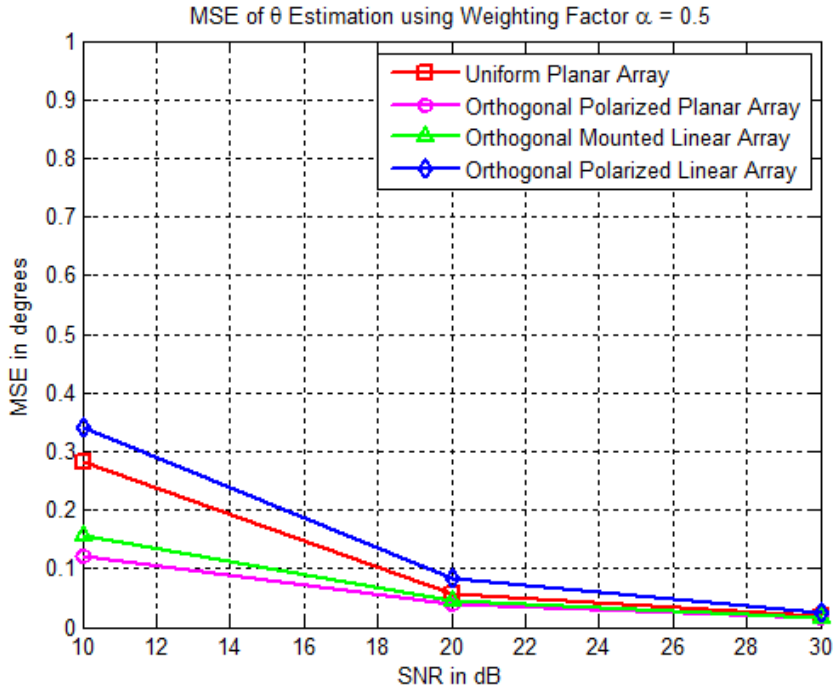

Figure 5.21: Comparison of MSE of θ Estimation using Weighting Factor

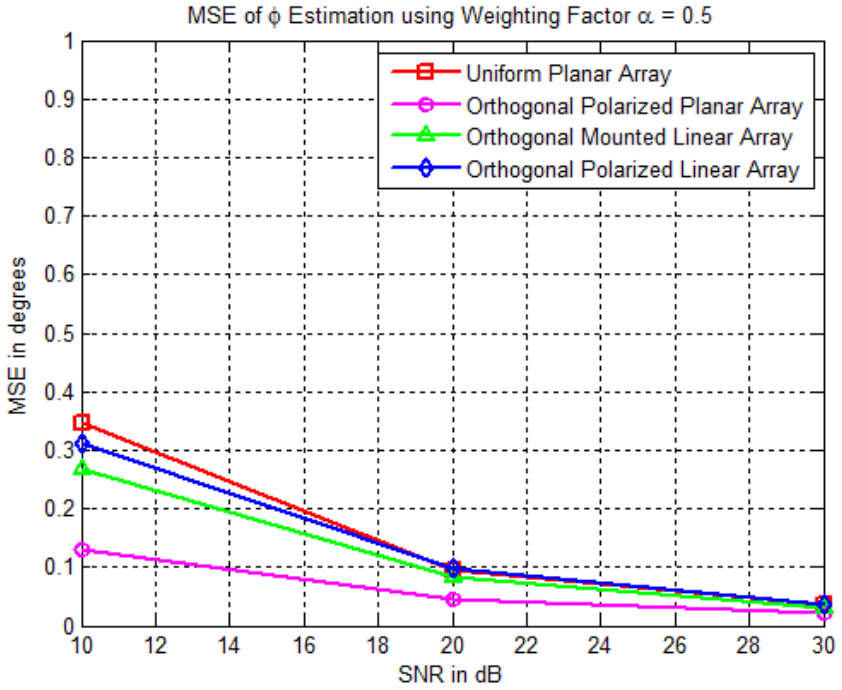

Figure 5.22: Comparison of MSE of ϕ Estimation using Weighting Factor

The analysis is carried by incorporating weighting factor approach for data covariance matrix in the 2D-DOA estimation and tracking. A weighting factor $\alpha = 0.5$ is incorporated in the construction of data covariance matrix, which induces the weighted average of the current and immediate past data samples. The simulation analysis with weighting factor approach is illustrated by plots of MSE versus SNR for the conventional single polarized array configuration and the proposed orthogonal polarized array configurations. The MSE θ_{mse} and ϕ_{mse} for all the array configurations are shown in Figures 5.21 and 5.22 respectively. The results of the Figures 5.21 and 5.22 clearly depict the performance improvement in the tracking behaviour of 2D-DOA estimation of all the array configuration, when compared to instantaneous samples approach. The consistency in the improved tracking behaviour of 2D-DOA estimation is evident in both the θ_{mse} and ϕ_{mse} of estimations for all the array configurations. At low SNRs, all the array configurations exhibit lesser than 0.4° estimation error in both the θ and ϕ estimations. The analysis invariably infers that, OPPA is best among all other array configurations, in the tracking behaviour of the trajectory of 2D-DOA, by estimating θ and ϕ with least MSE values. The OMLA configuration continues to perform better, when compared to OPLA and single polarized UPA configurations. The OPLA shows a slightly inferior performance in its θ estimations at lower SNR, when compared to the single polarized UPA configuration. The ϕ angle estimations with OPLA is more accurate when compared to single polarized UPA configuration. However, at medium and higher SNR scenarios, the OPLA and UPA show on an average the same tracking behaviour with negligibly small difference.

5.6.3 MSE Performance Analysis of Tracking Behaviour of 2D-DOA Estimation with Forgetting Factor

The MSE performance analysis for the low, medium and high SNR scenarios is extended further with formation of data covariance matrix with forgetting factor approach. The conventional single polarized UPA as well as the proposed OPPA, OMLA and OPLA configuration are analysed for its MSE performance by incorporating the forgetting factor approach in the formation of data covariance matrix in the 2D-DOA estimation and tracking technique.

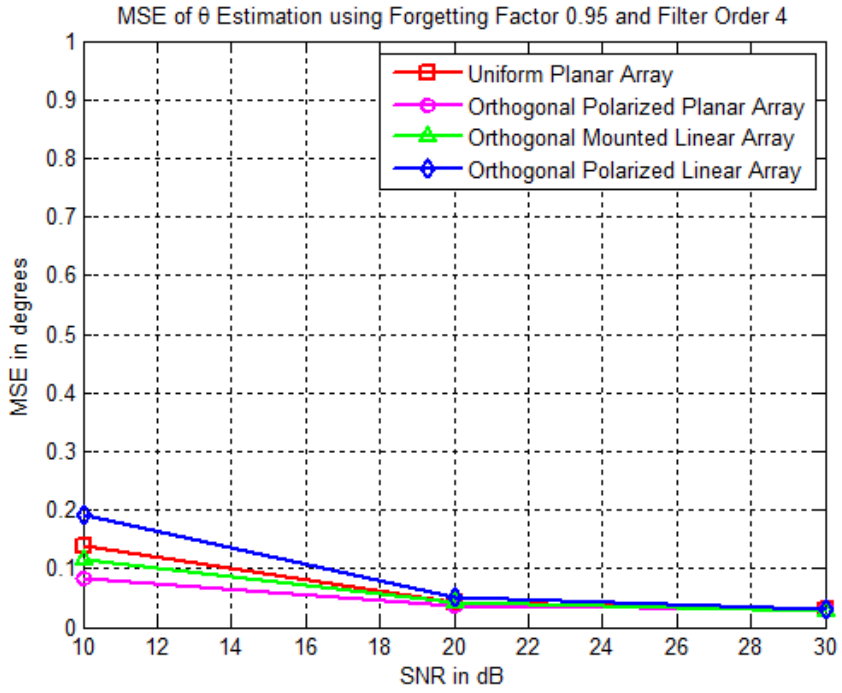

Figure 5.23: Comparison of MSE of θ Estimation using Forgetting Factor

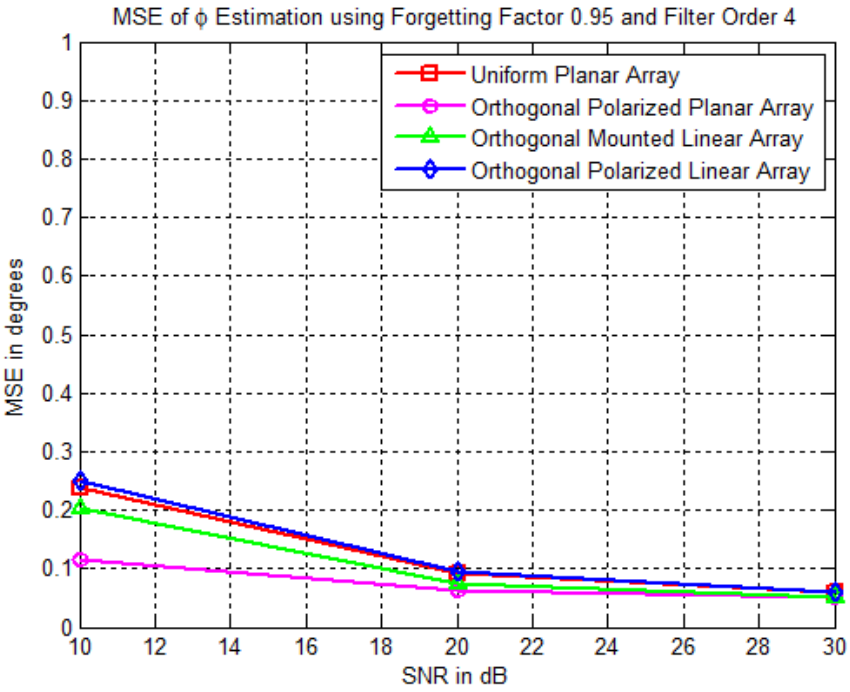

Figure 5.24: Comparison of MSE of ϕ Estimation using Forgetting Factor

The forgetting factor $\beta = 0.95$ and order of the smoothing filter $q = 4$ are incorporated in the simulation based on the extensive analysis of the approach. The tracking behaviour of 2D-DOA estimation with forgetting factor approach is superior in its performance, which is evident from the previous analysis presented earlier. The tracking behaviour of 2D-DOA estimation realized with forgetting factor based covariance matrix is consistently better when compared to those realized with the instantaneous approach as well as weighting factor approach. The results of the Figures 5.23 and 5.24 exhibiting the better MSE performance of θ and ϕ respectively are clear indicators of the superior performance of 2D-DOA tracking behaviour. The forgetting factor approach shows the MSE lesser than 0.25° at lower SNR scenario, which is the least estimation error, when compared to the instantaneous and weighting factor approaches. The results of the Figures 5.23 and 5.24 infer the individual performance of the array configurations considered in the simulation analysis. The OPPA configuration continues to exhibit least estimation error in both, θ and ϕ estimations, and thus shows the superior performance in the trajectory estimation of 2D-DOA. The OMLA proves to be next best alternate to OPPA configuration in the estimation accuracy of both θ and ϕ angles. The OPLA and the UPA configurations show similar performance as with case of weighting factor approach with reduced estimation error. The linear arrangement of elements in OPLA for 2D-DOA estimation limits the estimation performance at low SNR, when compared with the single polarized UPA configuration. However, the advantage of linear arrangement can also be factor that needs to be considered along the estimation accuracy.

Table 5.1: Comparison of MSE of Antenna Configurations for 2D-DOA Tracking

Configuration	**SNR in dB**	**Instantaneous Samples**		**Weighting Factor** $\alpha = 0.5^\circ$		**Forgetting Factor** $\beta = 0.95$ **and** $q = 4$	
		θ_{mse}	ϕ_{mse}	θ_{mse}	ϕ_{mse}	θ_{mse}	ϕ_{mse}
Conventional	10	0.7995	0.9610	0.2812	0.3456	0.1376	0.2381
Uniform Planar	20	0.0826	0.1304	0.0559	0.0939	0.0426	0.0919
Array	30	0.0247	0.0409	0.0199	0.0357	0.0305	0.0597
Orthogonal	10	0.1671	0.1762	0.1200	0.1301	0.0826	0.1146
Polarized Planar	20	0.0499	0.0559	0.0389	0.0450	0.0380	0.0622
Array	30	0.0156	0.0176	0.0159	0.0230	0.0297	0.0520
Orthogonal	10	0.2293	0.3635	0.1554	0.2684	0.1144	0.2029
Mounted Linear	20	0.0633	0.1115	0.0462	0.0834	0.0420	0.0739
Array	30	0.0194	0.0343	0.0172	0.0304	0.0290	0.0504
Linear	10	0.4961	0.4325	0.3411	0.3123	0.1912	0.2509
Orthogonal	20	0.1386	0.1351	0.0843	0.0994	0.0515	0.0952
Array	30	0.0384	0.0420	0.0261	0.0361	0.0307	0.0587

5.7 Summary

The simulation analysis of 2D-DOA estimation and tracking using the conventional single polarized and orthogonal polarized array configurations are performed. The tracking behaviour of 2D-DOA estimation with various array configurations are analysed by comparing the computed MSE between true trajectory of the signal model and estimated trajectory. Different schemes such as instantaneous samples approach, weighting factor approach and forgetting factor approach have been utilized for the formation of data covariance matrix involved in the MUSIC algorithm. The resulting MSEs for θ and ϕ angles of 2D-DOA are computed using the data covariance matrix using three different approaches. The results of the various analysis are tabulated for the low, medium and high SNR scenarios in the Table 5.1.

Chapter 6

DOA Estimation of Wideband Sources

This chapter presents the analysis and simulation of 1D and 2D-DOA estimation of wideband signal sources. A comparison of performance between the conventional wideband DOA estimation schemes with proposed subband filter approach is carried. A study on proposed subband filter approach for 2D-DOA estimation of wideband sources with single polarized UPA and the orthogonal polarized array configurations is performed for single and two sources for a wide range of SNR scenarios.

6.1 Introduction

Further to the analysis of 2D-DOA estimation and tracking, the single polarised conventional UPA and the proposed orthogonal polarized array configurations are evaluated for the 2D-DOA estimation of wideband signal sources. A signal whose energy is spread over a bandwidth, that is large in comparison to the signal center frequency is said to be wideband signal. The estimation of the DOA of wave-fronts carrying wideband signal is one of the critical tasks in DOA estimation. The rotational signal subspace and signal subspace transformation and many beamspace processing techniques are cited in literature for DOA of wideband sources (Sellone, 2005). The localization of a wideband signal exploiting the array of wideband antenna elements using the conventional narrow band techniques will fail. The limitation of narrowband techniques is that they exploit only the time delays which directly translate to a phase shift in the frequency domain (Stoica & Moses, 1997; Yoon, 2004). The performance of the subband filter approach for wideband 2D-DOA estimation, proposed in this chapter has been compared with performance of conventional ICM and CSSM techniques discussed in Chapter 2.

Conventionally DOA estimation is carried through CSSM and ICM methods. In CSSM, averaging of the spectrum is carried out after the focusing (transformation) of the subspace vectors to the desired frequency. Whereas in ICM, the averaging is performed without the transformation of subspace vectors. However the number of subspace computations

involved in EVD or SVD significantly increases the computational burden of CSSM and ICM methods. Also these methods suffer in their accuracy due to their high susceptibility to the noise present in the spatial samples.

6.2 Sub-band Filtering Approach

This section presents an analytical formulation for a subband filtering approach for the DOA estimation of wideband signal. The wideband signal received in the antenna array is passed through the set of filters. The filters are designed as sub-bands of the frequency spectrum (Vaidyanathan, 1993; Woods & O'Neil, 1986). The subband filtering technique is proposed for DOA estimation of wideband signals and it overcomes the limitations associated with the CSSM and ICM techniques. The block diagram of the subband filtering with two subbands is shown in Figure 6.1. In the proposed technique, there are two subband filters namely low band and high band. The low pass and high pass sub band filters are 2^{nd} order FIR type with normalized frequency response. The impulse response of the subbands

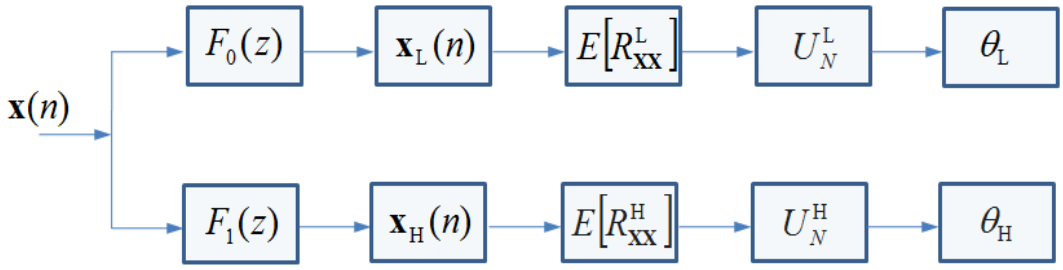

Figure 6.1: Two Subband Approach for Wideband DOA Estimation

is designed with subband filter design Equation (6.1). The normalized frequency spectrum is split into L number of subbands.

$$\mathbf{F}_l(z) = e^{\frac{i2\pi lg}{L}} \tag{6.1}$$

where L is the total number of subbands, in which l^{th} subband filter $\mathbf{F}_l(z)$ is designed with Equation (6.1). Here $l = 0, 1, \ldots, L-1$ and g is coefficient of the l^{th} subband filter $g = 0, 1, \ldots, L-1$. The block diagram shown in Figure 6.1 represents a two subband filtering approach in which $L = 2$ is applied. In the two subband approach the normalized frequency spectrum is divided into low pass subband filter $\mathbf{F}_0(z)$ and a high pass subband filter $\mathbf{F}_1(z)$. The frequency response of the low pass and high pass subband filters is shown in Figure 6.2. For wideband DOA estimation, the obtained samples from the array $\mathbf{x}_n$ is

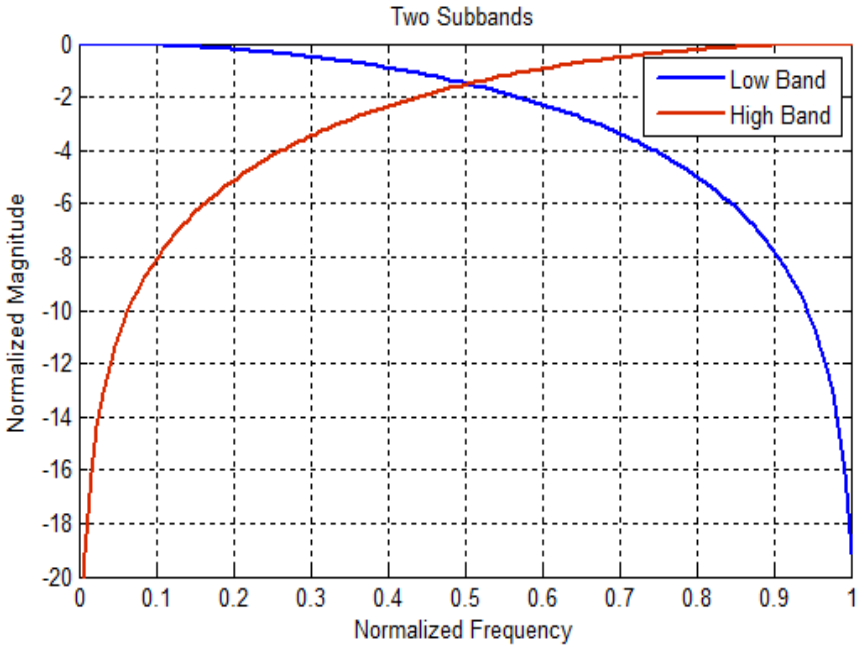

Figure 6.2: Two Subband Filters for Subband Technique

filtered through the designed filter banks. The covariance matrix of respective low and high band filtered signal components is computed as given in Equations (6.2) and (6.3) respectively.

$$\mathbf{R}_{\mathbf{xx}}^{\mathbf{L}} = E[\mathbf{x_L}(n)\mathbf{x_L}(n)^H] \tag{6.2}$$

$$\mathbf{R}_{\mathbf{xx}}^{\mathbf{H}} = E[\mathbf{x_H}(n)\mathbf{x_H}(n)^H] \tag{6.3}$$

In Equation (6.3), the subscript **H** refers to high band and the superscript $(.)^H$ refers to Hermitian conjugate. The covariance matrix of the low band and high band signal components is subjected to EVD or SVD to compute its noise subspace $\mathbf{U}_N$. This noise subspace is utilized in the conventional MUSIC algorithm for the estimation of DOA from the low band component θ_L and the high band component θ_H.

6.3 Simulation Analysis of DOA Estimation of Wideband Sources

Simulation of DOA estimation of wideband signal is carried by invoking wideband DOA estimation methods such as the conventional ICM, CSSM and the proposed two subband method for its performance analysis.

6.3.1 Wideband Signal Model

A ULA consisting of 15 antenna elements is modelled with its element exhibiting unity omni-directional gain. A wideband signal model of frequency range 9.1 GHz to 9.5 GHz was modelled to incident on ULA at a DOA angle $\theta = -30^{\circ}$. Narrow band signal sources

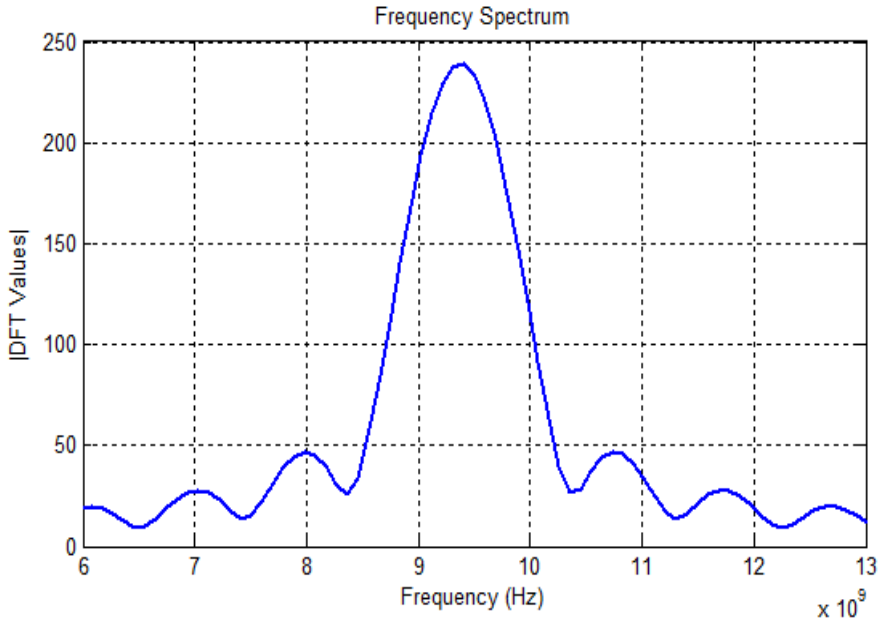

Figure 6.3: Wideband Source with Frequency Spread

in the frequencies ranging from 9.1 GHz to 9.5 GHz are averaged to form a wideband signal. The frequency spectrum of the wideband signal source is shown in Figure 6.3. The frequency spectrum of the wideband source is mapped to discrete frequencies. The wideband signal source with discrete frequency bins are shown in Figure 6.4. The discrete frequency components of the wideband signal are shown in Figure 6.4. The discrete frequency components with significant magnitude are considered for the wideband DOA estimation. The significant magnitude is chosen by fixing a threshold magnitude of DFT. In this simulation, a threshold magnitude of 200 is considered.

6.3.2 Incoherent Method for DOA Estimation of Wideband Signal

The conventional technique of incoherent method is applied for the above mentioned wideband signal model for DOA estimation. The performance of incoherent method is analysed for various SNR scenarios. The 12 discrete frequencies with significant magnitude are utilized in the DOA estimation. Final wideband DOA estimation is obtained with

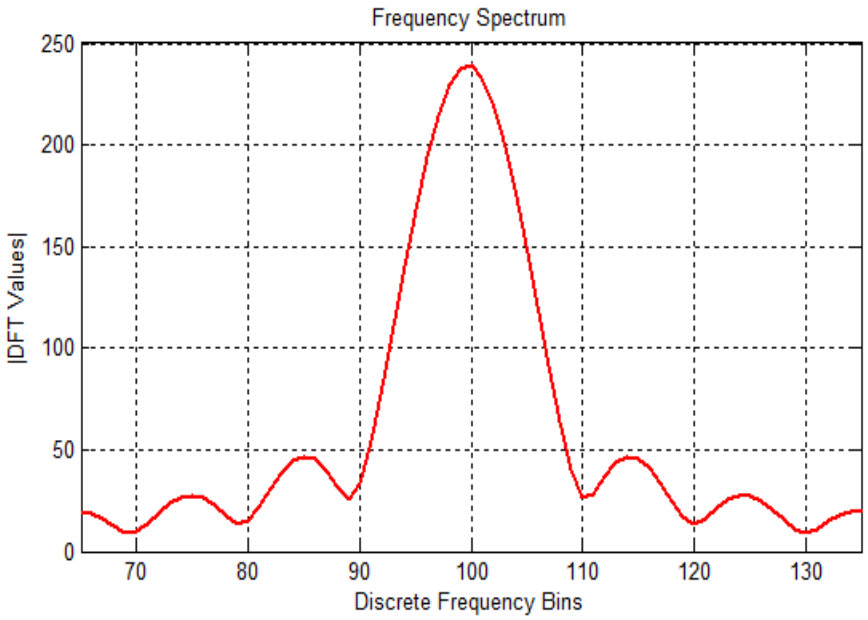

Figure 6.4: Wideband Source Mapped to Discrete Frequencies

the product of the each estimation with discrete frequencies. Each of discrete frequency components of wideband signal spectrum and its DOA estimation for 30 dB SNR are shown in Figure 6.5. Figure 6.5 shows individual discrete frequencies of wideband source

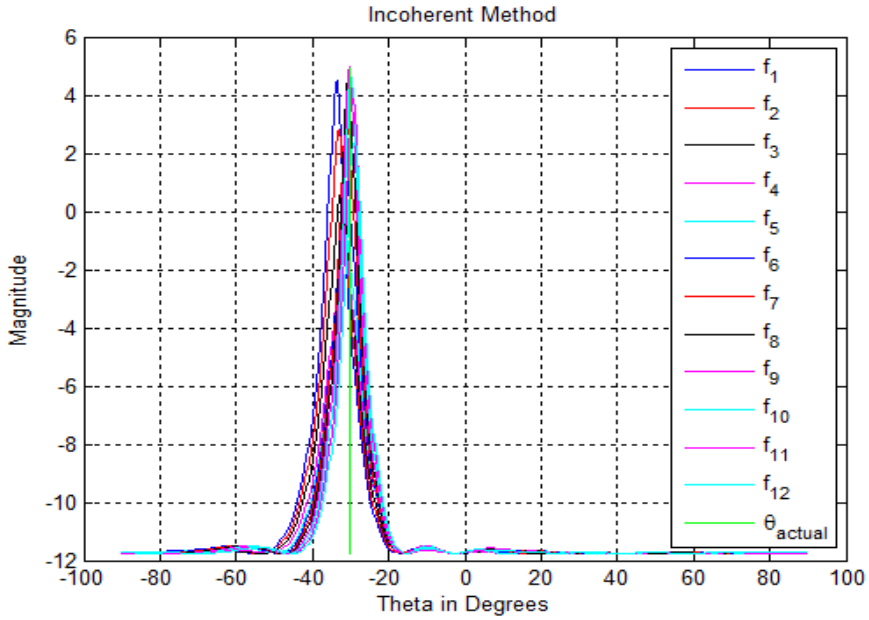

Figure 6.5: Wideband DOA Estimation with Discrete Frequencies of Incoherent Method with 30 dB SNR

which act as narrow band signal component in the wideband DOA estimation. Since the frequency spread over a range of frequencies leads to perturbations of the phase of the signal, the peak of DOA estimation with discrete frequency components will be around the actual DOA angle. The higher magnitude of the DOA estimation with all the discrete frequency components are due to higher SNR of 30 dB and the estimated peaks around the -30° are evident in the result. It is pertinent to point that in the simulations of results of Figure 6.5, the signal was modelled for DOA of -30°.

Further the simulation is carried for 20 dB SNR scenario. The discrete frequency components of wideband DOA estimation for 20 dB SNR are shown in Figure 6.6. The reduced magnitude of peaks of DOA estimation with discrete frequencies is due to moderate SNR is evident in the simulation results. Also the increased spread of the DOA estimation in Figure 6.6 is due to the moderate SNR of the scenario. The product of the DOA estimation

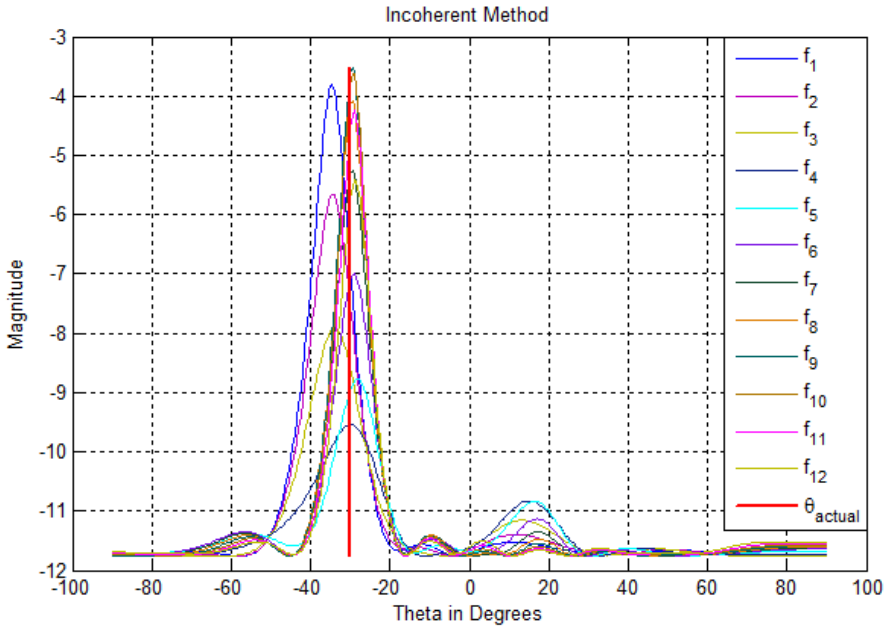

Figure 6.6: Wideband DOA Estimation with Discrete Frequencies of Incoherent Method with 20 dB SNR

with discrete frequency components produces the wideband DOA estimation of incoherent method. The magnitude of the DOA estimation of incoherent method for the 20 dB SNR is shown in Figure 6.7.

The results of wideband DOA estimation at 10 dB SNR for discrete frequency components are shown in Figure 6.8. The results of 10 dB SNR show the poor magnitude of frequency component as well as wider spread of estimation peaks. The amount of noise

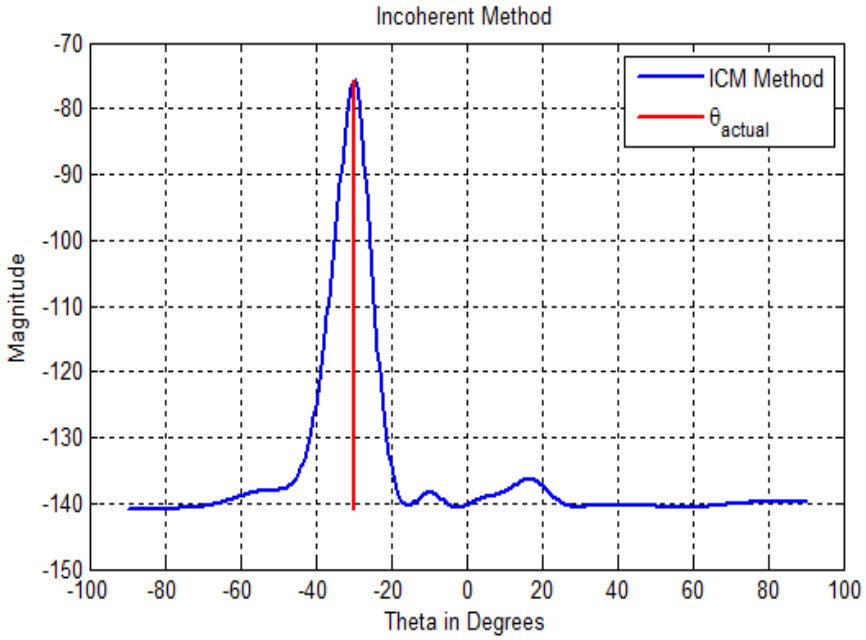

Figure 6.7: Wideband DOA Estimation with Incoherent Method with 20 dB SNR

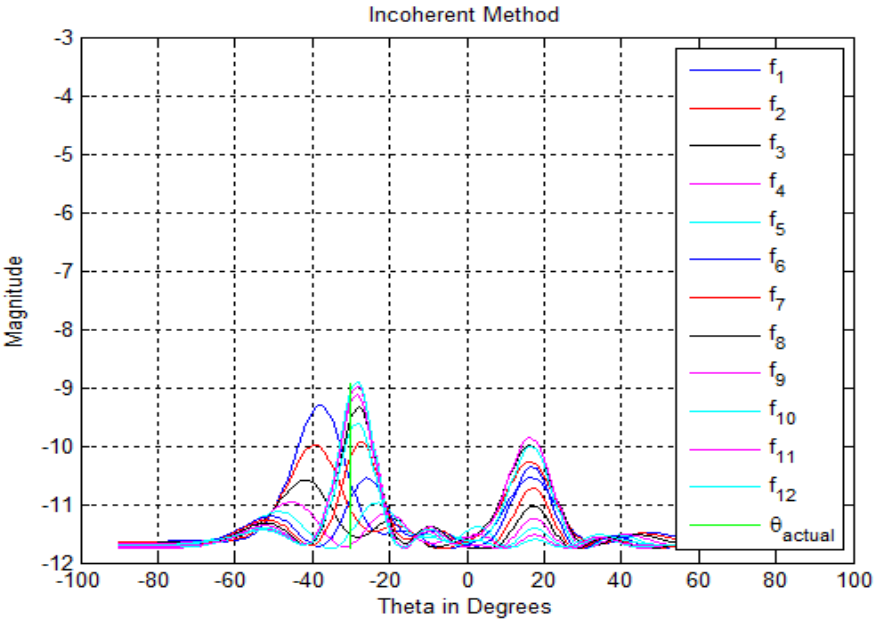

Figure 6.8: Wideband DOA Estimation with Discrete Frequencies of Incoherent Method with 10 dB SNR

present in the signal at 10 dB SNR is more and the noise energy is accumulated with phase of the wideband signal at each of the array element. Thus the incoherent method is inferior in distinguishing the frequency components along with phase information. Hence in DOA

estimation, the accumulation of phase of wideband signal leads to emerge at some arbitrary angle apart from actual DOA angle. The DOA estimation with the discrete components at 10 dB SNR shown in Figure 6.8 leads to poorer estimation of DOA. The incoherent method is evaluated over range of SNR, which verifies that the method is inferior in estimation of DOA at lower SNRs due the accumulated energy in the phase information.

6.4 Coherent Signal Subspace Method (CSSM) for Wideband DOA Estimation

The CSSM focuses the signal subspace components of individual discrete frequencies to a focusing frequency. The focusing frequency will be typically chosen as center frequency of wideband signal spectrum. The wideband signal model for the ULA of 15 elements is further subjected to the DOA estimation with CSSM. The same wideband signal model for the DOA angle of -30° is incorporated for the performance analysis. The CSSM

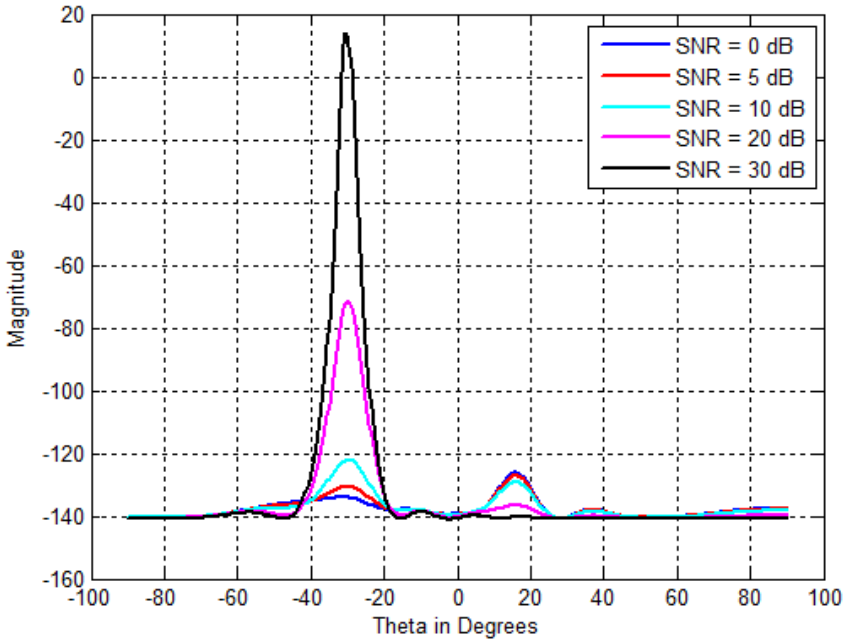

Figure 6.9: Wideband DOA Estimation with CSSM Method for various SNRs

improves the accuracy of the individual signal subspace of discrete frequency components to a particular focussing frequency. The CSSM is analysed for various SNR scenarios. The performance of wideband DOA estimation with CSSM is shown in Figure 6.9. As it is anticipated, at higher SNR, the CSSM estimates the DOA accurately with higher magnitude and sharper peak. As the SNR decreases, sharpness of detected peak diminishes with lower

magnitude, which can be clearly seen in the results of Figure 6.9. Similar to incoherent method, the CSSM is also inferior in estimation accuracy of DOA at lower SNR of 10 dB and lesser. Also the additional peaks shown around 15° have a higher magnitude than the original magnitude at lower SNR scenarios, which leads to false estimation of DOA angle. But additional peaks are of very low magnitude.

6.4.1 Subband Technique for Wideband DOA Estimation

The proposed subband technique for DOA estimation of wideband signal decomposes the signal with a set of subband components. The subband components are obtained by subjecting wideband signal to a set of filter banks. Without loss of generality, the DOA analysis of wideband signal is extended for the proposed subband based technique. The same wideband signal modelled utilizing ULA of 15 elements for the DOA angle of -30° is subjected to the proposed subband method. The performance analysis of subband technique is carried with the filter bank of two filters.

The DOA estimation of wideband signal with subbanding technique is carried by filtering the wideband signal with subband filter response as shown in Figure 6.2. The normalized frequency response of the two subband filters which have a low band and high band is shown in Figure 6.2. The filtered low band and high band components of signal are utilized individually for the DOA estimation.

The DOA estimation of wideband signal utilizing low band and high band signal components for 20 dB SNR scenario, as well as actual DOA angle are shown in Figure 6.10. The result depicts a overlapping of the plots corresponding to DOA estimation through low band and high band signal components. A perfect estimation of DOA angle is clearly seen from the result of the Figure 6.10. The proposed subband technique is evaluated for the wideband signal model with 10 dB SNR. The results of wideband DOA estimation for the 10 dB are shown in Figure 6.11. The results of Figure 6.11 infer, that DOA estimation through low band signal component show a consistent behaviour in the estimation of DOA angle as with case for 20 dB scenario seen above. A negligibly small diminish in the magnitude of estimation peak through high band signal component is seen. However both the low band and high band signal components estimate the DOA angle perfectly at modelled DOA angle of -30°. The AWGN has the uniform noise spectral density across the spectrum. But the influence of the noise is more in high frequency signal components than that in low frequency signal components. With the sub-band filtering

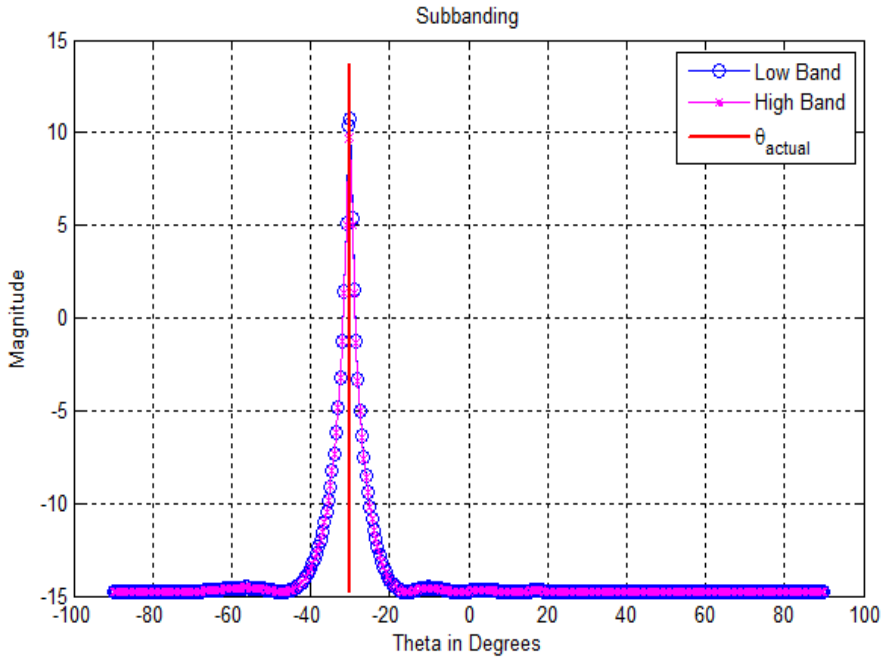

Figure 6.10: Wideband DOA Estimation with Subband Technique with 20 dB SNR

concept, the normalized spectrum is split into two equal halves namely low band and high band. For the signal modelled with fixed SNR, the low band filter facilitates noise removal and therefore the influence of the noise is less pronounced on the signals filtered through low band filter. In the case of high band filter, the noise removal is relatively less pronounced. The signal filtered with high band filter experiences significant influence of the noise and it is proportional to the modelled SNR. Therefore the DOA estimation realised through high frequency band components is prone to relatively higher severity compared to the estimation obtained through low frequency band components. Thus, the change in the SNR in signal has not influenced the accuracy of DOA estimate as shown in Figure 6.11. Further analysis of the subband technique is evaluated for the same wideband signal model at 5 dB SNR scenario. The corresponding results of subband based DOA estimation for the 5 dB SNR are depicted in Figure 6.12. The results of DOA estimation with low band signal component are consistent with the same magnitude and sharpness of estimation peak along the actual DOA angle as with the case seen in 20 dB and 10 dB SNR scenario. A significant reduction in the magnitude of the detection peak of estimation through high band signal component is evident in the results of Figure 6.11. However, even with the reduced magnitude of peak, the DOA estimation accuracy is still maintained at the actual DOA of -30°. The performance of the subband technique is evaluated even

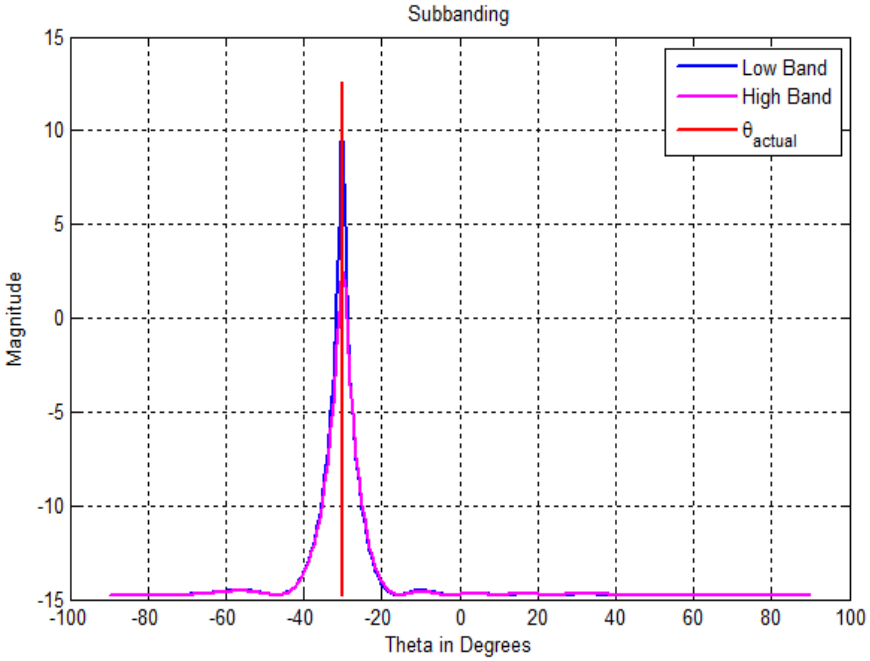

Figure 6.11: Wideband DOA Estimation with Subband Technique with 10 dB SNR

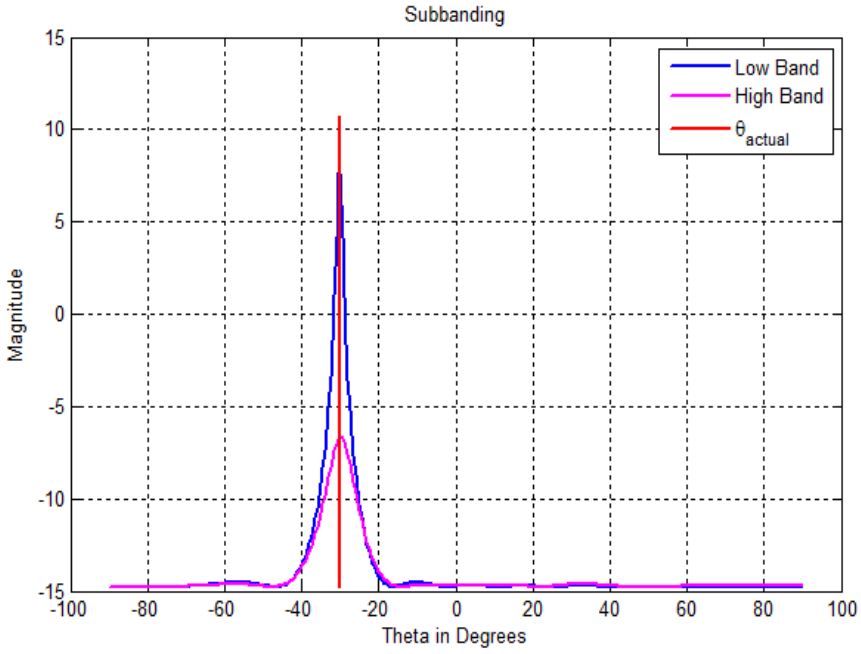

Figure 6.12: Wideband DOA Estimation with Subband Technique with 5 dB SNR

at 0 dB SNR in which the signal and noise carry equal power. The results of subband based DOA estimation thorough low band and high band signal components are shown

in Figure 6.13. The consistent estimate through low band signal component continued even at 0 dB SNR without losing its large magnitude and sharpness of detection profile along the actual DOA angle. The estimation through high band signal component exhibits significantly diminished peak magnitude and also lose its sharpness of peak. The reduced sharpness of peak leads to degraded estimation accuracy of DOA. The analysis of results

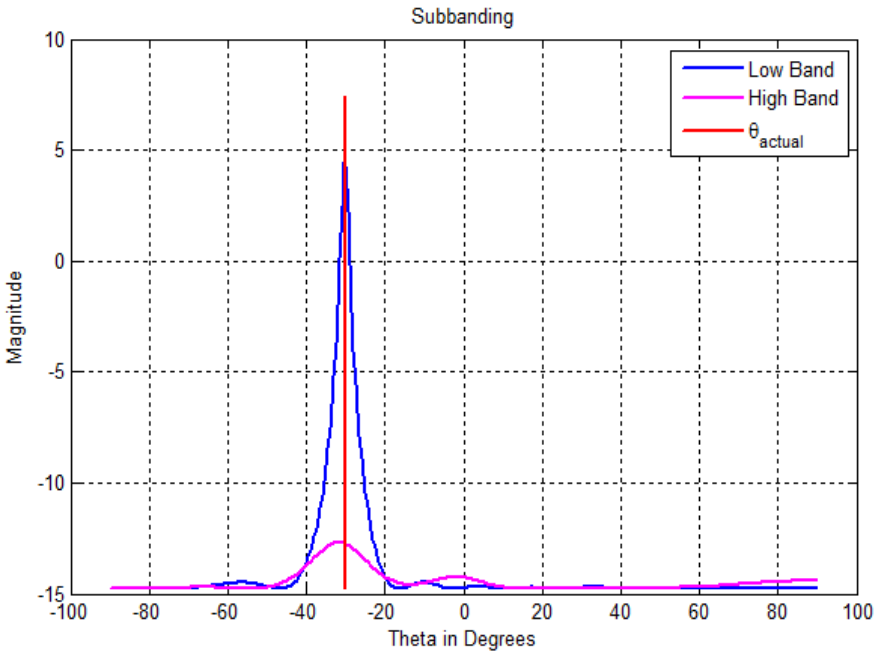

Figure 6.13: Wideband DOA Estimation with Subband Technique with 0 dB SNR

with subband filter based approach of DOA estimate of wideband signal, illustrates that, the subband based DOA estimation through low band signal component is consistent in the estimation of DOA through its higher magnitude of detection peak and sharpness along actual DOA at -30°. The consistent behaviour is clearly evident at all SNR scenarios. However the DOA estimation through high band signal component shows diminished magnitude of detection peak in the estimation at lower SNRs and also loses its sharpness leading to reduced estimation accuracy. In summary, it can concluded that, only the low band signal component is sufficient to estimate the DOA of wideband signal at all SNRs. The high band signal component can be utilized at high and medium range of SNRs and it cannot be relied upon at very lower SNR scenarios. The average of the DOA estimation of wideband signal through low band and high band signal components is not preferred due to the inconsistent nature of the magnitudes of detection peak and sharpness of the estimations realisable through high band signal components.

6.5 Comparison of DOA Estimation Techniques for Wideband Signal

The performance of wideband DOA estimations methods involving the conventional incoherent method, coherent signal subspace method and the proposed subbanding techniques are compared. The results of Figure 6.14 illustrate that the wideband DOA estimation performance of the three methods at high, medium and lower SNR scenarios. In subband based technique, only the low band signal component is utilized for the DOA estimation of wideband signal, since the earlier analysis has proved that it facilitates consistent estimation. Figure 6.14 shows the comparison of the three methods of DOA estimation for a DOA

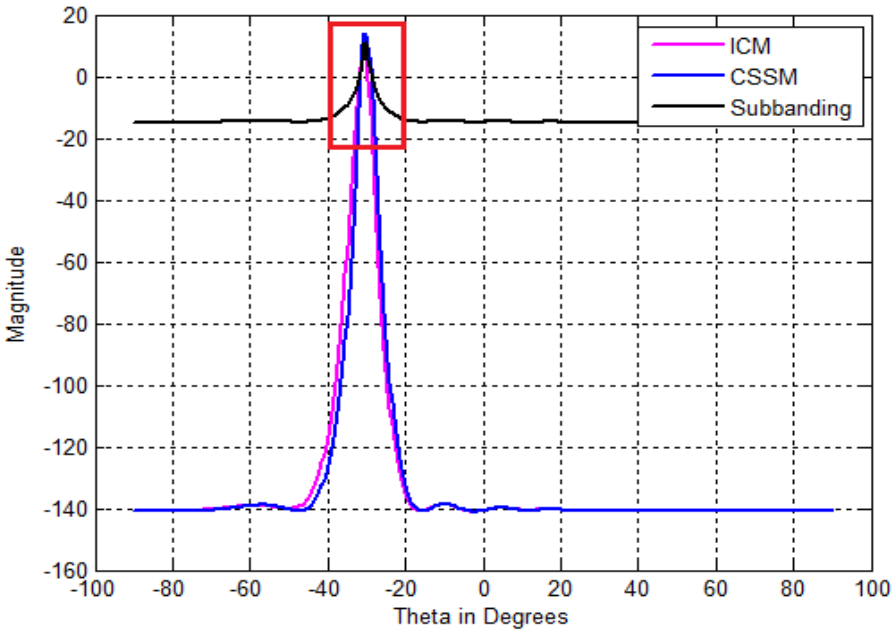

Figure 6.14: Comparison of Wideband DOA Estimation with 30 dB SNR

of -30°. The results of Figure 6.14 reveal the following. The performance of CSSM and incoherent method of wideband DOA estimation is similar. However, the proposed subband filtering approach of DOA estimation of wideband signal exhibits much improved performance. The Figure 6.15 shows the zoomed plot of the peak magnitudes of Figure 6.14. The peak magnitudes of all the three DOA estimation methods of wideband signal are approximately the same, whereas the incoherent and coherent schemes suffer from a accuracy of 0.5° in DOA estimate at times due to white Gaussian noise present in it. The results also show the accurate DOA estimation at -30° is exhibited by the proposed subband based technique. The simulation of comparative analysis is further carried for

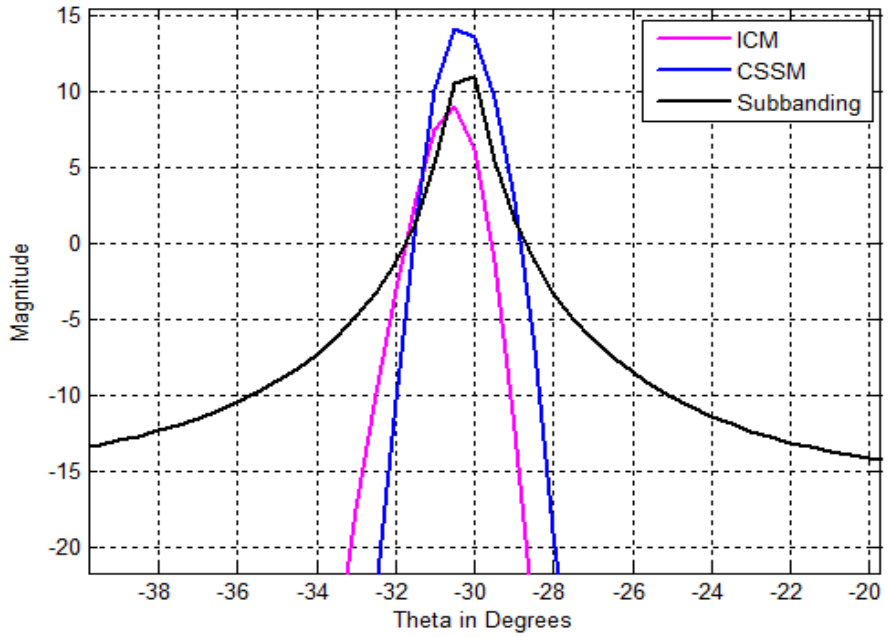

Figure 6.15: Comparison of Wideband DOA Estimation with 30 dB SNR

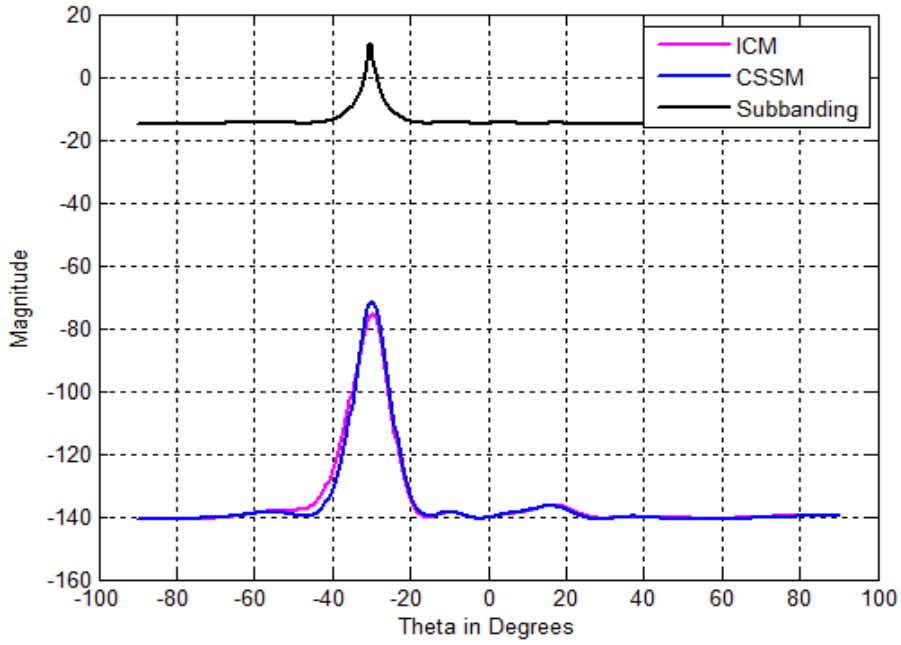

Figure 6.16: Comparison of Wideband DOA Estimation with 20 dB SNR

wideband signal model with 20 dB SNR scenario. The results corresponding to 20 dB SNR are shown in Figure 6.16. The results infer that, the DOA estimation through incoherent

and coherent methods, the peak magnitudes of the estimation peak diminish significantly. Also it is noted, that performance behaviour of incoherent and coherent estimation schemes are similar with negligibly small difference. However, the behaviour of DOA estimation of wideband signal through the low band signal component of subbanding technique has not changed and the consistency is apparent as with the case of 30 dB SNR which can be seen in results of Figure 6.16. The simulation for 10 dB SNR scenario is incorporated in the

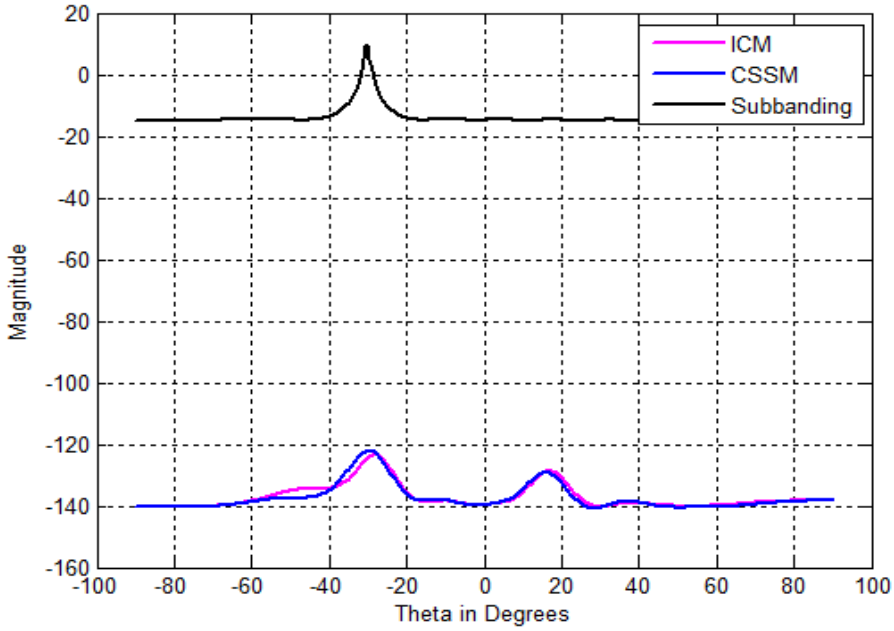

Figure 6.17: Comparison of Wideband DOA Estimation with 10 dB SNR

wideband signal model. The results in the Figure 6.17 infer, further reduction in the peak magnitudes as well as the sharpness of detection profile are associated with incoherent and coherent methods. In addition, the additional peak appears at $+15^{\circ}$ which leads to erroneous DOA estimation. However, the subband technique does not lose its accuracy in the DOA estimation at 10 dB SNR. The comparison of three wideband DOA estimation methods are evaluated further and analysed for 0 dB SNR scenario. The results for the wideband signal model at 0 dB SNR are shown in Figure 6.18. The results depict the peak of incoherent and coherent method completely vanish around the actual DOA angle of -30° and the additional peaks retain certain magnitude, and hence contributing to misleading inference in the DOA estimation. The superior performance of DOA estimation through low band signal component of the subband technique is evident in the results of Figure 6.18, without any change in its estimation behaviour at all SNR scenario. There is no

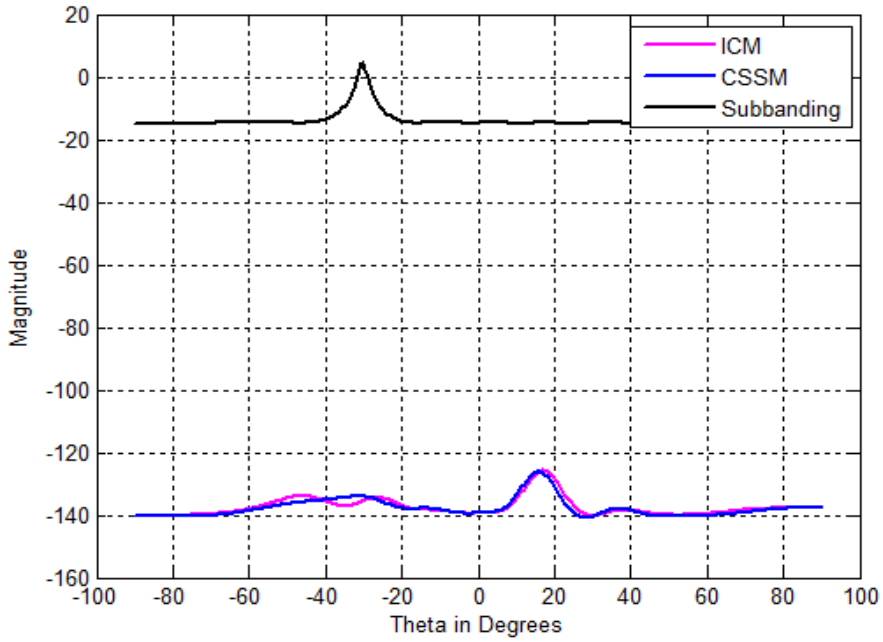

Figure 6.18: Comparison of Wideband DOA Estimation with 0 dB SNR

undesired additional peaks in the subband technique. In summary, the subbanding scheme proves its robust performance in DOA estimation of wideband signal in the presence of white Gaussian noise irrespective of its SNR.

6.5.1 Computation Time Analysis of Wideband DOA Methods

The computation time of the incoherent, coherent signal subspace and the proposed subband based wideband DOA estimation methods is compared. The computation time of all the three methods is tabulated in Table 6.1. To derive the results shown Table 6.1, the processor Intel Core(TM)2 Duo CPU with the clock speed of 2.40 GHz is used. In the computation

Table 6.1: Computation Time for Wideband DOA Methods

Wideband Band DOA Methods	**Computation Time**
Incoherent Method	0.8608s
CSSM	1.1135s
Subband Technique	0.0409s

of DOA estimation of wideband signal, incoherent and coherent methods take more time due to the computation of EVD or SVD for the subspace decompositions for every discrete frequency bins in it. The proposed two subband filter approach involves only two set of

eigen value decomposition for low band and high band signal components. Comparatively, the proposed subband technique is approximately 20 times faster than the conventional incoherent and CSSM methods. Thus the proposed subband technique possesses the desirable advantage in terms of minimum computation time. Also the computation time of subband technique can be further reduced by completely neglecting the computation of high band component, since it is prone to degraded DOA estimation performance at lower SNRs.

6.6 Simulation of DOA Estimation Techniques for Two Wideband Sources

In view of evaluation of the proposed subband based DOA estimation of wideband signal presented in section 6.5, further analysis is carried for the case of estimation of DOA of two wideband sources. The performance DOA estimation techniques for two wideband sources for various SNR levels is analysed by incorporating the conventional incoherent and coherent schemes as well as with the proposed subband approach. The comparative performance of estimating the modelled DOA estimation techniques for two wideband sources for different cases are analysed and the results are presented in the subsection to follow.

6.6.1 Estimation of DOA of Two Wideband Sources $\theta_1 = 10^\circ$, and $\theta_2 = 40^\circ$

The modelling of DOA estimation techniques of wideband sources for the actual DOA angles $\theta_1 = 10^\circ$, and $\theta_2 = 40^\circ$ is carried out to perform the simulation analysis for various SNR levels. The results shown in Figures 6.19, 6.20 and 6.21 are the comparative performance of the DOA estimation schemes of two wideband sources for 30 dB, 10 dB and 0 dB SNR levels respectively.

The normalized magnitude of the DOA estimation peaks is shown in the results of Figures 6.19, 6.20 and 6.21. The actual DOA angles of the signal model are also shown in results for reference. The simulation results in the Figure 6.19 infer that, the ICM and CSSM methods estimate the DOA of two wideband sources with significantly different magnitudes. Also the accuracy of DOA estimation suffers when compared with the subband scheme of DOA estimation. The estimated DOAs through the subband technique correlate accurately with the DOA of modelled sources. Similar to the case of single source, results of DOA estimation by low subband component and high subband component overlap and amounting to an equal performance in the DOA estimation at higher SNR scenario. The

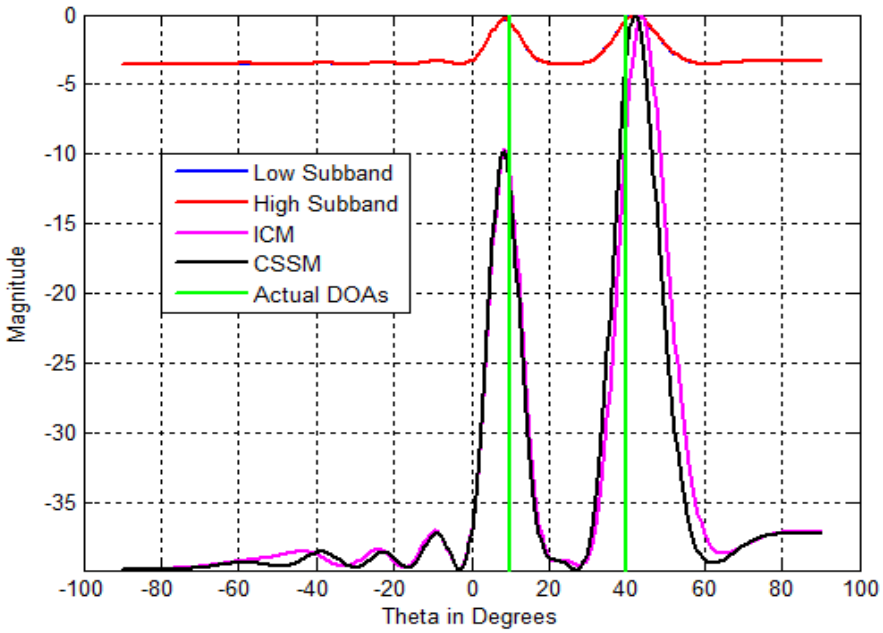

Figure 6.19: DOA Estimation of Two Wideband Sources with the Signal Model $\theta_1 = 10^\circ$, and $\theta_2 = 40^\circ$ for 30 dB SNR

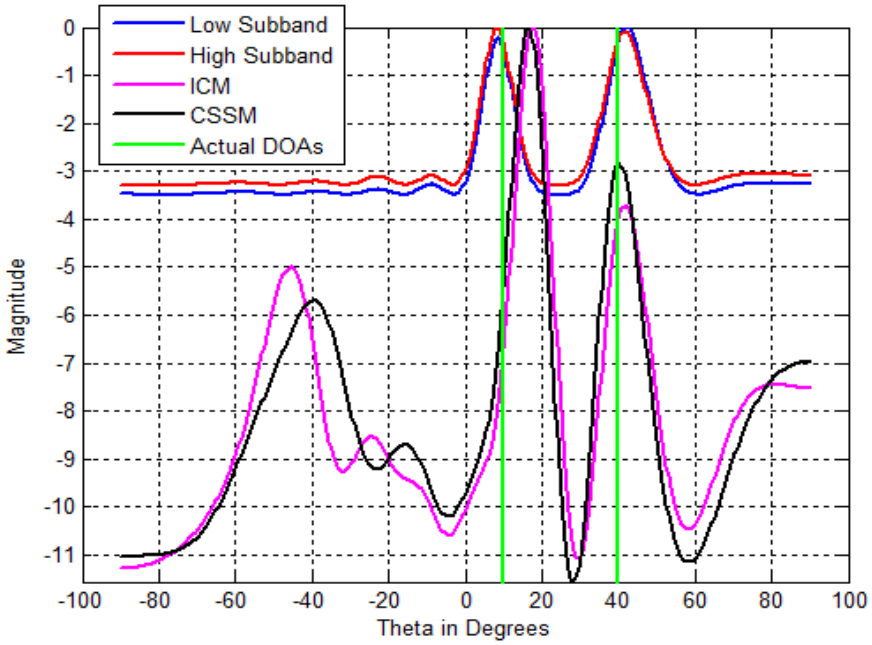

Figure 6.20: DOA Estimation of Two Wideband Sources with the Signal Model $\theta_1 = 10^\circ$, and $\theta_2 = 40^\circ$ for 10 dB SNR

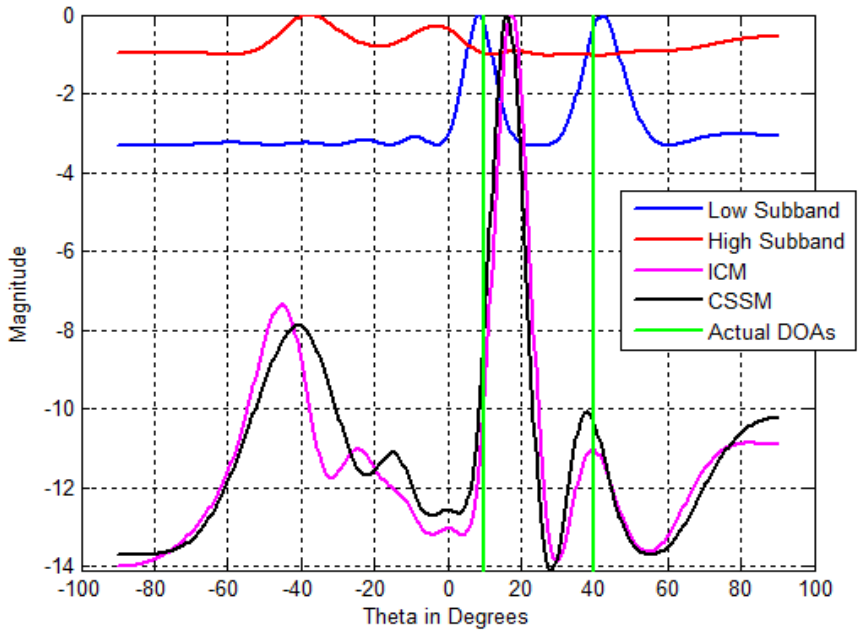

Figure 6.21: DOA Estimation of Two Wideband Sources with the Signal Model $\theta_1 = 10^\circ$, and $\theta_2 = 40^\circ$ for 0 dB SNR

results of Figure 6.20 depict simulations for two wideband source with 10 dB SNR. The results show the inferior performance of the ICM and CSSM methods in the estimation of DOA of source at $\theta_1 = 10^\circ$ with poor accuracy. The DOA of source at $\theta_2 = 40^\circ$ is estimated with a lower magnitude. Difference in the magnitudes of the detection peaks of two sources is significant with ICM and CSSM. However, the consistency of DOA estimation with equal magnitudes of detected peaks of DOA of both sources realized with subband technique is noteworthy. The DOA estimation through high subband component shows a minor difference in the magnitude of detected peaks when compared with the low subband component.

Figure 6.21 illustrates the estimation performance DOA of two wideband sources with 0 dB SNR. The influence of noise in the two wideband sources can be clearly seen in the results of Figure 6.21. The estimation of DOA by both ICM and CSSM is associated with poor accuracy and they exhibit reduced magnitude of detection peak. The low subband technique proves its consistent performance in the estimation of two DOA angles even at 0 dB SNR. The high band component fails to estimate DOA of sources, since it is heavily influenced by the additive noise.

6.6.2 Estimation of DOA of Two Wideband Sources $\theta_1 = -10°$, and $\theta_2 = 20°$

The consistent behaviour of the proposed subband based DOA estimation scheme of wideband signal is evaluated in comparison with incoherent and coherent schemes for various source angles and SNRs. The two wideband sources are modelled at $\theta_1 = -10°$, and $\theta_2 = 20°$.

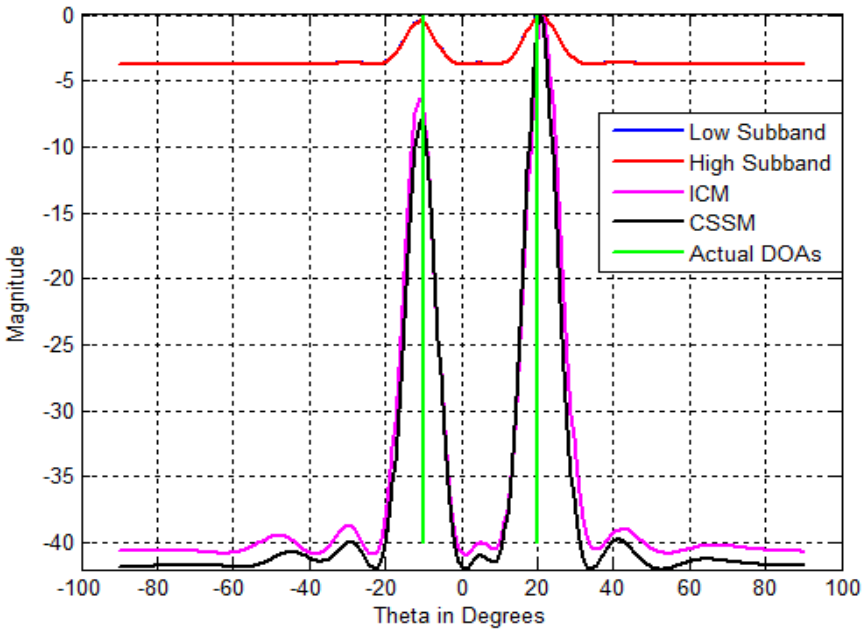

Figure 6.22: DOA Estimation of Two Wideband Sources with the Signal Model $\theta_1 = -10°$, and $\theta_2 = 20°$ for 30 dB SNR

The simulation for the above illustrated scenario and their results of DOA estimations of wideband signals are provided in the Figures 6.22, 6.23 and 6.24 for the SNR of 30 dB, 10 dB and 0 dB respectively. These results depict, the clear distinction of DOA of two sources by the estimation through low band component of the subband approach. The high band component of subband approach fails to perform the estimation of DOA as well as in distinguishing sources at SNR lower than 10 dB. The coherent and incoherent approaches estimate the DOA of two sources with significantly different peak magnitudes for SNR of 30 dB and 10 dB. They fail to estimate the DOA of the sources as well as in distinguishing sources at 0 dB SNR.

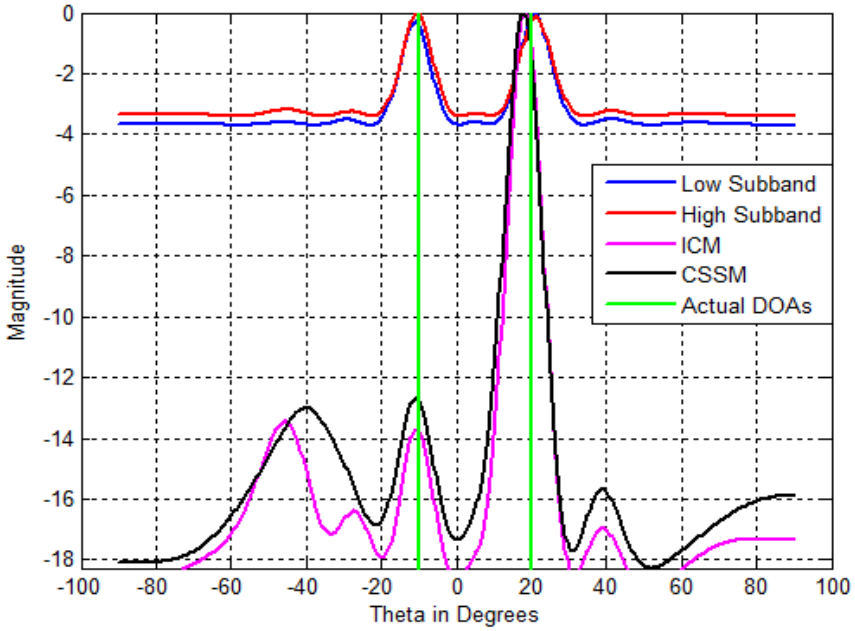

Figure 6.23: DOA Estimation of Two Wideband Sources with the Signal Model $\theta_1 = -10^\circ$, and $\theta_2 = 20^\circ$ for 10 dB SNR

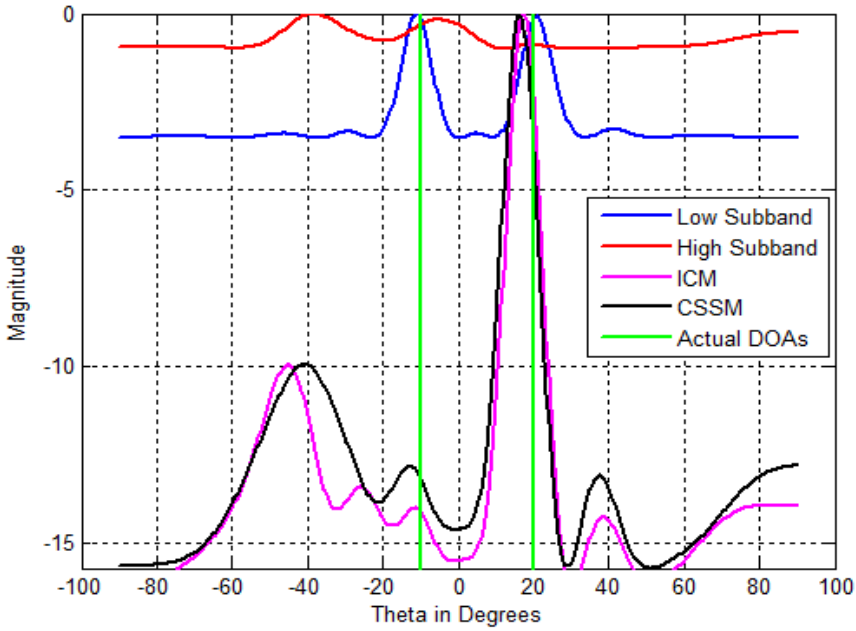

Figure 6.24: DOA Estimation of Two Wideband Sources with the Signal Model $\theta_1 = -10^\circ$, and $\theta_2 = 20^\circ$ for 0 dB SNR

6.6.3 Estimation of DOA of Two Wideband Sources $\theta_1 = -30°$, and $\theta_2 = 40°$

Further analysis is carried for the case of DOA estimation of two sources modelled at $\theta_1 = -30°$, and $\theta_2 = 40°$. The results of the simulations in the Figures 6.25 6.26 and 6.27 are for the SNR of 30 dB, 10 dB and 0 dB respectively. The results of the simulations

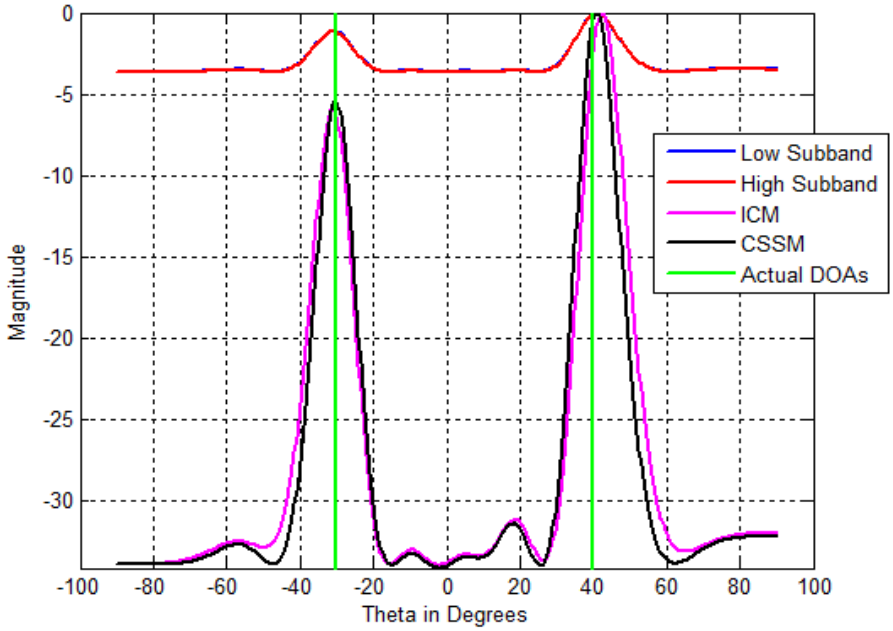

Figure 6.25: DOA Estimation of Two Wideband Sources with the Signal Model $\theta_1 = -30°$, and $\theta_2 = 40°$ for 30 dB SNR

shown in Figures 6.25, 6.26 and 6.27 are comparable with the previous simulation analysis. The consistent behaviour in the results of DOA estimation of wideband signal by subband based technique clearly reveal its utility in all the scenarios of SNR.

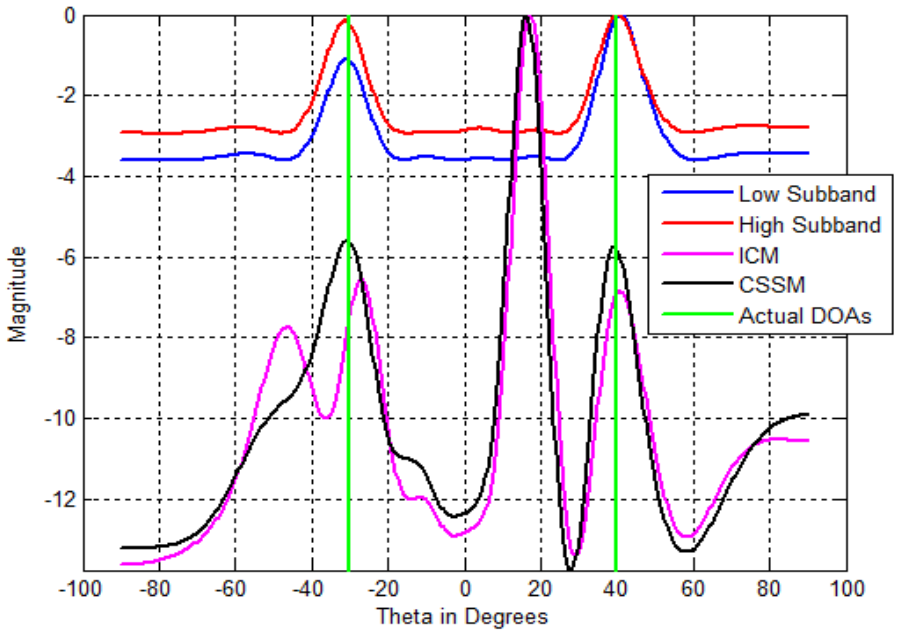

Figure 6.26: DOA Estimation of Two Wideband Sources with the Signal Model $\theta_1 = -30°$, and $\theta_2 = 40°$ for 10 dB SNR

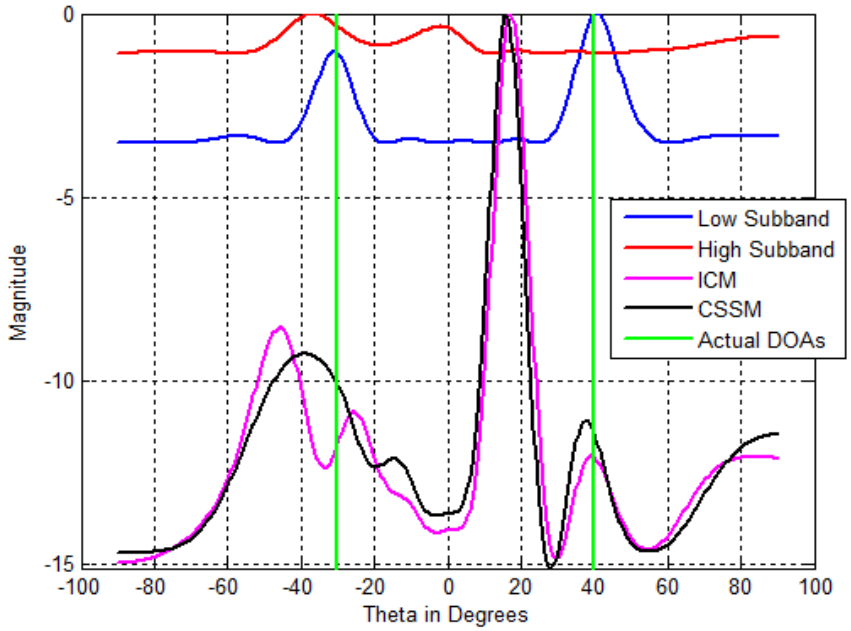

Figure 6.27: DOA Estimation of Two Wideband Sources with the Signal Model $\theta_1 = -30°$, and $\theta_2 = 40°$ for 0 dB SNR

6.7 Simulation of 2D-DOA Estimation of Wideband Source by Using Subband Technique

The discussion of the previous section was on the estimation of 1D-DOA of one or more wideband signals. The 2D-DOA estimation of wideband source using the proposed subband filter technique is carried to evaluate its performance with the conventional single polarized array and the proposed orthogonal polarized array configurations in this section.

6.7.1 Wideband Signal Model for 2D-DOA

The 1D signal model for DOA estimation of wideband sources shown in Equation (2.61) can be extended for the case of 2D-DOA estimation, in which case both the elevation angle θ and azimuth angle ϕ are involved in the modelling. For the case of P number of far-field wideband sources, observed by M antennas arranged in an array geometry with additive white Gaussian noise, the spectral output of the array of the wideband sources for frequency f and time sample t is given by the Equations (6.4)

$$\mathbf{x}(f,t) = \mathbf{A}(f,\theta,\phi)\mathbf{s}(f,t) + \mathbf{n}(t) \tag{6.4}$$

Where $\mathbf{A}(f,\theta,\phi)$ is array steering matrix of size $P \times M$, whose columns are spanned by array steering vector $\mathbf{a}(f,\theta,\phi)$ for the frequency f.

$$\mathbf{x}(f,t) = \sum_{i=f_L}^{f_H} \sum_{p=1}^{P} \mathbf{a}(f_i,\theta_p,\phi_p)\mathbf{s}_p(f_i,t) + \mathbf{n}(t) \tag{6.5}$$

Here the $\mathbf{x}(f,t)$ is the observation of wideband signal for frequencies ranging from f_L to f_H at time instant t. The signal source $\mathbf{s}(f_i,t)$ is represented as $\left[\mathbf{s}_1(f,t), \quad \mathbf{s}_2(f,t), \quad \ldots \quad ,\mathbf{s}_P(f,t)\right]^T$. The noise vector $\mathbf{n}(t)$ is spectrally and spatially uncorrelated. The noise is also uncorrelated with the source signals. The array manifold matrix of size $M \times P$ can be defined as

$$\mathbf{A}(f,\theta,\phi) = \left[\mathbf{a}(f,\theta_1,\phi_1), \quad \mathbf{a}(f,\theta_2,\phi_2), \quad \ldots \quad ,\mathbf{a}(f,\theta_P,\phi_P)\right] \tag{6.6}$$

The array manifold matrix has the array steering vector $\mathbf{a}(f,\theta_p,\phi_p)$ for the p^{th} source at frequency f in its columns space. The array steering vector for a elevation angle θ and azimuth angle ϕ for case of arbitrary array configuration is defined as

$$\mathbf{a}(f,\theta,\phi) = \left[e^{-j\frac{2\pi f}{c}\beta_1(\theta,\phi)}, \quad e^{-j\frac{2\pi f}{c}\beta_2(\theta,\phi)}, \quad \cdots, \quad e^{-j\frac{2\pi f}{c}\beta_M(\theta,\phi)}\right]^T \tag{6.7}$$

Where,

$$\beta_m(\theta,\phi) = x_m \sin\theta\cos\phi + y_m \sin\theta\sin\phi + z_m\cos\theta \tag{6.8}$$

Here x_m, y_m and z_m are co-ordinates of the m^{th} antenna element positioned in the array. In case of antenna elements of linear array mounted along x-axis, its y and z co-ordinates of its elements will be zero. Similarly for a planar array mounted in $x-y$ plane, the z co-ordinate will be zero. For three dimensional array or conformal array, all the three axes take their co-ordinate values. For the proposed orthogonal polarized array configurations, the vertical and horizontal polarized components of the RWG denoted by $E_{\phi}(f,\theta,\phi)$ and $E_{f,\theta}(\theta,\phi)$ should be multiplied with the array steering vector for the respective polarized elements of the array and frequency f.

The simulation analysis of the proposed subband technique for 1D-DOA estimation of wideband source is extended for the 2D-DOA by invoking the conventional single polarized UPA and the proposed orthogonal polarized array configurations. The 2D-DOA for single wideband source is modelled for the DOA angles of $\theta = 15^{\circ}$ and $\phi = 30^{\circ}$. The simulation is performed for the estimation of 2D-DOA for the single wideband source for the modelled elevation angle θ and azimuth angle ϕ.

6.7.2 2D-DOA Estimation of Wideband Source Using Conventional Single Polarized UPA

The conventional single polarized UPA discussed in the Chapter 4 is utilized for estimation of 2D-DOA of single wideband source modelled for 0 dB SNR. The results of the 2D-DOA estimation of wideband source with single polarized UPA are depicted in Figure 6.28.

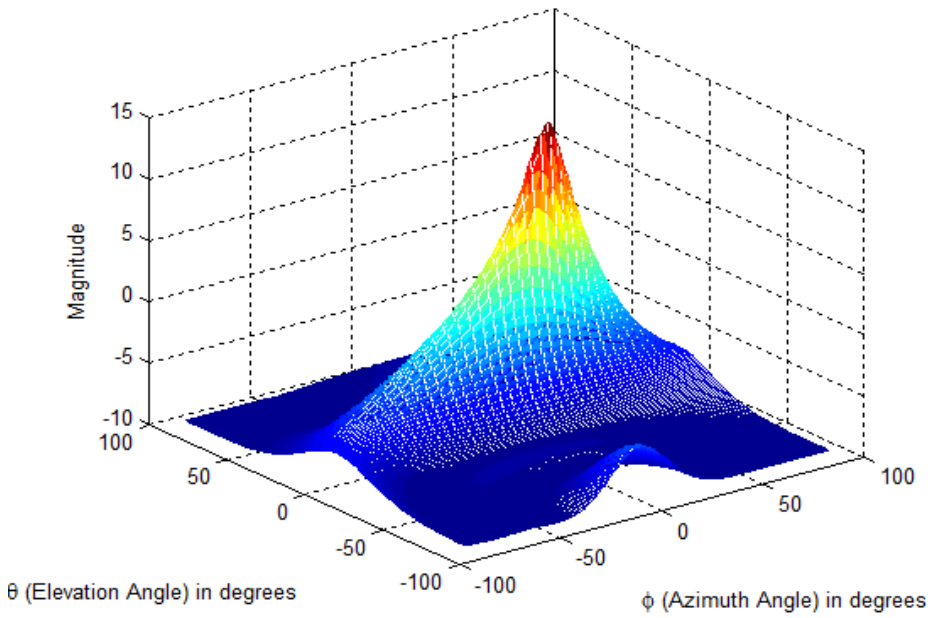

Figure 6.28: 2D-DOA Estimation of Wideband Sources with Uniform Planar Array for the Signal Model $\theta = 15^\circ$ and $\phi = 30^\circ$ for 0 dB SNR

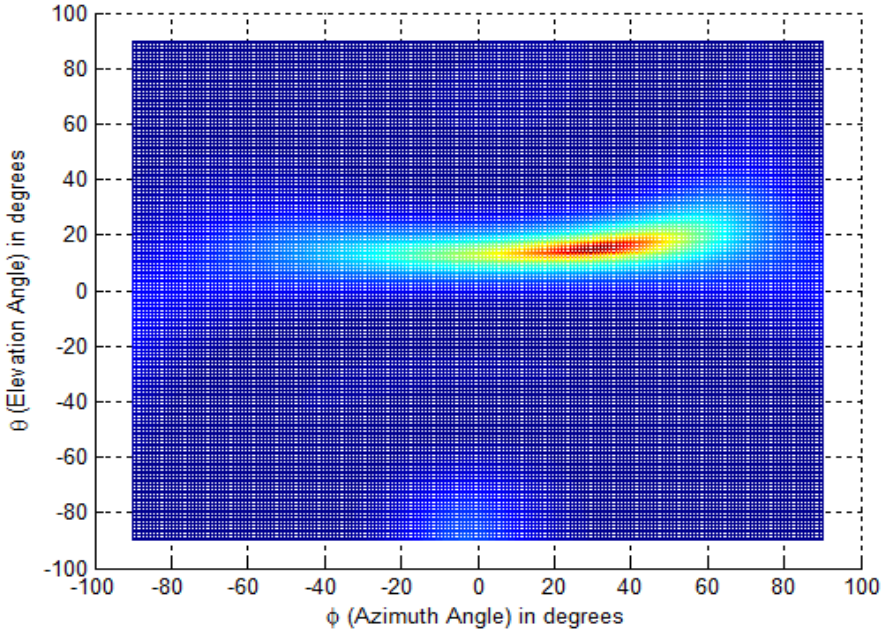

Figure 6.29: 2D-DOA Estimation of Wideband Sources with Uniform Planar Array for the Signal Model $\theta = 15^\circ$ and $\phi = 30^\circ$ for 0 dB SNR - 2D View of Simulation Result

The spread of the profile of the detection peak above a certain magnitude can be clearly seen around the actual DOA angle in the 2D view of the result, depicted in Figure 6.29. Due to higher noise as well the single polarized array configuration, the performance of 2D-DOA estimation of wideband source with singly polarized UPA is not satisfactory.

6.7.3 2D-DOA Estimation of Wideband Source with OPPA

The performance of 2D-DOA estimation of wideband source with OPPA has been analysed. The wideband signal model for OPPA configuration is performed for a single source with angles $\theta = 15^\circ$ and $\phi = 30^\circ$.

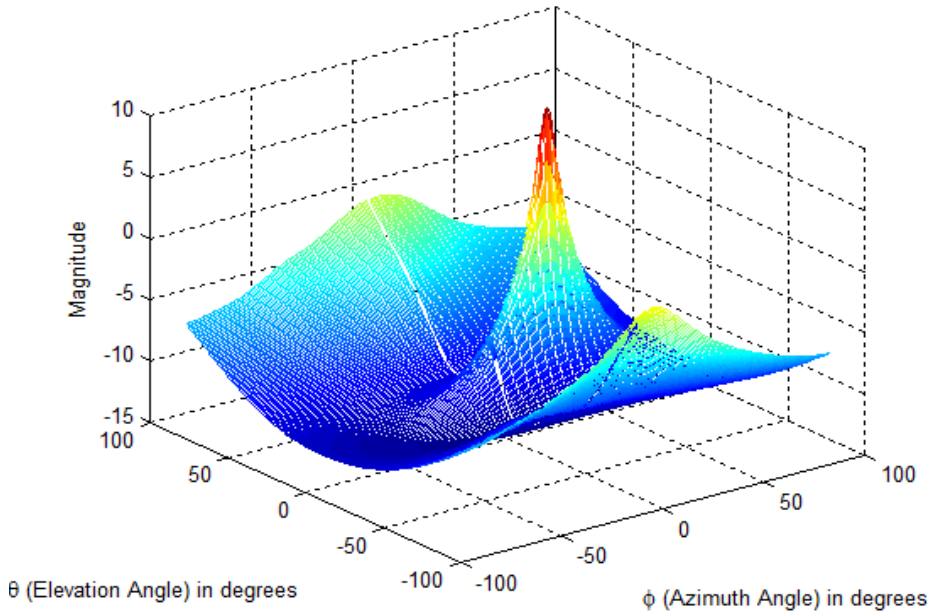

Figure 6.30: 2D-DOA Estimation of Wideband Sources with Orthogonal Polarized Planar Array for the Signal Model $\theta = 15^\circ$ and $\phi = 30^\circ$ for 0 dB SNR

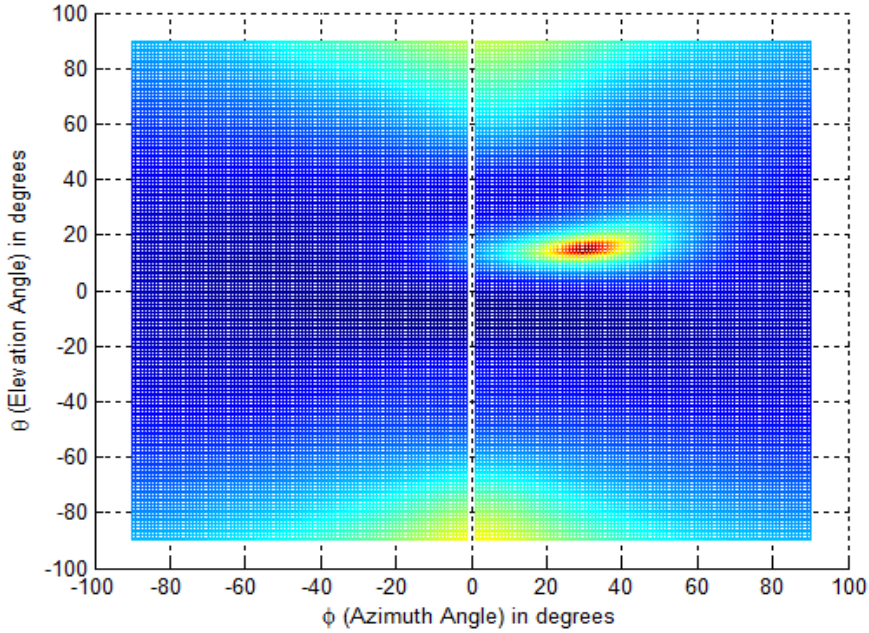

Figure 6.31: 2D-DOA Estimation of Wideband Sources with Orthogonal Polarized Planar Array for the Signal Model $\theta = 15^{\circ}$ and $\phi = 30^{\circ}$ for 0 dB SNR - 2D View of Simulation Result

The performance of 2D-DOA estimation of wideband source for 0 dB SNR using OPPA is shown in the Figure 6.30 and the same result is depicted in 2D view in Figure 6.31. The results of Figures 6.30 and 6.31 clearly indicate the reduction in the spread of profile of detection peak leading to less ambiguity in the estimated DOA angles.

6.7.4 2D-DOA Estimation of Wideband Source with OMLA

Without incorporating any changes, the wideband signal model of the previous subsection is extended to analyse the performance of OMLA configuration for 2D-DOA estimation of single wideband source. Keeping the 2D-DOA signal model same as in the previous array configuration, the 2D-DOA estimation of a wideband source has been carried out.

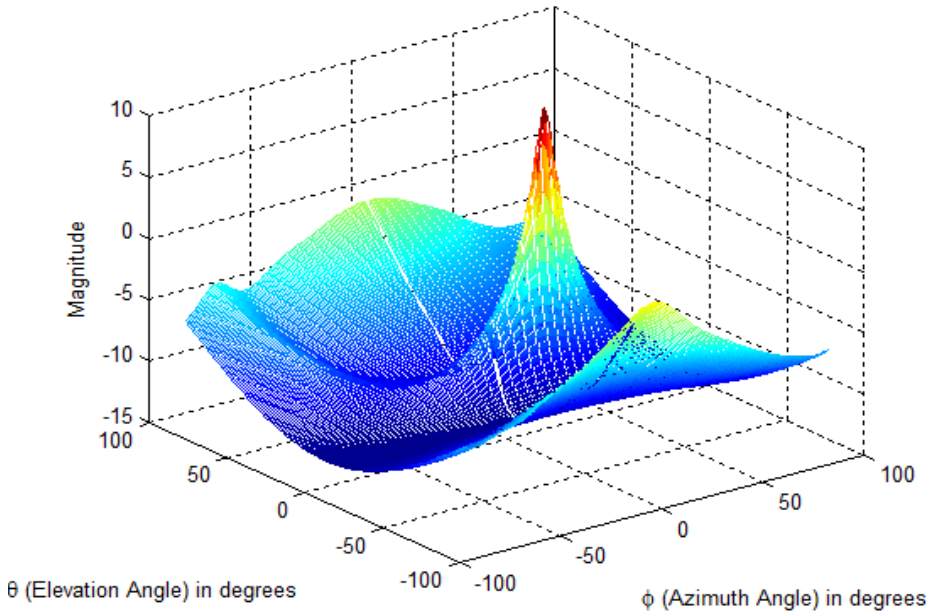

Figure 6.32: 2D-DOA Estimation of Wideband Sources with Orthogonal Mounted Linear Array for the Signal Model $\theta = 15^{\circ}$ and $\phi = 30^{\circ}$ for 0 dB SNR

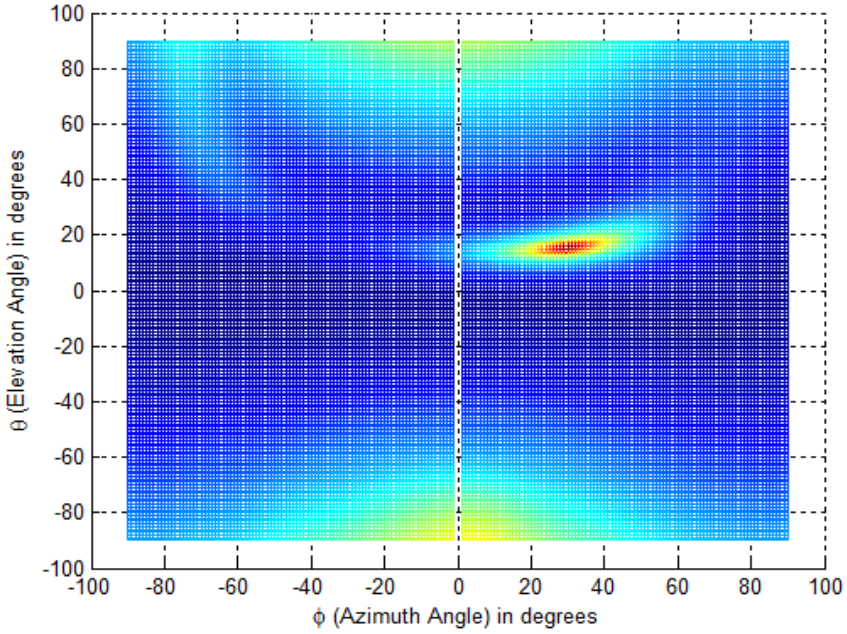

Figure 6.33: 2D-DOA Estimation of Wideband Sources with Orthogonal Mounted Linear Array for the Signal Model $\theta = 15^{\circ}$ and $\phi = 30^{\circ}$ for 0 dB SNR - 2D View of Simulation Result

The simulation results of 2D-DOA estimation of wideband signal using the OMLA are shown in Figure 6.32 and the 2D view is depicted in the Figure 6.33. The results of the simulation of Figures 6.32 and 6.33 confirm that the OMLA facilitates the reduction in the spread of detection profile leading to improved accuracy of 2D-DOA estimation.

6.7.5 2D-DOA Estimation of Wideband Source with OPLA

The OPLA is also evaluated for its performance in 2D-DOA estimation for the case of wideband signal scenario. The signal model for single wideband source used in the three previous array configuration is retained for the simulation. The simulation results of 2D-DOA of wideband signal with OPLA are depicted in Figure 6.34.

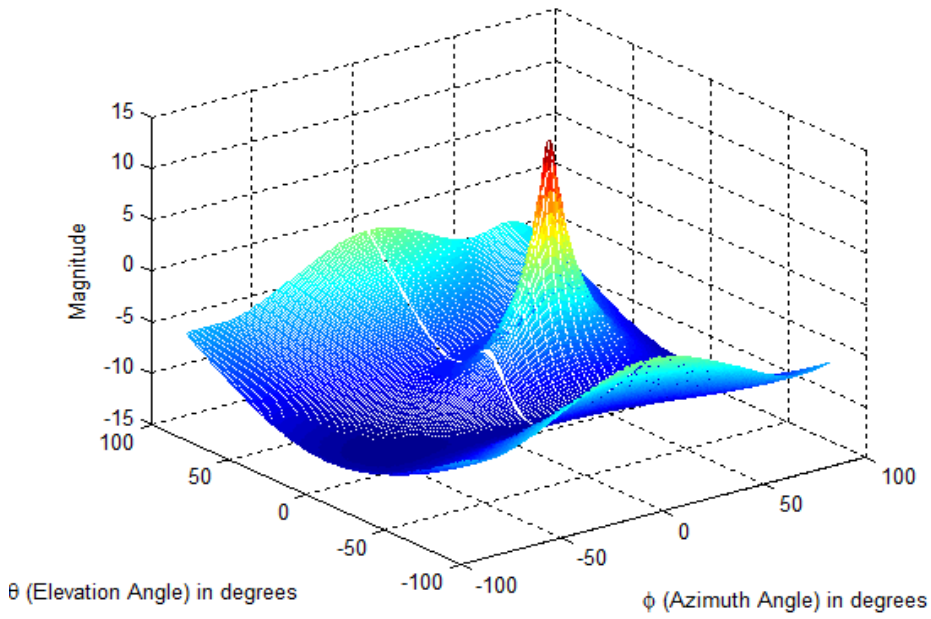

Figure 6.34: 2D-DOA Estimation of Wideband Sources with Orthogonal Polarized Linear Array for the Signal Model $\theta = 15^{\circ}$ and $\phi = 30^{\circ}$ for 0 dB SNR

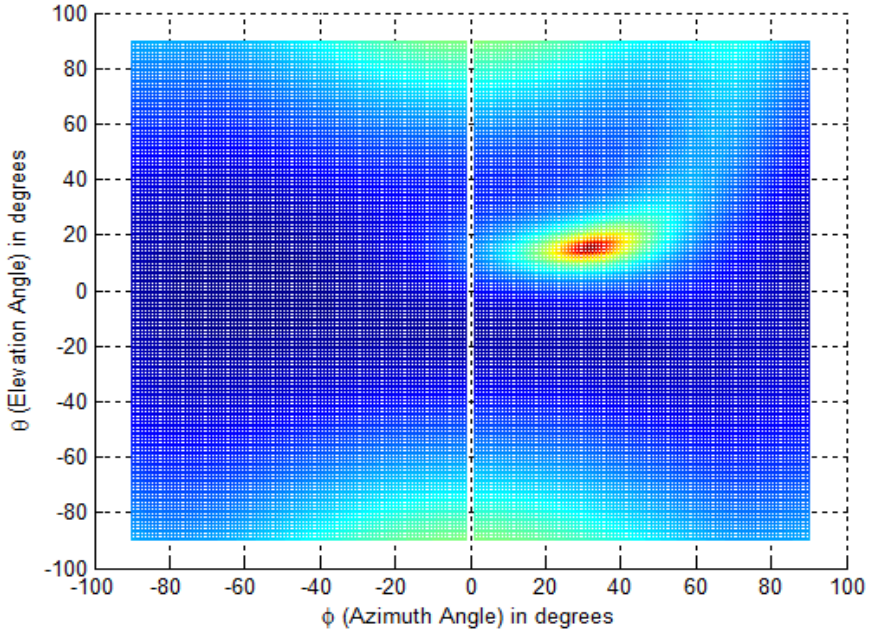

Figure 6.35: 2D-DOA Estimation of Wideband Sources with Orthogonal Polarized Linear Array for the Signal Model $\theta = 15^{\circ}$ and $\phi = 30^{\circ}$ for 0 dB SNR - 2D View of Simulation Result

The result of the simulation are also depicted in 2D view in Figure 6.35. The simulation results of the OPLA, in which the spread of the detection peak profile is slightly wide. when compared with the other two orthogonal polarized array configurations. This wider spread is due to the linear arrangement of the array configuration. In the simulation results of 2D-DOA of single wideband source using the four array configurations discussed, SNR of 0 dB has been considered. It is obvious to expect that the estimation performance of 2D-DOA using the discussed array configurations will improve with increase in SNR. Appendix B thus for to presents additional results of 2D-DOA estimation of single wideband source at higher SNR values using various array configurations. It is clearly evident from the simulation results, the orthogonal polarized array configuration is helpful in improving the 2D-DOA estimation of wideband signals with improved accuracy when compared to the conventional single polarized UPA.

6.7.6 RMSE Performance Analysis of Subband Based 2D-DOA Estimation of Wideband Signal with Single and Orthogonal Polarized Array Configurations

From the analysis of simulation results of the previous subsections, it is clear that the proposed wideband DOA estimation scheme based on subband filter exhibits consistency and superiority in the 1D-DOA estimation in all SNR scenarios. This subbanding technique is further analysed for its RMSE performance for the range of SNRs using the conventional single and the proposed orthogonal polarized array configurations. The wideband signal model for the conventional single polarized UPA and the proposed orthogonal polarized array configurations namely, OPPA, OMLA and OPLA modelled in the previous subsections is used for RMSE analysis. The DOA for the wideband signal model is carried for $\theta = 15^\circ$ and $\phi = 30^\circ$. This wideband signal model is subjected for the analysis invoking the proposed subbanding technique for the wideband 2D-DOA estimation at 0 to 30 dB SNR scenarios. As per the previous analysis, the low band signal component for the estimation of DOA of the wideband source is utilized and the estimation through high band signal components is ignored in the simulation.

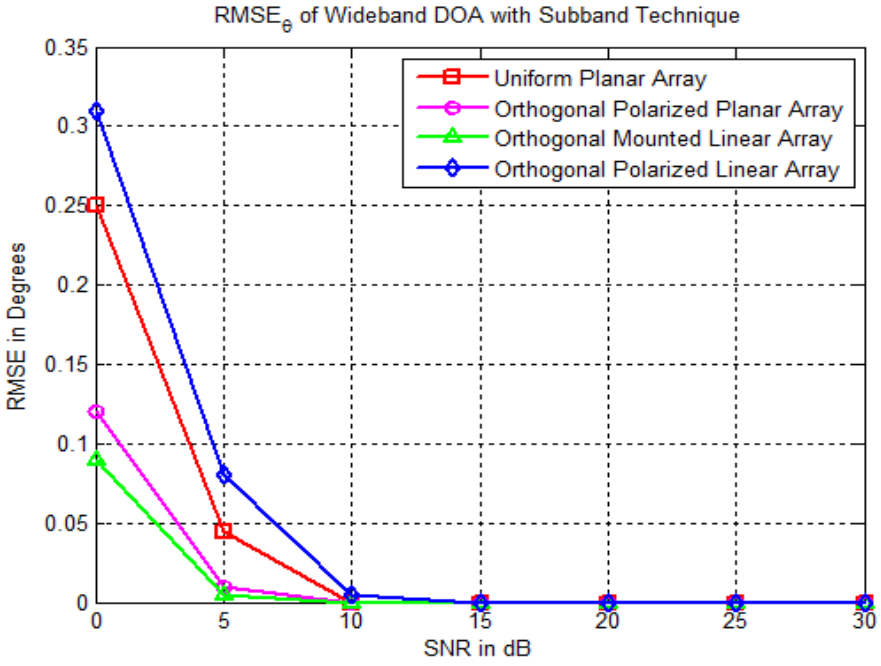

Figure 6.36: RMSE Comparison for θ Angle Estimation of 2D-DOA Estimation of Wideband Signal for Single and Orthogonal Polarized Array Configurations

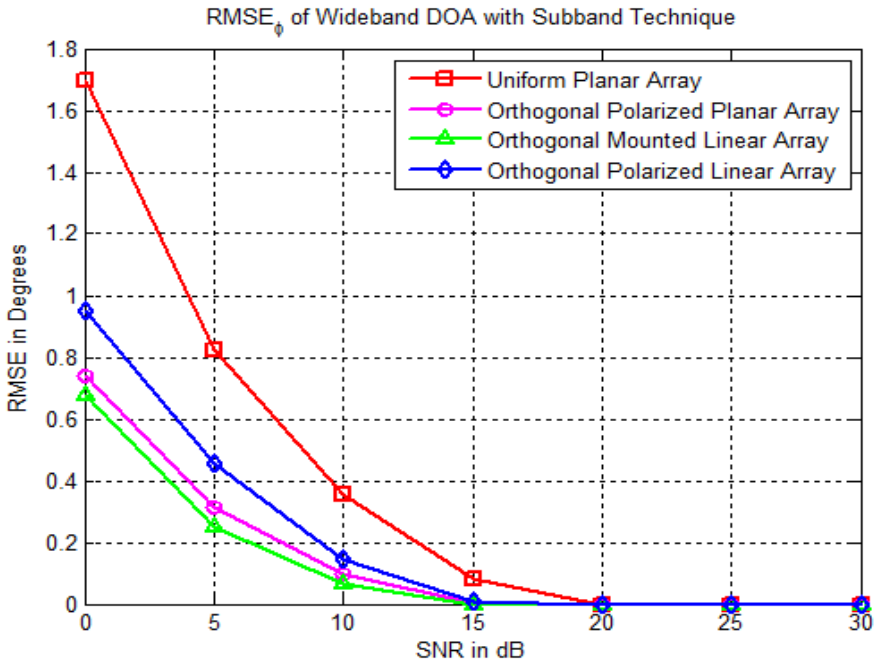

Figure 6.37: RMSE Comparison for ϕ Angle Estimation of 2D-DOA Estimation of Wideband Signal for Single and Orthogonal Polarized Array Configurations

The RMSE performance of DOA estimation of wideband signal for both the θ and ϕ angles of 2D-DOA is analysed for 0 to 30 dB SNR scenarios. The results of the RMSE performance of θ and ϕ angles of 2D-DOA estimations are illustrated in Figures 6.36 and 6.37 respectively. Comparison of the wideband estimation performance is seen individually for the elevation angle θ and the azimuth angle ϕ estimations for the single and orthogonal polarizes array configurations. The analysis of influence of array configuration on the 2D-DOA estimation presented in the previous chapters for narrow band cases and tracking performances has been extended for the case of wideband sources also. At lower SNR, the estimation of ϕ angle is less accurate when compared to the estimation ofθ angle. The single polarized UPA configuration is more prone for error in the estimation of azimuth ϕ angle, when compared to the proposed orthogonal array configurations. The OMLA and OPPA configurations are better in their performance. These two array configurations show almost similar performance with least RMSE in their θ and ϕ angle estimation. The OPLA suffers slightly due to its linear geometric arrangement in the 2D-DOA estimation. However OPLA shows improved DOA estimation of wideband source when compared with the azimuth angle ϕ estimation of conventional single polarized UPA configuration.

6.8 Simulation of 2D-DOA Estimation of Two Wideband Source by Using Subband Technique

The simulation analysis of the proposed subband technique for DOA of wideband source is further extended for the 2D-DOA of two wideband sources. The two wideband incoming sources and the estimation of 2D-DOA are carried by invoking the conventional single polarized UPA and the proposed orthogonal polarized arrays. The 2D-DOA for two wideband sources are modelled for the DOA angles $(\theta_1 = 52^\circ\ ,\ \phi_1 = 28^\circ)$ and $(\theta_2 = 40^\circ\ ,\ \phi_2 = 65^\circ)$.

6.8.1 2D-DOA Estimation of Two Wideband Sources with Conventional Single Polarized UPA

The conventional single polarized UPA discussed in the previous chapters is utilized for estimation of 2D-DOA of two wideband sources modelled for 0 dB SNR. The results of the 2D-DOA estimation with single polarized UPA are shown in Figure 6.38. The magnitudes of detection peaks corresponding to 2D-DOA of two sources are different. Additional fictitious peak is also seen in the results leading to ambiguity in the estimation of 2D-DOA.

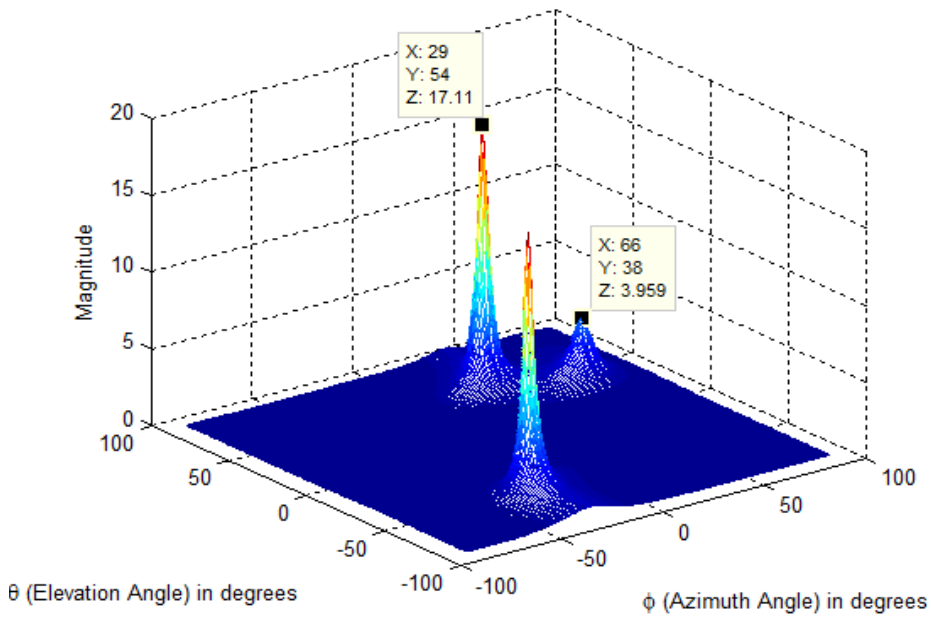

Figure 6.38: 2D-DOA Estimation of Two Wideband Sources with Uniform Planar Array for the Signal Model $(\theta_1 = 52^\circ\ ,\ \phi_1 = 28^\circ)$ and $(\theta_2 = 40^\circ\ ,\ \phi_2 = 65^\circ)$ for 0 dB SNR

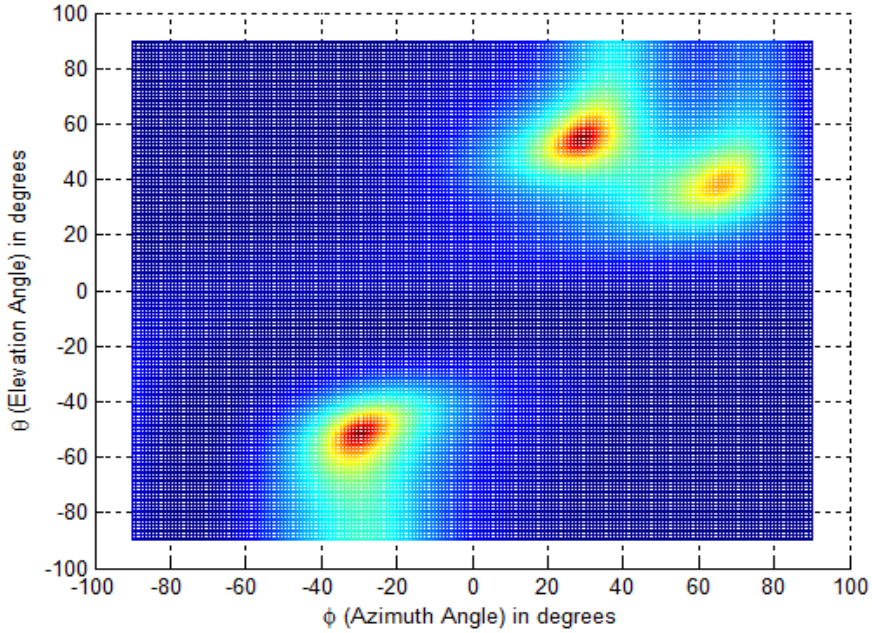

Figure 6.39: 2D-DOA Estimation of Two Wideband Sources with Uniform Planar Array for the Signal Model $(\theta_1 = 52^\circ\ ,\ \phi_1 = 28^\circ)$ and $(\theta_2 = 40^\circ\ ,\ \phi_2 = 65^\circ)$ for 0 dB SNR - 2D View of Simulation Result

A spread of peak magnitudes around the DOA of the two modelled wide band sources are seen in results of Figure 6.39. The additional peak at angle $(-50^\circ, -30^\circ)$ is a spurious peak. The availability of only single polarized component, uniform covariance of the received data as well as the lack of provision for further reduction of inter-element spacing induce the additional spurious peak in the estimation. Also, the results of the simulation at higher SNR also confirm that the magnitude of spurious peak is not reducing. The results of 2D-DOA estimation at higher SNR scenario are shown in Figures C.1, C.2, C.3, C.4, C.5 and C.6 of Appendix C.

6.8.2 2D-DOA Estimation of Two Wideband Sources with OPPA

The proposed OPPA configuration is evaluated for its performance in estimating the 2D-DOA of two wideband sources. The results of the 2D-DOA estimation with two wideband sources are presented in Figure 6.40 for 0 dB SNR.

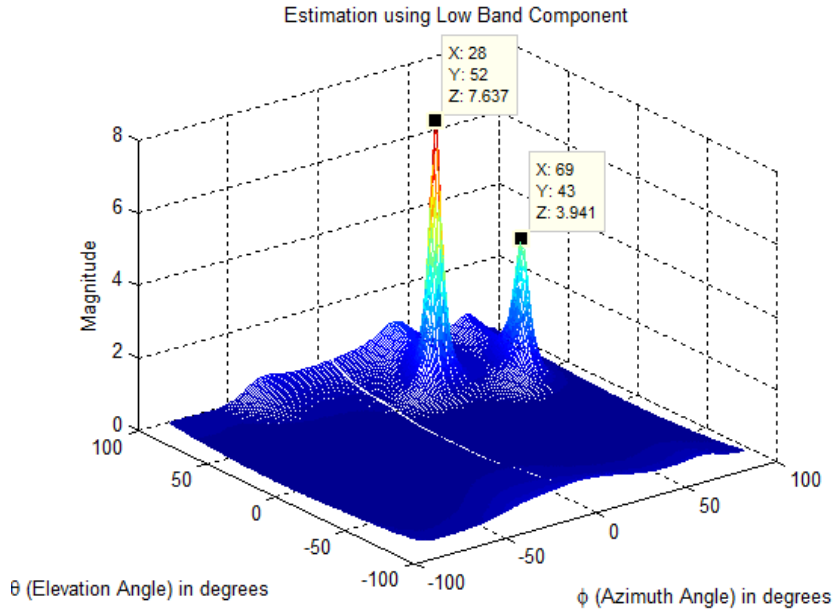

Figure 6.40: 2D-DOA Estimation of Two Wideband Sources with Orthogonal Polarized Planar Array for the Signal Model $(\theta_1 = 52^\circ\ ,\ \phi_1 = 28^\circ)$ and $(\theta_2 = 40^\circ\ ,\ \phi_2 = 65^\circ)$ for 0 dB SNR

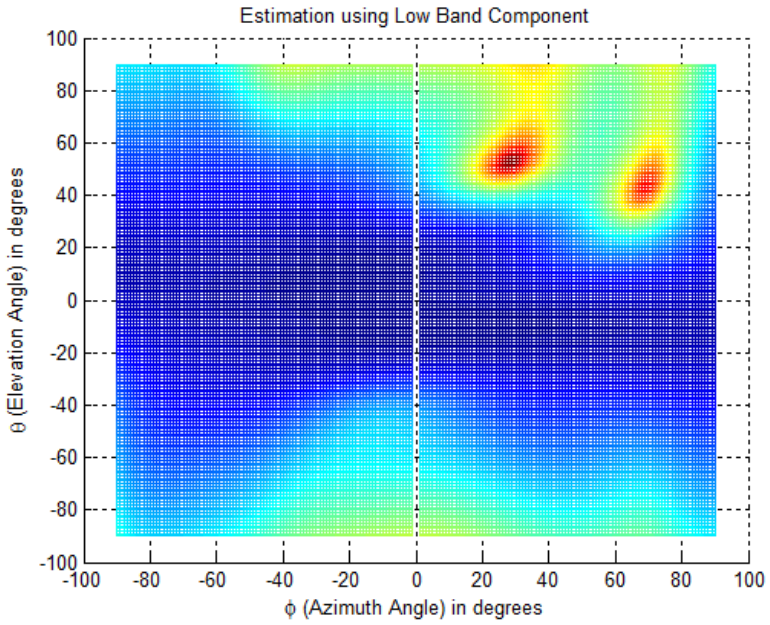

Figure 6.41: 2D-DOA Estimation of Two Wideband Sources with Orthogonal Polarized Planar Array for the Signal Model $(\theta_1 = 52^\circ\ ,\ \phi_1 = 28^\circ)$ and $(\theta_2 = 40^\circ\ ,\ \phi_2 = 65^\circ)$ for 0 dB SNR - 2D View of Simulation Result

The 2D view of the simulation results is depicted in Figure 6.41. The results of Figures 6.40 and 6.41 show that the OPPA facilitates the improved estimation of the 2D-DOA of two wideband sources without any spurious peak. The improved estimation of the two sources despite the case of 0 dB SNR is accomplished, due to the availability of the data covariances of both the vertical and horizontal polarized components along both x and y axes. The improved results of the estimation of 2D-DOA of two wideband sources, estimated through OPPA at higher SNRs are presented in Figures C.7, C.8, C.9, C.10, C.11 and C.12 of Appendix C.

6.8.3 2D-DOA Estimation of Two Wideband Sources with OMLA

The 2D-DOA estimation of two wideband sources is also accomplished with the proposed OMLA. The two wideband sources of the simulations are modelled for 0 dB SNR. The results of 2D-DOA estimation of two wideband sources are shown in Figure 6.42. The same results are also captured in 2D view in Figure 6.43 to get the additional information on the spread of the detection peaks.

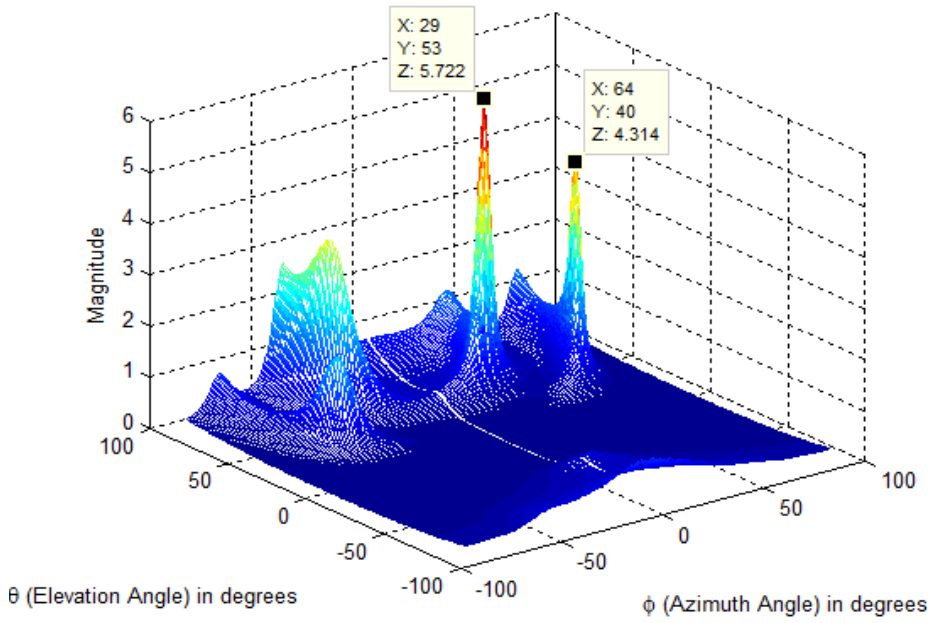

Figure 6.42: 2D-DOA Estimation of Two Wideband Sources with Orthogonal Mounted Linear Array for the Signal Model $(\theta_1 = 52^\circ\ ,\ \phi_1 = 28^\circ)$ and $(\theta_2 = 40^\circ\ ,\ \phi_2 = 65^\circ)$ for 0 dB SNR

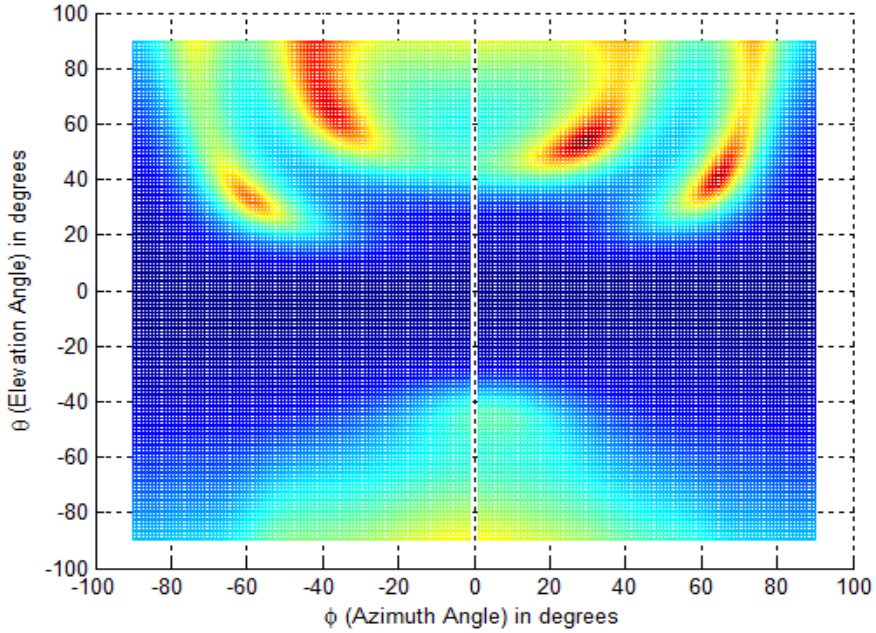

Figure 6.43: 2D-DOA Estimation of Two Wideband Sources with Orthogonal Mounted Linear Array for the Signal Model $(\theta_1 = 52^\circ\ ,\ \phi_1 = 28^\circ)$ and $(\theta_2 = 40^\circ\ ,\ \phi_2 = 65^\circ)$ for 0 dB SNR - 2D View of Simulation Result

The results of Figure 6.42 reveal the higher magnitudes of detection peaks. The OMLA has limited covariance data of both the horizontal and vertical polarized components in both the x and y axes. In addition, the wideband nature of the two sources at 0 dB SNR, the spurious peaks of Figure 6.42 with reduced magnitudes than the peaks corresponding to the actual DOA of sources can be seen in the results. However, the magnitude of these spurious peak diminish as SNR of the data covariances increases. The results of diminishing magnitude of spurious peaks at higher SNRs can be seen in the results presented Figures C.13, C.14, C.15, C.16, C.17 and C.18 in Appendix C.

6.8.4 2D-DOA Estimation of Two Wideband Sources with OPLA

The simulation of 2D-DOA estimation is also carried for the proposed OPLA, keeping the same DOA angles of the source modelling. The estimation performance of 2D-DOA with OPLA as well as the corresponding detection peak and the spread of profile of detection peak can be seen in the results of Figure 6.44 and 6.45 respectively.

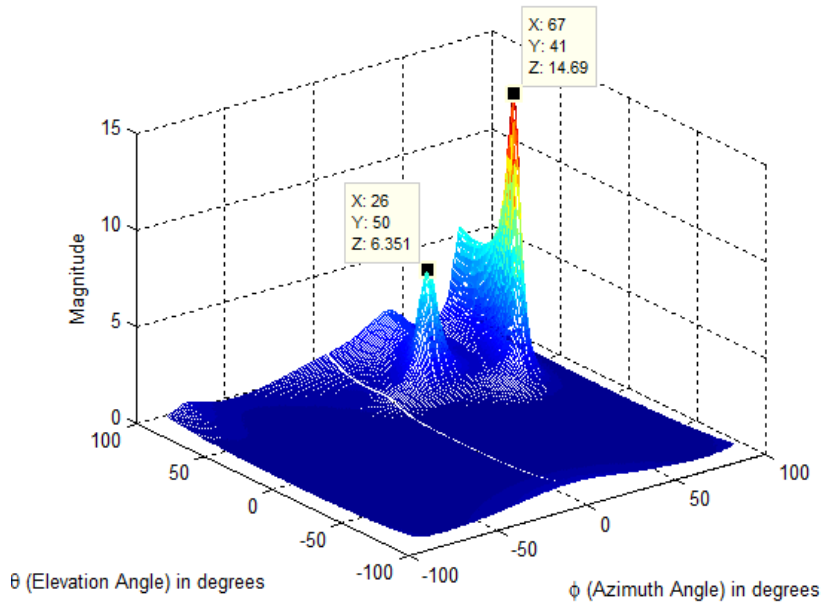

Figure 6.44: 2D-DOA Estimation of Two Wideband Sources with Orthogonal Polarized Linear Array for the Signal Model $(\theta_1 = 52^\circ\ ,\ \phi_1 = 28^\circ)$ and $(\theta_2 = 40^\circ\ ,\ \phi_2 = 65^\circ)$ for 0 dB SNR

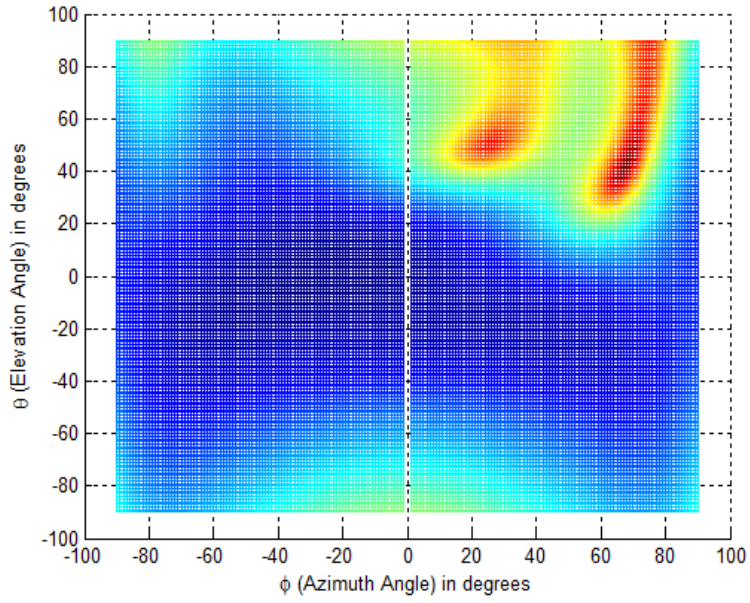

Figure 6.45: 2D-DOA Estimation of Two Wideband Sources with Orthogonal Polarized Linear Array for the Signal Model $(\theta_1 = 52^\circ\ ,\ \phi_1 = 28^\circ)$ and $(\theta_2 = 40^\circ\ ,\ \phi_2 = 65^\circ)$ for 0 dB SNR - 2D View of Simulation Result

The results of Figure 6.44 and 6.45 indicate more spread in the estimation profile of the two DOA sources at low SNR (0 dB). There is a wider spread of the two detected peaks corresponding to the estimated DOA angles. The samples received through the array elements of OPLA will have the data covariance of both vertical and horizontal polarized components along one (x) axis only. The non-availability of the data covariance along the y axis of 2D-DOA estimation leads to spread of the peak magnitudes in the DOA of the two sources. However, the reduction in spread of estimation peaks is evident in the results of the higher SNR simulation shown in the Figures C.19, C.20, C.21, C.22, C.23 and C.24 of Appendix C.

6.9 Summary

This chapter dealt with extension of DOA estimation technique of narrow band signal to wideband signal source. A detailed discussion on formulation of analysis for wideband DOA estimation based on incoherent, coherent and subband filtering techniques is presented in this chapter. Results of numerous simulation studies have been presented in the chapter to analyse the performance of the proposed wideband technique under the scenarios of low, moderate and high SNR. Through the simulation studies, it is evidently clear that only the proposed subband filtering is able to estimate the DOA of wideband signal consistently for all the SNR scenarios. A significant computation time reduction (20 times faster than incoherent and 27 times faster than CSSM) is realized for the proposed subband filter based DOA estimation of wideband sources when compared with conventional incoherent and coherent schemes.

Further, it is noticed that the DOA estimation derived through the low band component of the subband filtering technique is accurate and shows the consistency at all SNR scenarios. The DOA estimation derived through the high band component of the subband filter cannot be relied upon particularly at low SNR scenarios such as 0 dB. The influence of the geometrical configuration of the array on the accuracy of wideband DOA estimation has been analysed using the 4 array configurations which have been dealt in chapters 3 and 4 of this thesis. From the presented comparative analysis of DOA estimation through orthogonally polarized array configurations, it is inferred that OPPA has better DOA estimation capability because of the presence of spatial phase variation in its array configuration (along both the axes). In addition to OPPA, OMLA also exhibits better performance in 2D-DOA estimation, since its geometrical configuration is a limiting case

of OPPA. The performance of the 2D-DOA of wideband sources with OPPA has been found to be more accurate and consistent for various simulation scenarios.

Chapter 7

Conclusions

This chapter intends to summarize and facilitate recapitulation of succinct summary, inferences, technical conclusions derived out of the undertaken research study of this thesis. The potential avenues for further explorations and investigations of the research study presented in this thesis are also emphasised.

7.1 Research Summary

The topic of parameter estimation has attracted many researchers over the past several decades. The estimation of the parameter DOA and its multi disciplinary approach pose challenges to RF and signal processing engineers. The estimation of DOA of electromagnetic sources continues to warrant the performance improvement of the DOA estimation algorithms dealing with single and multiple sources. In addition, there is a greater emphasis for tracking of DOA of dynamic sources. There is growing need to extend the DOA estimation algorithms established for narrow band sources to wideband sources. There is always a desirable need to minimize the computational complexity of proven DOA algorithms without compromising the accuracy and reliability.

In this context, this research was motivated towards the utilization of orthogonal polarized antenna array configurations for the improvement of accuracy and resolution of DOA estimation invoking the classical MUSIC algorithm. By utilizing orthogonal polarized elements of the antenna array, a closed form solution was derived for the estimation of 2D-DOA with 1D search technique to realize reduced computation complexity. This thesis proposes novel orthogonally polarized array configurations to facilitate enhanced accuracy and resolution of 2D-DOA estimation algorithms for single and multiple sources. The novel orthogonal polarized array configurations include OPLA, OPPA and OMLA.

The improved capability of distinguishing two closely spaced sources is realized with the proposed orthogonal polarized arrays when compared to single polarized UPA configuration. This thesis also analysed the proposed array configurations for their potential

in tracking of 2D-DOA of sources. The combination of orthogonally polarized array configurations and the conventional MUSIC algorithm is extended to analyse the tracking behaviour of 2D-DOA estimation of dynamic sources. Further, this thesis also covered the development of 1D and 2D-DOA estimation of wideband sources using the proposed orthogonally polarized array configurations. A novel subbanding technique for wideband DOA technique was proposed and its improved performance was substantiated through a comparative study involving conventional algorithms for estimation of DOA of wideband sources.

7.2 Conclusions

The technical observations, inferences, original contributions and conclusions of this research are briefly reviewed in the following subsections.

7.2.1 Formulation of Closed Form solution for 2D-DOA Estimation with OPLA

Formulation of an analysis to derive the closed form expression for the estimation of 2D-DOA of a single source using the linear array configuration constituted the primary theme of the 3^{rd} chapter of this thesis. Under the purview of this topic, the following conclusions can be derived from the simulation studies.

- The OPLA configuration can be used to estimate the DOA with classical subspace based MUSIC algorithm. The derived closed form expression can be used along with the classical subspace based technique to estimate the 2D-DOA. The search dimensions are reduced from 2D to 1D thereby minimizing the computational complexity involved in 2D-DOA estimation.

- The derived solution estimates both azimuth and elevation angles of distant sources utilizing a linear array configuration. The proposed one-dimensional search is a consequence of utilizing the linear array configuration with its alternate elements orthogonally polarized.

- The distinct feature of the proposed one-dimensional search technique leading to a significant reduction in the computation time for two-dimensional DOA estimation using MUSIC algorithm has been illustrated through the simulation studies.

- The proposed formulation can be extended to any other antenna whose radiation pattern can be represented through an analytical expression involving separable form of elevation angle θ and azimuth angle ϕ.

- Simulation results of 2D-DOA obtained with conventional single polarized UPA (2×2) have been correlated with those obtained through OPLA and very good correlation exists between the results of the above two array configurations. The proposed one-dimensional search technique has resulted in an acceleration of computation time by factors of 50 and 150 for 1° and 0.5° search intervals respectively.

7.2.2 2D-DOA Estimation with Orthogonal Polarized Arrays

Formulation of an analysis to estimate the 2D-DOA of multiple sources with enhanced accuracy and improved resolution is the main focus of the 4^{th} chapter of this thesis.

- The simulations and analysis have been carried out to confirm that the orthogonally polarized elements of antenna array have significant influence in the accuracy and resolution of the estimation of 2D-DOA.

- The proposed OPLA as a physical arrangement can be treated as a linear array. Thus a linear array configuration and its ability to estimate the 2D-DOA is the novel part of the proposed OPLA.

- The proposed configuration of OPPA has improved accuracy of estimation of 2D-DOA when compared with single polarized UPA.

- The proposed OMLA configuration estimates the two DOA sources with higher magnitudes when compared with the other proposed orthogonally polarized and conventional UPA configuration.

- The improved capability of the orthogonally polarized arrays in distinguishing the closely spaced sources is also substantiated through the simulation studies.

- The OPPA and the OMLA clearly distinguish the DOA of sources with minimum angular separation of 10°. The conventional single polarized UPA configuration could resolve the two sources whose angular separation was 18° or more, which is inferior when compared with the proposed OPPA and OMLA configurations.

- The orthogonally polarized linear elements resolve DOA of the two sources with angular separation of 10° with increased inter-element spacing.
- The consistent accurate estimation of the 2D-DOA for two sources and three sources under high, medium and low SNR scenario with the proposed orthogonally polarized array configurations and the derivable higher resolution have been substantiated from the simulation analysis.

7.2.3 Orthogonal Polarized Arrays for Tracking of 2D-DOA for Dynamic Sources

The primary emphasis of the 5^{th} chapter of this thesis has been the extension of the analysis of the orthogonally polarized array configurations to track the 2D-DOA of dynamic sources using different schemes of formation of covariance matrix.

- The simulation analysis of tracking behaviour of 2D-DOA with the conventional single polarized and orthogonal polarized array configurations has been carried out. The tracking behaviour of 2D-DOA estimation algorithms is analysed by comparing the computed MSE between true trajectory and estimated trajectory.
- The MSE for θ and ϕ angles of tracking the estimation of 2D-DOA is computed by utilizing the different approaches in the formation of data covariance matrix such as instantaneous samples approach, weighting factor and forgetting factor approaches.
- The results of the analysis are tabulated for the low, medium and high SNR scenarios in the Table 5.1. The comparative analysis reveals, that the OPPA outperforms the other array configurations with least MSE in the 2D-DOA estimation and as well as in tracking of 2D-DOA estimation.
- The OMLA performs better, when compared to UPA and OPLA configurations.
- The OPLA performs almost equally with UPA at medium and high SNR scenarios. Due to the linear geometric configuration, the OPLA shows, a small degradation in θ estimations when compared to UPA at low SNR.
- The forgetting factor approach in the covariance matrix formation tracks the 2D-DOA estimation more accurately when compared to instantaneous samples and weighting factor approaches.

7.2.4 Subband Filter Technique for DOA Estimation of Wideband Sources

The various analytical and simulation studies on DOA estimation of narrow band sources have been extended to the scenario of wideband signal too. The conclusions derived from the pertinent simulation studies on the estimation of 2D-DOA of wideband sources are presented in this subsection.

- The subband filter approach for DOA estimation of wideband source is proposed and the performance of estimation of DOA of the proposed approach has been compared with conventional wideband DOA estimation methods namely incoherent and coherent signal subspace methods.
- The comparative analysis of the proposed subband filter based wideband DOA estimation scheme outperforms the conventional incoherent and coherent signal subspace method.
- A significant reduction in computation time (20 times faster than incoherent and 27 times faster than CSSM) is realized for the proposed subband filter based DOA estimation of wideband sources.
- The proposed two subband filter approach yields the DOA estimation through the two components namely low band and high band signals. The estimation of DOA derived through the signal component of low band exhibits satisfactory performance in low, medium and high SNR scenarios including the case of 0 dB.
- The accuracy of the estimation of DOA of wideband signal through incoherent and coherent methods as well as through the high band signal of the subband filter approach is satisfactory only in high SNR. However they have the limitation of degraded performance in low and medium SNR cases.
- Among the various array configurations used in the estimation of DOA of wideband sources, the OPPA and OMLA exhibit the feature of improved estimation through low RMSE even in low SNR scenario.
- The performance analysis of DOA estimation of two wideband signals has also been carried out using the proposed subband filter approach and the simulation results reveal the relative performance improvement compared to the conventional incoherent and coherent subspace methods.

- The accuracy of 2D-DOA estimation of wideband sources obtained through the signal component of low band is consistently better when compared to the other approaches cited above and the relative performance accuracy is significantly higher particularly in medium and low SNR scenarios.
- The conventional single polarized UPA exhibits spurious peaks at an arbitrary DOA angle which tend to mislead the DOA estimation, whereas the proposed orthogonal array configurations estimate the DOA angles of the sources without spurious peaks.
- The orthogonally polarized array configurations proposed in this thesis continue to facilitate better performance of the 2D-DOA estimation of two wideband signal sources.

7.3 Contributions

The following are the contributions of this thesis whose emphasis is on the estimation and tracking of 2D-DOA applying MUSIC algorithm.

- Derivation of the closed form expression for the estimation of 2D-DOA of a single source using the orthogonally polarized linear array configuration.
- Novel orthogonal polarized array configurations for improved accuracy and resolution estimation of 2D-DOA.
- Improved tracking accuracy of 2D-DOA estimation by utilizing orthogonal polarized array configurations as well as forgetting factor approach based covariance matrix.
- Enhanced accuracy in estimation of 2D-DOA of wideband sources by invoking subband filter approach.

7.4 Suggestions for Future Work

Research is a voyage of discovery. It is a path for unknown to the known and at times, known to the unknown. The philosophy of research always provides impetus to look for avenues to enhance the scope of current state of knowledge and understanding of any topic of interest to research community. With these words, potential avenues to further advance the research topic of this thesis are highlighted.

7.4.1 Orthogonal Polarized Arrays

- Like the rectangular waveguides as antenna, chosen in this thesis, other potential waveguides and antenna elements suitable to be applied for DOA estimation can be explored for their utility in orthogonal polarized array configuration for estimation of 2D-DOA.

- Invoking dual polarized antenna elements for DOA estimation by simultaneous reception of both the horizontal and vertical polarized components might yield novelty as well as paving the way for a new direction in modelling of antenna arrays and signal processing algorithms.

- Analysis to investigate the influence of mutual coupling of the various array configurations proposed in this thesis is yet to be formalised and the same can constitute a significant part for the future work.

7.4.2 Tracking of 2D-DOA

- The repeated computation of SVD during the tracking of 2D-DOA can be circumvented by the Bi-SVD and modified Bi-SVD algorithms for reduction in the computation complexity.

- An implicit assumption of linear movement of the DOA sources is associated with the research of this thesis. However, tracking of estimation of 2D-DOA with non-linear movements of non-stationary signal sources is worth pursuing further.

- The extraction of DOA information and tracking the estimation of DOA in the presence of non-linear movements of single and multiple signal sources in a dynamic changing environment pose significant challenges in the estimation algorithm.

- A forgetting factor based smoothing of covariance data matrix is carried out in this thesis. Further a prediction based tracking algorithm for linear and non-linear movements of non-stationary DOA sources can be analysed by invoking Kalman Filter and Extended Kalman Filter based techniques.

- A Gaussian white noise process is utilized for the simulation analysis in most of this thesis. Instead consideration of a non-Gaussian noise with non-linearity in the signal model is a worth while exercise of practical significance.

7.4.3 Wideband DOA Estimation Techniques

- The proposed two subband approaches can be extended to multiple filter bank approach for further improvements in estimation of DOA of wideband sources.
- The polyphase decomposition scheme in the multirate filter bank approaches may offer potential scope for improvements in the estimation of DOA of wideband sources.
- The Short Time Fourier Transform (STFT), Wavelet Filters and Gabor Filters can also be incorporated in estimation of DOA of wideband sources.

APPENDIX A

Mutual Coupling Analysis of RWG

This appendix is aimed to present the simulation studies pertaining to the mutual coupling between the RWG elements when configured in linear array and OPLA configuration. The simulation results presented in this appendix clearly substantiate the desirable feature of reduced mutual coupling between the RWG elements when configured as OPLA.

A.1 Analysis of Mutual Coupling

The simulation analysis of mutual coupling between antennas involves the geometric modelling of the radiating structure of the antennas. For the purpose of simulation analysis, the following dimensions of X band RWG have been assumed for standard RWG operating in dominant TE_{10} mode. The width $a = 2.32$ cm and height $b = 1$ cm. The linear array configuration with two RWG elements is shown in Figure A.1.

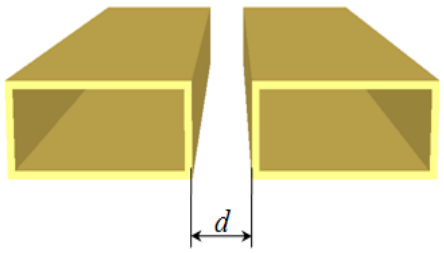

Figure A.1: Mutual Coupling of Rectangular Waveguide Array for Conventional Linear Arrangement for Two Elements

In Figure A.1 the edge to edge separation between the two RWGs is denoted by d. With this arrangement of the array, the inter-element spacing between the center of aperture of the two RWGs $d + a$ neglecting the wall thickness. Traditionally the elements of the antenna array are assumed to be point sources and physical dimensions of the antenna are not considered in the analysis. However, in this thesis, the inter-element spacing between the successive elements includes the edge to edge separation and the relevant physical

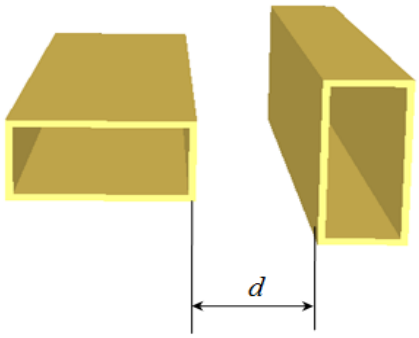

Figure A.2: Mutual Coupling of Rectangular Waveguide Array for Orthogonal Arrangement for Two Elements

dimensions of the waveguide. As a consequence, the usual constraint of $\frac{\lambda}{4} \leq d \leq \frac{\lambda}{2}$ cannot be satisfied, λ being wavelength. The geometry of the RWG elements of linear array of Figure A.1 is modelled in Empire 3D EM solver which is based on FDTD technique.

The S parameters (S_{12} or S_{21}) corresponding to the mutual coupling between the two

Table A.1: Mutual Coupling Analysis between the Rectangular Waveguides

Inter-element Spacing d in mm	**Mutual Coupling in Conventional Uniform Linear Array**	**Mutual Coupling in Orthogonal Polarized Array**
16 mm	-40 dB	-98 dB
8 mm	-38 dB	-95 dB
4 mm	-30 dB	-86 dB
2 mm	-25 dB	-85 dB
0 mm	-20 dB	-85 dB

RWGs are simulated by varying the value of d. For the simulation studies, the frequency of operation is 9.375 GHz. In the second configuration of linear array comprising the two RWGs, the two elements are oriented as shown in Figure A.2 to ensure that one of the RWGs receives only vertical or azimuth polarization and the other RWG receives only horizontal or elevation polarization. In Figure A.2 also d refers to the distance between the edges of the two RWGs. The S parameters corresponding to the mutual coupling between the RWGs of the Figure A.2 are simulated for various values of d which are identical to the ones used in earlier simulation pertaining to array shown in Figure A.1. Table A.1 presents a comparative performance of the mutual coupling exhibited by the two different array configurations shown in Figure A.1 and A.2. From the simulation results of the Table A.1 it is evident that the mutual coupling between the two RWGs of array shown in Figure

A.1 varies between -20 dB and -40 dB for the chosen range of d. For the same chosen range of d the mutual coupling between the adjacent elements of the array shown in Figure A.2 ranges between -85 dB and -98 dB. The reduced mutual coupling between the RWGs of Figure A.2 is attributed to relative orthogonal orientation of the two RWGs. In Table A.1 the scenario of $d = 0$ corresponds to the case of the two RWGs touching each other through the side walls. In a physical arrangement of RWGs, the two elements cannot be brought any closer than with $d = 0$. The results of Table A.1 show that the orthogonally oriented adjacent elements (Figure A.2) experience a mutual coupling -85 dB when the two RWGs touch each other. For an analogous case of two RWGs in conventional linear array configuration (Figure A.1), the mutual coupling between them is -20 dB at $d = 0$. This clearly indicates that the relative orthogonal orientation of adjacent elements results in significant reduction in the mutual coupling which is desirable for improved accuracy of DOA estimation. Therefore the novel orthogonal polarized array configurations proposed in this thesis namely OPLA, OPPA and OMLA are featured with reduced mutual coupling between the adjacent elements even when they are in very proximity.

APPENDIX B

Results of Estimation of 2D-DOA of Single Wideband Source for different SNRs

Additional simulation results pertaining to the estimation of 2D-DOA of single wideband source are presented in this Appendix. The improved accuracy and reliability of the MUSIC based DOA estimation algorithm using various orthogonally polarized array configurations are illustrated for varying SNR scenario. All the results presented in this Appendix are obtained through subband based technique of DOA estimation of single wideband source. In particular, only low band signal component of the subband technique is considered in the simulation results presented in this Appendix.

B.1 Estimation of 2D-DOA of Single Wideband Source With Conventional Single Polarized UPA

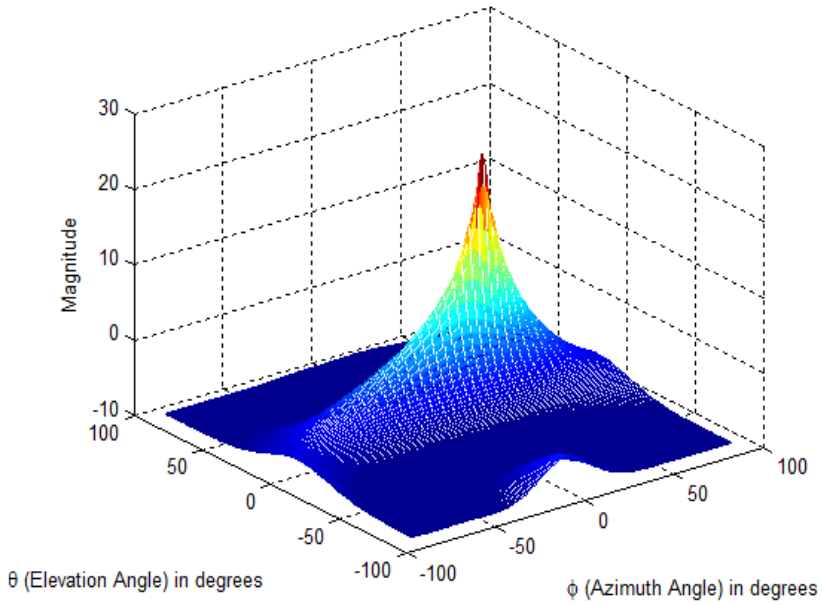

Figure B.1: 2D DOA Estimation of Single Wideband Source with UPA for the Signal Model $\theta = 15^\circ$ and $\phi = 30^\circ$ for 10 dB SNR

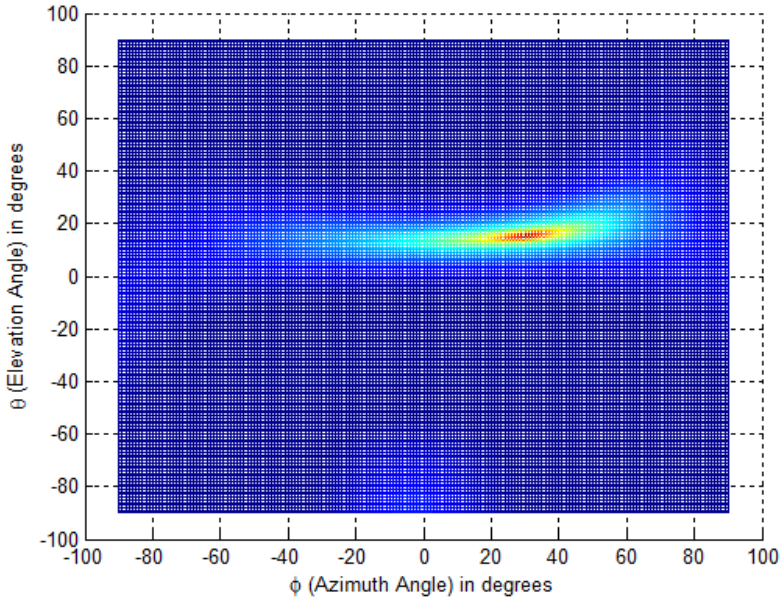

Figure B.2: 2D DOA Estimation of Single Wideband Source with UPA for the Signal Model $\theta = 15^\circ$ and $\phi = 30^\circ$ for 10 dB SNR - 2D View of Simulation Result

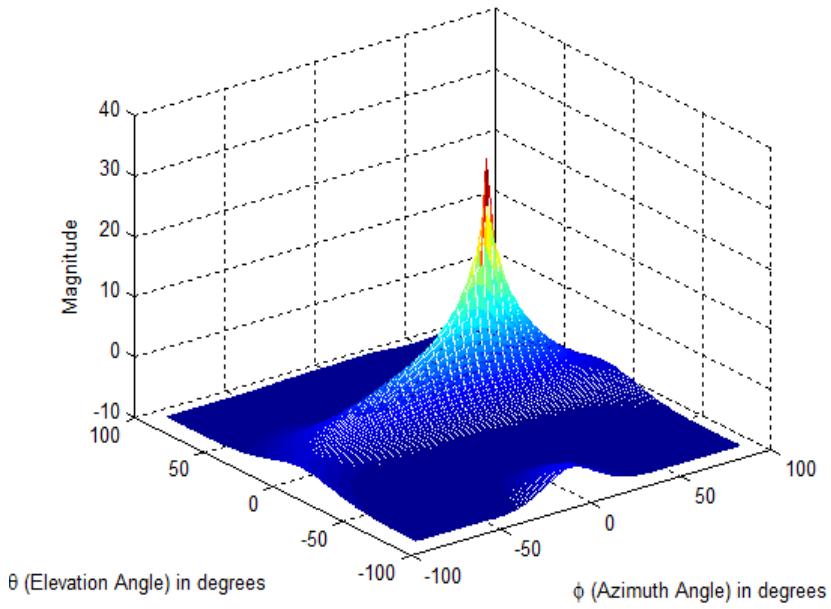

Figure B.3: 2D DOA Estimation of Single Wideband Source with UPA for the Signal Model $\theta = 15^\circ$ and $\phi = 30^\circ$ for 20 dB SNR

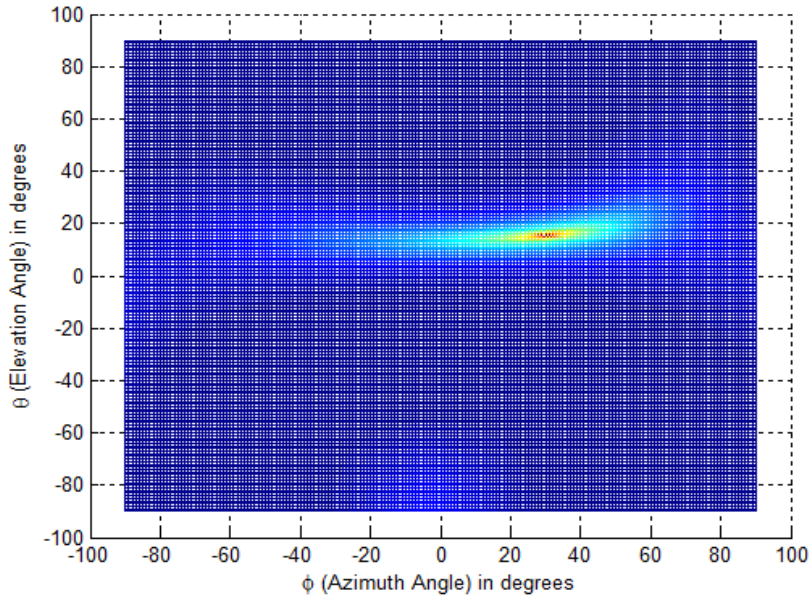

Figure B.4: 2D DOA Estimation of Single Wideband Source with UPA for the Signal Model $\theta = 15^\circ$ and $\phi = 30^\circ$ for 20 dB SNR - 2D View of Simulation Result

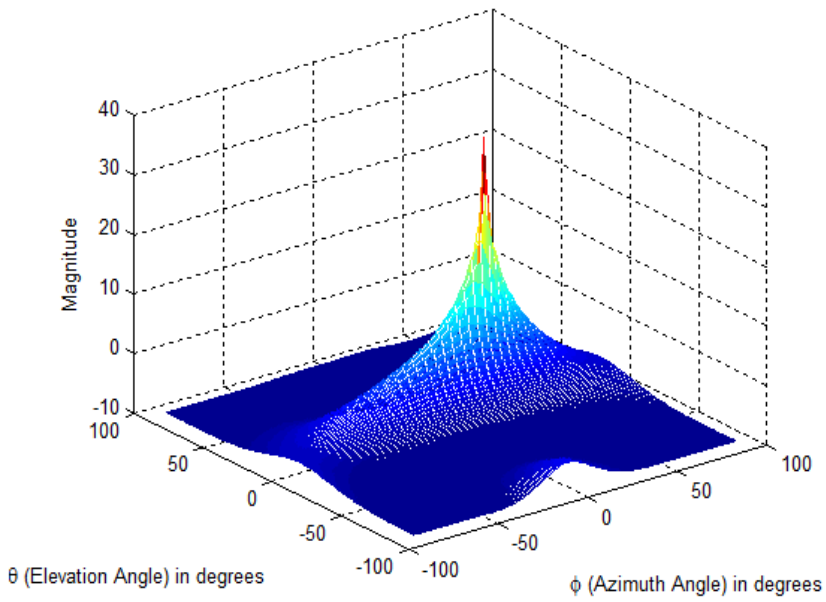

Figure B.5: 2D DOA Estimation of Single Wideband Source with UPA for the Signal Model $\theta = 15^\circ$ and $\phi = 30^\circ$ for 30 dB SNR

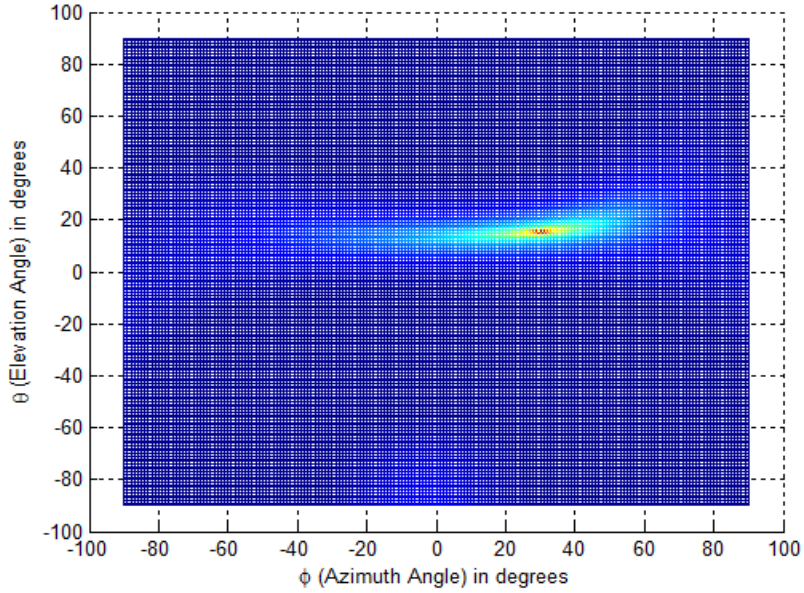

Figure B.6: 2D DOA Estimation of Single Wideband Source with UPA for the Signal Model $\theta = 15^\circ$ and $\phi = 30^\circ$ for 30 dB SNR - 2D View of Simulation Result

B.2 Estimation of 2D-DOA of Single Wideband Source With OPPA

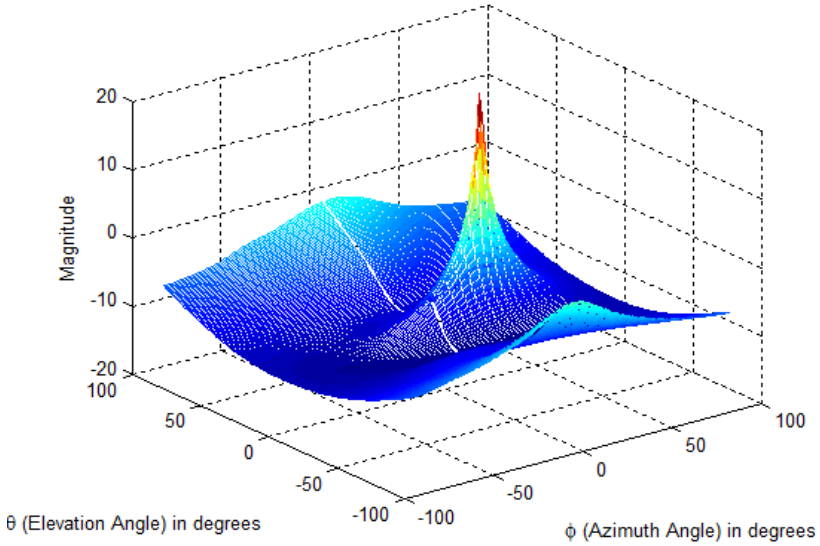

Figure B.7: 2D DOA Estimation of Single Wideband Source with OPPA for the Signal Model $\theta = 15^\circ$ and $\phi = 30^\circ$ for 10 dB SNR

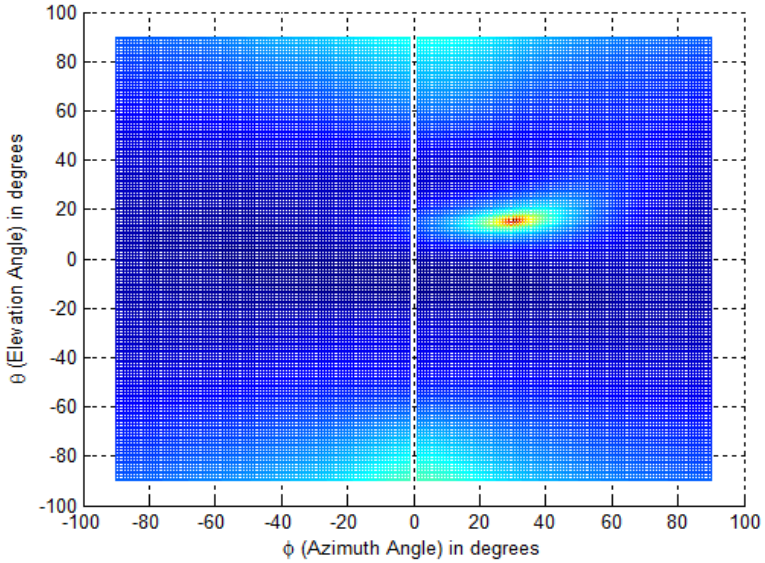

Figure B.8: 2D DOA Estimation of Single Wideband Source with OPPA for the Signal Model $\theta = 15^\circ$ and $\phi = 30^\circ$ for 10 dB SNR - 2D View of Simulation Result

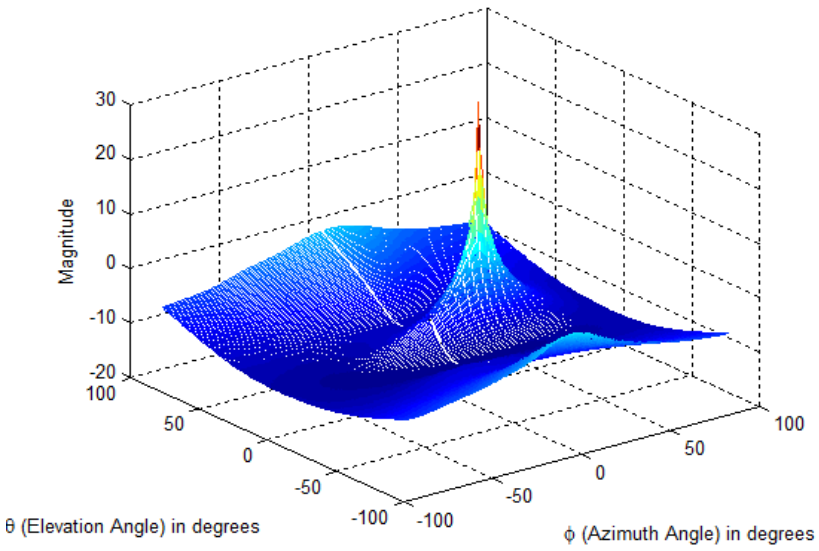

Figure B.9: 2D DOA Estimation of Single Wideband Source with OPPA for the Signal Model $\theta = 15^\circ$ and $\phi = 30^\circ$ for 20 dB SNR

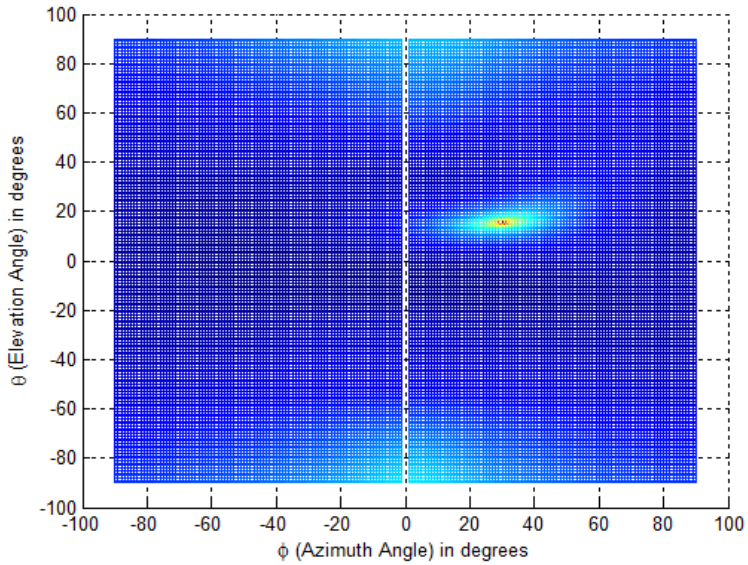

Figure B.10: 2D DOA Estimation of Single Wideband Source with OPPA for the Signal Model $\theta = 15^\circ$ and $\phi = 30^\circ$ for 20 dB SNR - 2D View of Simulation Result

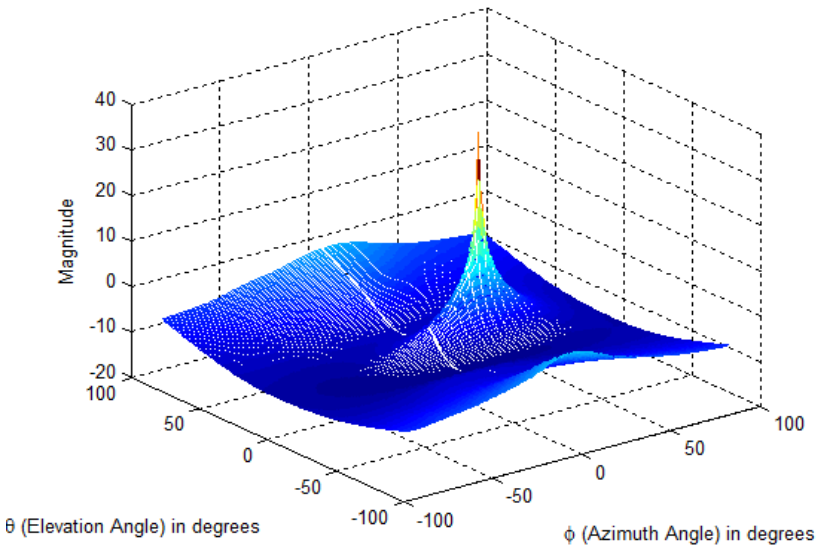

Figure B.11: 2D DOA Estimation of Single Wideband Source with OPPA for the Signal Model $\theta = 15^\circ$ and $\phi = 30^\circ$ for 30 dB SNR

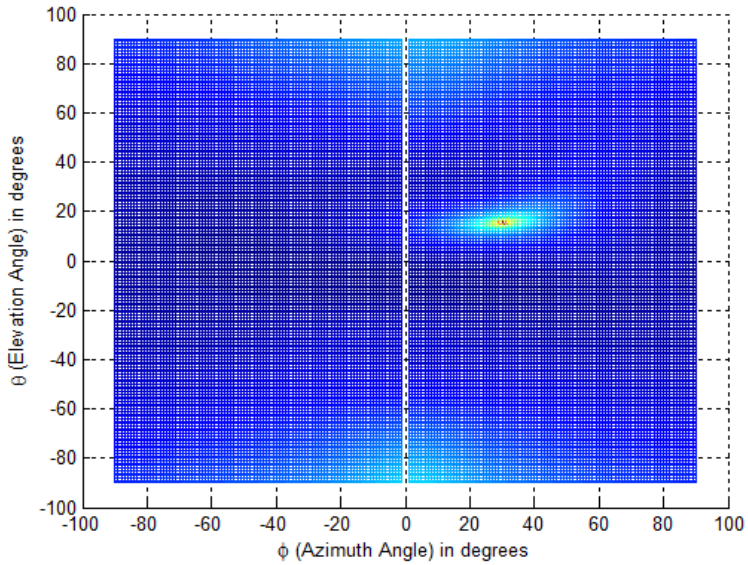

Figure B.12: 2D DOA Estimation of Single Wideband Source with OPPA for the Signal Model $\theta = 15^\circ$ and $\phi = 30^\circ$ for 30 dB SNR - 2D View of Simulation Result

B.3 Estimation of 2D-DOA of Single Wideband Source With OMLA

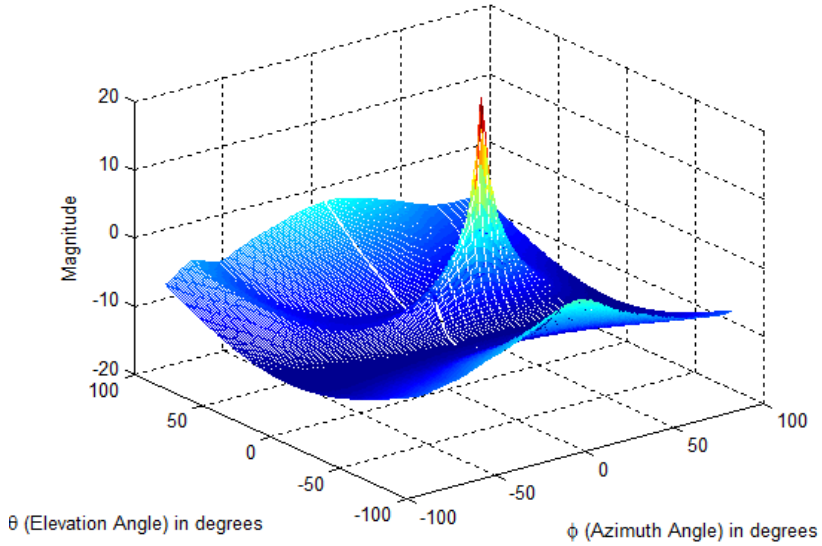

Figure B.13: 2D DOA Estimation of Single Wideband Source with OMLA for the Signal Model $\theta = 15^\circ$ and $\phi = 30^\circ$ for 10 dB SNR

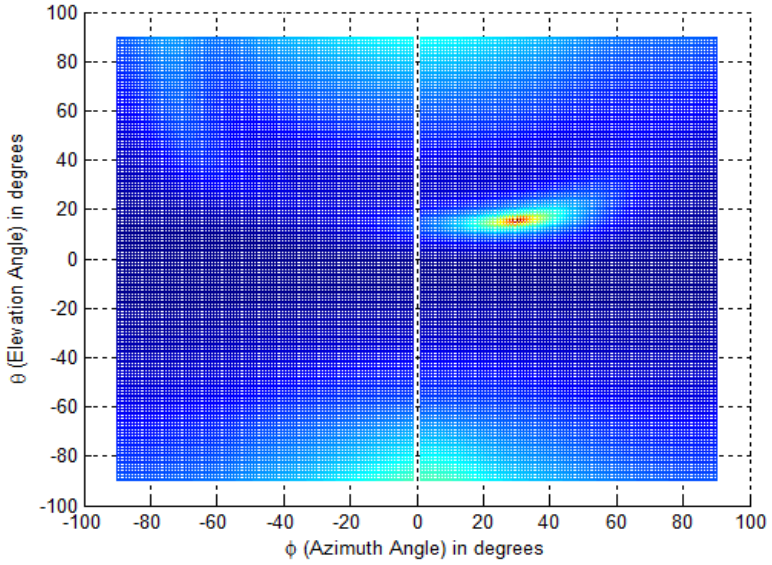

Figure B.14: 2D DOA Estimation of Single Wideband Source with OMLA for the Signal Model $\theta = 15^\circ$ and $\phi = 30^\circ$ for 10 dB SNR - 2D View of Simulation Result

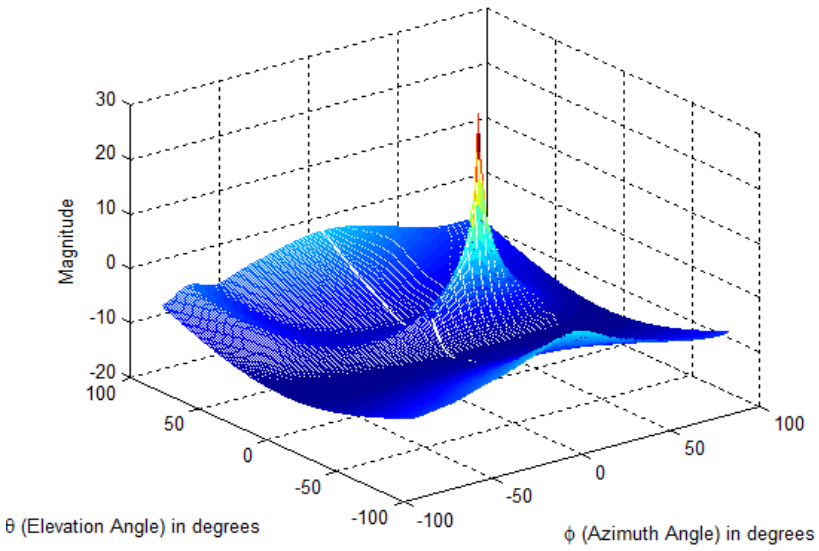

Figure B.15: 2D DOA Estimation of Single Wideband Source with OMLA for the Signal Model $\theta = 15^\circ$ and $\phi = 30^\circ$ for 20 dB SNR

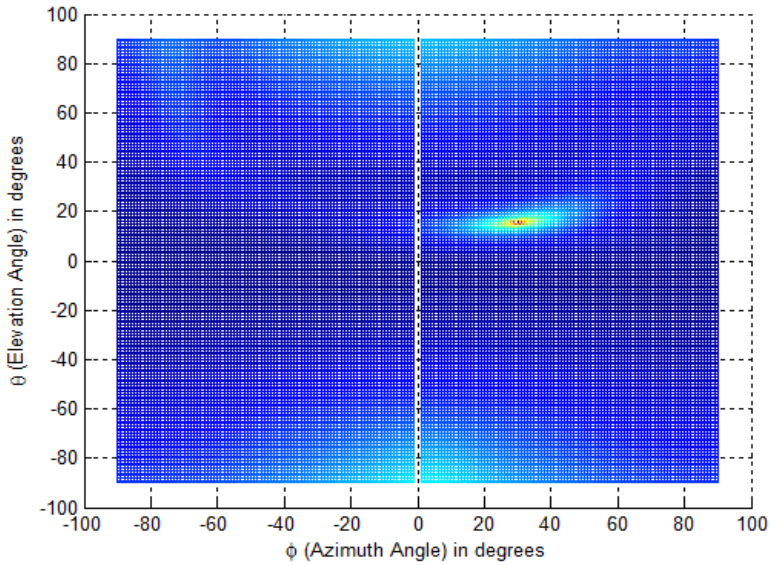

Figure B.16: 2D DOA Estimation of Single Wideband Source with OMLA for the Signal Model $\theta = 15^\circ$ and $\phi = 30^\circ$ for 20 dB SNR - 2D View of Simulation Result

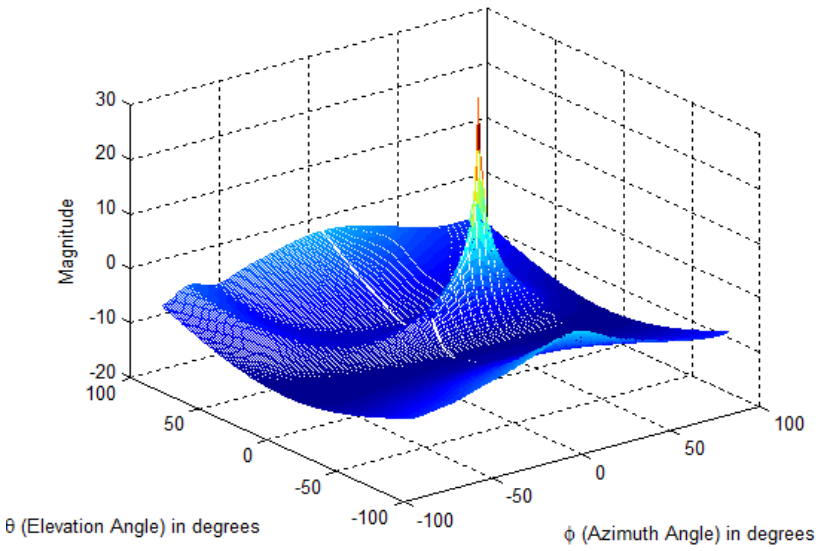

Figure B.17: 2D DOA Estimation of Single Wideband Source with OMLA for Signal Model $\theta = 15^\circ$ and $\phi = 30^\circ$ for 30 dB SNR

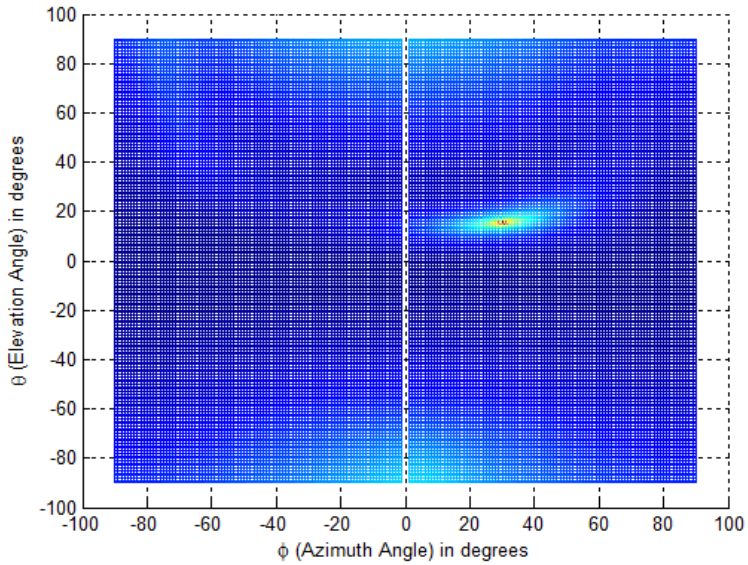

Figure B.18: 2D DOA Estimation of Single Wideband Source with OMLA for the Signal Model $\theta = 15^\circ$ and $\phi = 30^\circ$ for 30 dB SNR - 2D View of Simulation Result

B.4 Estimation of 2D-DOA of Single Wideband Source With OPLA

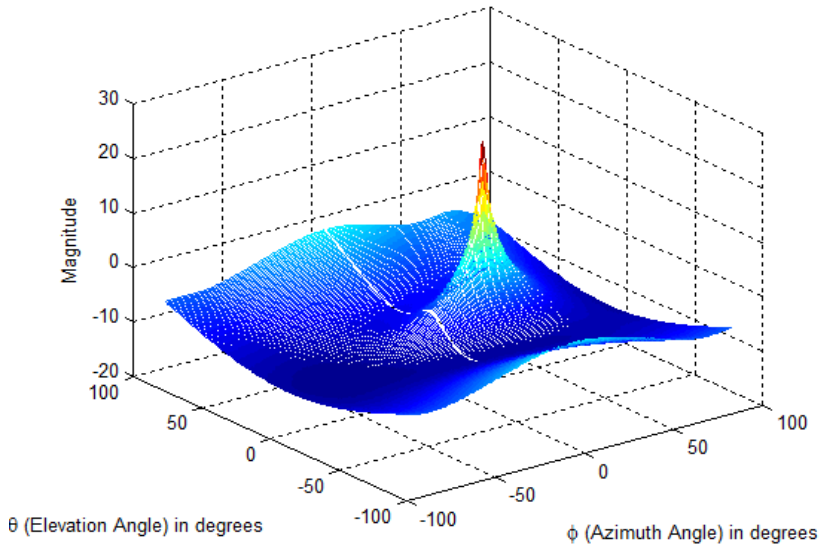

Figure B.19: 2D DOA Estimation of Single Wideband Source with OPLA for the Signal Model $\theta = 15^\circ$ and $\phi = 30^\circ$ for 10 dB SNR

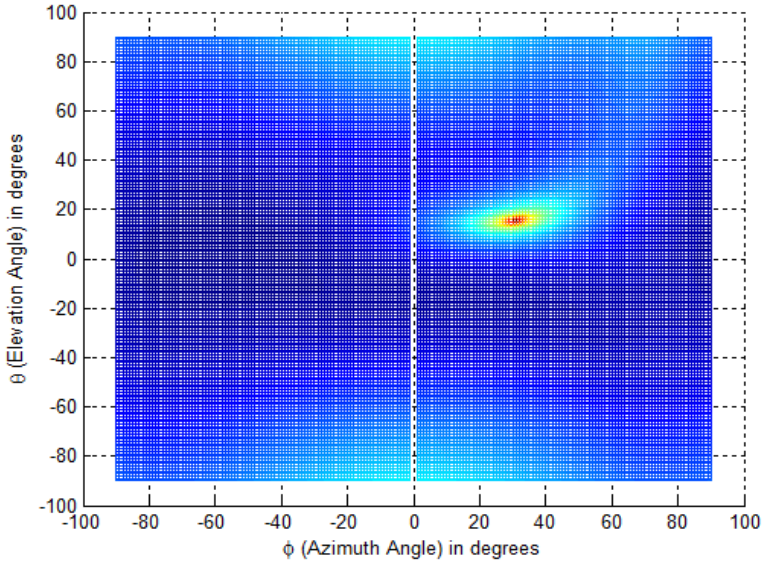

Figure B.20: 2D DOA Estimation of Single Wideband Source with OPLA for the Signal Model $\theta = 15^\circ$ and $\phi = 30^\circ$ for 10 dB SNR - 2D View of Simulation Result

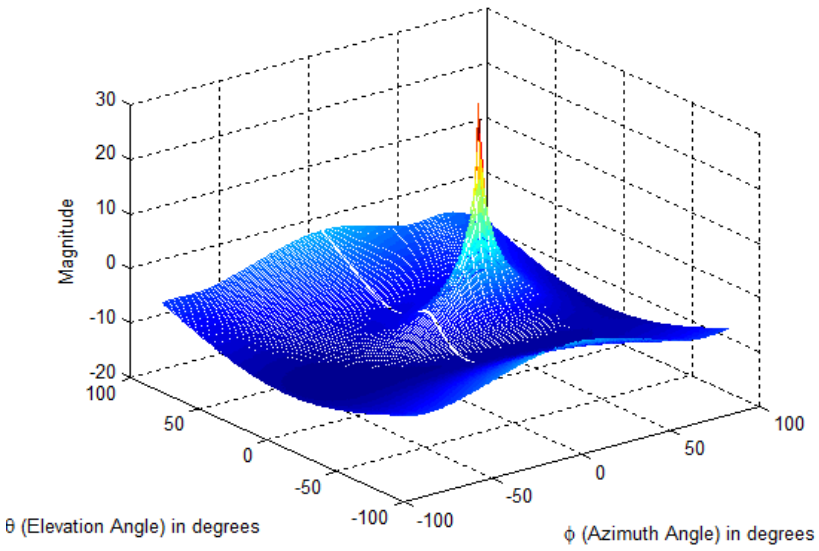

Figure B.21: 2D DOA Estimation of Single Wideband Source with OPLA for the Signal Model $\theta = 15^\circ$ and $\phi = 30^\circ$ for 20 dB SNR

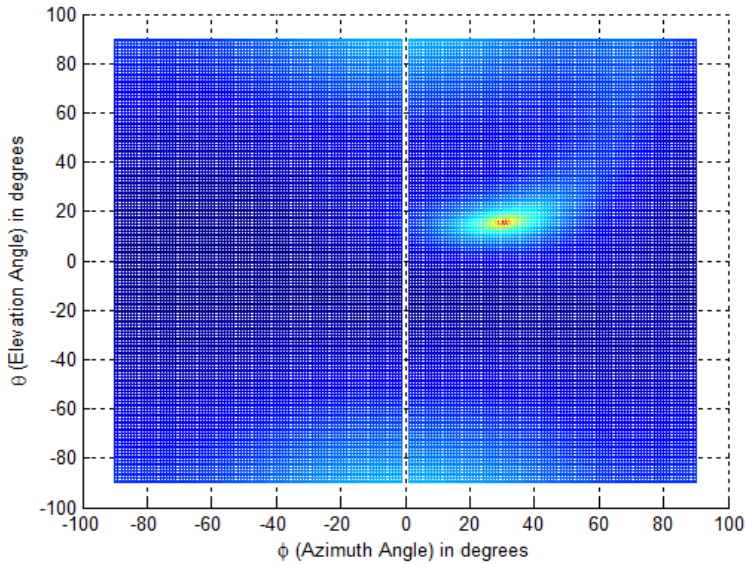

Figure B.22: 2D DOA Estimation of Single Wideband Source with OPLA for the Signal Model $\theta = 15^\circ$ and $\phi = 30^\circ$ for 20 dB SNR - 2D View of Simulation Result

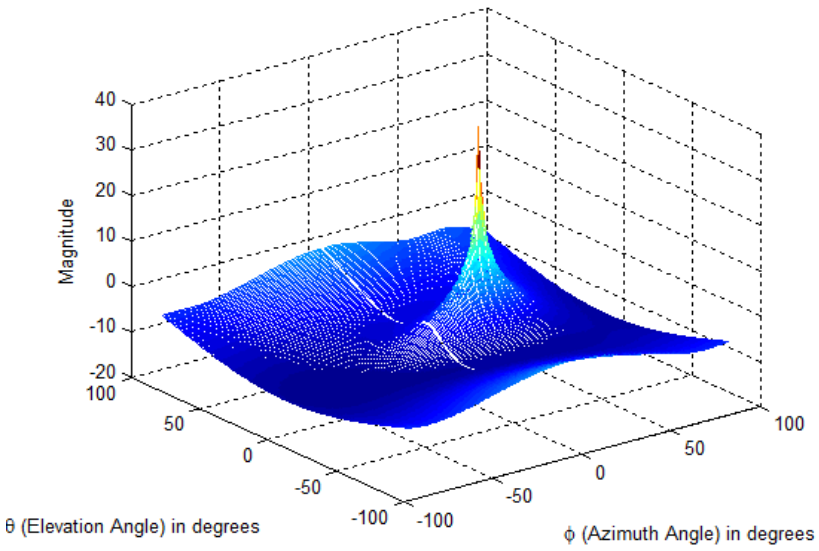

Figure B.23: 2D DOA Estimation of Single Wideband Source with OPLA for the Signal Model $\theta = 15^\circ$ and $\phi = 30^\circ$ for 30 dB SNR

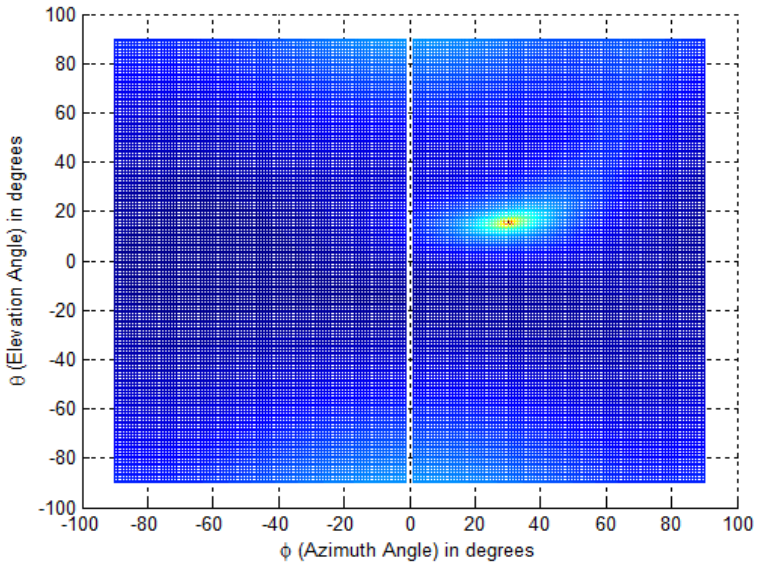

Figure B.24: 2D DOA Estimation of Single Wideband Source with OPLA for the Signal Model $\theta = 15^\circ$ and $\phi = 30^\circ$ for 30 dB SNR - 2D View of Simulation Result

APPENDIX C

Results of Estimation of 2D-DOA of Two Wideband Sources for different SNRs

Appendix C is an extension of the previous Appendix B. While the focus of the Appendix B was on the estimation of DOA of a single wideband source, this Appendix is intended to present additional simulation results pertaining to the estimation of 2D-DOA of two wideband sources. All the other introductory remarks of Appendix B are valid for this Appendix also.

C.1 Estimation of 2D-DOA of Two Wideband Sources With Conventional Single Polarized UPA

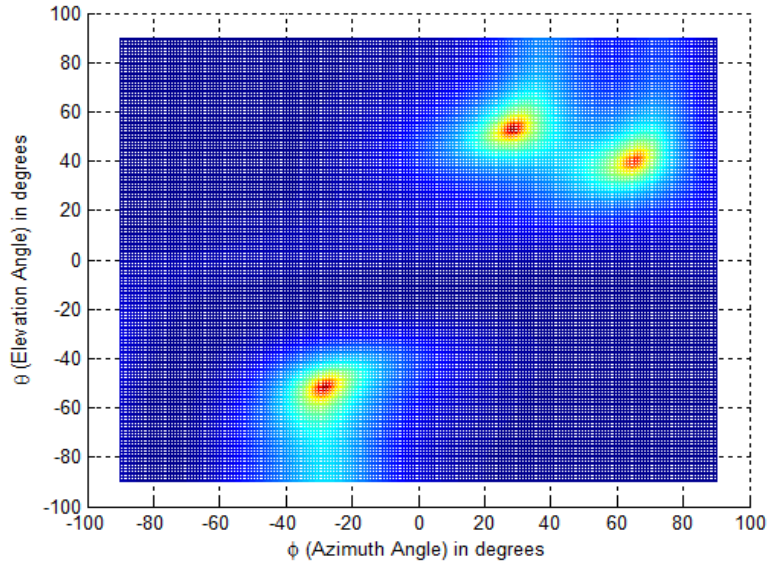

Figure C.2: 2D DOA Estimation of Two Wideband Sources with UPA for the Signal Model $(\theta_1 = 52^\circ\ ,\ \phi_1 = 28^\circ)$ and $(\theta_2 = 40^\circ\ ,\ \phi_2 = 65^\circ)$ for 10 dB SNR - 2D View of Simulation Result

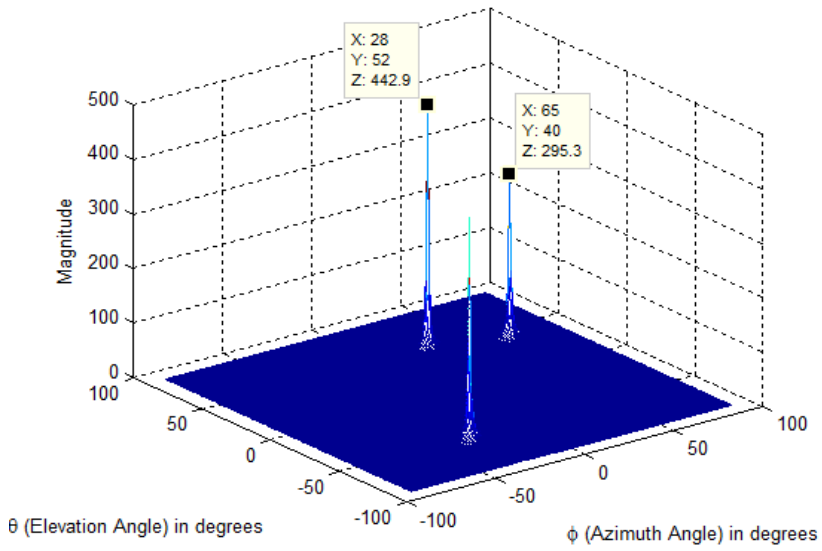

Figure C.3: 2D DOA Estimation of Two Wideband Sources with UPA for the Signal Model $(\theta_1 = 52^\circ\ ,\ \phi_1 = 28^\circ)$ and $(\theta_2 = 40^\circ\ ,\ \phi_2 = 65^\circ)$ for 20 dB SNR

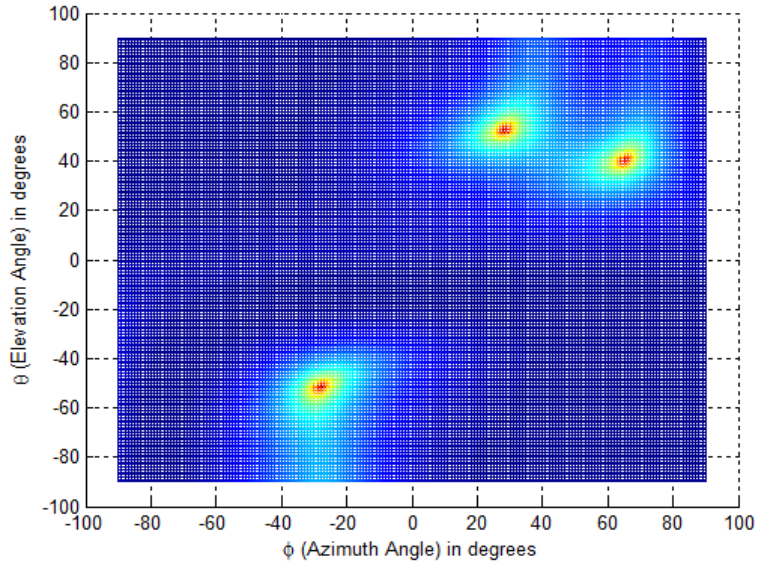

Figure C.4: 2D DOA Estimation of Two Wideband Sources with UPA for the Signal Model $(\theta_1 = 52^\circ\ ,\ \phi_1 = 28^\circ)$ and $(\theta_2 = 40^\circ\ ,\ \phi_2 = 65^\circ)$ for 20 dB SNR - 2D View of Simulation Result

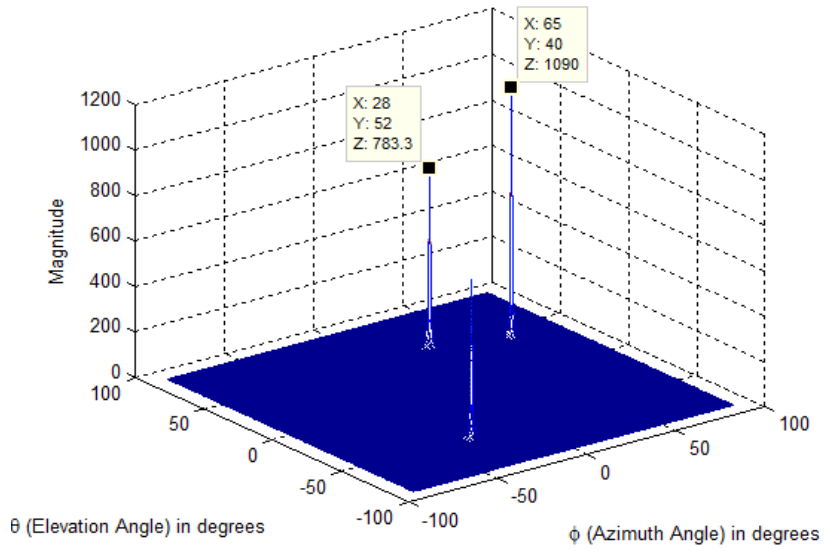

Figure C.5: 2D DOA Estimation of Two Wideband Sources with UPA for the Signal Model $(\theta_1 = 52^\circ\ ,\ \phi_1 = 28^\circ)$ and $(\theta_2 = 40^\circ\ ,\ \phi_2 = 65^\circ)$ for 30 dB SNR

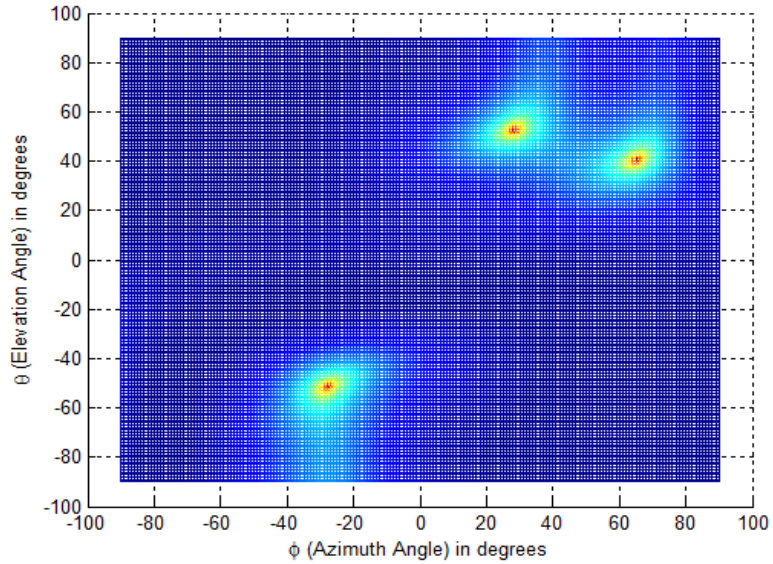

Figure C.6: 2D DOA Estimation of Two Wideband Sources with UPA for the Signal Model $(\theta_1 = 52^\circ\ ,\ \phi_1 = 28^\circ)$ and $(\theta_2 = 40^\circ\ ,\ \phi_2 = 65^\circ)$ for 30 dB SNR - 2D View of Simulation Result

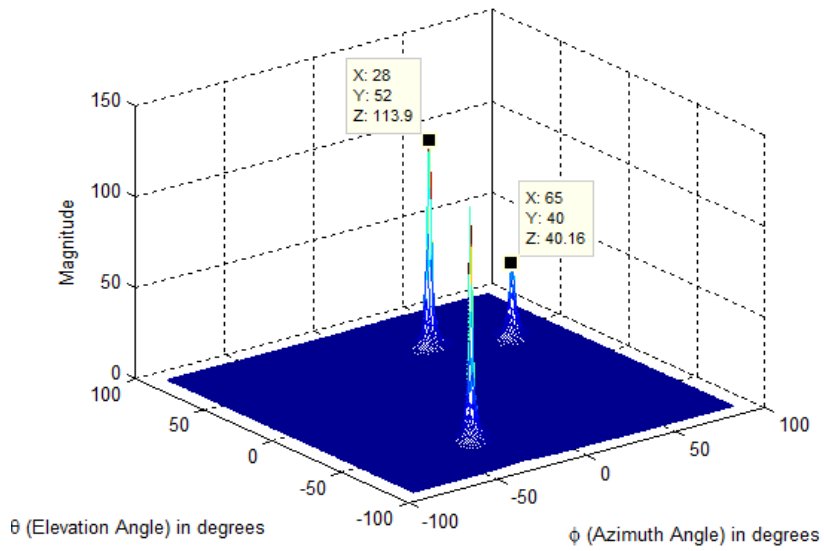

Figure C.1: 2D DOA Estimation of Two Wideband Sources with UPA for the Signal Model $(\theta_1 = 52^\circ\ ,\ \phi_1 = 28^\circ)$ and $(\theta_2 = 40^\circ\ ,\ \phi_2 = 65^\circ)$ for 10 dB SNR

C.2 Estimation of 2D-DOA of Two Wideband Sources With OPPA

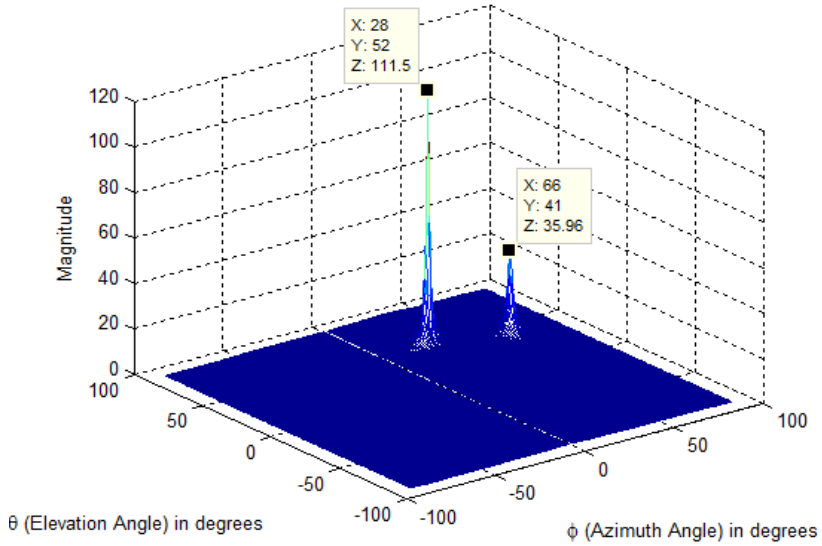

Figure C.7: 2D DOA Estimation of Two Wideband Sources with OPPA for the Signal Model $(\theta_1 = 52^\circ\ ,\ \phi_1 = 28^\circ)$ and $(\theta_2 = 40^\circ\ ,\ \phi_2 = 65^\circ)$ for 10 dB SNR

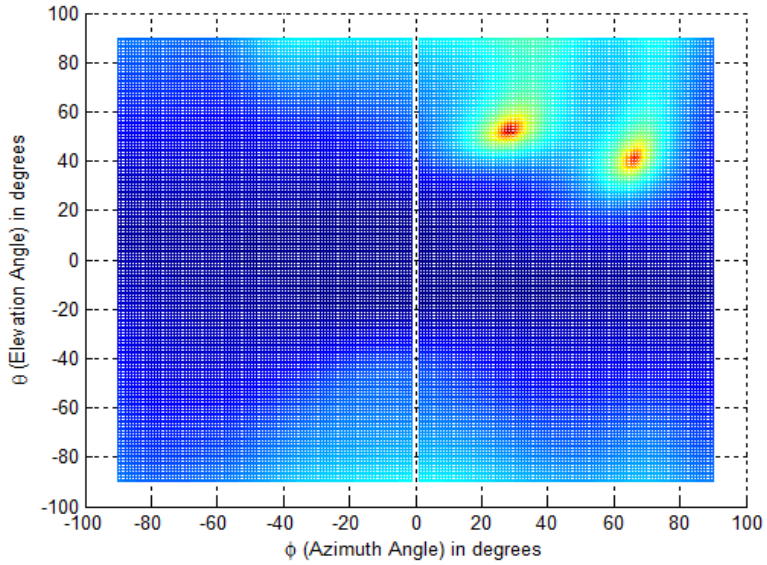

Figure C.8: 2D DOA Estimation of Two Wideband Sources with OPPA for the Signal Model $(\theta_1 = 52^\circ\ ,\ \phi_1 = 28^\circ)$ and $(\theta_2 = 40^\circ\ ,\ \phi_2 = 65^\circ)$ for 10 dB SNR - 2D View of Simulation Result

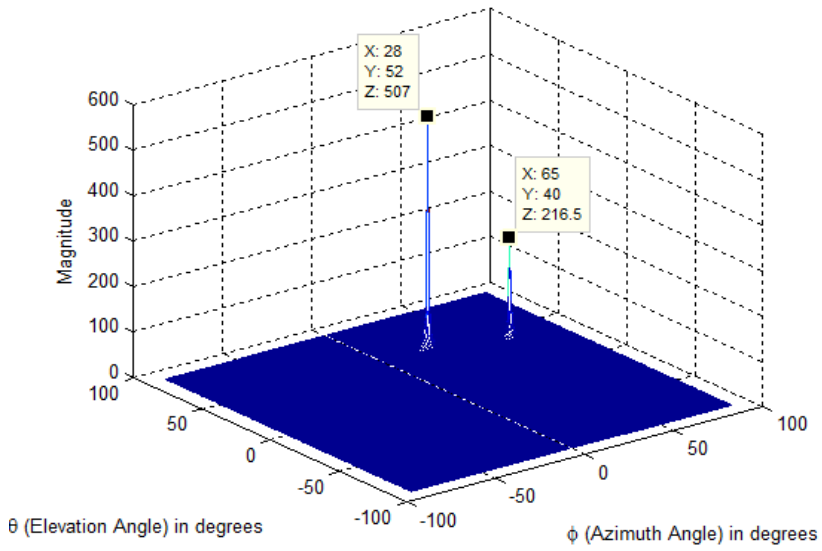

Figure C.9: 2D DOA Estimation of Two Wideband Sources with OPPA for the Signal Model $(\theta_1 = 52^\circ\ ,\ \phi_1 = 28^\circ)$ and $(\theta_2 = 40^\circ\ ,\ \phi_2 = 65^\circ)$ for 20 dB SNR

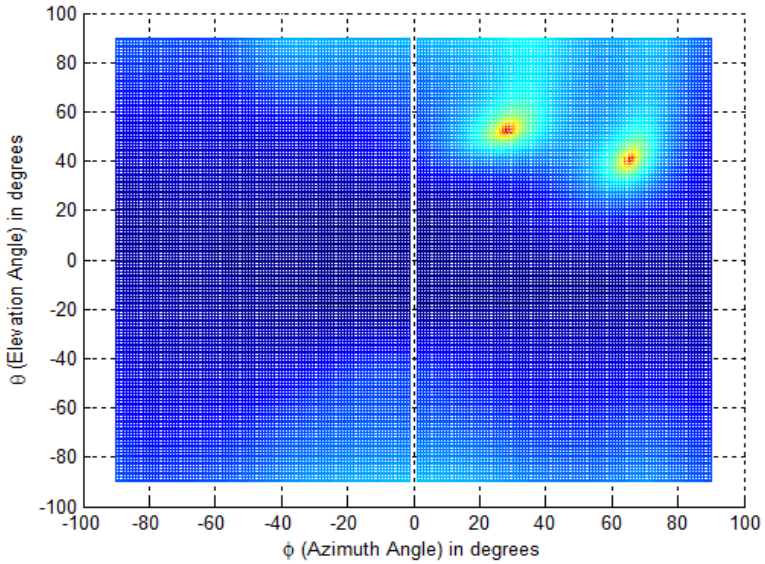

Figure C.10: 2D DOA Estimation of Two Wideband Sources with OPPA for the Signal Model $(\theta_1 = 52^\circ\ ,\ \phi_1 = 28^\circ)$ and $(\theta_2 = 40^\circ\ ,\ \phi_2 = 65^\circ)$ for 20 dB SNR - 2D View of Simulation Result

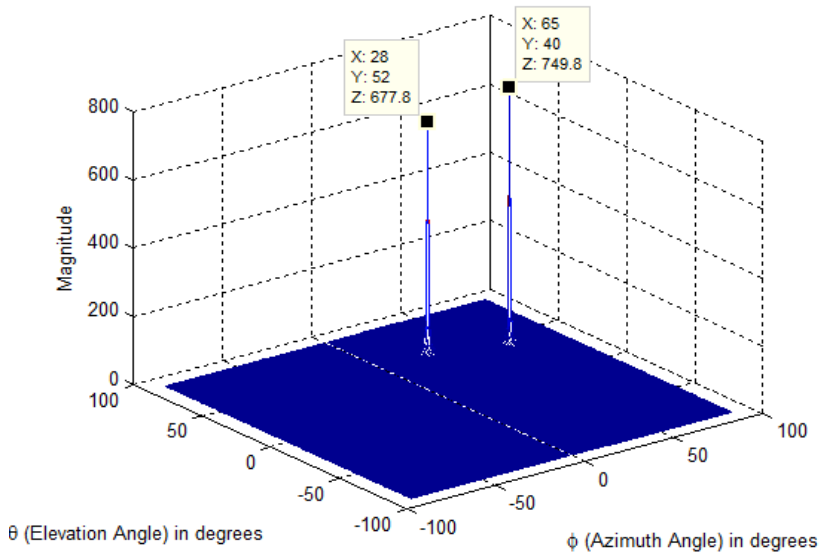

Figure C.11: 2D DOA Estimation of Two Wideband Sources with OPPA for the Signal Model $(\theta_1 = 52^\circ\ ,\ \phi_1 = 28^\circ)$ and $(\theta_2 = 40^\circ\ ,\ \phi_2 = 65^\circ)$ for 30 dB SNR

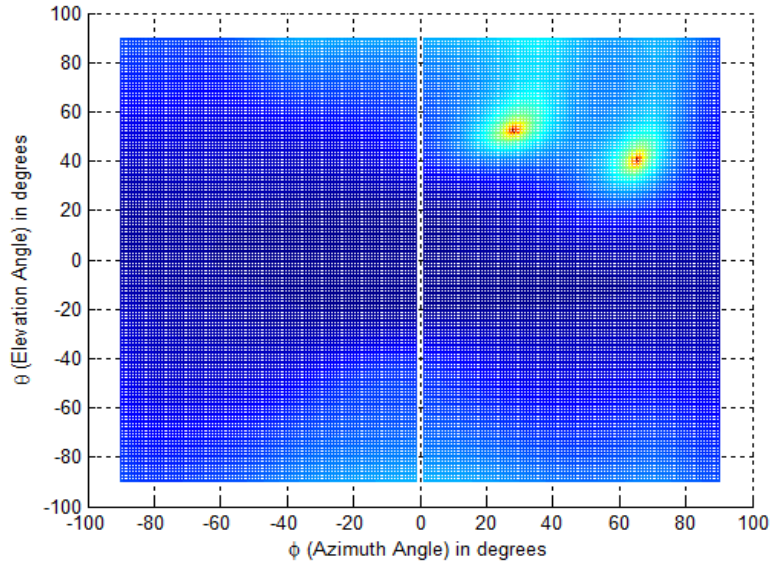

Figure C.12: 2D DOA Estimation of Two Wideband Sources with OPPA for the Signal Model $(\theta_1 = 52^\circ\ ,\ \phi_1 = 28^\circ)$ and $(\theta_2 = 40^\circ\ ,\ \phi_2 = 65^\circ)$ for 30 dB SNR - 2D View of Simulation Result

C.3 Estimation of 2D-DOA of Two Wideband Sources With OMLA

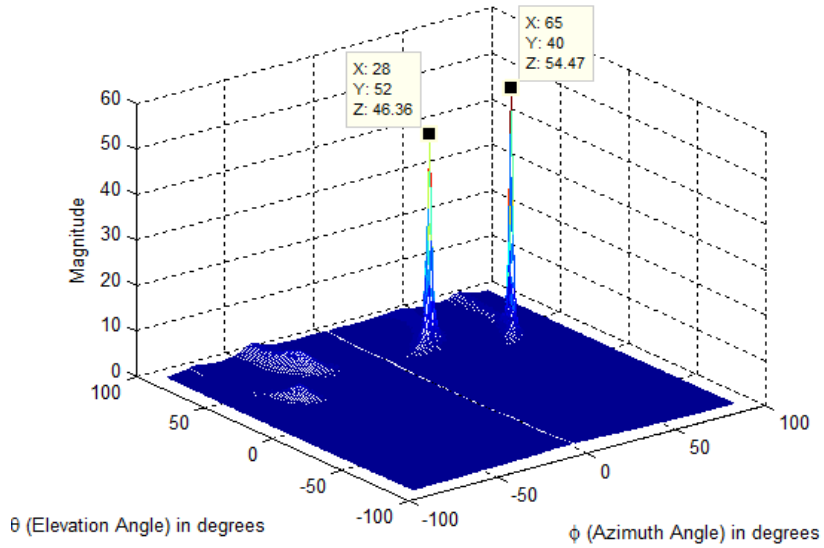

Figure C.13: 2D DOA Estimation of Two Wideband Sources with OMLA for the Signal Model $(\theta_1 = 52^\circ\ ,\ \phi_1 = 28^\circ)$ and $(\theta_2 = 40^\circ\ ,\ \phi_2 = 65^\circ)$ for 10 dB SNR

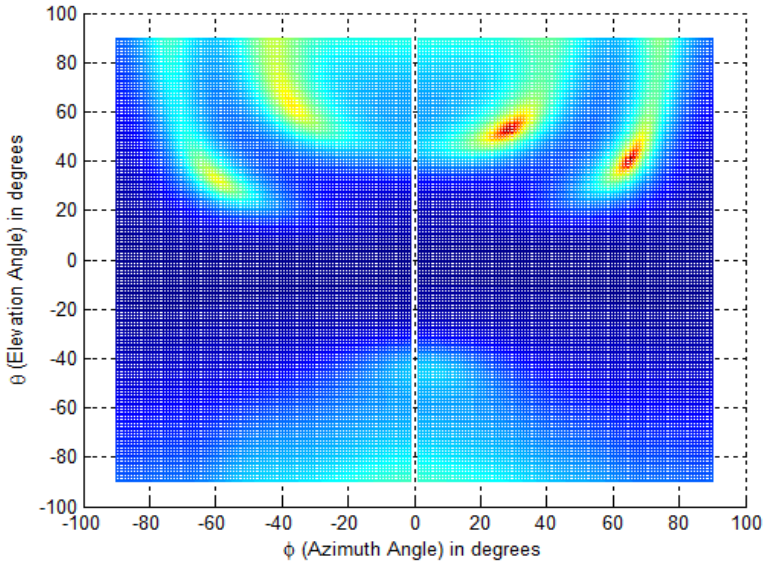

Figure C.14: 2D DOA Estimation of Two Wideband Sources with OMLA for the Signal Model $(\theta_1 = 52^\circ\ ,\ \phi_1 = 28^\circ)$ and $(\theta_2 = 40^\circ\ ,\ \phi_2 = 65^\circ)$ for 10 dB SNR - 2D View of Simulation Result

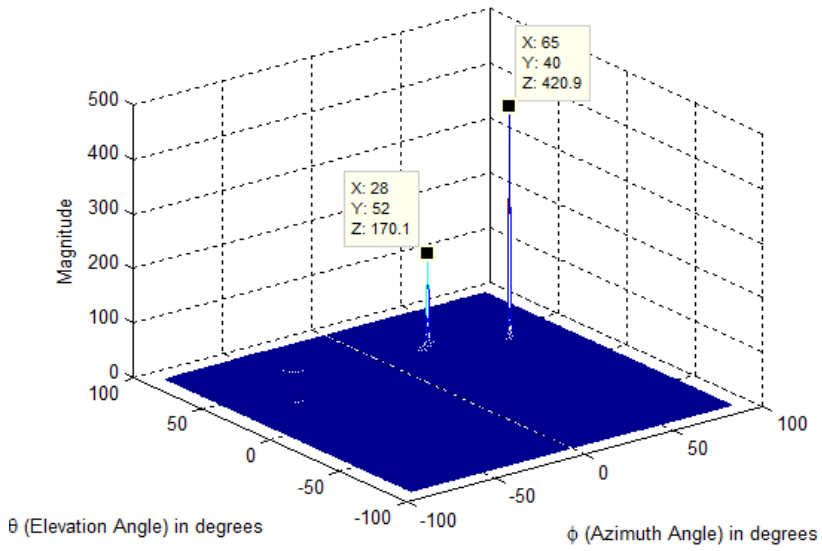

Figure C.15: 2D DOA Estimation of Two Wideband Sources with OMLA for the Signal Model $(\theta_1 = 52^\circ\ ,\ \phi_1 = 28^\circ)$ and $(\theta_2 = 40^\circ\ ,\ \phi_2 = 65^\circ)$ for 20 dB SNR

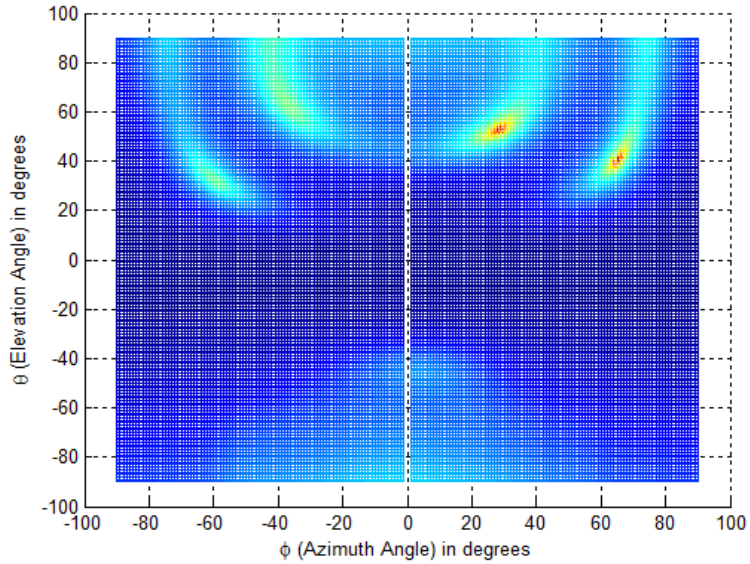

Figure C.16: 2D DOA Estimation of Two Wideband Sources with OMLA for the Signal Model $(\theta_1 = 52^\circ\ ,\ \phi_1 = 28^\circ)$ and $(\theta_2 = 40^\circ\ ,\ \phi_2 = 65^\circ)$ for 20 dB SNR - 2D View of Simulation Result

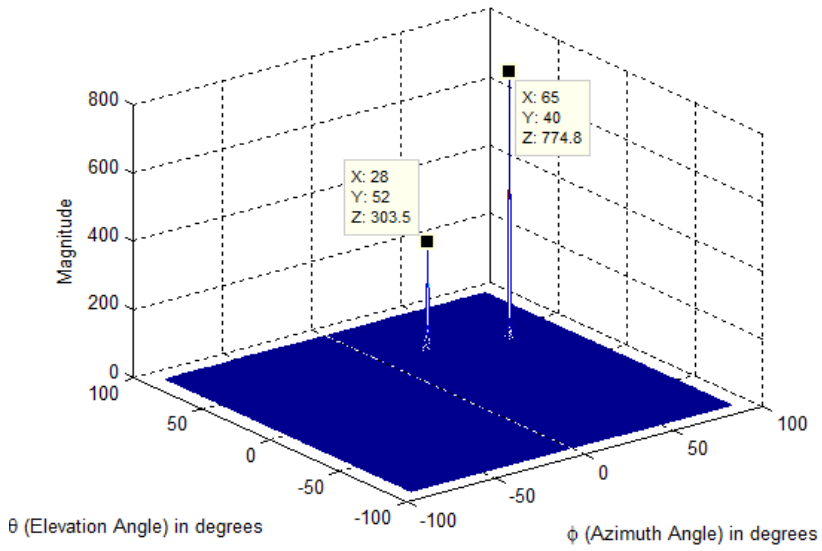

Figure C.17: 2D DOA Estimation of Two Wideband Sources with OMLA for the Signal Model $(\theta_1 = 52^\circ\ ,\ \phi_1 = 28^\circ)$ and $(\theta_2 = 40^\circ\ ,\ \phi_2 = 65^\circ)$ for 30 dB SNR

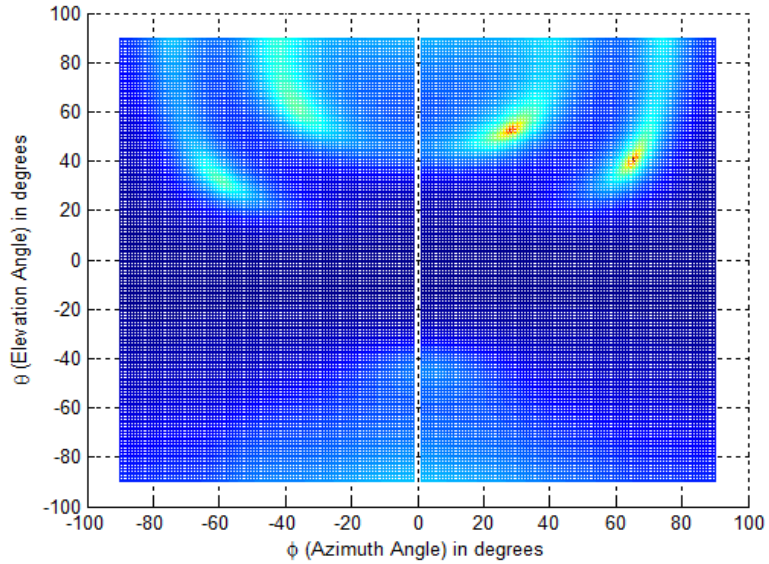

Figure C.18: 2D DOA Estimation of Two Wideband Sources with OMLA for the Signal Model $(\theta_1 = 52^\circ\ ,\ \phi_1 = 28^\circ)$ and $(\theta_2 = 40^\circ\ ,\ \phi_2 = 65^\circ)$ for 30 dB SNR - 2D View of Simulation Result

C.4 Estimation of 2D-DOA of Two Wideband Sources With OPLA

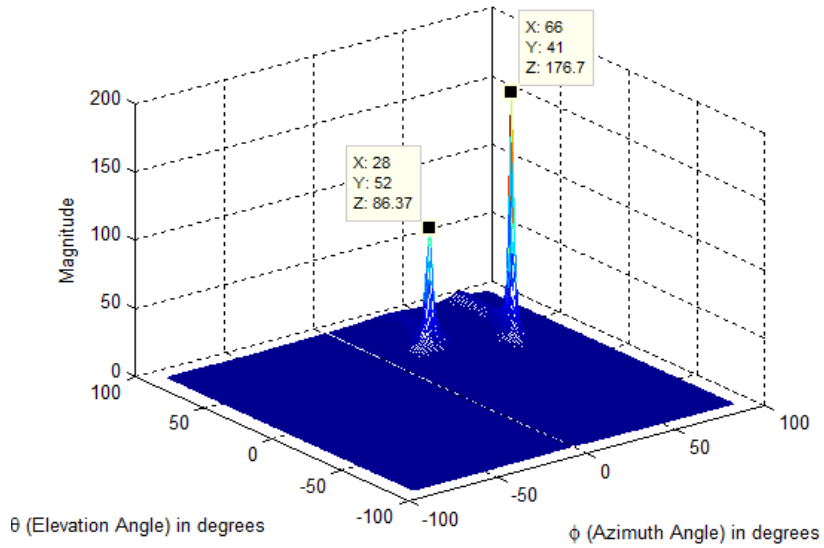

Figure C.19: 2D DOA Estimation of Two Wideband Sources with OPLA for the Signal Model $(\theta_1 = 52^\circ\ ,\ \phi_1 = 28^\circ)$ and $(\theta_2 = 40^\circ\ ,\ \phi_2 = 65^\circ)$ for 10 dB SNR

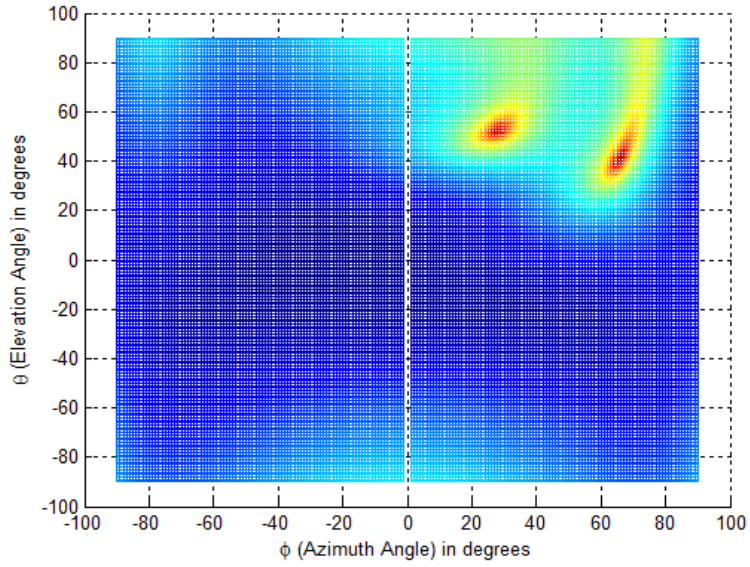

Figure C.20: 2D DOA Estimation of Two Wideband Sources with OPLA for the Signal Model $(\theta_1 = 52^\circ\ ,\ \phi_1 = 28^\circ)$ and $(\theta_2 = 40^\circ\ ,\ \phi_2 = 65^\circ)$ for 10 dB SNR - 2D View of Simulation Result

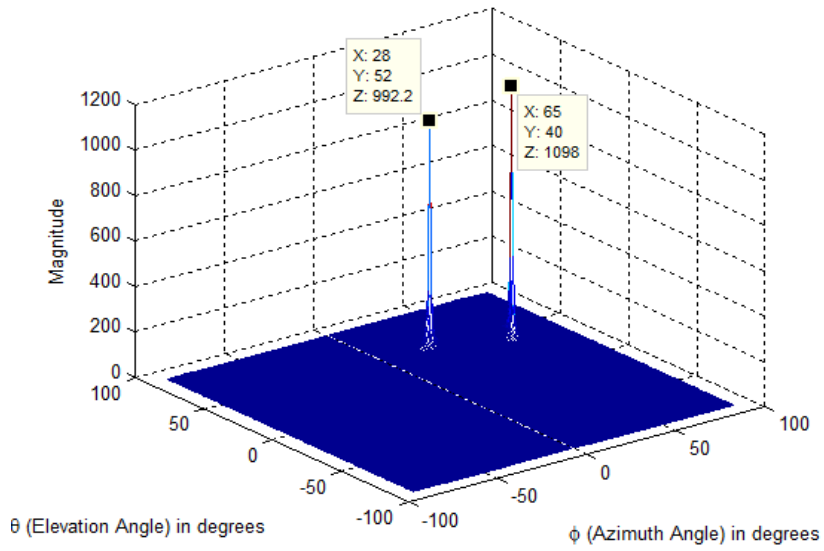

Figure C.21: 2D DOA Estimation of Two Wideband Sources with OPLA for the Signal Model $(\theta_1 = 52^\circ\ ,\ \phi_1 = 28^\circ)$ and $(\theta_2 = 40^\circ\ ,\ \phi_2 = 65^\circ)$ for 20 dB SNR

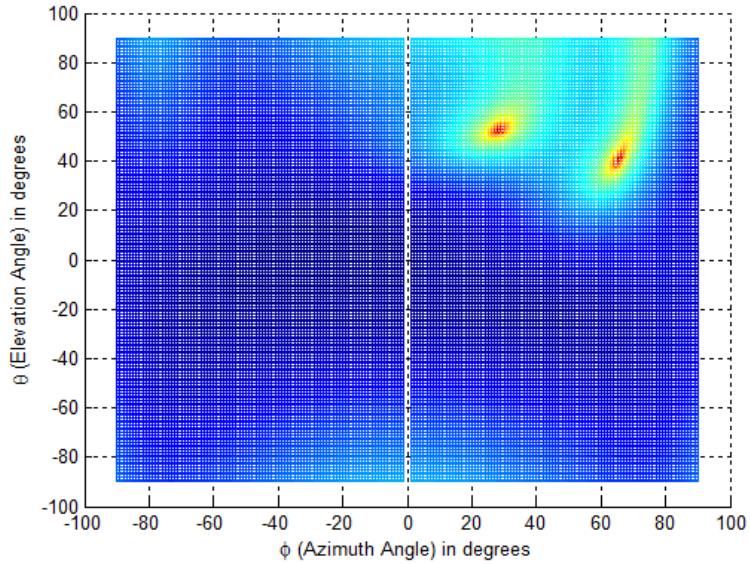

Figure C.22: 2D DOA Estimation of Two Wideband Sources with OPLA for the Signal Model $(\theta_1 = 52^\circ\ ,\ \phi_1 = 28^\circ)$ and $(\theta_2 = 40^\circ\ ,\ \phi_2 = 65^\circ)$ for 20 dB SNR - 2D View of Simulation Result

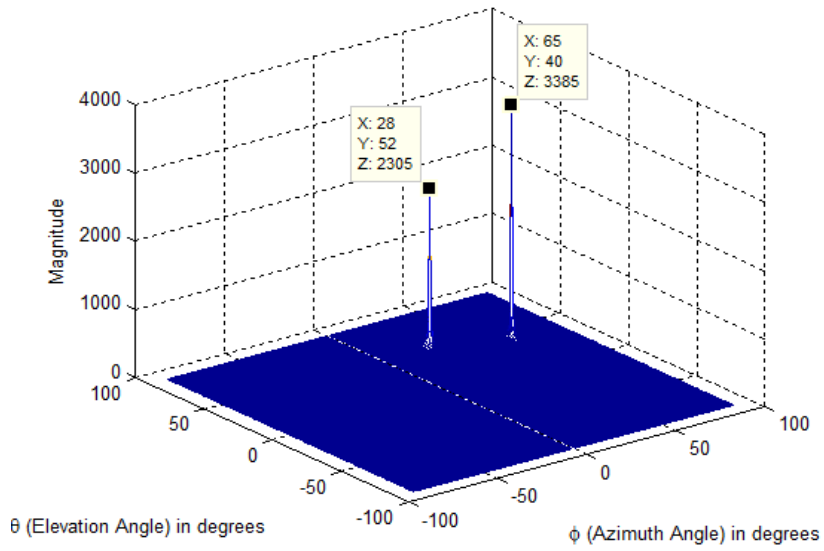

Figure C.23: 2D DOA Estimation of Two Wideband Sources with OPLA for the Signal Model $(\theta_1 = 52^\circ\ ,\ \phi_1 = 28^\circ)$ and $(\theta_2 = 40^\circ\ ,\ \phi_2 = 65^\circ)$ for 30 dB SNR

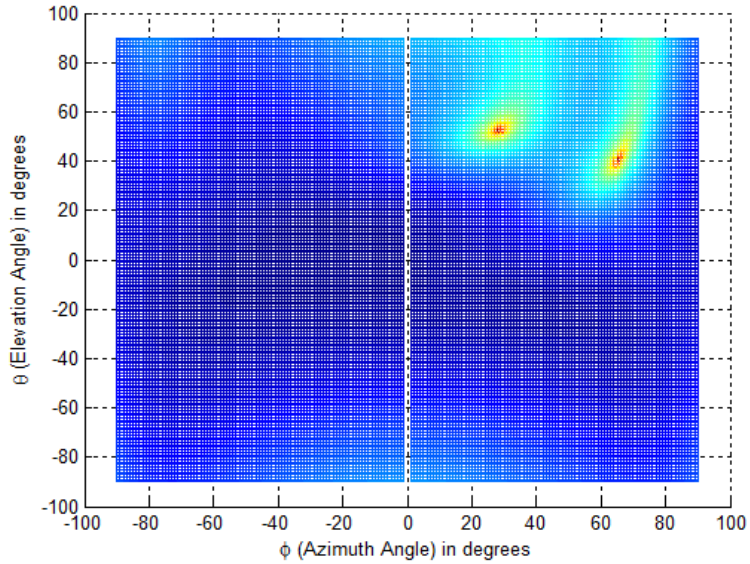

Figure C.24: 2D DOA Estimation of Two Wideband Sources with OPLA for the Signal Model $(\theta_1 = 52^\circ\ ,\ \phi_1 = 28^\circ)$ and $(\theta_2 = 40^\circ\ ,\ \phi_2 = 65^\circ)$ for 30 dB SNR - 2D View of Simulation Result

APPENDIX D

Low Risk Research Ethics Approval Checklist

Annexure – 7 (for Sl. No. 11 of PHD01)

Low Risk Research Ethics Approval Checklist

Applicant Details

Name B. RAMASWAMY KARTHIKEYAN	E-mail karthikeyan@msrsas.org
Department EEE	Date
Course Ph.D	Title of Project Development of Novel Approaches for High Resolution DOA Techniques.

Project Details

Summary of the project in jargon-free language and in not more than 120 words:

- Research Objectives
- Research Design (e.g. Experimental, Desk-based, Theoretical etc)
- Methods of Data Collection

Participants in your research

1. Will the project involve human participants?	Yes	No ✓

If you answered **Yes** to this questions, this may **not** be a low risk project.

- If you are a student, please discuss your project with your Supervisor.
- If you are a member of staff, please discuss your project with your Faculty Research Ethics Leader or use the Medium to High Risk Ethical Approval or NHS or Medical Approval Routes.

Risk to Participants

2. Will the project involve human patients/clients, health professionals, and/or patient (client) data and/or health professional data?	Yes	No ✓
3. Will any invasive physical procedure, including collecting tissue or other samples, be used in the research?	Yes	No ✓
4. Is there a risk of physical discomfort to those taking part?	Yes	No ✓
5. Is there a risk of psychological or emotional distress to those taking part?	Yes	No ✓
6. Is there a risk of challenging the deeply held beliefs of those taking part?	Yes	No ✓
7. Is there a risk that previous, current or proposed criminal or illegal acts will be revealed by those taking part?	Yes	No ✓
8. Will the project involve giving any form of professional, medical or legal advice, either directly or indirectly to those taking part?	Yes	No ✓

If you answered **Yes** to **any** of these questions, this may **not** be a low risk project.

- If you are a student, please discuss your project with your Supervisor.
- If you are a member of staff, please discuss your project with your Faculty Research Ethics Leader or use the Medium to High Risk Ethical Approval or NHS or Medical Approval Routes.

Risk to Researcher

9. Will this project put you or others at risk of physical harm, injury or death?	Yes	No
10. Will project put you or others at risk of abduction, physical, mental or sexual abuse?	Yes	No
11. Will this project involve participating in acts that may cause psychological or emotional distress to you or to others?	Yes	No
12. Will this project involve observing acts which may cause psychological or emotional distress to you or to others?	Yes	No
13. Will this project involve reading about, listening to or viewing materials that may cause psychological or emotional distress to you or to others?	Yes	No
14. Will this project involve you disclosing personal data to the participants other than your name and the University as your contact and e-mail address?	Yes	No
15. Will this project involve you in unsupervised private discussion with people who are not already known to you?	Yes	No
16. Will this project potentially place you in the situation where you may receive unwelcome media attention?	Yes	No
17. Could the topic or results of this project be seen as illegal or attract the attention of the security services or other agencies?	Yes	No
18. Could the topic or results of this project be viewed as controversial by anyone?	Yes	No

If you answered **Yes** to **any** of these questions, this is **not** a low risk project. Please:

- If you are a student, discuss your project with your Supervisor.
- If you are a member of staff, discuss your project with your Faculty Research Ethics Leader or use the Medium to High Risk Ethical Approval route.

Informed Consent of the Participant

19. Are any of the participants under the age of 18?	Yes	No
20. Are any of the participants unable mentally or physically to give consent?	Yes	No
21. Do you intend to observe the activities of individuals or groups without their knowledge and/or informed consent from each participant (or from his or her parent or guardian)?	Yes	No

If you answered **Yes** to **any** of these questions, this may **not** be a low risk project. Please:

- If you are a student, discuss your project with your Supervisor.
- If you are a member of staff, discuss your project with your Faculty Research Ethics Leader or use the Medium to High Risk Ethical Approval route.

Participant Confidentiality and Data Protection

22. Will the project involve collecting data and information from human participants who will be identifiable in the final report?	Yes	No ✓
23. Will information not already in the public domain about specific individuals or institutions be identifiable through data published or otherwise made available?	Yes	No ✓
24. Do you intend to record, photograph or film individuals or groups without their knowledge or informed consent?	Yes	No ✓
25. Do you intend to use the confidential information, knowledge or trade secrets gathered for any purpose other than this research project?	Yes	No ✓

If you answered **Yes** to **any** of these questions, this may **not** be a low risk project:

- If you are a student, discuss your project with your Supervisor.
- If you are a member of staff, discuss your project with your Faculty Research Ethics Leader or use the Medium to High Risk Ethical Approval or NHS or Medical Approval routes.

Gatekeeper Risk

26. Will this project involve collecting data outside University buildings?	Yes	No ✓
27. Do you intend to collect data in shopping centres or other public places?	Yes	No ✓
28. Do you intend to gather data within nurseries, schools or colleges?	Yes	No ✓
29. Do you intend to gather data within National Health Service premises?	Yes	No ✓

If you answered **Yes** to **any** of these questions, this is **not** a low risk project. Please:

- If you are a student, discuss your project with your Supervisor.
- If you are a member of staff, discuss your project with your Faculty Research Ethics Leader or use the Medium to High Risk Ethical Approval or NHS or Medical Approval routes.

Other Ethical Issues

30. Is there any other risk or issue not covered above that may pose a risk to you or any of the participants?	Yes	No ✓
31. Will any activity associated with this project put you or the participants at an ethical, moral or legal risk?	Yes	No ✓

If you answered **Yes** to these questions, this may **not** be a low risk project. Please:

- If you are a student, discuss your project with your Supervisor.
- If you are a member of staff, discuss your project with your Faculty Research Ethics Leader.

Principal Investigator Certification

If you answered **No** to **all** of the above questions, then you have described a low risk project. Please complete the following declaration to certify your project and keep a copy for your record as you may be asked for this at any time.

Agreed restrictions to project to allow Principal Investigator Certification

Please identify any restrictions to the project, agreed with your Supervisor or Faculty Research Ethics Leader to allow you to sign the Principal Investigator Certification declaration.

Participant Information Leaflet attached. Informed Consent Forms attached.

Principal Investigator's Declaration

Please ensure that you:

- Tick all the boxes below and sign this checklist.
- Students must get their Supervisor to countersign this declaration.

I believe that this project **does not require research ethics approval**. I have completed the checklist and kept a copy for my own records. I realise I may be asked to provide a copy of this checklist at any time.	
I confirm that I have answered all relevant questions in this checklist honestly.	
I confirm that I will carry out the project in the ways described in this checklist. I will immediately suspend research and request a new ethical approval if the project subsequently changes the information I have given in this checklist.	

Signatures

If you submit this checklist and any attachments by e-mail, you should type your name in the signature space. An email attachment sent from your University inbox will be assumed to have been signed electronically.

Principal Investigator

Signed [redacted] (Principal Investigator or Student)

Date 10.5.2011

Students storing this checklist electronically must append to it an email from your Supervisor confirming that they are prepared to make the declaration above and to countersign this checklist. This-email will be tak[redacted]countersignature.

Student's Supervisor

Countersigned [redacted] (Supervisor)

Date 10.5.2011

I have read this checklist and confirm that it covers all the ethical issues raised by this project fully and frankly. I also confirm that these issues have been discussed with the student and will continue to be reviewed in the course of supervision.

References

Abed-Meraim, K., Chkeif, A., & Hua, Y. (2000). Fast orthonormal past algorithm. *Signal Processing Letters, IEEE*, *7*(3), 60–62.

Allen, B., & Ghavami, M. (2006). *Adaptive array systems: fundamentals and applications*. John Wiley & Sons.

Balanis, C. A. (2011). *Modern antenna handbook*. John Wiley & Sons.

Balanis, C. A. (2012). *Antenna theory: analysis and design*. John Wiley & Sons.

Bartlett, M. S. (1950). Periodogram analysis and continuous spectra. *Biometrika*, 1–16.

Bunch, J. R., Nielsen, C. P., & Sorensen, D. C. (1978). Rank-one modification of the symmetric eigenproblem. *Numerische Mathematik*, *31*(1), 31–48.

Capon, J. (1969). High-resolution frequency-wavenumber spectrum analysis. *Proceedings of the IEEE*, *57*(8), 1408–1418.

Champagne, B. (1994). Adaptive eigendecomposition of data covariance matrices based on first-order perturbations. *Signal Processing, IEEE Transactions on*, *42*(10), 2758–2770.

Chandran, S. (2005). *Advances in direction-of-arrival estimation*. Artech House.

Chen, J. C., Yao, K., & Hudson, R. E. (2002). Source localization and beamforming. *Signal Processing Magazine, IEEE*, *19*(2), 30–39.

Chen, S.-W., Jen, C.-W., & Chang, A.-C. (2009). High-resolution doa estimation based on independent noise component for correlated signal sources. *Neural Computing and Applications*, *18*(4), 381–385.

Chick, D. F., Collins, P., Goodman, S., Martin, R., & Terzuoli Jr, A. (2011). Direction finding with mutually orthogonal antennas. In *Antennas and propagation (apsursi), 2011 ieee international symposium on* (pp. 2853–2856).

Choudhury, R. R., & Vaidya, N. H. (2003). Impact of directional antennas on ad hoc routing. In *Personal wireless communications* (pp. 590–600).

Chryssomallis, M. (2000). Smart antennas. *Antennas and Propagation Magazine, IEEE*, *42*(3), 129–136.

Coldrey, M., & Viberg, M. (2006). Generalization and analysis of the conventional

beamformer for localization of spatially distributed sources. In *In proc. 14th european signal processing conference, eusipco 2006.*

Comon, P., & Golub, G. H. (1990). Tracking a few extreme singular values and vectors in signal processing. *Proceedings of the IEEE*, *78*(8), 1327–1343.

Di Claudio, E. D., & Parisi, R. (2001). Waves: weighted average of signal subspaces for robust wideband direction finding. *Signal Processing, IEEE Transactions on*, *49*(10), 2179–2191.

Doran, M., Doron, M., Weiss, A. J., et al. (1993). Coherent wide-band processing for arbitrary array geometry. *Signal Processing, IEEE Transactions on*, *41*(1), 414.

Doron, M. A., & Weiss, A. J. (1992). On focusing matrices for wide-band array processing. *Signal Processing, IEEE Transactions on*, *40*(6), 1295–1302.

Feng, D., Bao, M., Ye, Z., Guan, L., & Li, X. (2011). A novel wideband doa estimator based on khatri–rao subspace approach. *Signal Processing*, *91*(10), 2415–2419.

Fuhl, J., Rossi, J.-P., & Bonek, E. (1997). High-resolution 3-d direction-of-arrival determination for urban mobile radio. *Antennas and Propagation, IEEE Transactions on*, *45*(4), 672–682.

Golub, G. H. (1973). Some modified matrix eigenvalue problems. *Siam Review*, *15*(2), 318–334.

Golub, G. H., & Van Loan, C. F. (2012). *Matrix computations* (Vol. 3). JHU Press.

Gu, J.-F., Zhu, W.-P., & Swamy, M. (2015). Joint 2-d doa estimation via sparse l-shaped array. *Signal Processing, IEEE Transactions on*, *63*(5), 1171–1182.

Hansen, R. C. (2009). *Phased array antennas* (Vol. 213). John Wiley & Sons.

Harabi, F., Changuel, H., & Gharsallah, A. (2007). Direction of arrival estimation method using a 2-l shape arrays antenna. *Progress In Electromagnetics Research*, *69*, 145–160.

Hayes, M. H. (2009). *Statistical digital signal processing and modeling*. John Wiley & Sons.

Haykin, S. (2008). *Communication systems*. John Wiley & Sons.

Haykin, S. S. (2008). *Adaptive filter theory*. Pearson Education India.

He, Z.-Q., Shi, Z.-P., Huang, L., & So, H. C. (2015). Underdetermined doa estimation for wideband signals using robust sparse covariance fitting. *Signal Processing Letters, IEEE*, *22*(4), 435–439.

Hu, W., Zhang, A., & Wang, C. (2014). 2d direction of arrival estimation for cross array in the presence of mutual coupling. *International Journal of Antennas and Propagation*,

2014.

Inoue, Y., Mori, K., & Arai, H. (2002). Doa estimation in consideration of the array element pattern. In *Vehicular technology conference, 2002. vtc spring 2002. ieee 55th* (Vol. 2, pp. 745–748).

Karasalo, I. (1986). Estimating the covariance matrix by signal subspace averaging. *Acoustics, Speech and Signal Processing, IEEE Transactions on*, *34*(1), 8–12.

Karthikeyan, B. R., Kadambi, G. R., & Vershinin, Y. A. (2015). A formulation of 1-d search technique for 2-d doa estimation using orthogonally polarized components of linear array. *IEEE Antennas and Wireless Propagation Letters*, *14*.

Kim, J.-T., Kim, S.-t., & Lee, K.-w. (2013). 1 ambiguity analysis method for the calibrated array manifold.

Kim, M., Takeuchi, T., & Chong, N. Y. (2004). A 3-axis orthogonal antenna for indoor localization. In *First international workshop on networked sensing systems* (pp. 59–62).

Kolar, V. (2004). *Challenges in directional antennas* (Unpublished master's thesis). State University of New York.

Kraus, J. (1992). *Electromagnetics*. McGraw-Hill.

Krim, H., & Viberg, M. (1996). Two decades of array signal processing research: the parametric approach. *Signal Processing Magazine, IEEE*, *13*(4), 67–94.

Lathi, B. P. (1998). *Modern digital and analog communication systems 3e osece*. Oxford university press.

Li, J. (1993). Direction and polarization estimation using arrays with small loops and short dipoles. *Antennas and Propagation, IEEE Transactions on*, *41*(3), 379–387.

Liang, J., & Liu, D. (2011). Two l-shaped array-based 2-d doas estimation in the presence of mutual coupling. *Progress In Electromagnetics Research*, *112*, 273–298.

Liao, B., Zhang, Z.-G., & Chan, S.-C. (2012). Doa estimation and tracking of ulas with mutual coupling. *Aerospace and Electronic Systems, IEEE Transactions on*, *48*(1), 891–905.

Manikas, A., Alexiou, A., & Karimi, H. (1997). Comparison of the ultimate direction-finding capabilities of a number of planar array geometries. In *Radar, sonar and navigation, iee proceedings-* (Vol. 144, pp. 321–329).

Marcos, S., Marsal, A., & Benidir, M. (1995). The propagator method for source bearing estimation. *Signal Processing*, *42*(2), 121–138.

Nadler, B. (2010). Nonparametric detection of signals by information theoretic criteria: per-

formance analysis and an improved estimator. *Signal Processing, IEEE Transactions on*, *58*(5), 2746–2756.

Ouyang, S., & Hua, Y. (2005). Bi-iterative least-square method for subspace tracking. *Signal Processing, IEEE Transactions on*, *53*(8), 2984–2996.

Owsley, N. L. (1978). Adaptive data orthogonalization. In *Acoustics, speech, and signal processing, ieee international conference on icassp'78.* (Vol. 3, pp. 109–112).

Pisarenko, V. F. (1973). The retrieval of harmonics from a covariance function. *Geophysical Journal International*, *33*(3), 347–366.

Rajagopalan, J. (1996). *An iterative algorithm for inversion of matrices* (Unpublished doctoral dissertation). Concordia University.

Rappaport, T. S., Reed, J., & Woerner, B. D. (1996). Position location using wireless communications on highways of the future. *Communications Magazine, IEEE*, *34*(10), 33–41.

Roy, R., & Kailath, T. (1989). Esprit-estimation of signal parameters via rotational invariance techniques. *Acoustics, Speech and Signal Processing, IEEE Transactions on*, *37*(7), 984–995.

Schmidt, R. O. (1986). Multiple emitter location and signal parameter estimation. *Antennas and Propagation, IEEE Transactions on*, *34*(3), 276–280.

Schreiber, R. (1986). Implementation of adaptive array algorithms. *IEEE transactions on acoustics, speech, and signal processing*, *34*, 1038–1045.

Sellone, F. (2005). Robust wideband doa estimation. In *Statistical signal processing, 2005 ieee/sp 13th workshop on* (pp. 277–282).

Sellone, F. (2006). Robust auto-focusing wideband doa estimation. *Signal Processing*, *86*(1), 17–37.

Shaghaghi, M., & Vorobyov, S. (2015). Subspace leakage analysis and improved doa estimation with small sample size.

Shan, T.-J., Wax, M., & Kailath, T. (1985). On spatial smoothing for direction-of-arrival estimation of coherent signals. *IEEE Transactions on Acoustics, Speech, and Signal Processing*, *33*(4), 806–811.

Silver, S. (1949). *Microwave antenna theory and design* (No. 19). Iet.

Stoica, P., & Moses, R. L. (1997). *Introduction to spectral analysis* (Vol. 1). Prentice hall Upper Saddle River, NJ.

Stoica, P., & Söderström, T. (1991). Statistical analysis of music and esprit estimates of sinusoidal frequencies. In *Acoustics, speech, and signal processing, 1991. icassp-91.,*

1991 international conference on (pp. 3273–3276).

Stoica, P., & Soderstrom, T. (1991). Statistical analysis of music and subspace rotation estimates of sinusoidal frequencies. *Signal Processing, IEEE Transactions on*, *39*(8), 1836–1847.

Strobach, P. (1997). Bi-iteration svd subspace tracking algorithms. *Signal Processing, IEEE Transactions on*, *45*(5), 1222–1240.

Tayem, N., & Kwon, H. M. (2005). L-shape 2-dimensional arrival angle estimation with propagator method. *Antennas and Propagation, IEEE Transactions on*, *53*(5), 1622–1630.

Tayem, N. A.-H. M. (2005). *Direction of arrival angle estimation schemes for wireless communication systems* (Unpublished doctoral dissertation). Wichita State University.

IEEE standard definitions of terms for antennas. (1983, June). *IEEE Std 145-1983*, 1-31. doi: 10.1109/IEEESTD.1983.82386

Tuncer, T. E., & Friedlander, B. (2009). *Classical and modern direction-of-arrival estimation*. Academic Press.

Vaidyanathan, P. P. (1993). *Multirate systems and filter banks*. Pearson Education India.

Van Trees, H. L. (2004). *Detection, estimation, and modulation theory, optimum array processing*. John Wiley & Sons.

Van Veen, B. D., & Buckley, K. M. (1988). Beamforming: A versatile approach to spatial filtering. *IEEE assp magazine*, *5*(2), 4–24.

Vershinin, Y. A. (2014). Adaptive control system for solution of fault tolerance problem. In *Iaeng transactions on engineering technologies* (pp. 197–207). Springer.

Visser, H. J. (2006). *Array and phased array antenna basics*. John Wiley & Sons.

Wang, H., & Kaveh, M. (1985). Coherent signal-subspace processing for the detection and estimation of angles of arrival of multiple wide-band sources. *Acoustics, Speech and Signal Processing, IEEE Transactions on*, *33*(4), 823–831.

Wax, M. (1989). Detection of the number of coherent signals by the mdl principle. *IEEE Trans. Acoust., Speech, Signal Processing*, *37*(8), 1190–1196.

Wax, M., & Kailath, T. (1985). Detection of signals by information theoretic criteria. *Acoustics, Speech and Signal Processing, IEEE Transactions on*, *33*(2), 387–392.

Wei, Y., & Guo, X. (2014). Pair-matching method by signal covariance matrices for 2d-doa estimation. *Antennas and Wireless Propagation Letters, IEEE*, *13*, 1199–1202.

Weiss, A. J., & Friedlander, B. (1993). Direction finding for diversely polarized signals

using polynomial rooting. *Signal Processing, IEEE Transactions on*, *41*(5), 1893–1905.

Wong, K. T., Li, L., & Zoltowski, M. D. (2004). Root-music-based direction-finding and polarization estimation using diversely polarized possibly collocated antennas. *IEEE Antennas and Wireless Propagation Letters*, *3*(1), 129–132.

Wong, K. T., & Zoltowski, M. D. (1998). Closed-form direction-finding with arbitrarily spaced electromagnetic vector-sensors at unknown locations. In *Acoustics, speech and signal processing, 1998. proceedings of the 1998 ieee international conference on* (Vol. 4, pp. 1949–1952).

Woods, J. W., & O'Neil, S. D. (1986). Subband coding of images. *Acoustics, Speech and Signal Processing, IEEE Transactions on*, *34*(5), 1278–1288.

Wu, Y., Liao, G., & So, H.-C. (2003). A fast algorithm for 2-d direction-of-arrival estimation. *Signal processing*, *83*(8), 1827–1831.

Yang, B. (1995). Projection approximation subspace tracking. *Signal Processing, IEEE Transactions on*, *43*(1), 95–107.

Yang, J.-F., & Kaveh, M. (1988). Adaptive eigensubspace algorithms for direction or frequency estimation and tracking. *Acoustics, Speech and Signal Processing, IEEE Transactions on*, *36*(2), 241–251.

Yilmazer, N., Koh, J., & Sarkar, T. K. (2006). Utilization of a unitary transform for efficient computation in the matrix pencil method to find the direction of arrival. *Antennas and Propagation, IEEE Transactions on*, *54*(1), 175–181.

Yoon, Y.-S. (2004). *Direction-of-arrival estimation of wideband sources using sensor arrays* (Unpublished doctoral dissertation). Georgia Institute of Technology.

Yoon, Y.-S., Kaplan, L. M., & McClellan, J. H. (2006). Tops: new doa estimator for wideband signals. *Signal Processing, IEEE Transactions on*, *54*(6), 1977–1989.

Yoshimura, S., Ushijima, Y., Nishiyama, E., & Aikawa, M. (2011). Microstrip array antenna for orthogonal linear polarization discrimination. In *Proc. international symposium on antenna and propagation, wed1-2.*

Yu, H., Liu, J., Huang, Z., Zhou, Y., & Xu, X. (2007). A new method for wideband doa estimation. In *Wireless communications, networking and mobile computing, 2007. wicom 2007. international conference on* (pp. 598–601).

Zhang, J., Dai, J., & Ye, Z. (2010). An extended tops algorithm based on incoherent signal subspace method. *Signal Processing*, *90*(12), 3317–3324.